

Anchorage of Headed Reinforcement in Concrete

by

Richard Alan DeVries, B.S.C.E., M.S.E.

Dissertation

Presented to the Faculty of the Graduate School of

The University of Texas at Austin

in Partial Fulfillment

of the Requirements

for the Degree of

Doctor of Philosophy

The University of Texas at Austin

December 1996

Anchorage of Headed Reinforcement in Concrete

Approved by Dissertation Committee:

Supervisor: J. O. Jirsa

J. E. Breen

M. E. Kreger

J. M. Roesset

E. B. Becker

For my family and for Linda

Acknowledgments

I would like to express my thanks and gratitude to Dr. Jirsa whose gracious and generous support and friendship helped me accomplish this goal. My gratitude is extended to my supervising committee, Dr. Breen, Dr. Kreger, Dr. Roesset and Dr. Becker, for their assistance, suggestions and inspiration. Also I would like to thank David Mitchell and Kjell Dahl of HRC for their guidance and sponsorship, without which this project would have been impossible.

The staff of the Ferguson Structural Engineering Laboratory, Laurie Golding, Sharon Cunningham, April Jenkins, Blake Stasney, Wayne Fontenot, Wayne Little, Pat Ball, Ray Madonna and Ryan Green were invaluable in the completion of my research. As were Saleem Marwat and Tarek Bashandy who provided indispensable help.

I treasure my parents for their love and support and to whom I can say, "Yes, I'm done now." Finally, my gratefulness to my wife Linda who kept me sane and made writing a dissertation more fun than I could imagine.

Richard DeVries
August 1996
Austin, Texas

Anchorage of Headed Reinforcement in Concrete

Publication No. _____

Richard Alan DeVries, Ph.D.

The University of Texas at Austin, 1996

Supervisor: James O. Jirsa

Recent advances in welding technology have made it cost effective to attach steel plates to reinforcing bars. Headed reinforcing bars have been used in the construction of offshore oil platforms and there is interest in using headed reinforcement as longitudinal reinforcement in concrete members. It is felt that headed reinforcement will offer several advantages over straight and hooked reinforcing bars such as reduced congestion, lower bond slip and improved confinement of joints.

Over 140 pullout tests were conducted to determine the effects of several variables on the anchorage of headed bars in concrete. Variables studied include:

clear cover, corner placement, close spacing, concrete strength, embedment depth, development length, transverse reinforcement and head geometry.

The affects of variables on the pullout-cone capacity of headed reinforcement with low ratios of embedment depth to edge distance were tested. A pullout-cone failure is characterized by a cone of concrete centered around the head being pulled out with the headed bar. The critical variables affecting the pullout-cone capacity were the embedment depth, concrete strength and perimeter of the head. Edge and corner placement reduced the pullout-cone capacity. The results of these tests led to a design procedure for the pullout-cone capacity based on the Concrete Capacity Design Method for anchorage to concrete.

The affects of variables on the blowout capacity of headed reinforcement with large ratios of embedment depth to edge distance were also considered. A blowout failure is characterized by a spalling of cover perpendicular to the bar. The critical variables affecting the blowout capacity were edge distance, concrete strength and net bearing area of the head. Corner placement and close spacing of bars reduced the blowout capacity. A design procedure for the blowout capacity was formulated based on regression analyses of the data and a physical model of the observed behavior. The design procedure takes into account the primary variables, close spacing and corner placement.

The tests showed that headed reinforcement is a viable alternative to current methods of anchorage. Combining the two design procedures will allow engineers to design the anchorage of headed reinforcement in a wide range of applications.

Table of Contents

Acknowledgments.....	v
Abstract	vi
List of Tables.....	xiii
List of Figures	xvi
CHAPTER 1	
INTRODUCTION AND BACKGROUND.....	1
1.1 INTRODUCTION.....	1
1.2 MANUFACTURING OF HEADED REINFORCEMENT.....	4
1.3 APPLICATIONS OF HEADED REINFORCEMENT	6
1.4 PREVIOUS RESEARCH.....	6
1.5 GOALS.....	8
1.6 SCOPE	9
CHAPTER 2 PULLOUT TESTS	
OVERVIEW OF TESTING AND DEFINITIONS.....	11
2.1 INTRODUCTION.....	11
2.2 TEST SETUPS	13
2.3 DEFINITIONS	17
Embedment Depth.....	17
Development Length	17
Edge Distance, Clear Cover and Spacing.....	18
Head Orientation and Geometry.....	20
Transverse Reinforcement.....	21
2.4 CONSTRUCTION OF SPECIMENS	22
Shallow-Embedment Tests	22
Deep-Embedment Tests	25
2.5 MATERIALS	28
Concrete	28
Steel.....	32
2.6 TESTING PROCEDURE.....	34
2.7 EQUIPMENT AND MEASUREMENTS	34
2.8 TEST PROGRAMS.....	38

**CHAPTER 3 SHALLOW-EMBEDMENT PULLOUT TESTS
EFFECT OF VARIABLES ON ANCHORAGE..... 39**

3.1 OVERVIEW OF RESULTS 39
 3.2 GENERAL BEHAVIOR UNDER LOAD 42
 3.3 TRANSVERSE REINFORCEMENT 45
 3.4 DEVELOPMENT LENGTH..... 50
 3.5 CONCRETE STRENGTH 55
 3.6 HEAD AREA AND ASPECT RATIO 57
 3.7 EDGE DISTANCE..... 58
 3.8 EMBEDMENT DEPTH..... 60
 3.9 SUMMARY 62

**CHAPTER 4 SHALLOW EMBEDMENT TESTS
COMPARISON WITH CONCRETE CAPACITY DESIGN METHOD 63**

4.1 INTRODUCTION..... 63
 4.2 CONCRETE CAPACITY DESIGN METHOD..... 64
 4.3 COMPARISON OF RESULTS..... 69
 4.4 COEFFICIENT ADJUSTMENT 77
 4.5 ADJUSTING FOR HEAD AREA..... 82
 4.6 DESIGN EQUATION 88
 4.7 CONCLUSION 93

**CHAPTER 5 DEEP-EMBEDMENT PULLOUT TESTS
EFFECT OF VARIABLES ON ANCHORAGE..... 94**

5.1 OVERVIEW OF RESULTS 94
 5.2 GENERAL BEHAVIOR UNDER LOAD 102
 5.3 DEFLECTIONS 106
 5.4 EMBEDMENT DEPTH..... 109
 5.5 HEAD ORIENTATION 112
 5.6 TRANSVERSE REINFORCEMENT 114
 5.7 DEVELOPMENT LENGTH..... 122
 5.8 HEAD GEOMETRY 129
 Head Area 136
 Head Aspect Ratio..... 137
 Head Shape 137
 Head Thickness..... 141
 5.9 CONCRETE STRENGTH 158
 5.10 COVER 161
 Corner Bars 164
 Close Spacing..... 166
 5.11 SUMMARY 168

CHAPTER 6 DEEP-EMBEDMENT PULLOUT TESTS COMPARISON WITH PREVIOUS RESEARCH AND DESIGN METHODS	169
6.1 INTRODUCTION.....	169
6.2 BEARING STRENGTH OF CONCRETE.....	170
Experimental Studies.....	170
Code Provisions: ACI 318 Section 10.17.....	174
6.3 PRESTRESS ANCHORAGE.....	175
Experimental Studies.....	175
Code Provisions	179
6.4 ANCHOR BOLTS.....	180
Experimental Studies: University of Texas	180
Experimental Studies: University of Stuttgart	184
Code Provisions: Proposed ACI 318 Section 23.11	186
Code Provisions: CEB Method	187
6.5 SUMMARY	192
CHAPTER 7 DEEP-EMBEDMENT PULLOUT TESTS REGRESSION ANALYSIS	196
7.1 INTRODUCTION.....	196
7.2 REGRESSION ANALYSIS PROCEDURE	197
7.3 HEAD AREA	199
7.4 CONCRETE STRENGTH.....	203
7.5 EDGE DISTANCE.....	203
7.6 BEST-FIT EQUATION	209
CHAPTER 8 DEEP-EMBEDMENT PULLOUT TESTS PHYSICAL MODEL	212
8.1 INTRODUCTION.....	212
8.2 PHYSICAL MODEL	213
8.3 EQUATIONS OF THE PHYSICAL MODEL	214
8.4 EQUATION FROM PHYSICAL MODEL AND REGRESSION.....	226
8.5 SUMMARY	228
CHAPTER 9 DEEP-EMBEDMENT PULLOUT TESTS FORMULATION OF DESIGN PROCEDURES FOR SIDE BLOWOUT CAPACITY	229
9.1 INTRODUCTION.....	229
9.2 REVIEW OF EQUATIONS.....	230
9.3 SIMPLIFICATION OF CONCRETE STRENGTH TERM.....	231
9.4 SIMPLIFICATION OF NET BEARING AREA TERM	232
9.5 SIMPLIFICATION OF EDGE DISTANCE TERM	234
9.6 EQUATION FOR CHARACTERISTIC APPLICATION.....	235
9.7 COMPARISON OF CHARACTERISTIC EQUATION WITH PHYSICAL MODEL.....	236
9.8 DEVELOPMENT LENGTH.....	240
9.9 CORNER PLACEMENT AND CLOSE SPACING	241

9.10 95% FRACTILE OF CHARACTERISTIC EQUATION	245
9.11 COMPARISON WITH OTHER RESEARCH.....	248
University of Stuttgart	248
University of Texas	250
9.12 SUMMARY	257
CHAPTER 10	
DESIGN IMPLICATIONS FOR HEADED REINFORCEMENT	258
10.1 INTRODUCTION.....	258
10.2 FAILURE MODE.....	259
10.3 MINIMUM DISTANCES FOR BAR YIELD	265
10.4 BEAM-COLUMN JOINT DESIGN EXAMPLE.....	269
10.5 COLUMN-FOOTING DESIGN EXAMPLE.....	274
CHAPTER 11	
SUMMARY AND CONCLUSIONS.....	278
11.1 SUMMARY	278
11.2 CONCLUSIONS	279
Shallow-Embedment Tests	279
Deep-Embedment Tests	282
11.3 AREAS FOR FURTHER RESEARCH.....	285
Bibliography.....	287
Vita.....	294

List of Tables

Table 2.1 - Mix Designs for Pullout Tests	29
Table 2.2 - Concrete Data for Shallow-Embedment Tests.....	30
Table 2.3 - Concrete Data for Deep-Embedment Tests	31
Table 2.4 - Standard Head Sizes	33
Table 2.5 - Headed Bar Strengths	33
Table 2.6 - Head Strengths	33
Table 2.7 - Transverse Reinforcement Strengths	33
Table 3.1 - Parameters of Shallow-Embedment Tests	40
Table 3.2 - Results of Shallow-Embedment Tests	41
Table 3.3 - Parameters and Results of Shallow-Embedment Tests for Transverse Reinforcement.....	48
Table 3.4 - Parameters and Results of Shallow-Embedment Tests on Development Length	51
Table 3.5 - Prediction of Effect of Development Length on Capacity	53
Table 3.6 - Parameters and Results for Shallow-Embedment Tests on Concrete Strength.....	56
Table 3.7 - Parameters and Results of Shallow-Embedment Tests on Head Area and Aspect Ratio.....	58
Table 3.8 - Parameters and Results of Shallow-Embedment Tests Comparing Edge Distance.....	59
Table 4.1 - Calculations of CCD Capacities for Shallow-Embedment Tests	74
Table 4.2 - Calculations of CCD Capacities with New Coefficient for Shallow-Embedment Tests.....	79
Table 4.3 - Calculations of CCD Capacities with Head Area for Shallow- Embedment Tests	85
Table 4.4 - Calculations of CCD Design Capacities with Head Area for Shallow-Embedment Tests.....	90
Table 5.1 - Parameters and Results of Deep-Embedment Tests	95
Table 5.2 - Parameters and Results of Deep-Embedment Tests on Paired Bars.....	99
Table 5.3 - Parameters and Results of Deep-Embedment Tests with Bearing Failures	101

Table 5.4 - Parameters and Results for Tests on Embedment Depth	111
Table 5.5 - Parameters and Results of Tests with Different Head Orientation.....	113
Table 5.6 - Parameters for Tests with Transverse Reinforcement	117
Table 5.7 - Results from Tests with Transverse Reinforcement	118
Table 5.8 - Parameters and Results of Tests with Development Length.....	124
Table 5.9 - Predicted Anchorage Capacity Based on Orangun's Equation.....	127
Table 5.10 - Predicted Anchorage Capacities Based on ACI Provisions for Development Length	130
Table 5.11 - Parameters and Results of Tests on Head Geometry	133
Table 5.12 - Nominal and Actual Head Sizes for Tests on Head Geometry	134
Table 5.13 - Parameters and Results for Tests on Head Aspect Ratio	138
Table 5.14 - Parameters and Results for Tests on Head Shape	140
Table 5.15 - Parameters and Results for Tests on Head Thickness	142
Table 5.16 - Comparison of Measured and Predicted Head Strains	147
Table 5.17 - Comparison of Measured and Predicted Head Strains	150
Table 5.18 - Summary of Tests with Head Yielding.....	151
Table 5.19 - Minimum Thicknesses of Heads Based on Hawkins' Equation	155
Table 5.20 - Minimum Thicknesses for Rigid Heads Based on Roberts' Criteria.....	157
Table 5.21 - Minimum Head Thicknesses for Rigid Heads Based on Cantilever Beam Model	158
Table 5.22 - Parameters and Results for Tests on Concrete Strength	160
Table 5.23 - Nominal and Actual Head Sizes for Tests on Concrete Strength	160
Table 5.24 - Comparison of Capacities for Tests with Different Concrete Strengths.....	161
Table 5.25 - Parameters and Results for Tests on Edge Distance	163
Table 5.26 - Comparison of Effect of Edge Distance on Capacity	164
Table 5.27 - Comparison of Capacities of Edge and Corner Bar Tests	166
Table 5.28 - Parameters and Results of Tests on Closely Spaced Bars	167
Table 6.1 - Summary of Statistical Measures for Comparisons of Edge Bar Capacities	193
Table 6.2 - Summary of Statistical Measures for Comparisons of Corner Bar Capacities	195
Table 6.3 - Summary of Statistical Measures for Comparison of All Deep- Embedment Test Capacities	195
Table 7.1 - Results of Regression Analyses for Head Area	200
Table 7.2 - Parameters and Results for Deep-Embedment Tests on Edge Bars with No Development Length.....	204

Table 7.3 - Results of Regression Analyses for Edge Distance	207
Table 8.1 - Statistical Measures of Measured Sizes of Blowout Failures	218
Table 9.1 - Statistical Measures of Equations from Regressions and Physical Model	230
Table 9.2 - Parameters and Results of Tests by Furche and Eligehausen	249
Table 9.3 - Parameters and Results of Tests by Hasselwander	251
Table 9.4 - Summary of Statistical Measures for Various Comparisons Based on Design Equations (Equations 9.20, 9.15 and 9.16)	255
Table 9.5 - Example Calculations for Blowout Capacities	256

List of Figures

Figure 1.1 - Force Transfer for Smooth (Undeformed) Bar	2
Figure 1.2 - Anchorage Method Used by Hennibique [25].....	2
Figure 1.3 - Force Transfer for Deformed Bar	3
Figure 1.4 - Force Transfer for Hooked Bar.....	3
Figure 1.5 - Headed Reinforcing Bar	3
Figure 1.6 - Force Transfer for Headed Bar	4
Figure 1.7 - Friction Welding Process.....	5
Figure 1.8 - Headed Reinforcing in Offshore Platform Construction	7
Figure 2.1 - Pullout-Cone Failure.....	12
Figure 2.2 - Side-Blowout Failure.....	13
Figure 2.3 - Basic Test Setup for Shallow-Embedment Tests	14
Figure 2.4 - Shallow-Embedment Test Setup for Center Bar	14
Figure 2.5 - Shallow-Embedment Test Setup for Edge Bar.....	15
Figure 2.6 - Basic Test Setup for Deep-Embedment Tests	16
Figure 2.7 - Embedment Depth	17
Figure 2.8 - Comparison of Embedment Depth and Development Length.....	18
Figure 2.9 - Cover Parameters.....	19
Figure 2.10 - Head Dimensions and Orientation.....	20
Figure 2.11 - Parameters for Transverse Reinforcement.....	21
Figure 2.12 - Forms for Shallow-Embedment Tests	23
Figure 2.13 - Construction of Shallow-Embedment Specimens	23
Figure 2.14 - Placement of Concrete for Shallow-Embedment Tests.....	24
Figure 2.15 - Forms for Deep-Embedment Tests.....	25
Figure 2.16 - Construction of Deep-Embedment Specimens.....	26
Figure 2.17 - Placement of Concrete for Deep-Embedment Tests.....	28
Figure 2.18 - Concrete Strengths for Shallow-Embedment Tests.....	30
Figure 2.19 - Concrete Strength for Deep-Embedment Tests	31
Figure 2.20 - Test Equipment.....	35
Figure 2.21 - Shallow-Embedment Test Setup and Equipment.....	36
Figure 2.22 - Deep-Embedment Test Setup and Equipment.....	36

Figure 3.1 - Deflection of Headed Reinforcing Bar with Shallow Embedment.....	42
Figure 3.2 - Pullout-Cone Failure of Headed Bar with Shallow Embedment.....	43
Figure 3.3 - Deflection of Headed Bar with Shallow Embedment and Bar Yielding.....	44
Figure 3.4 - Deflection of Headed Bar with Shallow Embedment and Bar Fracture.....	45
Figure 3.5 - Model of Transverse Reinforcement for Shallow-Embedment Tests	46
Figure 3.6 - Configurations of Transverse Reinforcement for Shallow-Embedment Tests	47
Figure 3.7 - Comparison of Capacities for Tests on Transverse Reinforcement	48
Figure 3.8 - Deflections of Headed Bars with and without Transverse Reinforcement	49
Figure 3.9 - Comparison of Capacities of Shallow-Embedment Tests on Development Length	51
Figure 3.10 - Comparison of Deflection of Headed Bars with and without Development Length	54
Figure 3.11 - Comparison of Capacities of Shallow-Embedment Tests on Concrete Strength.....	56
Figure 3.12 - Deflection of Headed Bars with Different Concrete Strengths	57
Figure 3.13 - Comparison of Deflections of Tests with Different Heads	58
Figure 3.14 - Deflections of Headed Bars with Different Edge Distances.....	59
Figure 3.15 - Comparison of Capacities versus Embedment Depth	60
Figure 3.16 - Comparison of Deflections of Headed Bars with Different Embedment Depths	61
Figure 4.1 - CCD Pullout Cone.....	65
Figure 4.2 - CCD Failure Area.....	66
Figure 4.3 - CCD Failure Area for Edge Placements.....	67
Figure 4.4 - CCD Failure Area for Groups.....	68
Figure 4.5 - Extent of Failure Surface for Edge Bar with Shallow Embedment.....	70
Figure 4.6 - Extent of Failure Surface for Edge Bar with Shallow Embedment.....	71
Figure 4.7 - Extent of Failure Surface for Corner Bar with Shallow Embedment.....	71
Figure 4.8 - Comparison of Predicted Capacities from CCD Method with Measured Capacities of Shallow-Embedment Tests	73

Figure 4.9 - Comparison of Predicted Capacities from CCD Method with New Coefficient and Measured Capacities of Shallow- Embedment Tests	78
Figure 4.10 - Pullout-Cone Failure Area Based on Effective Perimeter	82
Figure 4.11 - Comparison of Predicted Capacities using CCD Method with Head Area and Measured Capacities for Shallow- Embedment Tests	84
Figure 4.12 - Comparison of Predicted Capacities with CCD Design Method with Head Area with Measured Capacities of Shallow-Embedment Tests.....	89
Figure 5.1 - Bearing Failure of Loaded Surface	99
Figure 5.2 - Setup for Retesting after Bearing Failure	100
Figure 5.3 - Setup for Retesting after Bearing Failure	101
Figure 5.4 - Deflection at Head for Bar without Development Length.....	102
Figure 5.5 - Wedge of Concrete Observed on Head after Failure	103
Figure 5.6 - Head Movement after Failure	104
Figure 5.7 - Cracking along Development Length during Testing.....	105
Figure 5.8 - Shearing of Concrete at Lugs.....	106
Figure 5.9 - Comparison of Head Slips for Various Deep-Embedment Tests	107
Figure 5.10 - Effect of Transverse Reinforcement on Head Slip	108
Figure 5.11 - Comparison of Head and Lead Slip.....	109
Figure 5.12 - Comparison of Capacities for Tests with Different Embedment Depths	111
Figure 5.13 - Comparison of Capacities of Tests with Different Head Orientations	113
Figure 5.14 - Tie Configurations for Edge Bars.....	115
Figure 5.15 - Tie Configurations for Corner Bars.....	115
Figure 5.16 - Comparison of Capacities of Tests with Transverse Reinforcement	119
Figure 5.17 - Comparison of Tie Force with Head Deflection.....	121
Figure 5.18 - Comparison of Capacities of Tests with Development Length	124
Figure 5.19 - Bar Force at Head versus Total Bar Load.....	125
Figure 5.20 - Comparison of Spacing for Circular and Rectangular Heads.....	132
Figure 5.21 - Head Dimensions and Geometric Properties.....	135
Figure 5.22 - Comparison of Capacities with Head Area	136
Figure 5.23 - Comparison of Capacities for Tests on Head Aspect Ratio	138
Figure 5.24 - Comparison of Capacities of Tests on Head Shape.....	140
Figure 5.25 - Comparison of Capacities for Tests on Head Thickness	142
Figure 5.26 - Strain Gauge Locations.....	143

Figure 5.27 - Comparison of Head Strains.....	144
Figure 5.28 - Head Thickness Design Parameters and Equations.....	145
Figure 5.29 - Inelastic Deformations of Thin Heads.....	152
Figure 5.30 - Comparison of Capacities for Tests with and without Head Yielding.....	152
Figure 5.31 - Hawkins' Variables for Flexible Plates and Headed Reinforcement Equivalents.....	154
Figure 5.32 - Measured Capacities versus Edge Distance.....	162
Figure 5.33 - Typical Failure Surface for Corner Bar.....	165
Figure 5.34 - Failure Surfaces of Tests on Closely Spaced Paired Bars.....	167
Figure 6.1 - Failure Mechanism Proposed by Hawkins.....	170
Figure 6.2 - Variables for Equation 6.1 by Hawkins.....	171
Figure 6.3 - Headed Reinforcement Variables for Equation 6.2.....	172
Figure 6.4 - Comparison of Measured and Predicted Capacities using Equation 6.2 by Hawkins.....	173
Figure 6.5 - Comparison of Measured and Predicted Capacities using Equation 6.3 from ACI 318 Section 10.17.....	175
Figure 6.6 - Comparison of Measured and Predicted Capacities using Equation 6.7 by Williams.....	177
Figure 6.7 - Comparison of Measured and Predicted Capacities using Equation 6.9 by Roberts.....	178
Figure 6.8 - Comparison of Measured and Predicted Capacities using Equation 6.11 based on CEB Model Code.....	180
Figure 6.9 - Comparison of Measured and Predicted Capacities using Equation 6.12 by Hasselwander.....	182
Figure 6.10 - Comparison of Measured and Predicted Capacities using Equation 6.13 by Hasselwander.....	184
Figure 6.11 - Comparison of Measured and Predicted Capacities using Equation 6.15 by Furche and Eligehausen.....	186
Figure 6.12 - Comparison of Measured and Predicted Capacities using Equation 6.14 from Proposed ACI 318 Section 23.11.....	187
Figure 6.13 - Basic Blowout Failure Area for CEB Method.....	189
Figure 6.14 - CEB Blowout Failure Area for Corner Placement.....	190
Figure 6.15 - CEB Blowout Failure Area for Close Spacing.....	190
Figure 6.16 - Comparison of Measured and Predicted Capacities using CEB Method - Equations 6.17 through 6.21.....	191
Figure 7.1 - Comparison of Best-Fit Equation for Head Area (Equation 7.2) with Test Results.....	201
Figure 7.2 - Comparison of Possible Failure Modes.....	202
Figure 7.3 - Comparison of Straight and Headed Bars with No Cover.....	206

Figure 7.4 - Comparison of Best-Fit Equation for Edge Distance (Equation 7.4) with Test Results.....	208
Figure 7.5 - Comparison of Measured Capacities with Capacities Predicted by Best-Fit Equation (Equation 7.6).....	211
Figure 8.1 - Pullout-Cone Failure.....	213
Figure 8.2 - Blowout Failure.....	215
Figure 8.3 - Geometry of Blowout Failure.....	217
Figure 8.4 - Dimensions of Blowout Failures.....	218
Figure 8.5 - Comparison of Blowout Area with Head Area.....	219
Figure 8.6 - Comparison of Blowout Area with Edge Distance.....	219
Figure 8.7 - Comparison of Theta with Head Area.....	220
Figure 8.8 - Comparison of Theta with Edge Distance.....	220
Figure 8.9 - Comparison of Blowout Area with Edge Distance and Predictive Equation.....	221
Figure 8.10 - Comparison of Alpha with f_b/f'_c	224
Figure 8.11 - Comparison of Measured Capacities with Capacities Predicted by Equation from Physical Model (Equation 8.11).....	225
Figure 9.1 - Comparison of Functions for Concrete Strength.....	232
Figure 9.2 - Comparison of Functions for Net Bearing Area.....	233
Figure 9.3 - Comparisons of Functions for Edge Distance.....	234
Figure 9.4 - Comparison of Measured Capacities with Capacities Predicted by Characteristic Equation (Equation 9.6).....	236
Figure 9.5 - Comparison of Measured and Predicted Alpha.....	239
Figure 9.6 - Comparison of Alpha with f_b/f'_c	239
Figure 9.7 - Comparison of Measured Capacities of Bars with Development Length with Capacities Predicted by Characteristic Equation (Equation 9.6).....	241
Figure 9.8 - Blowout Areas, A_{bo} , for Various Configurations.....	243
Figure 9.9 - Comparison of Measured Capacities of Corner and Paired Bars with Capacities Predicted by Modified Characteristic Equation (Equations 9.6, 9.15 and 9.16).....	245
Figure 9.10 - Comparison of Measured Capacities of Edge Bars with No Development Length with Capacities Predicted by Characteristic Design Equation (Equation 9.20).....	247
Figure 9.11 - Comparison of Measured Capacities of All Deep-Embedment Tests with Capacities Predicted by Design Equations (Equations 9.20, 9.15 and 9.16).....	247

Figure 9.12 - Comparison of Measured Capacities from Furche and Eligehausen with Design Equations (Equations 9.20, 9.15 and 9.16).....	250
Figure 9.13 - Comparison of Measured Capacities by Hasselwander with Capacities Predicted by Design Equations (Equations 9.20, 9.15 and 9.16).....	254
Figure 9.14 - Comparison of Measured Capacities for 187 Tests with Capacities Predicted by Design Equations (Equations 9.20, 9.15 and 9.16).....	255
Figure 10.1 - Anchorage Capacity of 20mm Bar with 50x50x12mm Head.....	261
Figure 10.2 - Anchorage Capacity of 20mm Bar with 35x70x16mm Head.....	261
Figure 10.3 - Anchorage Capacity of 25mm Bar with 70x70x16mm Head.....	262
Figure 10.4 - Anchorage Capacity of 25mm Bar with 40x80x18mm Head.....	262
Figure 10.5 - Anchorage Capacity of 35mm Bar with 90x90x20mm Head.....	263
Figure 10.6 - Anchorage Capacity of 35mm Bar with 55x100x25mm Head.....	263
Figure 10.7 - Relationship Between h_d and C_1 for Switch in Failure Mode	264
Figure 10.8 - Required Embedment Depth for Given Ratio of $f_s/(\text{root } f'_c)$	266
Figure 10.9 - Required Edge Distance for Given Ratio of $f_s/(\text{root } f'_c)$	268
Figure 10.10 - Parameters for Beam-Column Joint Design Example.....	269
Figure 10.11 - Pullout-Cone Failure for Beam-Column Joint Design Example.....	271
Figure 10.12 - Blowout Failure for Beam-Column Joint Design Example.....	272
Figure 10.13 - Partial Beam Section for Beam-Column Joint Design Example.....	273
Figure 10.14 - Parameters for Column-Footing Design Example.....	274
Figure 10.15 - Pullout-Cone Failure Area for Column-Footing Design Example.....	276
Figure 10.16 - Section of Footing for Column-Footing Design Example.....	277
Figure 11.1 - Pullout-Cone Failure for Headed Reinforcement.....	281
Figure 11.2 - Blowout Failure for Headed Reinforcement.....	284

Chapter 1

Introduction and Background

1.1 Introduction

The importance of transferring force between concrete and reinforcing steel has been recognized since the first applications of reinforced concrete. Early practices relied on friction and adhesion between the natural roughness of smooth bars (bars without additional projections or lugs rolled along the length) and concrete to transfer force (Figure 1.1). Some construction techniques, such as a patented method by the French engineer Hennibique, riveted plates to the ends of smooth reinforcing bars (Figure 1.2) [25]. The bearing of the plates on the surrounding concrete provided the mechanism for force transfer to anchor the bar in concrete. Advances in manufacturing of reinforcing steel made it more cost efficient to use deformed bars (bars with lugs) for reinforcement. The bearing of the bar deformations or lugs on the surrounding concrete transfers force along the

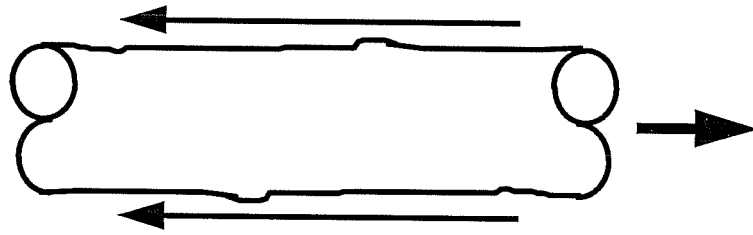


Figure 1.1 - Force Transfer for Smooth (Undeformed) Bar

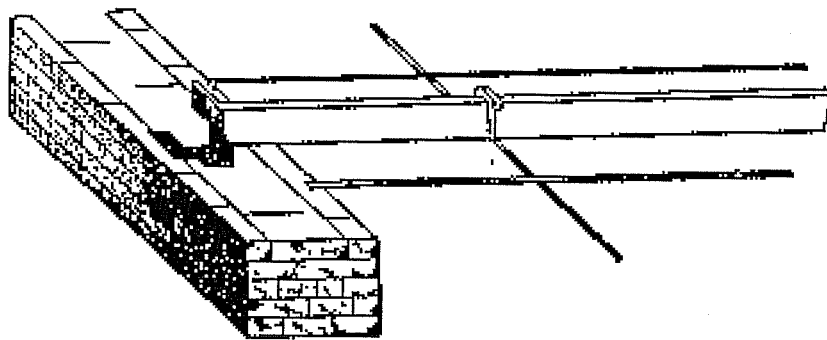


Figure 1.2 - Anchorage Method Used by Hennibique [25]

length of the anchored bar (Figure 1.3). In situations where there is not sufficient length available for a straight bar to provide anchorage, the bar can be hooked with either a 90° or 180° hook. The bearing of the hook along with force transfer along the development length anchors the bar (Figure 1.4). Recent advances in welding technology have made it cost efficient to weld steel plates to ends of smooth or deformed bars creating a headed reinforcing bar (Figure 1.5). As with the

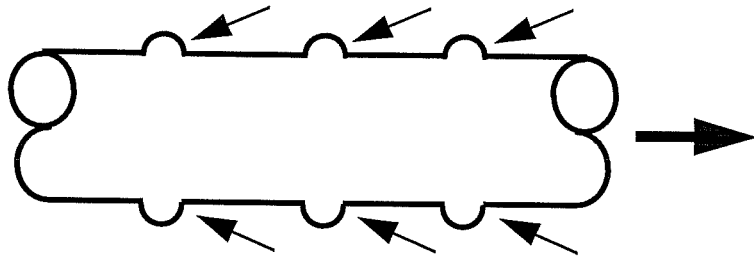


Figure 1.3 - Force Transfer for Deformed Bar

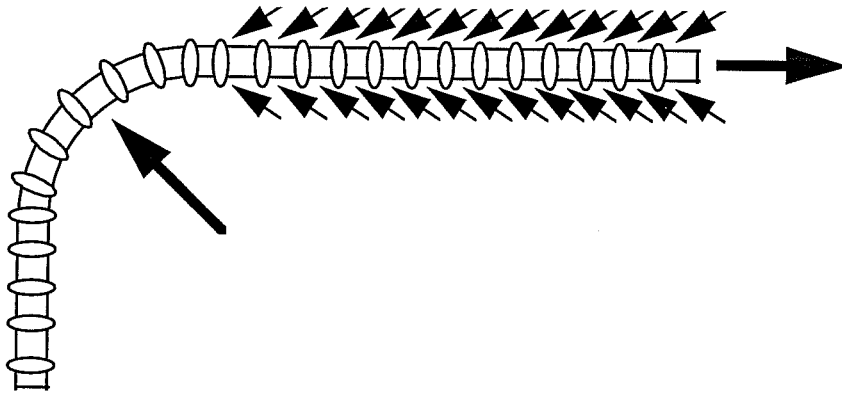


Figure 1.4 - Force Transfer for Hooked Bar

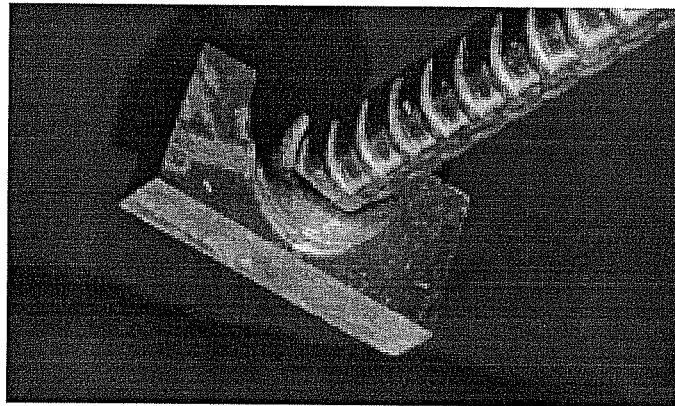


Figure 1.5 - Headed Reinforcing Bar

Hennibique technique, bearing of the plate against concrete anchors the bar, and when heads are attached to deformed bars, additional force may be transferred along the length (Figure 1.6).

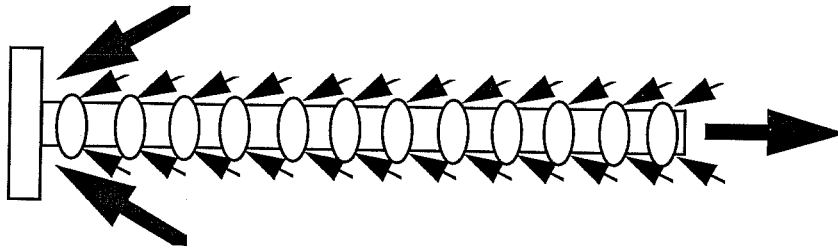


Figure 1.6 - Force Transfer for Headed Bar

The use of headed reinforcement may offer many advantages over straight or hooked bar anchorages such as improved confinement of joints, the ability to anchor larger bars than currently possible with hooked bars, lower slip of reinforcement, improved detailing and improved response to cyclic loading. In some applications the use of headed reinforcement may reduce the congestion of the reinforcing cage which would reduce erection time and cost.

1.2 Manufacturing of Headed Reinforcement

Headed reinforcement can be manufactured by a variety of techniques. The head can be welded to the bar with arc or induction welding or the bar can be

threaded and the head fastened with the threads. The requirements for the connection are that it must be strong enough to develop the expected bar force with negligible or acceptable deformations in the connection over the desired life of the structure. The manufacturing process of headed bars must be reliable and consistently produce acceptable connections.

One of the methods for manufacturing headed reinforcement is friction welding. In friction welding the steel head is rotated at approximately 1500 rpm; the steel bar is then pressed against the spinning head with sufficient force to generate enough heat of friction between the spinning head and bar to weld the two elements together (Figure 1.7). Friction welding has been used in the automotive industry and has produced reliable welds. The bar shown in Figure 1.5 was manufactured with the friction welding process. At the juncture of the bar and head a torus of steel called flashing forms during the welding process. The flashing is a byproduct of the process and can be removed without affecting the connection. The narrowest head that can be attached to a reinforcing bar is approximately 1.5 times the bar diameter. All the headed reinforcing bars used in this study were manufactured with the friction welding technique.

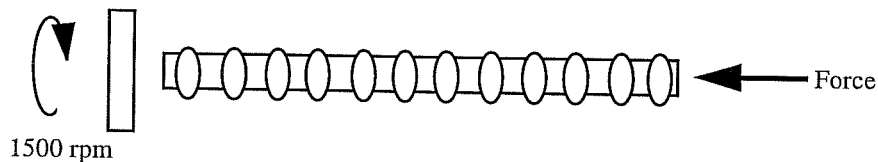


Figure 1.7 - Friction Welding Process

1.3 Applications of Headed Reinforcement

Headed reinforcement is a relatively new product and has not been used in many applications. Headed reinforcing bars have been extensively used in the construction of offshore oil platforms where hooked bars have traditionally been used to anchor longitudinal reinforcement or bars bent for ties and transverse reinforcement. Hooks and bent-bar ties create a large amount of congestion in the reinforcing cage which leads to difficulties during construction. Using headed reinforcement removes the tail extensions of hooks and allows fewer larger bars to be used, greatly reducing the congestion of the reinforcing cage (Figure 1.8). It has been found that the use of headed reinforcement can greatly decrease the time needed to erect the reinforcement resulting in large cost savings [37]. Headed reinforcement has also been used in a few projects for strengthening and repairing footings of highway structures.

1.4 Previous Research

Research on headed reinforcement includes studies of friction welded connections and fatigue life of the connection [46, 47]. Studies have been conducted on the confinement provided by headed transverse reinforcement in slabs and walls [32, 35]. Research has also been done looking at the use of headed

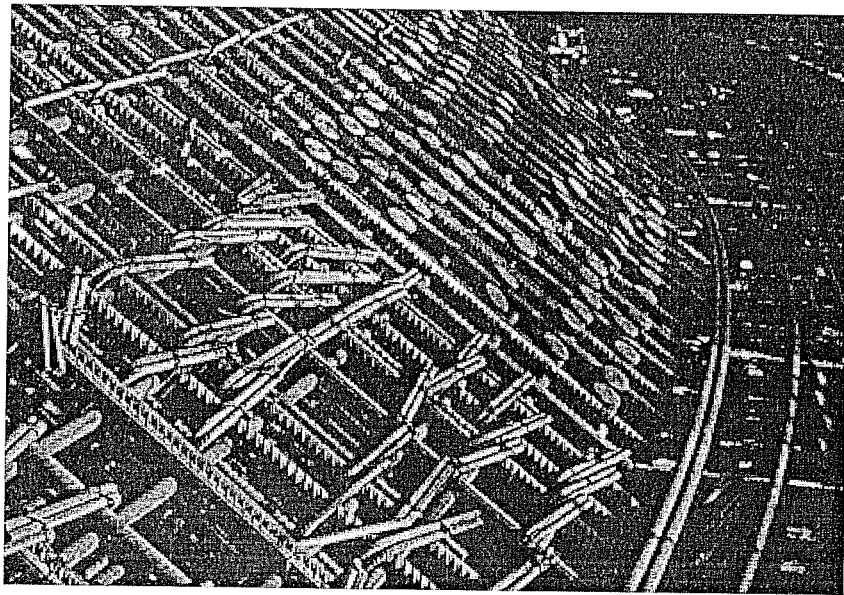
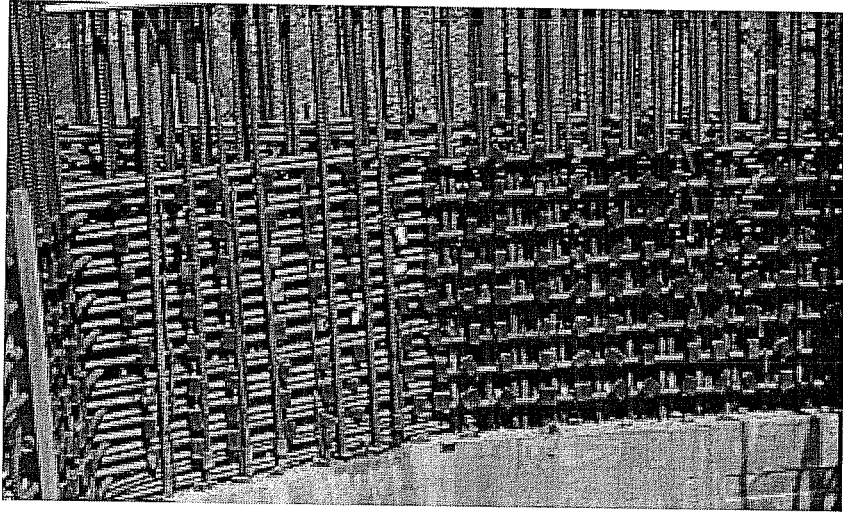


Figure 1.8 - Headed Reinforcing in Offshore Platform Construction

reinforcement for shear reinforcement in beams [7, 8]. Also a few tests which were part of larger research projects were conducted on beam-column joint specimens using headed reinforcement for longitudinal reinforcement [15, 38]. None of these previous research projects have focused on variables affecting the anchorage capacity of headed reinforcement.

1.5 Goals

The data discussed in this report is based on examinations of variables affecting anchorage capacity and behavior of headed reinforcement in concrete. The goal of this research is to produce comprehensive design recommendations to predict the anchorage capacity of headed reinforcement.

The design recommendations should be both rational and transparent. A rational design recommendation is based on a description or model explaining observations. In transparent recommendations, the effects of each variable are obvious by keeping required calculations as simple as possible. While it is possible to create an accurate equation to predict capacities that is not based on any model or requires difficult calculations, rational and transparent recommendations allow an engineer to use the recommendations for situations that may not have been directly tested or in field situations.

To help propose rational and transparent design recommendations, the proposed design methods will begin with a characteristic equation. The characteristic equation will predict the capacity for a characteristic application, for example a single headed reinforcing bar not affected by edges or close spacing. The characteristic equation is meant to predict the capacity for a common situation. For situations with different conditions than the characteristic application, the value predicted by the characteristic equation is modified by additional factors. The current ACI provisions for development of hooked bars follow this pattern. A basic or characteristic value is calculated (the basic hooked bar development length) and then modified for other conditions (lightweight aggregate, sufficient number of ties, larger covers than that on which the characteristic equation is based, etc.).

1.6 Scope

In order to propose design recommendations, over 140 pullout tests were conducted on headed reinforcing bars. Many factors were tested to determine their effects on the anchorage capacity and behavior of headed reinforcement. Included were variables associated with the placement of headed reinforcement in concrete members: embedment depth, clear cover over the bar, spacing of adjacent bars and orientation of the heads. Also, variables associated with the

geometry of a headed bar were tested: bar diameter, head size, head shape and head thickness. In addition variables associated with typical structures such as transverse reinforcement in the anchorage zone of headed bars and additional development length were tested. The variables were chosen to create a comprehensive study of headed reinforcement and were varied over a range of values that would encompass typical applications of headed reinforcement.

Chapter 2

Pullout Tests Overview of Testing and Definitions

2.1 Introduction

Other than yield or fracture of the steel bar, two failure modes will govern the majority of applications of headed reinforcement in concrete members: pullout-cone and side blowout. A pullout-cone failure is characterized by a cone of concrete around the reinforcing bar or anchor bolt being pulled out of the surrounding concrete as a unit (Figure 2.1). Pullout-cone failures are likely when the ratio of embedment depth to side cover (distance to the edge of concrete) is small. For example, an anchor bolt with a shallow embedment placed in the center of a slab would probably result in a pullout-cone failure when placed in tension. A series of shallow-embedment pullout tests were conducted to define the conditions for pullout failures.

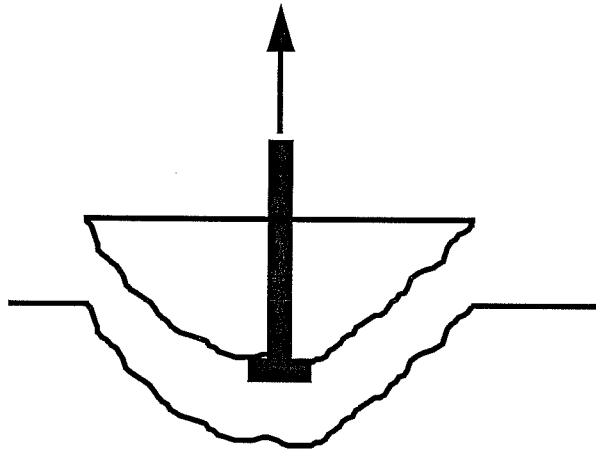


Figure 2.1 - Pullout-Cone Failure

A side-blowout failure is characterized by spalling of a portion of the concrete cover over the head (Figure 2.2). Side-blowout failures are likely when the ratio of embedment depth to side cover is large. For example, a headed reinforcing bar used to provide anchorage for the longitudinal reinforcement in a beam or column with minimum clear cover over the bar might experience a side blowout failure when placed in tension. A series of deep-embedment pullout tests were conducted to define the conditions for side blowout failures. In reinforced concrete members where headed reinforcement is used, it is assumed the embedment depth will be much greater than the cover over the bar.

Variables considered in these series of tests include: embedment depth; development length; clear cover; corner placement; concrete strength; transverse reinforcement; head orientation; head area; head aspect ratio; head thickness and

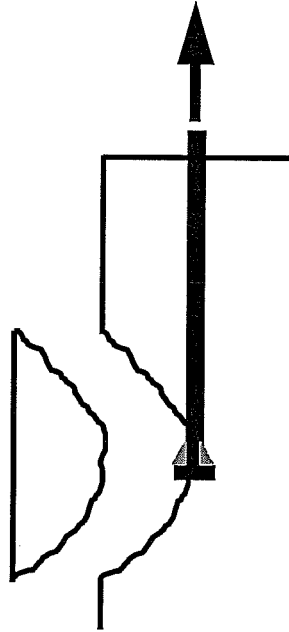


Figure 2.2 - Side-Blowout Failure

head shape. Definitions of these variables, construction of the specimens, test procedures, equipment and overviews of the test programs are presented in this chapter.

2.2 Test Setups

The basic test setup for the shallow-embedment pullout tests is illustrated in Figure 2.3. The test setup for a bar placed away from an edge is shown in Figure 2.4 and the test setup for a bar placed near an edge is shown in Figure 2.5. The shallow-embedment setup consisted of a headed bar with a ratio of

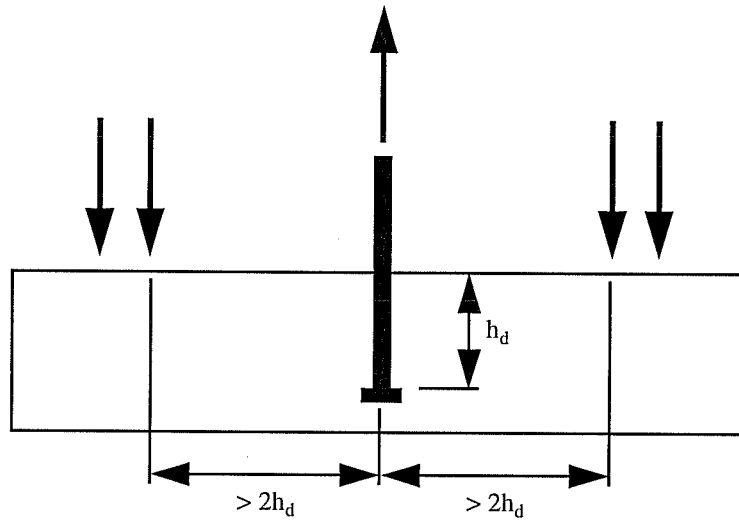


Figure 2.3 - Basic Test Setup for Shallow-Embedment Tests

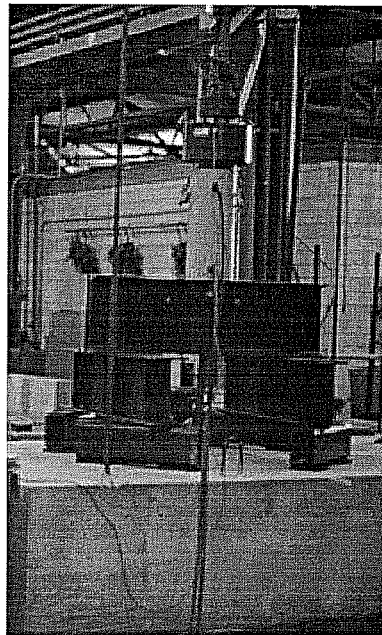


Figure 2.4 - Shallow-Embedment Test Setup for Center Bar

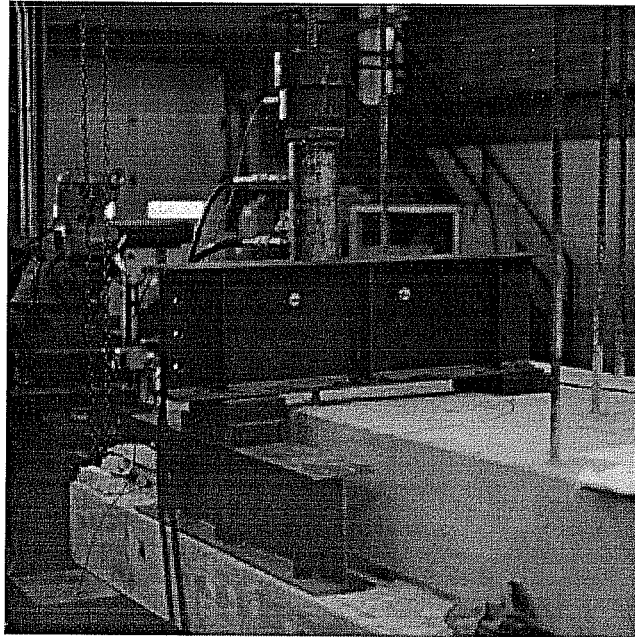


Figure 2.5 - Shallow-Embedment Test Setup for Edge Bar

embedment depth to clear cover less than five. With shallow embedments, the confinement of the concrete from the bearing reaction of the tests may affect the anchorage strength. To minimize these possible effects, the bearing reactions from the loading beams were placed far enough away from the anchorage zone so that the failure cone could develop without interference from the loading apparatus.

The basic test setup for the deep-embedment pullout tests is shown in Figure 2.6. Ratios of embedment depth to clear cover greater than five were used. With deep embedments, the confinement effects of the bearing reaction were assumed to have little effect on the anchorage strength. For this reason the loading ram bore directly on the concrete above the anchorage zone. This

assumption was verified with a series of tests reported in Section 5.4. To ensure level and equal bearing on the concrete surface, a steel plate with a single center hole was grouted to the surface around the bar before testing.

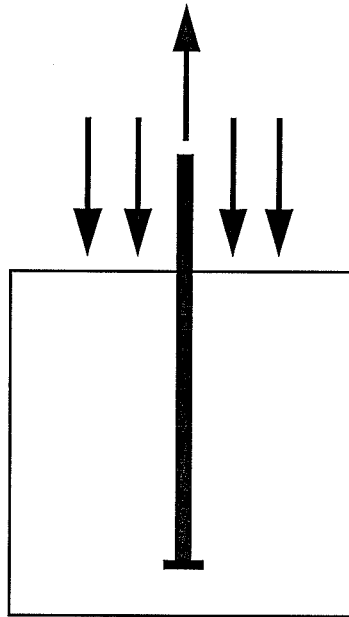


Figure 2.6 - Basic Test Setup for Deep-Embedment Tests

2.3 Definitions

Embedment Depth

The embedment depth defines the size of a possible pullout cone. The embedment depth, h_d , is defined as the distance from the top, or loaded, surface of the test specimen to the top of the head (Figure 2.7). In concrete members the embedment depth for headed reinforcement in tension would be defined as the distance, parallel with the bar, measured from the head, to a critical section (a point of maximum stress in the bar).

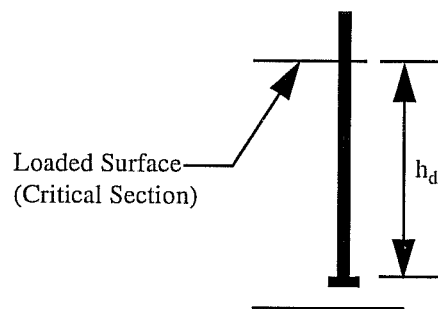


Figure 2.7 - Embedment Depth

Development Length

The development length, l_d , for headed reinforcement is defined as the length along a deformed bar bonded to the concrete from the head to a critical section. If a smooth reinforcing bar or bolt is attached to a head, then the development length is zero. The amount of development length was controlled

during testing by sheathing the bars with rigid PVC tubes. The ends of the tubes were sealed with silicon caulk to prevent any paste from bonding with the bar. Development length and embedment depth for the test setups are compared in Figure 2.8.

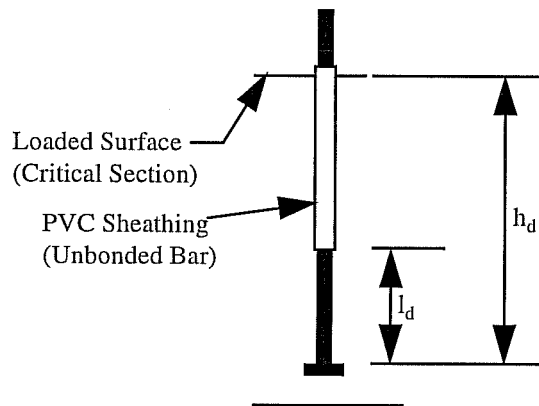


Figure 2.8 - Comparison of Embedment Depth and Development Length

Edge Distance, Clear Cover and Spacing

Four parameters associated with cover or spacing of headed reinforcement are illustrated in Figure 2.9. The minimum edge distance, C_1 , is defined as the distance from the closest edge of concrete to the center of the bar. The distance perpendicular to C_1 from the center of the bar to the second closest orthogonal edge is C_2 which will always be greater than or equal to C_1 . All dimensions measured parallel with C_1 are denoted with the subscript 1, and all dimensions parallel with C_2 are denoted with the subscript 2. Clear cover over the bar, C_{c1} and C_{c2} , is defined as the distance from the surface of the bar to closest edge. C_{c2}

will always be greater than or equal to C_{c1} . Clear covers over the head, C_{h1} and C_{h2} , are defined as the distance from the edge of the head to the concrete edge. Depending on the geometry of the head, C_{h2} may or may not be greater than C_{h1} . The head dimensions are denoted as h_1 and h_2 . The spacing between the centers of two adjacent bars is C_{sp1} and C_{sp2} depending on the direction (or plane) in which multiple bars are placed.

Head Orientation and Geometry

In all tabulations and notation used herein, the order of the head dimensions represents the head orientation with the h_1 dimension listed first followed by the h_2 dimension and t representing the thickness. The head aspect ratio is defined as the ratio of the largest head plan dimension to the smallest head plan dimension. For a square head the aspect ratio is 1:1, with higher ratios representing longer and narrower rectangles. These designations are illustrated in Figure 2.10.

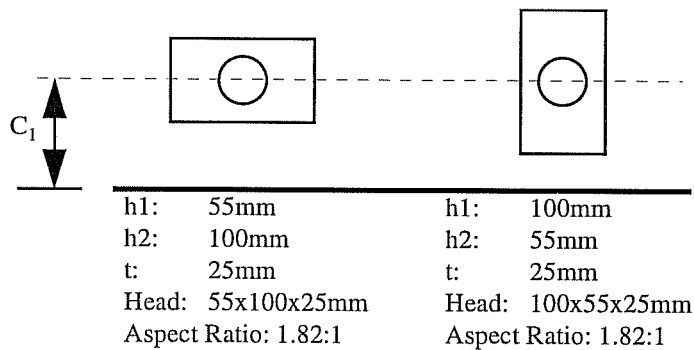


Figure 2.10 - Head Dimensions and Orientation

Transverse Reinforcement

Transverse reinforcement is described with four parameters: number of transverse ties, **Number**; diameter of individual ties, d_{btr} ; distance from the head to the first transverse tie measured along the bar, S_{p1} ; and spacing of remaining ties, S_p , (Figure 2.11). The area of transverse reinforcement in the anchorage zone, A_{tr} , is the total area of transverse reinforcement in tension across the failure plane (the surface of the pullout cone or blowout failure). The number of ties, the diameter of the ties and the number of legs of each tie crossing the failure plane providing tensile resistance to the failure determine A_{tr} .

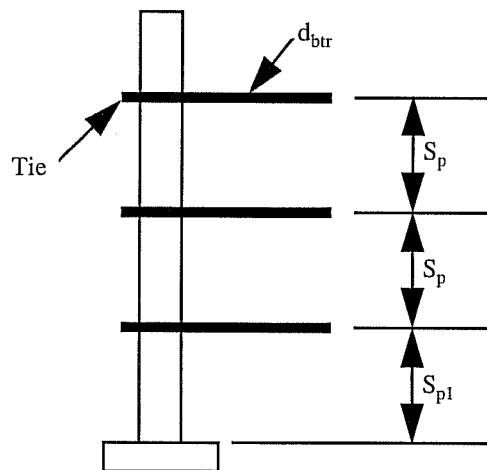


Figure 2.11 - Parameters for Transverse Reinforcement

2.4 Construction of Specimens

Shallow-Embedment Tests

Three large concrete blocks were constructed for the shallow-embedment pullout tests. Each block was 530mm (21 in.) deep with 8 to 11 headed reinforcing bars cast within the block. The plan dimensions of the blocks were 1520mm by 2900mm (5 ft. 0 in. by 9 ft. 6 in.). The bars were spaced far enough apart to avoid overlap of the anticipated failure surfaces. The blocks were cast in bolted plywood forms. For two of the blocks a ledge was cast along the two long sides to provide an area for the bearing reaction for edge and corner bar tests.

The form and bars are shown in Figure 2.12 before placement of concrete. Various parts of the formwork and supports used to ensure correct placement of the headed bars are shown in Figure 2.13. A frame was attached to the forms above the top surface of concrete and the bars were tied to the frame to prevent movement during casting. The embedment depth of the headed reinforcement was controlled with a piece of copper tubing placed under the head, supporting the bar at the proper depth.

After placing the bars in the form, transverse reinforcement, if any, was placed within the embedment depth. The transverse reinforcement was tied to the bars and secured to prevent movement during casting. Additional reinforcement was placed in the forms below the heads, along the ledges, between the bars and

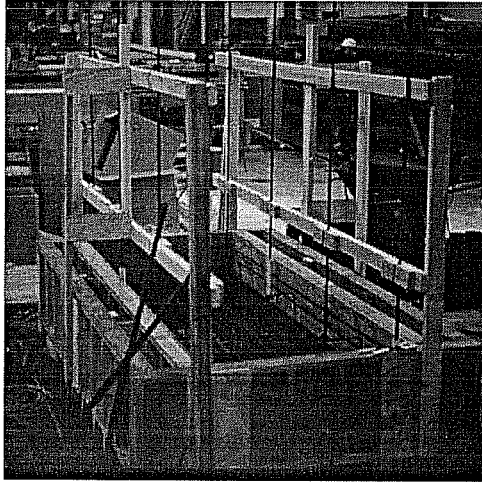


Figure 2.12 - Forms for Shallow-Embedment Tests

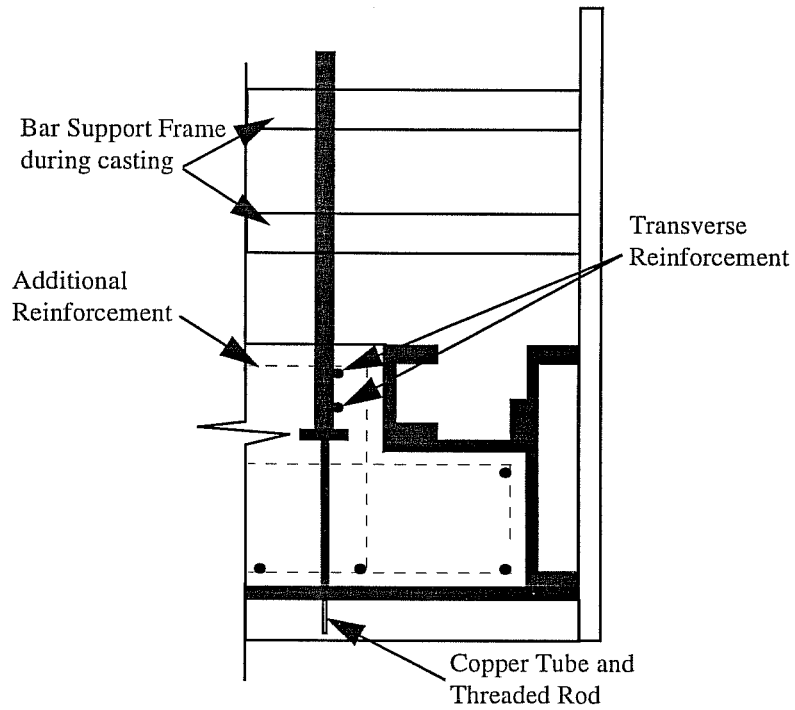


Figure 2.13 - Construction of Shallow-Embedment Specimens

near the top surface of the block to prevent cracks from extending through the block which would create difficulties in moving the block after testing. This additional reinforcement was placed so that it would not interfere with the formation of the failure around the headed bar.

The concrete was placed directly into the forms using the chute of the ready-mix concrete truck (Figure 2.14). The concrete was placed in three equal lifts and vibrated with stinger-type vibrators after each lift. Control cylinders were also cast at the same time as the block. After placement of the concrete, the top surface was finished with trowels. Wet burlap was placed on the top of the block after the surface was finished. The burlap was kept wet for one day after casting. The blocks were allowed to cure in the forms for approximately one week before the forms were removed. The blocks and cylinders were stored in the laboratory until testing and no additional curing procedures were used for either the blocks or cylinders.



Figure 2.14 - Placement of Concrete for Shallow-Embedment Tests

Deep-Embedment Tests

Eighteen concrete blocks were constructed for the deep-embedment pullout tests on headed reinforcement. Each concrete block was 920mm (36 in.) deep with 4 to 12 headed reinforcing bars cast around the perimeter. The plan dimensions of the blocks were either 920mm by 920mm (36 in. by 36 in.) or 1220mm by 1220mm (48 in. by 48 in.). The bars were spaced to preclude overlap of anticipated failure surfaces. The blocks were cast in bolted plywood forms.

The forms and bars are shown in Figure 2.15 before placement of concrete. Supports and spacers used to ensure correct placement of the headed bars are shown in Figure 2.16. Wood spacers controlled the amount of cover over the bar and heads. A frame was attached to the forms above the top surface of concrete.



Figure 2.15 - Forms for Deep-Embedment Tests

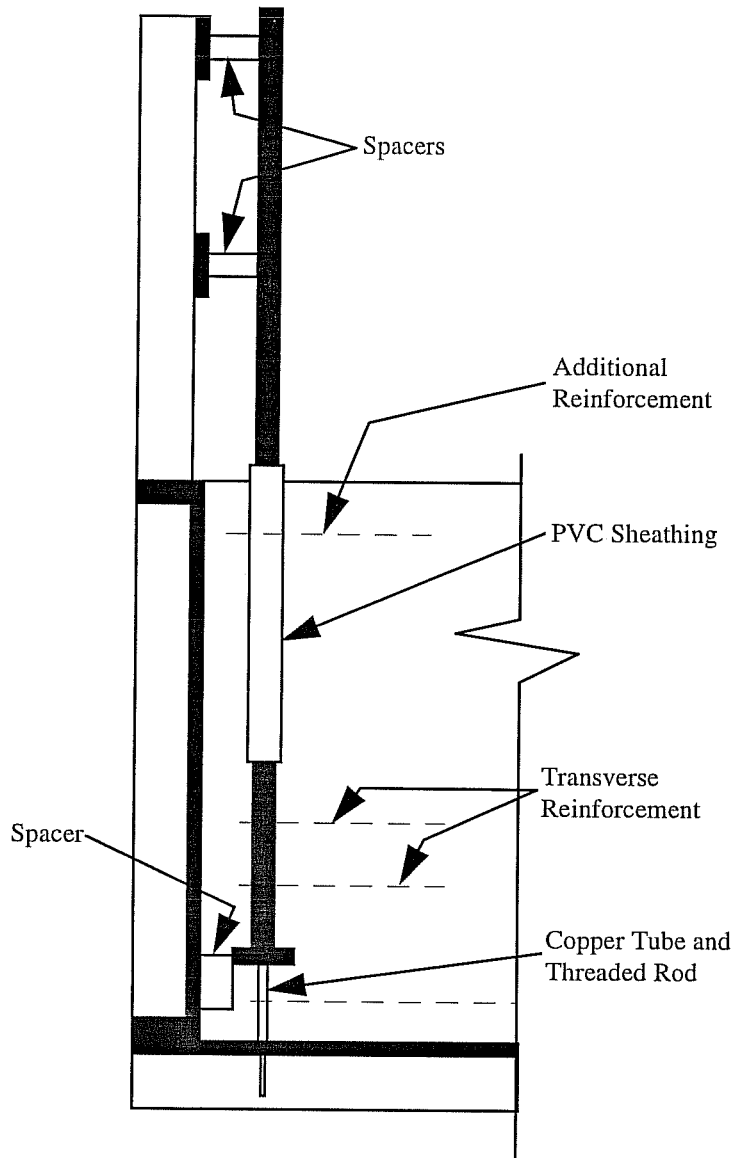


Figure 2.16 - Construction of Deep-Embedment Specimens

Wood spacers were attached to the frame and the bars were tied to the frame to provide the desired clear cover over the bar and to secure the bars during placement of concrete. Likewise, a wood spacer was placed on the interior face of the form at the head of the reinforcing bar to provide the desired cover over the head. The top edge of the head spacer was placed below the bearing surface of the head to avoid altering the bearing and cover at the head. The head was tied to the form against the spacer to insure the correct cover and to secure the bar during casting. The embedment depth of the headed reinforcement was controlled with a length of copper tubing placed under the head, supporting the bar at the proper depth.

After placing the bars in the form, transverse reinforcement, if any, was placed in the anchorage zone. The transverse reinforcement was tied to the bar and secured to prevent movement during casting. Additional reinforcement was placed in the forms below the heads and near the top surface of the block to prevent cracks originating at the head from extending through the block and creating difficulties in moving the block after testing. None of this additional reinforcement was placed near the anchorage zone of the headed bar.

The concrete was placed directly using the chute of the ready-mix concrete truck (Figure 2.17). The concrete was placed in three equal lifts and vibrated with stinger-type vibrators after each lift. Control cylinders were also cast at the same

time as the block. Two or three concrete blocks were cast at one time. After placement of the concrete, the top surface was finished with trowels and lifting anchors were positioned in the concrete. Each block was then allowed to cure for approximately one week before the form was removed. The blocks and cylinders were stored in the laboratory until testing without further curing.

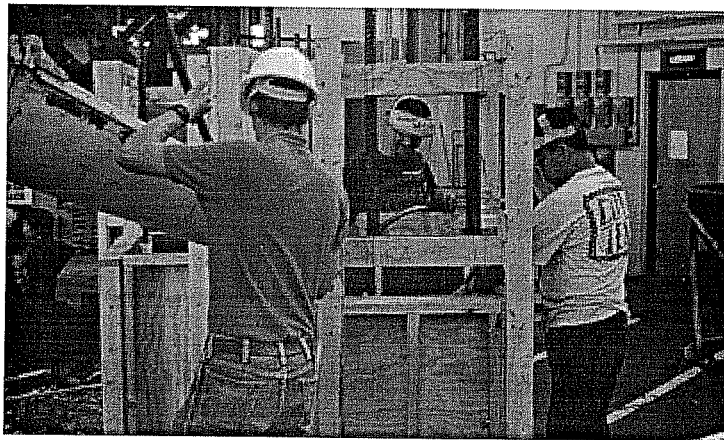


Figure 2.17 - Placement of Concrete for Deep-Embedment Tests

2.5 Materials

Concrete

The concrete was delivered by a local ready-mix company. Standard mix designs were used with nominal strengths between 21 and 69 MPa. The mix designs used for testing are listed in Table 2.1. No admixtures were used and all concrete mixes had 19mm (3/4 in.) maximum aggregate size. All mixes were

	Mix Design				
	UT3000	UT3500	UT4000	UT7000	UT10000
Nominal f'_c (psi)	3000	3500	4000	7000	10000
Max. Aggregate (in)	3/4	3/4	3/4	3/4	3/4
Cement (lb/cyd)	360	370	400	658	714
Fly Ash (lb/cyd)	0	0	0	0	254
Coarse Aggregate (lb/cyd)	1884	1876	1862	1712	1665
Fine Aggregate (lb/cyd)	1435	1432	1422	1280	1371
Water (lb/cyd)	266	266	267	292	290
Nominal f'_c (MPa)	21	24	28	48	69
Max. Aggregate (mm)	19	19	19	19	19

Table 2.1 - Mix Designs for Pullout Tests

ordered with a 102mm (4 in.) slump, though the amount of slump measured at the time of casting varied.

Control cylinders were tested to determine the compressive strength of the concrete. Three cylinders were tested 7, 14, 21 and 28 days after casting to determine the strength of the concrete. In addition, three control cylinders were tested on the day pullout tests were conducted. In Table 2.2, the slump and 28 day strength for three batches of concrete used for the shallow-embedment pullout tests are listed and Figure 2.18 is a plot of concrete strength with time. In Table 2.3, the slump and 28 day strength for the eight batches used for the deep-embedment tests are listed and in Figure 2.19 concrete strength is plotted against time.

Concrete Batch	Test Blocks	Mix Design	Slump (mm)	28 Day f'_c (MPa)	Nominal f'_c (MPa)
CB-2	T1	UT10000	165	79	69
CB-5	T2	UT4000	64	34	28
CB-6	T3	UT4000	102	28	28

Table 2. 2 - Concrete Data for Shallow-Embedment Tests

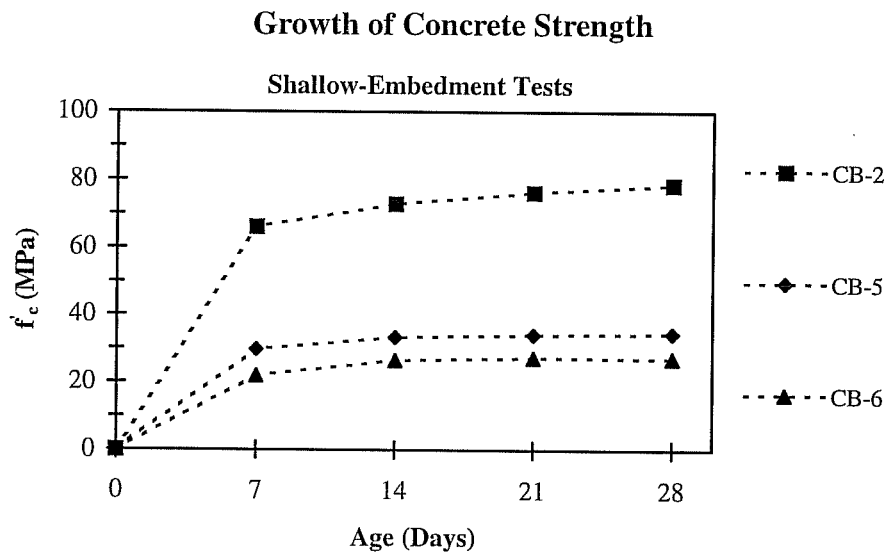


Figure 2.18 - Concrete Strengths for Shallow-Embedment Tests

Concrete Batch	Test Blocks	Mix Design	Slump (mm)	28 Day f'_c (MPa)	Nominal f'_c (MPa)
CB-7	C1, C2	UT4000	76	26	28
CB-8	C3, C4	UT4000	140	28	28
CB-9	C5, C6	UT4000	216	21	28
CB-10	C7, C8	UT4000	178	23	28
CB-11	C9, C10, C11	UT4000	64	27	28
CB-12	C12, C13	UT3500	51	22	24
CB-13	C15, C16, C17	UT3000	127	21	21
CB-14	C18, C19	UT7000	89	48	48

Table 2.3 - Concrete Data for Deep-Embedment Tests

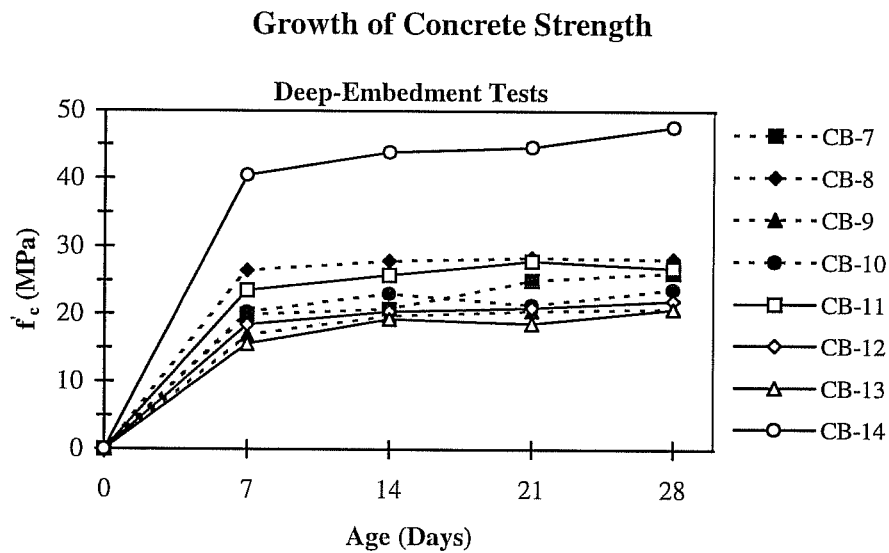


Figure 2.19 - Concrete Strength for Deep-Embedment Tests

Steel

The headed reinforcing steel was supplied by the sponsor. Three bar sizes were used for the headed reinforcement: 20; 25 and 35mm diameter. The majority of the bars had standard head sizes as designated by the manufacturer/sponsor. The standard head sizes are summarized in Table 2.4. In addition to the bars with standard head sizes, some 20mm and 25mm bars had 90x90x20mm and 100x55x25mm heads. The bars with large heads were used to determine the role of head geometry. For some tests the head area was reduced by saw cutting the head and the head thickness was reduced by removing material with a lathe. The head aspect ratio and head shape were also changed for a few tests by sawing the heads. The bars and heads had nominal yield strengths of 500 MPa. The actual yield and ultimate strengths of the bars and heads are listed in Tables 2.5 and 2.6.

Steel used for transverse reinforcement was obtained locally in traditional US sizes, #3, #4 and #6. For consistency, these sizes will be reported using metric equivalents: 10, 12 and 20mm, respectively. Transverse steel had a nominal yield strength of 420 MPa (60 ksi). Actual yield and ultimate strengths of the transverse reinforcement are listed in Table 2.7.

Transverse ties were either manufactured in the laboratory with a manual bending table, or fabricated locally using a hydraulic bending table. The ties were fabricated in accordance with ACI guidelines.

Bar Diameter (mm)	Standard Head Size (mm)	
	Square	Rectangular
20	50x50x12	70x35x16
25	70x70x16	80x40x18
35	90x90x20	100x55x25

Table 2.4 - Standard Head Sizes

Bar Diameter (mm)	Yield Stress (MPa)	Ultimate Stress (MPa)
20	554	679
25	571	709
35	542	686

Table 2.5 - Headed Bar Strengths

Head (mm)	Yield Stress (MPa)	Ultimate Stress (MPa)
50x50x12	516	655
70x35x16	514	669
70x70x16	505	654
80x40x18	515	660
90x90x20	494	631
100x55x25	508	660

Table 2.6 - Head Strengths

Bar Diameter (mm)	Yield Stress (MPa)	Ultimate Stress (MPa)
10	503	721
12	434	709
20	420	682

Table 2.7 - Transverse Reinforcement Strengths

2.6 Testing Procedure

Each bar was tested monotonically in tension until failure. Load was applied to the bar in stages and slowly to prevent any dynamic effects. The number of load stages for each bar depended on the expected capacity of the bar with at least 8 load stages imposed. At each load stage measurements of load, deflection, strain and crack width were taken. Photographs were taken to record cracking and failure. After failure, the loose (spalled) concrete cover was removed and the failure surface was photographed. For some tests, additional loading after failure was required to loosen the failed cover. For several tests with transverse reinforcement, loading was continued past peak load until the transverse reinforcement fractured.

2.7 Equipment and Measurements

The configuration of equipment used in the deep-embedment pullout tests is shown in Figure 2.20. Similar equipment was used for the shallow-embedment tests. Figures 2.21 and 2.22 are photographs of the equipment used for the shallow-embedment and deep-embedment tests respectively. Tensile load was applied to the bars using a center-hole hydraulic ram. Load was measured with an electronic load cell and checked with a pressure gauge. The output from the load cell was monitored and stored with a data acquisition system.

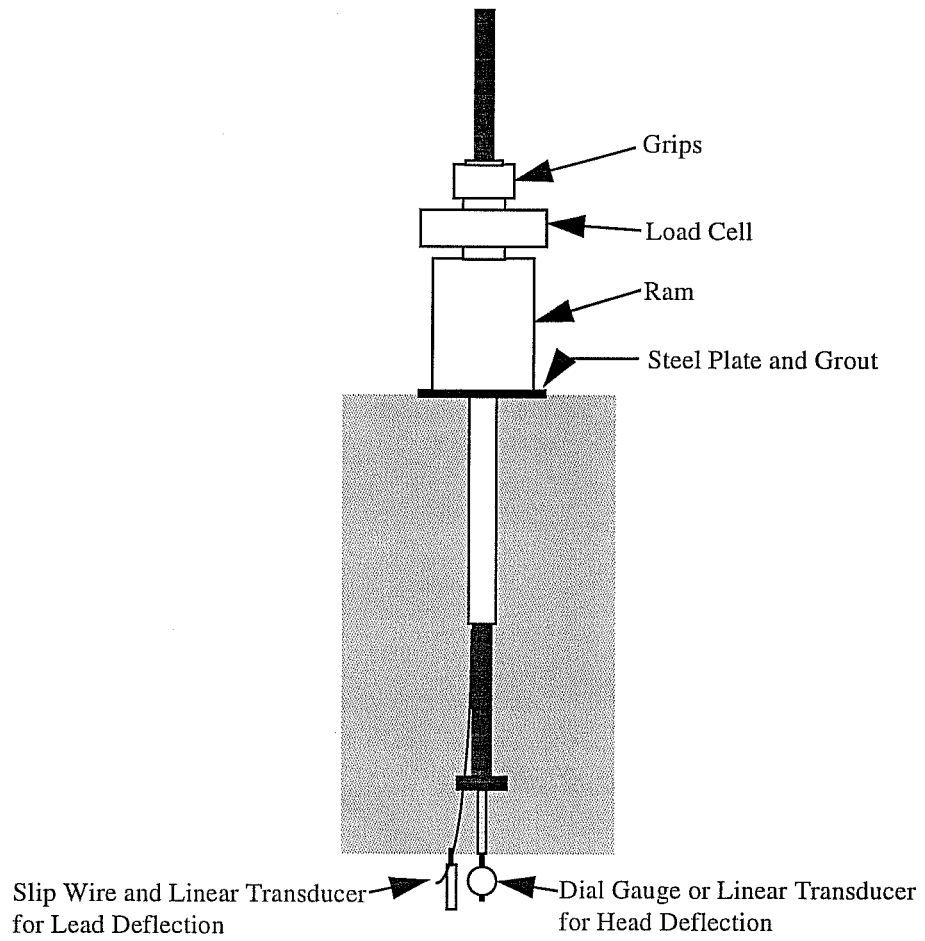


Figure 2.20 - Test Equipment

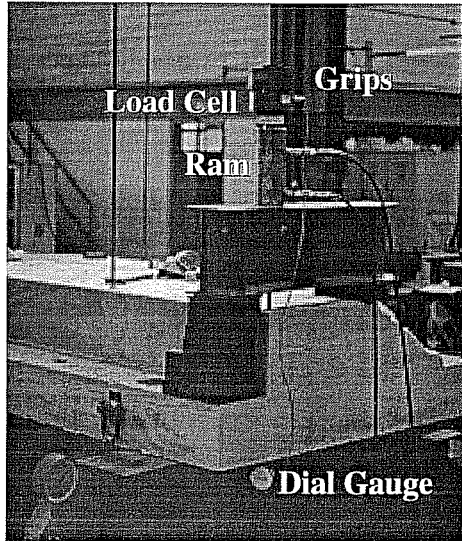


Figure 2.21 - Shallow-Embedment Test Setup and Equipment



Figure 2.22 - Deep-Embedment Test Setup and Equipment

For all tests, deflection of the head was measured. A small hole was drilled into the bottom of the heads and threaded. A piece of threaded rod was screwed into this hole and extended through the bottom of the form. The copper tubing used to support the headed bar at the proper depth also acted as sheathing for the threaded rod and prevented bonding of the rod with the concrete. During testing a dial gauge or linear transducer was attached to the rod and the head deflections were recorded. Dial gauge readings were recorded manually, while linear transducer readings were recorded with the loads by the data acquisition system.

For several deep-embedment tests with additional development length, the deflection at the beginning of the development length was also measured. For these measurements, a small hole was drilled into the bar. A piece of piano wire was pressed into this hole and crimped. The wire then extended through the bottom of the form. The wire was sheathed with flexible plastic tubing to prevent bonding with the concrete. The lead slip deflection measurements were monitored with a linear transducer attached to the wire and recorded using the data acquisition system.

Strains on the bottom surface of the head, along the bar and on transverse reinforcement were recorded with quarter-bridge foil strain gauges. The gauges were attached to the steel with glue and protected with two layers of waterproofing.

When gauges were attached to the bars or transverse reinforcement, some of the bar deformations had to be ground off to provide an adequate contact area on the steel bar. In these cases, care was taken to avoid reducing the net cross-section of the bar. Measurements of strain were recorded with the data acquisition system.

Finally, cracking was observed before failure in several tests. When cracks appeared they were marked on the concrete surface and the width of the cracks measured. The width was measured with a plastic crack comparator card and the measurements recorded manually.

2.8 Test Programs

Twenty-one headed reinforcing bars were tested using the shallow-embedment pullout test. Eight bars were cast in the center of blocks, seven along an edge and six in a corner.

A total of 123 tests were conducted using the deep-embedment setup. Seventy-seven single bars were cast along an edge and 40 single bars were cast in a corner. Six deep-embedment tests were conducted on pairs of closely-spaced edge bars.

Chapter 3

Shallow-Embedment Pullout Tests Effect of Variables on Anchorage

3.1 Overview of Results

The parameters for the 21 shallow-embedment tests are summarized in Table 3.1. The Test ID describes the concrete block number, $T_{_}$, and the test number within each block, $B_{_}$.

Two failure modes were expected in the shallow-embedment tests, pullout-cone failure and bar fracture. Three bar fractures were observed and the remaining 18 tests resulted in pullout-cone failures. Table 3.2 summarizes the results for the 21 shallow-embedment tests. In Table 3.2 P_U is the ultimate capacity of the anchorage and f'_c denotes the concrete strength measured on the day of testing.

Test ID	Bar Position	d_b (mm)	Nominal Head (mm)	C_1 (mm)	C_2 (mm)	h_d (mm)	l_d (mm)	Transverse Reinf.	Nominal f'_c (MPa)
T1B1	Center	20	50x50x12	457	457	36	0	None	69
T1B2	Center	20	70x35x16	457	457	36	0	None	69
T1B3	Center	20	50x50x12	457	457	113	0	None	69
T1B4	Center	20	70x35x16	457	457	113	0	None	69
T1B5	Center	35	90x90x20	457	457	80	0	None	69
T1B6	Center	35	100x55x25	457	457	80	0	None	69
T1B7	Center	35	90x90x20	457	457	209	0	None	69
T1B8	Edge	20	35x70x16	43	457	111	0	None	69
T1B9	Corner	25	70x70x16	84	84	136	0	None	69
T1B10	Edge	35	90x90x20	65	457	183	0	None	69
T2B1	Edge	20	50x50x12	51	457	229	0	None	28
T2B2	Edge	20	50x50x12	51	457	229	229	None	28
T2B3	Edge	20	50x50x12	51	457	229	0	STE-1	28
T2B4	Edge	20	50x50x12	51	457	229	229	STE-1	28
T2B5	Corner	20	50x50x12	51	51	229	0	None	28
T2B6	Corner	20	50x50x12	51	51	229	229	None	28
T2B7	Corner	20	50x50x12	51	51	229	0	STC-1	28
T2B8	Corner	20	50x50x12	51	51	229	229	STC-1	28
T3B4	Edge	20	50x50x12	51	457	229	0	None	28
T3B8	Corner	20	50x50x12	51	51	229	229	None	28
T3B11	Center	20	50x50x12	457	457	229	0	None	28

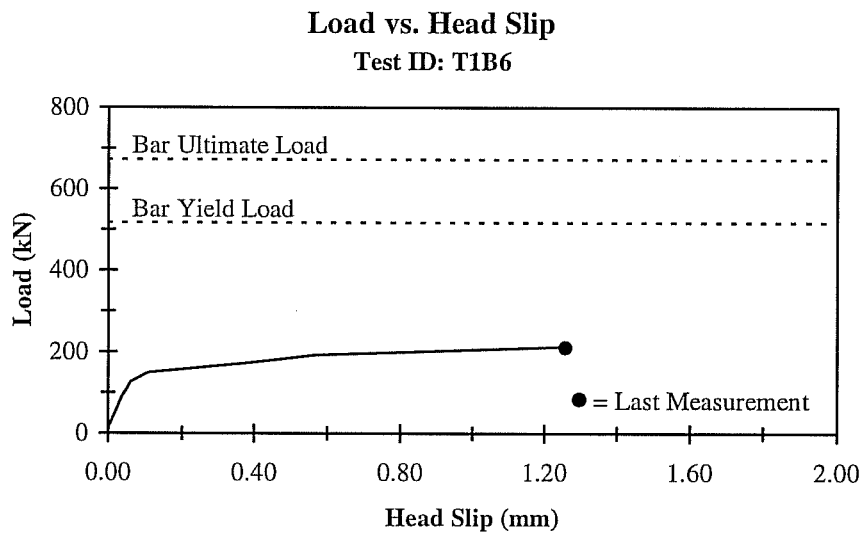
Table 3.1 - Parameters of Shallow-Embedment Tests

Test ID	d_b (mm)	Nominal Head (mm)	C_1 (mm)	C_2 (mm)	h_d (mm)	l_d (mm)	Trans. Reinf.	f'_c (MPa)	P_U (kN)	Failure Mode
T1B1	20	50x50x12	457	457	36	0	None	83	77	Pullout
T1B2	20	70x35x16	457	457	36	0	None	83	62	Pullout
T1B3	20	50x50x12	457	457	113	0	None	83	205	Bar Fracture
T1B4	20	70x35x16	457	457	113	0	None	83	208	Bar Fracture
T1B5	35	90x90x20	457	457	80	0	None	83	215	Pullout
T1B6	35	100x55x25	457	457	80	0	None	83	225	Pullout
T1B7	35	90x90x20	457	457	209	0	None	83	490	Pullout
T1B8	20	35x70x16	43	457	111	0	None	83	57	Pullout
T1B9	25	70x70x16	84	84	136	0	None	83	56	Pullout
T1B10	35	90x90x20	65	457	183	0	None	83	126	Pullout
T2B1	20	50x50x12	51	457	229	0	None	33	184	Pullout
T2B2	20	50x50x12	51	457	229	229	None	33	148	Pullout
T2B3	20	50x50x12	51	457	229	0	STE-1	33	160	Pullout
T2B4	20	50x50x12	51	457	229	229	STE-1	33	172	Pullout
T2B5	20	50x50x12	51	51	229	0	None	33	88	Pullout
T2B6	20	50x50x12	51	51	229	229	None	33	122	Pullout
T2B7	20	50x50x12	51	51	229	0	STC-1	33	89	Pullout
T2B8	20	50x50x12	51	51	229	229	STC-1	33	125	Pullout
T3B4	20	50x50x12	51	457	229	0	None	27	149	Pullout
T3B8	20	50x50x12	51	51	229	0	None	27	57	Pullout
T3B11	20	50x50x12	457	457	229	0	None	27	212	Bar Fracture

Table 3.2 - Results of Shallow-Embedment Tests

3.2 General Behavior under Load

A typical load-slip response of a headed bar with shallow-embedment and no yielding in the bar is shown in Figure 3.1. Slip is measured at the head. In general, the deflection at the head increases as the load increases. The relationship



Test ID	d_b (mm)	Nominal Head (mm)	C_1 (mm)	C_2 (mm)	h_d (mm)	l_d (mm)	Trans. Reinf.	f'_c (MPa)	P_U (kN)	Failure Mode
T1B6	35	100x55x25	457	457	80	0	None	83	225	Pullout

Figure 3.1 - Deflection of Headed Reinforcing Bar with Shallow Embedment

between load and slip is approximately linear at lower loads. As the load approaches the ultimate capacity of the anchorage, the slip increases and the load-slip curve begins to flatten out with large increases in deflection with little increase in load. This general shape for the load-slip curve was observed for all tests, though the ultimate capacities and slips differed. The pullout-cone failure was

sudden and the load carried by the anchorage dropped to zero after failure. No cracking was observed before failure.

The size of the pullout cone varied from test to test and depended upon placement of the bar, edge distance and head size. A typical pullout cone for an edge bar test without transverse reinforcement is shown in Figure 3.2. The failure surface was very large. The length of the failure measured parallel with the edge was approximately 1800mm (6 ft. 0 in.) long. It is unlikely that a failure surface this large would occur in actual concrete members.

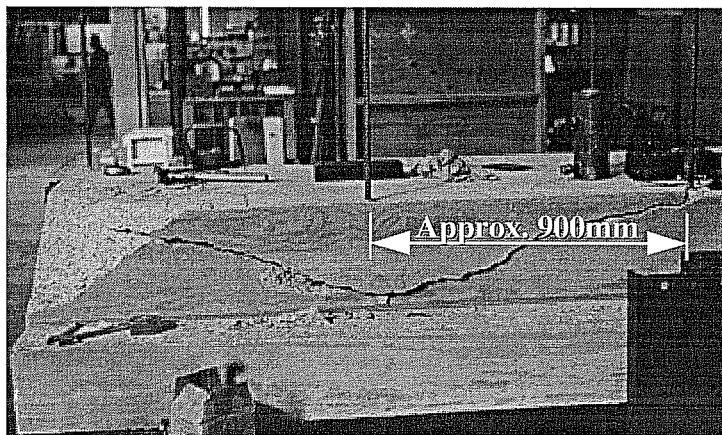
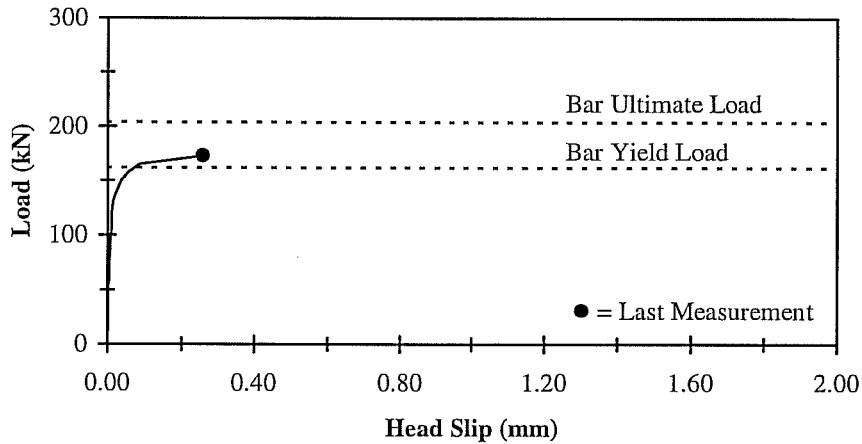


Figure 3.2 - Pullout-Cone Failure of Headed Bar with Shallow Embedment

In several tests, the bar yielded, went through the yield plateau and reached strain hardening. A typical load-slip diagram for a test reaching the yield load is shown in Figure 3.3. There was no change in the general displacement or cracking behavior for the tests that reached strain hardening. Based on these observations,

Load vs. Head Slip

Test ID: T2B4



Test ID	d_b (mm)	Nominal Head (mm)	C_1 (mm)	C_2 (mm)	h_d (mm)	l_d (mm)	Trans. Reinf.	f'_c (MPa)	P_U (kN)	Failure Mode
T2B4	20	50x50x12	51	457	229	229	STE-1	33	172	Pullout

Figure 3.3 - Deflection of Headed Bar with Shallow Embedment and Bar Yielding

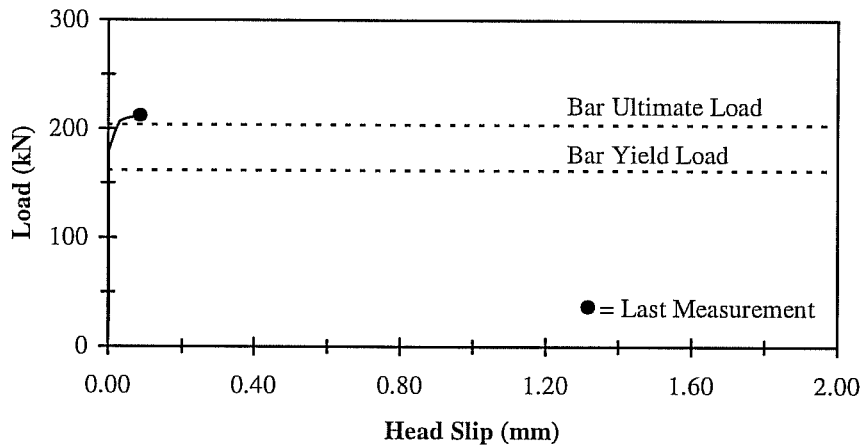
yielding of the bar had no impact on the ultimate capacity or behavior of the anchorage.

The test shown in Figure 3.1 appears to have a higher ultimate slip than the test shown in Figure 3.3. However, during testing the device measuring the slip was removed before failure and it is possible that the ultimate slip was not recorded. The last slip reading is denoted on the figures.

In Figure 3.4, the load-slip diagram for one of the three tests resulting in bar fracture is shown. The general shape of the load-slip curve was not affected by bar fracture.

Load vs. Head Slip

Test ID: T3B11



Test ID	d_b (mm)	Nominal Head (mm)	C_1 (mm)	C_2 (mm)	h_d (mm)	l_d (mm)	Trans. Reinf.	f'_c (MPa)	P_U (kN)	Failure Mode
T3B11	20	50x50x12	457	457	229	0	None	27	212	Bar Fracture

Figure 3.4 - Deflection of Headed Bar with Shallow Embedment and Bar Fracture

3.3 Transverse Reinforcement

It is probable that in most applications of headed reinforcement in concrete members transverse reinforcement will be present near the head. To test the effect of transverse reinforcement on headed reinforcement with shallow embedments a series of tests was conducted with transverse reinforcement along the embedment depth.

A likely type of transverse reinforcement in concrete members using headed reinforcement with shallow embedments as the longitudinal reinforcement is column bars in beam-column joints. In Figure 3.5, a typical detail for a beam-column joint and how this was modeled in the test setup is shown. Two types of transverse reinforcement were tested, one type for edge bars and one type for corner bars. The types are very similar to each other. The two types of transverse reinforcement tested are shown in Figure 3.6. The number of legs which provide

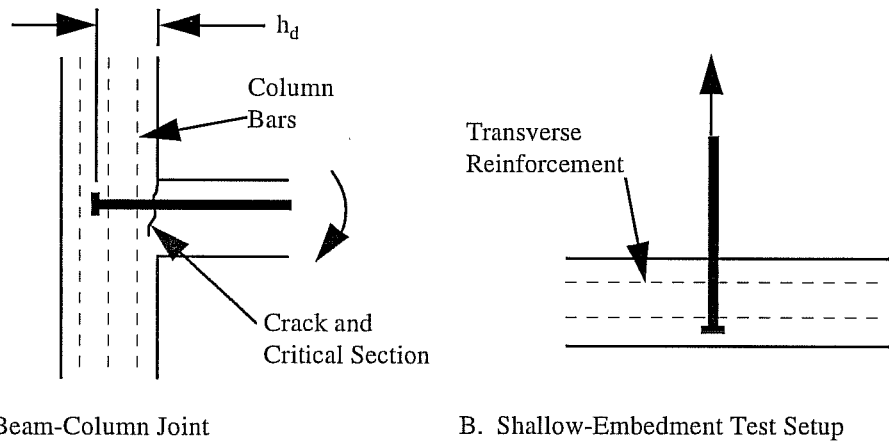


Figure 3.5 - Model of Transverse Reinforcement for Shallow-Embedment Tests

tensile resistance across the assumed failure plane are included in the figure. The total area of transverse reinforcement along the development length, A_{tr} , is calculated by multiplying the cross-sectional area of the tie bar by the number of legs crossing the failure surface and providing tensile resistance and the number of ties. Based on the assumed surface of the pullout cone, A_{tr} for all tests is zero and the transverse reinforcement should have no effect on the behavior. A total of

eight bars arranged in four pairs (four edge bars and four corner bars) were tested. The parameters and results for these tests are summarized in Table 3.3. The results from the four pairs of tests are compared in Figure 3.7. As expected, the arrangement of transverse reinforcement tested had no affect on the ultimate capacity of the anchorage. The largest differences in measured capacities for the four pairs was 14%, which is within normal experimental scatter for concrete tests. Based on the results of these tests, for transverse reinforcement to increase the capacity of a pullout-cone failure, it should be placed with a component parallel to the bar so that the transverse reinforcement will be mobilized by the pullout-cone failure.

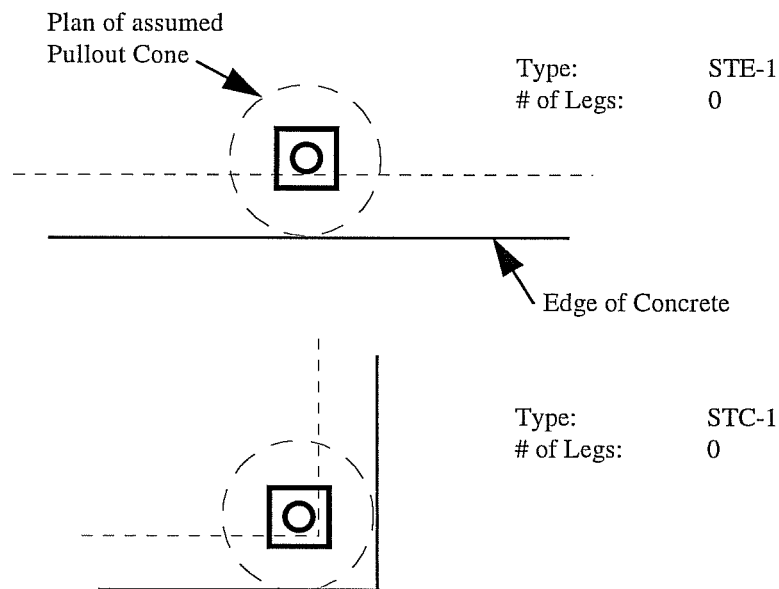


Figure 3.6 - Configurations of Transverse Reinforcement for Shallow-Embedment Tests

Test ID	d_b (mm)	Nominal Head (mm)	C_1 (mm)	C_2 (mm)	h_d (mm)	l_d (mm)	Trans. Reinf.	A_{tr} (mm ²)	f'_c (MPa)	P_U (kN)
T2B1	20	50x50x12	51	457	229	0	None	0	33	184
T2B3	20	50x50x12	51	457	229	0	STE-1	0	33	160
T2B2	20	50x50x12	51	457	229	229	None	0	33	148
T2B4	20	50x50x12	51	457	229	229	STE-1	0	33	172
T2B5	20	50x50x12	51	51	229	0	None	0	33	88
T2B7	20	50x50x12	51	51	229	0	STC-1	0	33	89
T2B6	20	50x50x12	51	51	229	229	None	0	33	122
T2B8	20	50x50x12	51	51	229	229	STC-1	0	33	125

Table 3.3 - Parameters and Results of Shallow-Embedment Tests for Transverse Reinforcement

Transverse Reinforcement

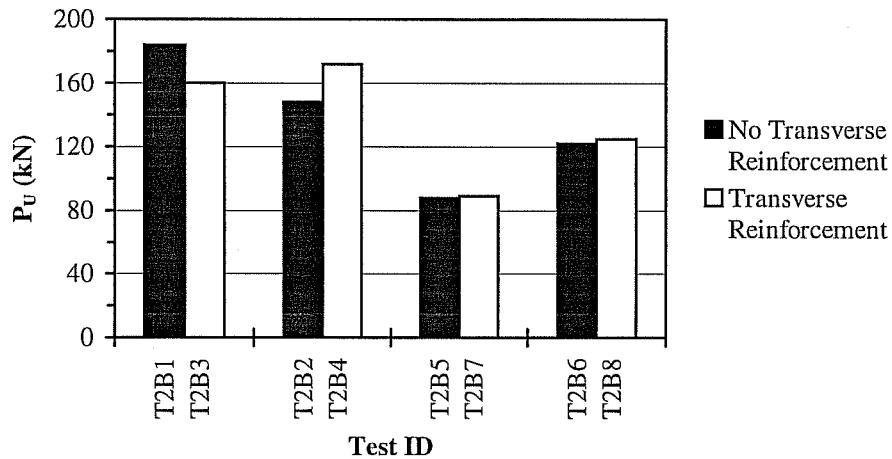
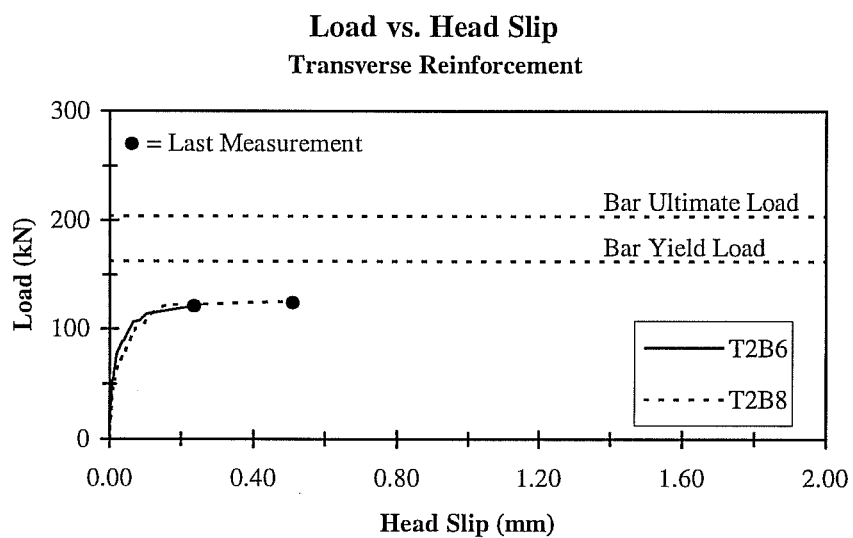


Figure 3.7 - Comparison of Capacities for Tests on Transverse Reinforcement

The head deflections of two tests with the only difference being the presence of transverse reinforcement are compared in Figure 3.8. Transverse reinforcement normal to the bar axis had no effect on the deflection behavior of the anchorage.



Test ID	d_b (mm)	Nominal Head (mm)	C_1 (mm)	C_2 (mm)	h_d (mm)	l_d (mm)	Trans. Reinf.	f'_c (MPa)	P_U (kN)	Failure Mode
T2B6	20	50x50x12	51	51	229	229	None	33	122	Pullout
T2B8	20	50x50x12	51	51	229	229	STC-1	33	125	Pullout

Figure 3.8 - Deflections of Headed Bars with and without Transverse Reinforcement

3.4 Development Length

The eight tests listed in Table 3.3 can be rearranged into four pairs with the only variable between tests in each pair being the development length. A summary of the parameters and results for these four pairs of tests is listed in Table 3.4. The measured capacities from the tests are compared in Figure 3.9. For three of the four pairs there was an increase in strength with increased development length.

Section 12.2.3 of the ACI 318-95 Building Code [1] uses the following equation to calculate the straight bar development length needed to reach the yield capacity of the bar, in customary US units:

$$\frac{l_d}{d_b} = \frac{3}{40} \frac{f_y}{\sqrt{f'_c}} \frac{\alpha\beta\gamma\lambda}{\left(\frac{c + K_{tr}}{d_b} \right)} \quad \text{eq. 3.1}$$

where l_d is the development length, d_b is the bar diameter, f_y is the yield stress of the bar, f'_c is the concrete strength, c is the minimum clear cover over the bar, and K_{tr} is a measure of the amount of transverse reinforcement. K_{tr} is taken as zero for the shallow-embedment pullout tests. The values of α , β , γ and λ are factors for casting position of bar, bar coatings, bar size and light-weight aggregate. For the shallow-embedment tests all four factors equal 1. Assuming a linear relationship for bond stress for development lengths less than calculated by

Test ID	d_b (mm)	Nominal Head (mm)	C_1 (mm)	C_2 (mm)	h_d (mm)	l_d (mm)	Trans. Reinf.	f'_c (MPa)	P_U (kN)
T2B1	20	50x50x12	51	457	229	0	None	33	184
T2B2	20	50x50x12	51	457	229	229	None	33	148
T2B3	20	50x50x12	51	457	229	0	STE-1	33	160
T2B4	20	50x50x12	51	457	229	229	STE-1	33	172
T2B5	20	50x50x12	51	51	229	0	None	33	88
T2B6	20	50x50x12	51	51	229	229	None	33	122
T2B7	20	50x50x12	51	51	229	0	STC-1	33	89
T2B8	20	50x50x12	51	51	229	229	STC-1	33	125

Table 3.4 - Parameters and Results of Shallow-Embedment Tests on Development Length

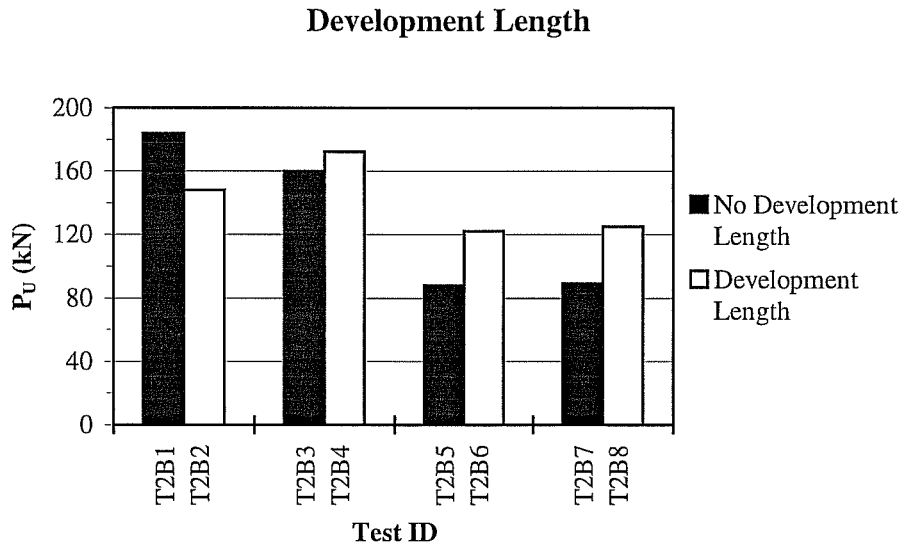


Figure 3.9 - Comparison of Capacities of Shallow-Embedment Tests on Development Length

Equation 3.1 and rearranging Equation 3.1 leads to an equation for the development force for a given development length:

$$F_{ld} = \frac{l_d}{l_{dACI}} F_y \quad \text{eq. 3.2}$$

where F_{ld} is the development force, l_d the actual development length, l_{dACI} the development length from Equation 3.1 and F_y the yield force of the bar. For each pair of tests listed in Table 3.4, the increase in capacity due to development length can be predicted using Equation 3.2:

$$P_{UPIld} = P_{U1} + (F_{ld2} - F_{ld1}) \quad \text{eq. 3.3}$$

where P_{UPIld} is the predicted capacity based on the measured capacity of the test with the least development length, P_{U1} , and the difference between the two predicted development forces from Equation 3.2 for both tests, F_{ld1} and F_{ld2} .

The measured capacities, the predicted development forces from Equation 3.2 and the predicted capacity from Equation 3.3 for the eight tests are listed and compared in Table 3.5. Equation 3.3, based on the current ACI code equation for development length, leads to an increase in capacity due to development length for the edge bars which is greater than observed, thus unconservative. The increase in capacity for corner bars is more accurately predicted by Equation 3.3.

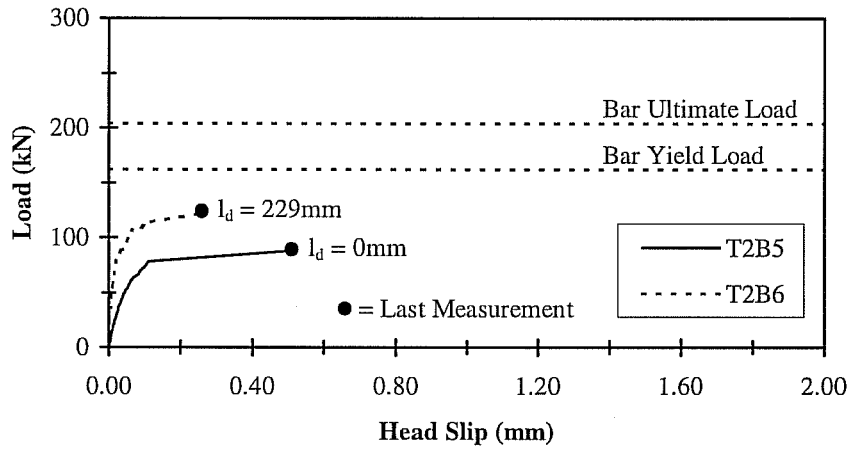
The head deflections for two tests in which the amount of development length was varied are compared in Figure 3.10. Development length did not change the general shape of the deflection curve. A decrease in deflection at low loads was noted with an increase in development length.

	Test ID 1	P_{U1} (kN)	F_{ld1} (kN)	Test ID 2	P_{U2} (kN)	F_{ld2} (kN)	$P_{U2}-P_{U1}$ (kN)	$F_{ld2}-F_{ld1}$ (kN)	$P_{UPI d}$ (kN)	$P_{U2}/P_{UPI d}$
Edge	T2B1	184	0	T2B2	148	37	-36	37	221	0.67
	T2B3	160	0	T2B4	172	37	12	37	197	0.87
Corner	T2B5	88	0	T2B6	122	37	34	37	125	0.97
	T2B7	89	0	T2B8	125	37	36	37	126	0.99

Maximum 0.99
 Minimum 0.67
 Average 0.88
 Standard Deviation 0.15

Table 3.5 - Prediction of Effect of Development Length on Capacity

Load vs. Head Slip
Development Length



Test ID	d_b (mm)	Nominal Head (mm)	C_1 (mm)	C_2 (mm)	h_d (mm)	l_d (mm)	Trans. Reinf.	f'_c (MPa)	P_U (kN)	Failure Mode
T2B5	20	50x50x12	51	51	229	0	None	33	88	Pullout
T2B6	20	50x50x12	51	51	229	229	None	33	122	Pullout

Figure 3.10 - Comparison of Deflection of Headed Bars with and without Development Length

3.5 Concrete Strength

In Table 3.6, the parameters and results of two pairs of tests are listed. The concrete strength is the only variable between tests in each pair. The capacities of these tests are compared in Figure 3.11. The effect of concrete strength on the anchorage capacity of headed reinforcement with shallow-embedments is difficult to quantify due to the low number of tests and the small difference in concrete strength. However, based on these limited results it appears that an increase in concrete strength increased the pullout-cone capacity of headed reinforcement.

The deflections at the head are compared in Figure 3.12 for two tests with different concrete strength. The concrete strength did not affect the deflections over the limited range of comparable load measurements for the two tests.

Test ID	d_b (mm)	Nominal Head (mm)	C_1 (mm)	C_2 (mm)	h_d (mm)	l_d (mm)	Trans. Reinf.	f_c (MPa)	P_U (kN)	Failure Mode
T2B1	20	50x50x12	51	457	229	0	None	33	184	Pullout
T3B4	20	50x50x12	51	457	229	0	None	27	149	Pullout
T2B5	20	50x50x12	51	51	229	0	None	33	88	Pullout
T3B8	20	50x50x12	51	51	229	0	None	27	57	Pullout

Table 3.6 - Parameters and Results for Shallow-Embedment Tests on Concrete Strength

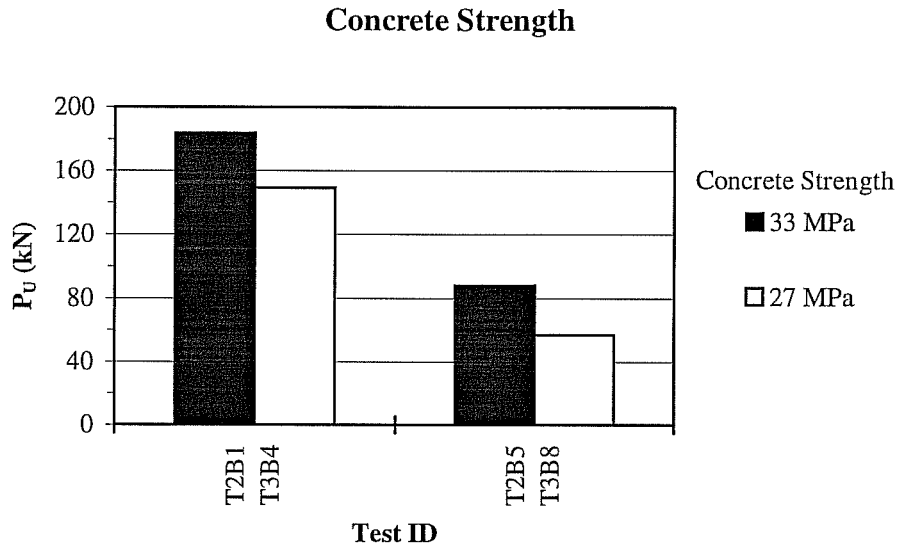
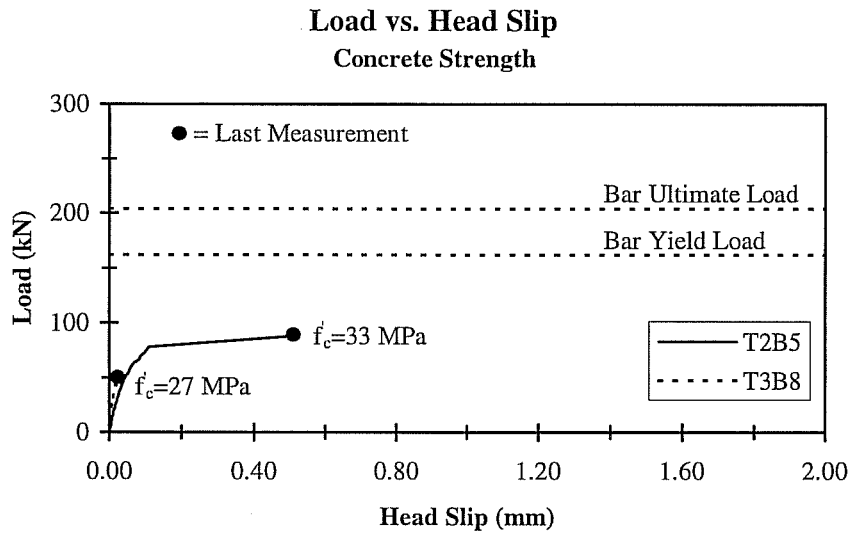


Figure 3.11 - Comparison of Capacities of Shallow-Embedment Tests on Concrete Strength



Test ID	d_b (mm)	Nominal Head (mm)	C_1 (mm)	C_2 (mm)	h_d (mm)	l_d (mm)	Trans. Reinf.	f'_c (MPa)	P_U (kN)	Failure Mode
T2B5	20	50x50x12	51	51	229	0	None	33	88	Pullout
T3B8	20	50x50x12	51	51	229	0	None	27	57	Pullout

Figure 3.12 - Deflection of Headed Bars with Different Concrete Strengths

3.6 Head Area and Aspect Ratio

The parameters and results for two tests with different head area and head aspect ratio are listed in Table 3.7. Based on these limited results, the head area or aspect ratio did not affect the capacity of headed reinforcement with a shallow embedment.

The deflections at the head for these two tests are compared in Figure 3.13. The deflection curves of the two tests were nearly identical before the final

measurements of the tests. The head area and head aspect ratio did not affect deflections.

3.7 Edge Distance

The edge distances varied from 51mm to 457mm. The parameters and results for three tests which were identical except for the edge distances are listed

Test ID	d_b (mm)	Nominal Head (mm)	A_h (mm ²)	Aspect Ratio	C_1 (mm)	C_2 (mm)	h_d (mm)	l_d (mm)	f'_c (MPa)	P_U (kN)	Failure Mode
T1B5	35	90x90x20	8100	1:1	457	457	80	0	83	215	Pullout
T1B6	35	100x55x25	5500	1.8:1	457	457	80	0	83	225	Pullout

Table 3.7 - Parameters and Results of Shallow-Embedment Tests on Head Area and Aspect Ratio

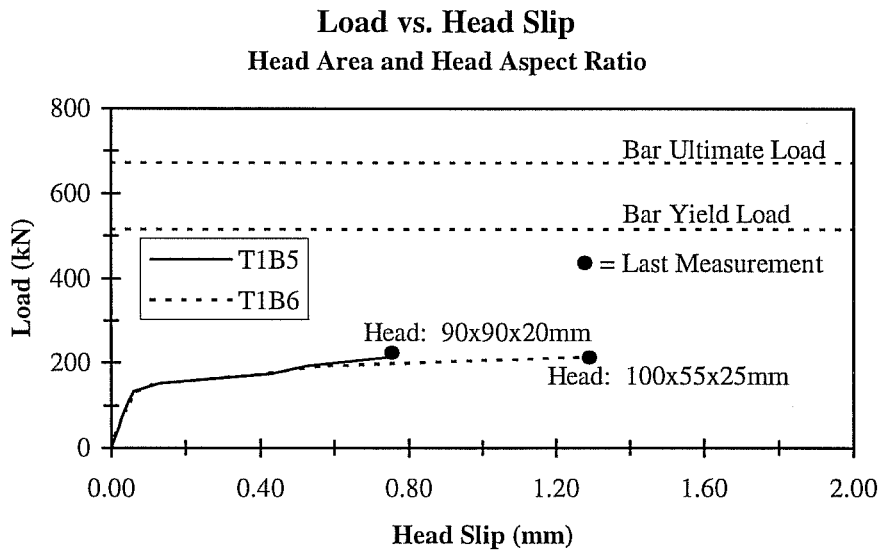


Figure 3.13 - Comparison of Deflections of Tests with Different Heads

in Table 3.8. In general, increasing the edge distance increased the capacity of the anchorage. Bars placed in corners had the weakest anchorages while bars placed far away from edges had the strongest anchorages.

The deflections at the head for these three tests are compared in Figure 3.14. A decrease in deflection at lower loads was observed with increase in edge distances.

Test ID	d_b (mm)	Nominal Head (mm)	C_1 (mm)	C_2 (mm)	h_d (mm)	l_d (mm)	Trans. Reinf.	f_c (MPa)	P_U (kN)	Failure Mode
T2B5	20	50x50x12	51	51	229	0	None	33	88	Pullout
T2B1	20	50x50x12	51	457	229	0	None	33	184	Pullout
T3B11	20	50x50x12	457	457	229	0	None	27	212	Bar Fracture

Table 3.8 - Parameters and Results of Shallow-Embedment Tests Comparing Edge Distance

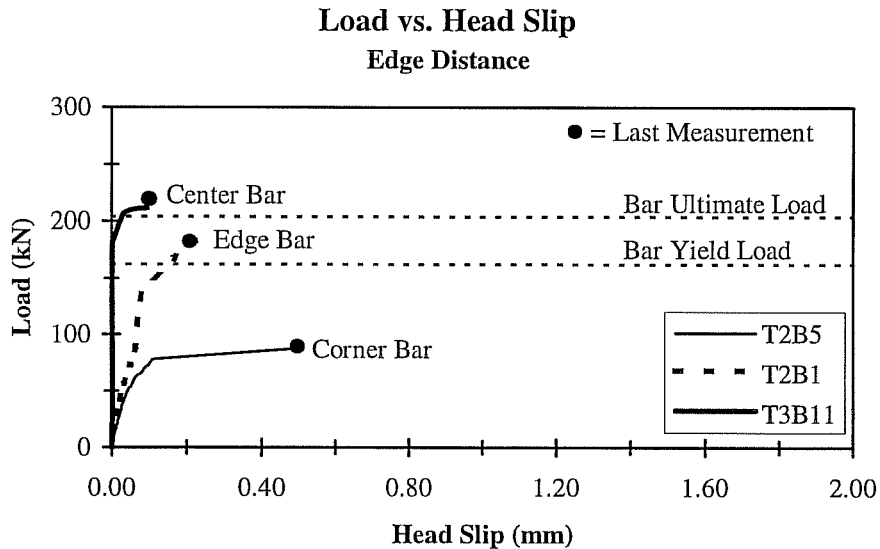


Figure 3.14 - Deflections of Headed Bars with Different Edge Distances

3.8 Embedment Depth

The measured capacities of the 21 shallow-embedment tests are plotted against embedment depth in Figure 3.15. There is a trend of increased capacity with increased embedment depth for each type of bar placement. The embedment depth defines the size of the pullout cone and the extent of the failure surface. Increasing the embedment depth should enlarge the failure surface and therefore the capacity.

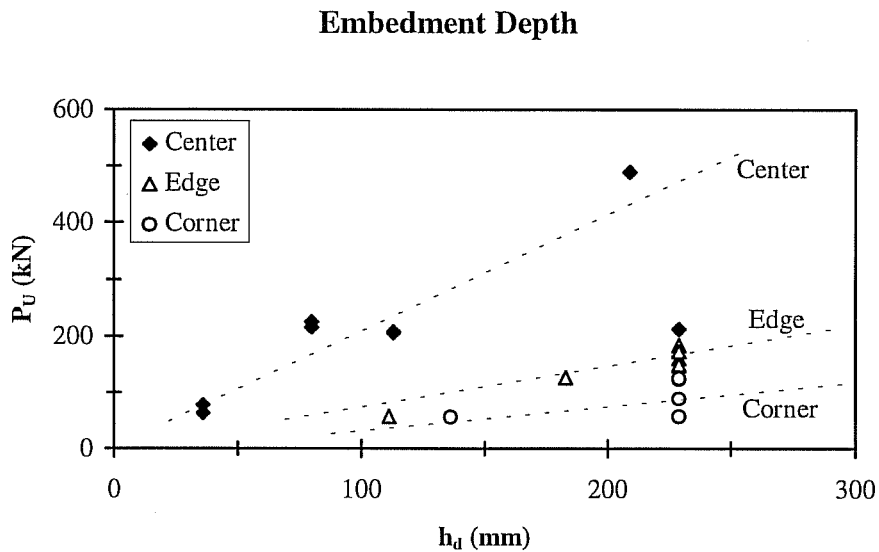
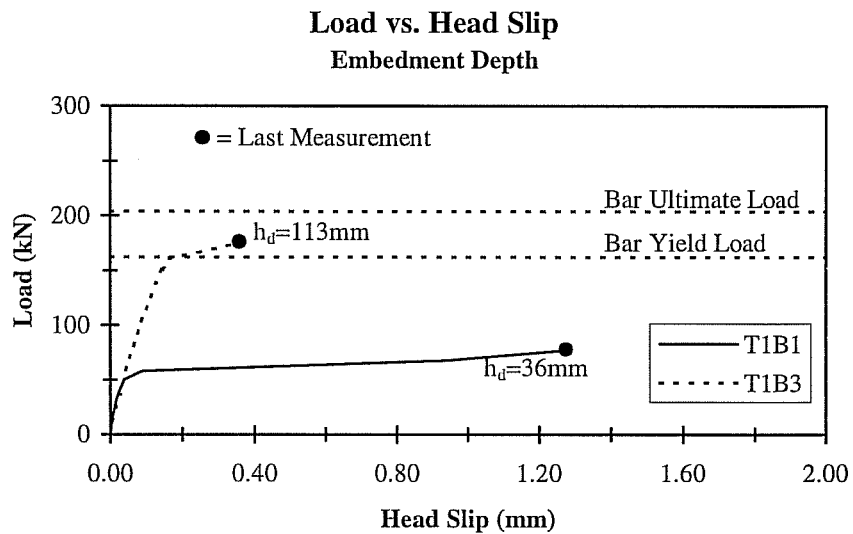


Figure 3.15 - Comparison of Capacities versus Embedment Depth

The deflections at the head for two identical tests with different embedment depths are compared in Figure 3.16. As with development length, the general shape of the deflection curve was not affected by the embedment depth. Unlike development length, there was no decrease in deflections at lower loads with increased embedment depth.



Test ID	d_b (mm)	Nominal Head (mm)	C_1 (mm)	C_2 (mm)	h_d (mm)	l_d (mm)	Trans. Reinf.	f'_c (MPa)	P_U (kN)	Failure Mode
T1B1	20	50x50x12	457	457	36	0	None	83	77	Pullout
T1B3	20	50x50x12	457	457	113	0	None	83	205	Bar Fracture

Figure 3.16 - Comparison of Deflections of Headed Bars with Different Embedment Depths

3.9 Summary

Based on results of 21 pullout tests on headed reinforcement with shallow embedments: embedment depth, bar position and concrete strength were the primary factors affecting the anchorage capacity of headed reinforcement with shallow embedments. Development length generally increased the anchorage capacity. The amount of increase could roughly be predicted using current code provisions for straight bar anchorages. Based on limited data, the amount of head area or head aspect ratio did not increase the capacity. Also the arrangement of transverse reinforcement tested did not affect the ultimate strength.

Chapter 4

Shallow-Embedment Pullout Tests Comparison with Concrete Capacity Design Method

4.1 Introduction

After reviewing the results of the 21 shallow-embedment pullout tests, the primary variables affecting the pullout-cone capacity of headed reinforcement were identified as embedment depth, concrete strength and edge distance. The Concrete Capacity Design method (CCD) is a comprehensive method for predicting the pullout-cone capacity of anchor bolts and headed studs. The CCD method is a rational and transparent approach for design and is the basis for the proposed Chapter 23 governing anchorage to concrete in the ACI 318 Code. In this chapter, the CCD method will be outlined and the results from the shallow-embedment tests will be compared with the capacities predicted by the CCD method. Adjustments to the CCD method for headed reinforcement will be proposed.

4.2 Concrete Capacity Design Method

The Concrete Capacity Design [17] method is based on a physical model in which the driving force is the tension on the bolt and the tension is resisted by an assumed distribution of stress in the concrete over a failure area. At ultimate load, the tension on the bolt is equal to the resisting capacity.

The assumed failure surface is a pyramid with its point at the head of the anchor, a square base and a height equal to the embedment depth (Figure 4.1). The concrete resists the load with a uniform distribution of tensile stress over the area of the pyramid base. The tensile capacity of the concrete is assumed to be a function of the square root of the compressive strength. The base area of the failure pyramid increases with the square of the embedment depth. However, it has been found that due to size effects from fracture mechanics theory, the resistance capacity of the concrete does not increase with the square of the embedment depth. The CCD pullout capacity of a single anchor bolt or headed stud unaffected by close spacing or edge influences is:

$$P_{UO} = 0.0155h_d^{1.5} \sqrt{f'_c} \quad \text{eq. 4.1}$$

where P_{UO} is the ultimate capacity in kN, f'_c is the compressive strength of concrete in MPa and h_d is the embedment depth in mm. The coefficient 15.5 represents a collection of constants and calibration factors. Equation 4.1 is the

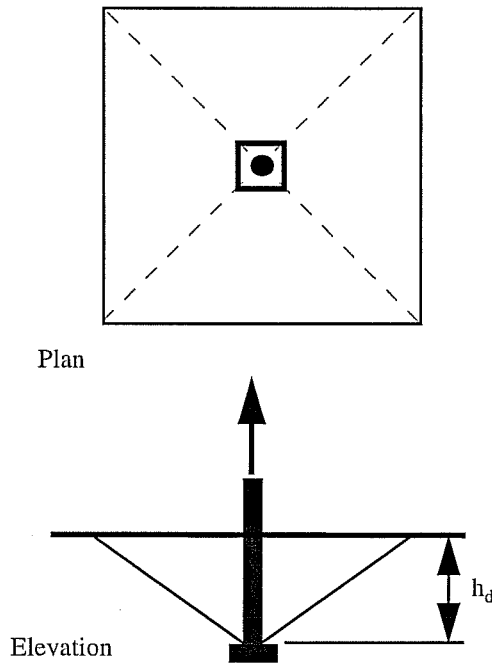


Figure 4.1 - CCD Pullout Cone

best-fit characteristic equation for the characteristic application of an anchor bolt: a single anchor not influenced by edges or adjacent anchors.

When an anchor bolt is placed near an edge or corner, the available failure area is less than assumed for Equation 4.1 and the resistance is reduced. The assumed size of the failure pyramid for an anchor away from an edge is a square measuring $3h_d$ on each side and the area is $9h_d^2$ (Figure 4.2). To take into account the reduced failure area, P_{UO} is multiplied by a ratio of the available area and the assumed area for a single anchor away from an edge:

$$P_U = \frac{A_N}{A_{NO}} P_{UO} \quad \text{eq. 4.2}$$

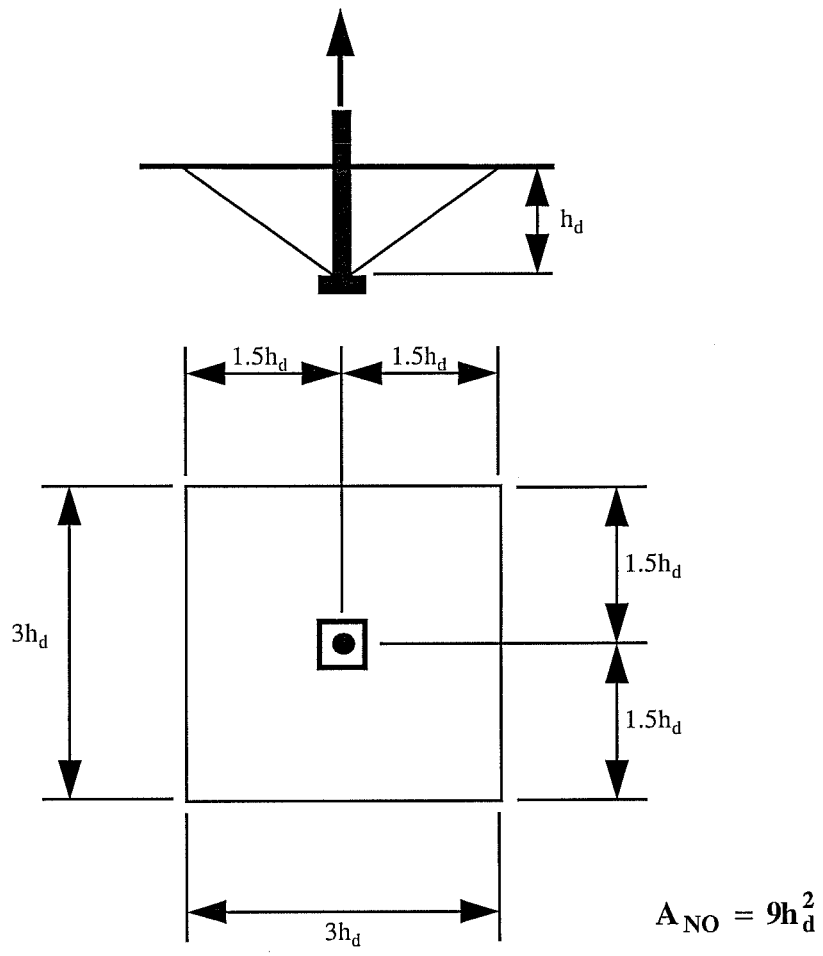
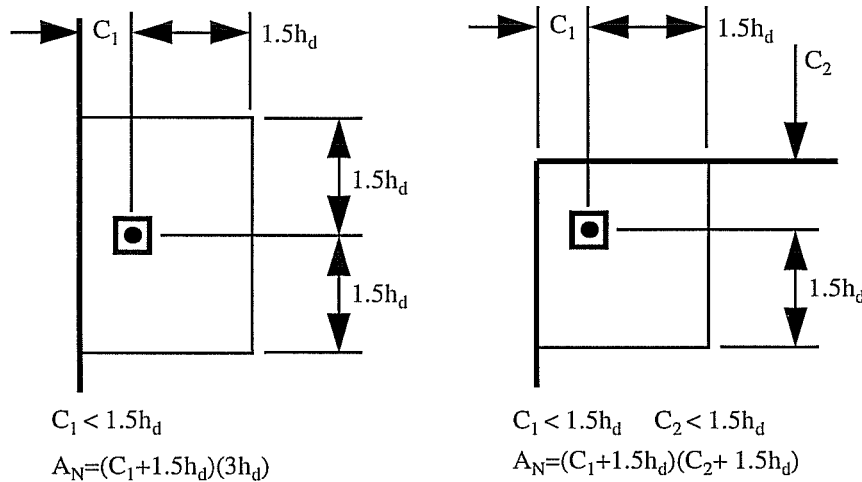


Figure 4.2 - CCD Failure Area

where A_N is the available area and A_{NO} equals $9h_d^2$. Failure areas, A_N , for typical edge placements are shown in Figure 4.3.

For groups of closely spaced anchor bolts the failure surfaces overlap and the capacity of the group is less than the combined capacity of an equal number of single anchors. The available failure area, A_N , is shown for several typical groups in Figure 4.4. Note that for a group it is possible for A_N to be greater than A_{NO} . However, A_N cannot be greater than A_{NO} times the number of anchors in the group. In other words the ratio of A_N to A_{NO} can be greater than one but not greater than the number of anchors in the group being considered. Equation 4.2 treats the group as one large anchor and will provide the capacity of the group as a whole. To find the ultimate load that could be placed on one anchor in a group,



A. Edge Placement

Figure 4.3 - CCD Failure Area for Edge Placements

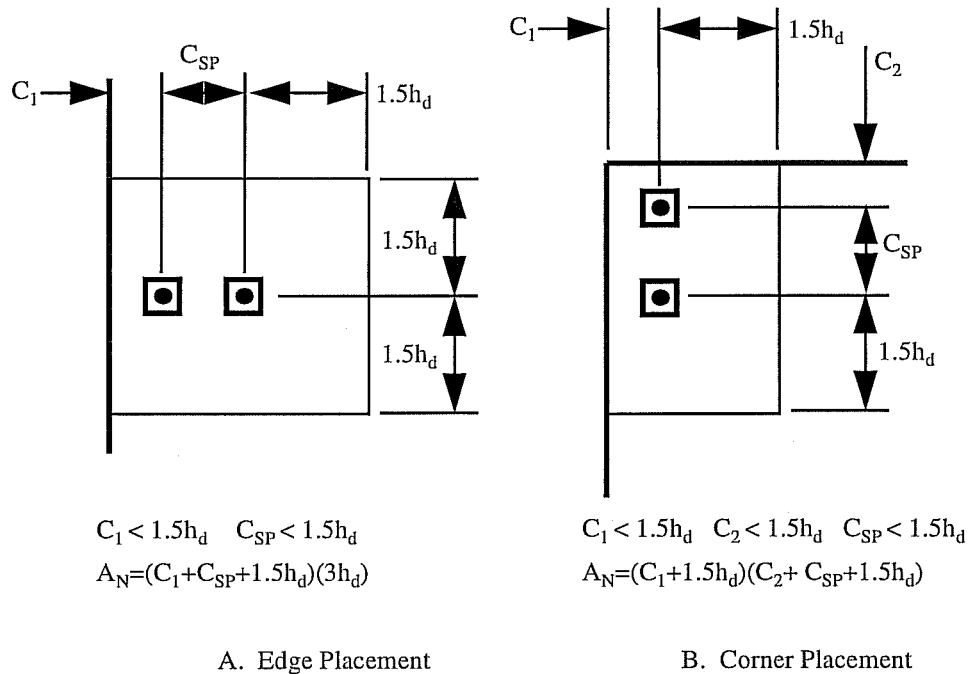


Figure 4.4 - CCD Failure Area for Groups

assuming that all anchors in the group are loaded equally, the capacity from Equation 4.2 is divided by the number of anchors in the group. One of the advantages of the CCD method over previous design methods for anchor bolts is the simplicity of calculating the failure area for anchors near an edge or for groups of anchors.

In addition to the reduction in capacity due to the decrease in failure area for edge placement or close spacing, the capacity is further reduced due to disturbances in the symmetrical state of stress which exists in the characteristic application of an anchor away from edges. To take this reduction into account the characteristic capacity is further modified:

$$P_U = \frac{A_N}{A_{NO}} \Psi P_{UO} \quad \text{eq. 4.3}$$

where Ψ is a factor taking into account the stress disturbances:

$$\Psi = 0.7 + 0.3 \frac{C_1}{1.5h_d} \leq 1.0 \quad \text{eq. 4.4}$$

where C_1 is the minimum edge distance. Note that $1.5h_d$ corresponds to the assumed failure area, A_{NO} , for the characteristic application. For anchors near three or four edges and when the largest edge distance, C_{max} , is less than $1.5h_d$ then the h_d term in Equations 4.1, 4.2 and 4.4 is limited to the largest edge distance, C_{max} , divided by 1.5.

4.3 Comparison of Results

The primary variables of the CCD method are the embedment depth, concrete strength and edge distance, matching the conclusions discussed in the previous chapter. The CCD method does not take into account transverse reinforcement which was found to have essentially no affect on the capacity in the shallow-embedment tests. The CCD method was developed for studs, bolts and expansion anchors which are generally smooth and hence does not take into account development length. It was found in the shallow-embedment tests with deformed reinforcement, development length does add capacity, though ignoring this increase would be conservative. The failure surface in the CCD method is

assumed to be $1.5h_d$ from the bar. For edge bar tests on headed reinforcement it was observed that the extent of the failure surface was approximately $1.5h_d$ from the bar measured perpendicular to the edge (Figure 4.5). The extent of the failure surface was approximately $4h_d$ from the bar measured parallel with the edge (Figure 4.6). For corner bar tests, the failure surface was approximately h_d from the bar (Figure 4.7).

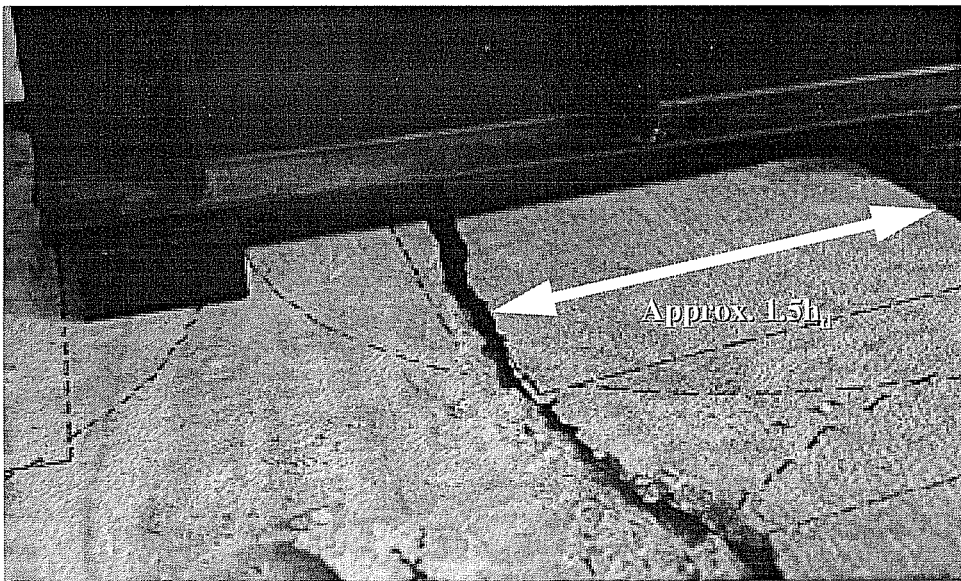


Figure 4.5 - Extent of Failure Surface for Edge Bar with Shallow Embedment

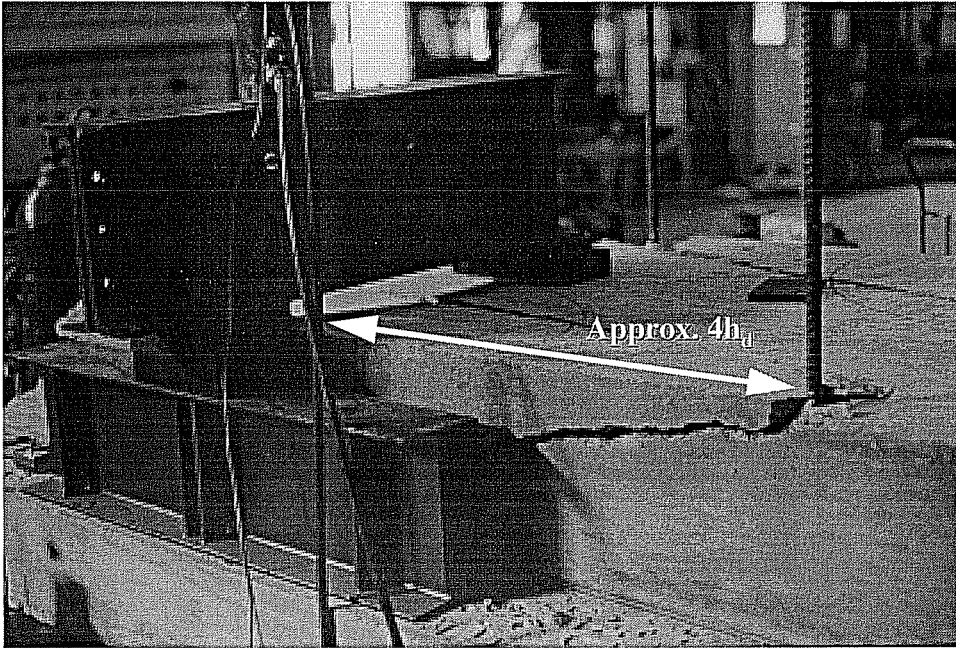


Figure 4.6 - Extent of Failure Surface for Edge Bar with Shallow Embedment

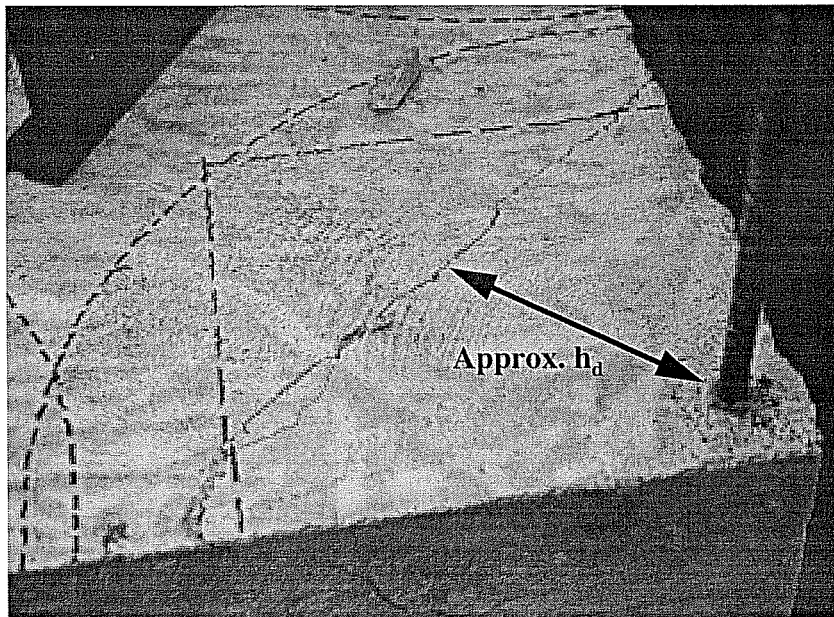


Figure 4.7 - Extent of Failure Surface for Corner Bar with Shallow Embedment

In Figure 4.8, the capacities for the 21 shallow-embedment tests of headed reinforcement are compared with the capacities predicted by the Best-Fit CCD method using the applicable modifications for edge or corner placement. The calculations for each test are summarized in Table 4.1. The CCD method underestimated (conservatively predicted) the capacity for 16 of the 21 tests. The CCD method underestimated the capacities for seven of eight center bar tests, five of seven edge bar tests and four of six corner bar tests. For the three center-bar shallow-embedment tests which resulted in a bar fracture, the CCD method underestimated the capacity of two tests. (In practice, the capacity provided by the CCD method is limited to the yield strength of the bar; however, this limit was ignored.) The capacities of all four tests with development length were underestimated by the CCD method. Three of the four tests whose capacities were less than provided by the CCD method (the CCD method was unconservative) had a concrete strength of 83 MPa.

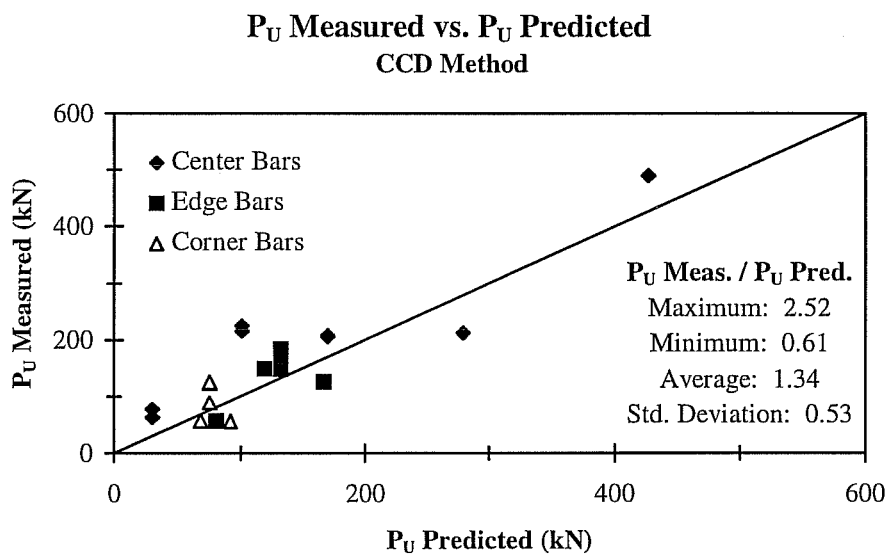


Figure 4.8 - Comparison of Predicted Capacities from CCD Method with Measured Capacities of Shallow-Embedment Tests

	Test ID - Center Bars							
	T1B1	T1B2	T1B3	T1B4	T1B5	T1B6	T1B7	T3B11
d_b (mm)	20	20	20	20	35	35	35	20
h₁ (mm)	50	70	50	70	90	100	90	50
h₂ (mm)	50	35	50	35	90	55	90	50
t (mm)	12	16	12	16	20	25	20	12
C₁ (mm)	457	457	457	457	457	457	457	457
C₂ (mm)	457	457	457	457	457	457	457	457
h_d (mm)	36	36	113	113	80	80	209	229
l_d (mm)	0	0	0	0	0	0	0	0
Trans. Reinf.	None	None	None	None	None	None	None	None
f'_c (MPa)	83	83	83	83	83	83	83	27
P_{UO} (kN)	31	31	170	170	101	101	427	279
A_n (mm²)	11664	11664	114921	114921	57600	57600	393129	471969
A_{no} (mm²)	11664	11664	114921	114921	57600	57600	393129	471969
A_n/A_{no}	1.00	1.00	1.00	1.00	1.00	1.00	1.00	1.00
PSI	1.00	1.00	1.00	1.00	1.00	1.00	1.00	1.00
P_{UCCD} (kN)	31	31	170	170	101	101	427	279
P_U (kN)	77	62	205	208	215	225	490	212
P_U/P_{UCCD}	2.52	2.03	1.21	1.23	2.13	2.23	1.15	0.76

Table 4.1a - Calculations of CCD Capacities for Shallow-Embedment Tests on Center Bars

	Test ID - Edge Bars						
	T1B8	T1B10	T2B1	T2B2	T2B3	T2B4	T3B4
d_b (mm)	20	35	20	20	20	20	20
h₁ (mm)	35	90	50	50	50	50	50
h₂ (mm)	70	90	50	50	50	50	50
t (mm)	16	20	12	12	12	12	12
C₁ (mm)	43	65	51	51	51	51	51
C₂ (mm)	457	457	457	457	457	457	457
h_d (mm)	111	183	229	229	229	229	229
l_d (mm)	0	0	0	229	0	229	0
Trans. Reinf.	None	None	None	None	STE-1	STE-1	None
f_c (MPa)	83	83	33	33	33	33	27
P_{UO} (kN)	165	350	309	309	309	309	279
A_n (mm²)	69764	186386	271022	271022	271022	271022	271022
A_{no} (mm²)	110889	301401	471969	471969	471969	471969	471969
A_n/A_{no}	0.63	0.62	0.57	0.57	0.57	0.57	0.57
PSI	0.78	0.77	0.74	0.74	0.74	0.74	0.74
P_{UCCD} (kN)	81	167	132	132	132	132	119
P_U (kN)	57	126	184	148	160	172	149
P_U/P_{UCCD}	0.71	0.76	1.39	1.12	1.21	1.30	1.25

Table 4.1b - Calculations of CCD Capacities for Shallow-Embedment Tests on Edge Bars

	Test ID - Corner Bars					
	T1B9	T2B5	T2B6	T2B7	T2B8	T3B8
d_b (mm)	25	20	20	20	20	20
h_1 (mm)	70	50	50	50	50	50
h_2 (mm)	70	50	50	50	50	50
t (mm)	16	12	12	12	12	12
C_1 (mm)	84	51	51	51	51	51
C_2 (mm)	84	51	51	51	51	51
h_d (mm)	136	229	229	229	229	229
l_d (mm)	0	0	229	0	229	229
Trans. Reinf.	None	None	None	STE-1	STE-1	None
f'_c (MPa)	83	33	33	33	33	27
P_{UO} (kN)	224	309	309	309	309	279
A_n (mm ²)	82944	155630	155630	155630	155630	155630
A_{no} (mm ²)	166464	471969	471969	471969	471969	471969
A_n/A_{no}	0.50	0.33	0.33	0.33	0.33	0.33
PSI	0.82	0.74	0.74	0.74	0.74	0.74
P_{UCCD} (kN)	92	76	76	76	76	69
P_U (kN)	56	88	122	89	125	57
P_U/P_{UCCD}	0.61	1.16	1.61	1.17	1.65	0.83

Table 4.1c - Calculations of CCD Capacities for Shallow-Embedment Tests on Corner Bars

4.4 Coefficient Adjustment

The Best-Fit CCD method underestimated the capacities for a majority of the tests on headed reinforcement. The CCD method is based on tests of anchor bolts which typically have smaller heads than the headed reinforcing bars tested. One way to adjust the CCD method for headed reinforcement is to change the coefficient in the characteristic equation. Because different types of anchors have different net bearing areas, different coefficients for different types of anchors are used in the characteristic equation. The value of 0.0155 in Equation 4.1 is for headed anchors when the bearing stress at failure at the head is less than $13\sqrt{f'_c}$. If the bearing stress at the head is higher, then the coefficient is reduced to 0.0135. For the twenty-one shallow-embedment tests, the average bearing stress at the head at failure was $8.3\sqrt{f'_c}$ with a range from $1.4\sqrt{f'_c}$ to $18.6\sqrt{f'_c}$. Since the bearing stress at the head, on average, was less than $13\sqrt{f'_c}$ perhaps a coefficient larger than 0.0155 could be used.

A new coefficient, k , was calculated from a linear regression analysis on the measured capacities for the 18 shallow-embedment tests that resulted in pullout-cone failures:

$$P_U = k \frac{A_N}{A_{NO}} \Psi \sqrt{f'_c} h_d^{1.5} \quad \text{eq. 4.5}$$

From the regression analysis, k is 0.0186. The measured capacities from the 18 pullout-cone failures are compared with the predicted capacities using this new coefficient in Figure 4.9. The calculations for each test are summarized in Table 4.2. The new coefficient results in a slightly better fit with the data than the CCD equation based on anchor bolts. The average values of the measured capacity divided by the predicted values using the new coefficient was 1.15 with a standard deviation of 0.46 compared with 1.34 and 0.53 using the original coefficient of 0.0155.

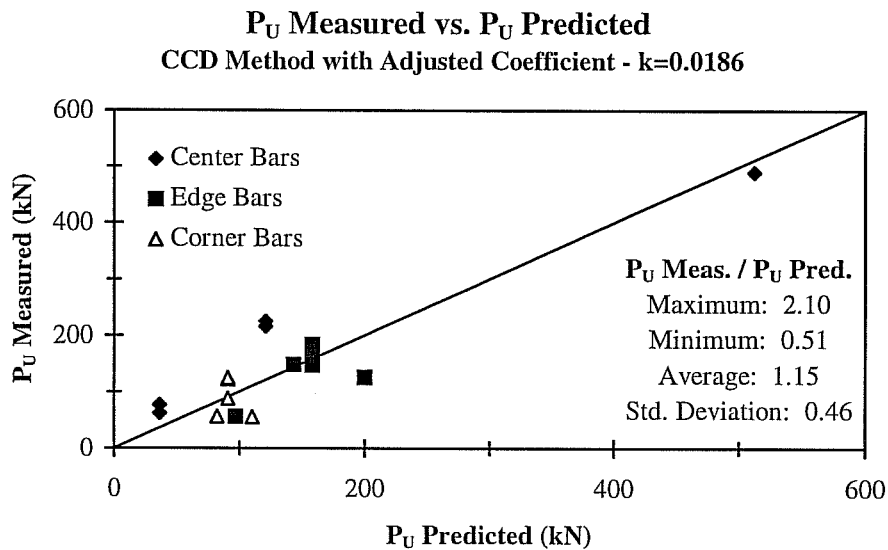


Figure 4.9 - Comparison of Predicted Capacities from CCD Method with New Coefficient and Measured Capacities of Shallow-Embedment Tests

	Test ID - Center Bars				
	T1B1	T1B2	T1B5	T1B6	T1B7
d_b (mm)	20	20	35	35	35
h₁ (mm)	50	70	90	100	90
h₂ (mm)	50	35	90	55	90
t (mm)	12	16	20	25	20
C₁ (mm)	457	457	457	457	457
C₂ (mm)	457	457	457	457	457
h_d (mm)	36	36	80	80	209
l_d (mm)	0	0	0	0	0
Trans. Reinf.	None	None	None	None	None
f'_c (MPa)	83	83	83	83	83
P_{UO} (kN)	37	37	121	121	512
A_n (mm²)	11664	11664	57600	57600	393129
A_{no} (mm²)	11664	11664	57600	57600	393129
A_n/A_{no}	1.00	1.00	1.00	1.00	1.00
PSI	1.00	1.00	1.00	1.00	1.00
P_{UCCD} (kN)	37	37	121	121	512
P_U (kN)	77	62	215	225	490
P_U/P_{UCCD}	2.10	1.69	1.77	1.86	0.96

Table 4.2a - Calculations of CCD Capacities with New Coefficient for Shallow-Embedment Tests on Center Bars

	Test ID - Edge Bars						
	T1B8	T1B10	T2B1	T2B2	T2B3	T2B4	T3B4
d_b (mm)	20	35	20	20	20	20	20
h_1 (mm)	35	90	50	50	50	50	50
h_2 (mm)	70	90	50	50	50	50	50
t (mm)	16	20	12	12	12	12	12
C_1 (mm)	43	65	51	51	51	51	51
C_2 (mm)	457	457	457	457	457	457	457
h_d (mm)	111	183	229	229	229	229	229
l_d (mm)	0	0	0	229	0	229	0
Trans. Reinf.	None	None	None	None	STE-1	STE-1	None
f'_c (MPa)	83	83	33	33	33	33	27
P_{UO} (kN)	198	419	370	370	370	370	335
A_n (mm ²)	69764	186386	271022	271022	271022	271022	271022
A_{no} (mm ²)	110889	301401	471969	471969	471969	471969	471969
A_n/A_{no}	0.63	0.62	0.57	0.57	0.57	0.57	0.57
PSI	0.78	0.77	0.74	0.74	0.74	0.74	0.74
P_{UCCD} (kN)	97	200	158	158	158	158	143
P_U (kN)	57	126	184	148	160	172	149
P_U/P_{UCCD}	0.59	0.63	1.16	0.93	1.01	1.09	1.04

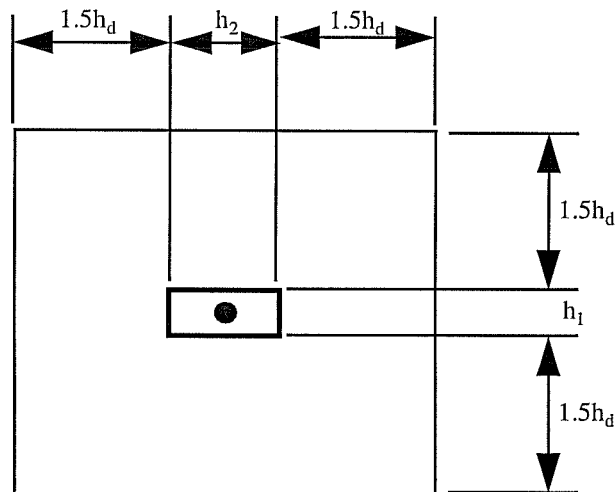
Table 4.2b - Calculations of CCD Capacities with New Coefficient for Shallow-Embedment Tests on Edge Bars

	Test ID - Corner Bars					
	T1B9	T2B5	T2B6	T2B7	T2B8	T3B8
d_b (mm)	25	20	20	20	20	20
h_1 (mm)	70	50	50	50	50	50
h_2 (mm)	70	50	50	50	50	50
t (mm)	16	12	12	12	12	12
C_1 (mm)	84	51	51	51	51	51
C_2 (mm)	84	51	51	51	51	51
h_d (mm)	136	229	229	229	229	229
l_d (mm)	0	0	229	0	229	229
Trans. Reinf.	None	None	None	STE-1	STE-1	None
f'_c (MPa)	83	33	33	33	33	27
P_{UO} (kN)	269	370	370	370	370	335
A_n (mm ²)	82944	155630	155630	155630	155630	155630
A_{no} (mm ²)	166464	471969	471969	471969	471969	471969
A_n/A_{no}	0.50	0.33	0.33	0.33	0.33	0.33
PSI	0.82	0.74	0.74	0.74	0.74	0.74
P_{UCCD} (kN)	110	91	91	91	91	82
P_U (kN)	56	88	122	89	125	57
P_U/P_{UCCD}	0.51	0.97	1.34	0.98	1.38	0.69

Table 4.2c - Calculations of CCD Capacities with New Coefficient for Shallow-Embedment Tests on Corner Bars

4.5 Adjusting for Head Area

The provisions of the proposed ACI 318 Chapter 23 [3] for anchorage to concrete allow the size of the available pullout cone to be measured from the effective perimeter of the head (Figure 4.10). This allows increases in capacity for anchor bolts with washers or for headed reinforcement which typically has heads larger than those on anchor bolts. The provisions limit the size of the effective perimeter for washers or plates attached to anchor bolts. However, it is reasonable to ignore this for headed reinforcement, since the heads are thicker than typical washers, and assume the effective perimeter is that of the head. (The effect of head thickness is discussed further in Section 5.8.) The only factor in the CCD method that changes with this approach is the value for A_N , and the ratio of



$$A_N = (3h_d + h_1)(3h_d + h_2)$$

Figure 4.10 - Pullout-Cone Failure Area Based on Effective Perimeter

A_N/A_{NO} which can now be greater than one for a single anchor. The value of A_N increased by an average of 36% when taking into account the size of the head for the 18 shallow-embedment tests resulting in pullout failures.

The measured capacities for the 18 shallow-embedment tests resulting in pullout failures are compared to the predicted capacities from the CCD method taking into account the head size in Figure 4.11. The calculations for each test are summarized in Table 4.3. Taking into account the head size resulted in better predictions of the pullout capacity of headed reinforcement. The average value of the measured capacity divided by the predicted capacity was 1.01 with a standard deviation of 0.28. The average was closer to unity than using the CCD method or the CCD method with the new coefficient, and the standard deviation was the lowest of the three approaches.

In the previous chapter, two tests which were identical except for head area and head aspect ratio were shown to have nearly identical ultimate capacities. For these two tests the head areas differed by over 45%. However, the assumed failure area using the CCD method and taking into account the perimeter of the heads differed by less than 9%.

P_U Measured vs. P_U Predicted
CCD Method Accounting for Head Size

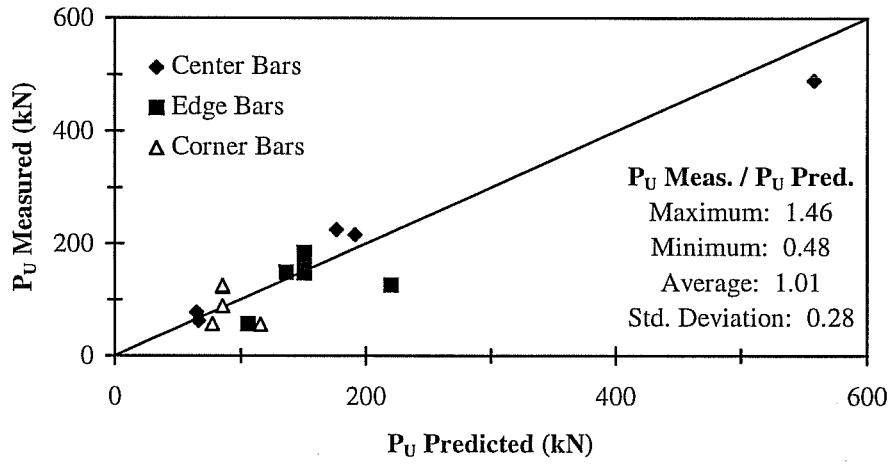


Figure 4.11 - Comparison of Predicted Capacities using CCD Method with Head Area and Measured Capacities for Shallow-Embedment Tests

	Test ID - Center Bars				
	T1B1	T1B2	T1B5	T1B6	T1B7
d_b (mm)	20	20	35	35	35
h_1 (mm)	50	70	90	100	90
h_2 (mm)	50	35	90	55	90
t (mm)	12	16	20	25	20
C_1 (mm)	457	457	457	457	457
C_2 (mm)	457	457	457	457	457
h_d (mm)	36	36	80	80	209
l_d (mm)	0	0	0	0	0
Trans. Reinf.	None	None	None	None	None
f'_c (MPa)	83	83	83	83	83
P_{UO} (kN)	31	31	101	101	427
A_n (mm ²)	24964	25454	108900	100300	514089
A_{no} (mm ²)	11664	11664	57600	57600	393129
A_n/A_{no}	2.14	2.18	1.89	1.74	1.31
PSI	1.00	1.00	1.00	1.00	1.00
P_{UCCD} (kN)	65	67	191	176	558
P_U (kN)	77	62	215	225	490
P_U/P_{UCCD}	1.18	0.93	1.13	1.28	0.88

Table 4.3a - Calculations of CCD Capacities with Head Area for Shallow-Embedment Tests on Center Bars

	Test ID - Edge Bars						
	T1B8	T1B10	T2B1	T2B2	T2B3	T2B4	T3B4
d_b (mm)	20	35	20	20	20	20	20
h_1 (mm)	35	90	50	50	50	50	50
h_2 (mm)	70	90	50	50	50	50	50
t (mm)	16	20	12	12	12	12	12
C_1 (mm)	43	65	51	51	51	51	51
C_2 (mm)	457	457	457	457	457	457	457
h_d (mm)	111	183	229	229	229	229	229
l_d (mm)	0	0	0	229	0	229	0
Trans. Reinf.	None	None	None	None	STE-1	STE-1	None
f'_c (MPa)	83	83	33	33	33	33	27
P_{UO} (kN)	165	350	309	309	309	309	279
A_n (mm ²)	91481	245696	309172	309172	309172	309172	309172
A_{no} (mm ²)	110889	301401	471969	471969	471969	471969	471969
A_n/A_{no}	0.82	0.82	0.66	0.66	0.66	0.66	0.66
PSI	0.78	0.77	0.74	0.74	0.74	0.74	0.74
P_{UCCD} (kN)	106	220	150	150	150	150	136
P_U (kN)	57	126	184	148	160	172	149
P_U/P_{UCCD}	0.54	0.57	1.22	0.98	1.06	1.14	1.09

Table 4.3b - Calculations of CCD Capacities with Head Area for Shallow-Embedment Tests on Edge Bars

	Test ID - Corner Bars					
	T1B9	T2B5	T2B6	T2B7	T2B8	T3B8
d_b (mm)	25	20	20	20	20	20
h_1 (mm)	70	50	50	50	50	50
h_2 (mm)	70	50	50	50	50	50
t (mm)	16	12	12	12	12	12
C_1 (mm)	84	51	51	51	51	51
C_2 (mm)	84	51	51	51	51	51
h_d (mm)	136	229	229	229	229	229
l_d (mm)	0	0	229	0	229	229
Trans. Reinf.	None	None	None	STE-1	STE-1	None
f'_c (MPa)	83	33	33	33	33	27
P_{UO} (kN)	224	309	309	309	309	279
A_n (mm ²)	104329	175980	175980	175980	175980	175980
A_{no} (mm ²)	166464	471969	471969	471969	471969	471969
A_n/A_{no}	0.63	0.37	0.37	0.37	0.37	0.37
PSI	0.82	0.74	0.74	0.74	0.74	0.74
P_{UCCD} (kN)	116	86	86	86	86	77
P_U (kN)	56	88	122	89	125	57
P_U/P_{UCCD}	0.48	1.03	1.42	1.04	1.46	0.74

Table 4.3c - Calculations of CCD Capacities with Head Area for Shallow-Embedment Tests on Corner Bars

4.6 Design Equation

In the proposed Chapter 23 for the ACI 318 Code, the proposed characteristic design equation for the pullout capacity of anchors has a coefficient of 0.0089 or 1/112:

$$P_{uo} = \frac{h_d^{1.5} \sqrt{f'_c}}{112} \quad \text{eq. 4.6}$$

In Figure 4.12, the measured capacity of the 18 shallow-embedment tests that resulted in pullout-cone failures are compared with the predicted values based on Equation 4.6 with all modification factors and taking into account the head perimeter. The calculations for each test are summarized in Table 4.4. The design method underestimated the capacity for 15 of the 18 tests. The three tests with capacities lower than predictions based on Equation 4.6 (the CCD method was unconservative) were edge or corner bars tests with a concrete strength of 83 MPa. From these results, basing the failure area on the perimeter of the head accurately models the effect of head area and head aspect ratio.

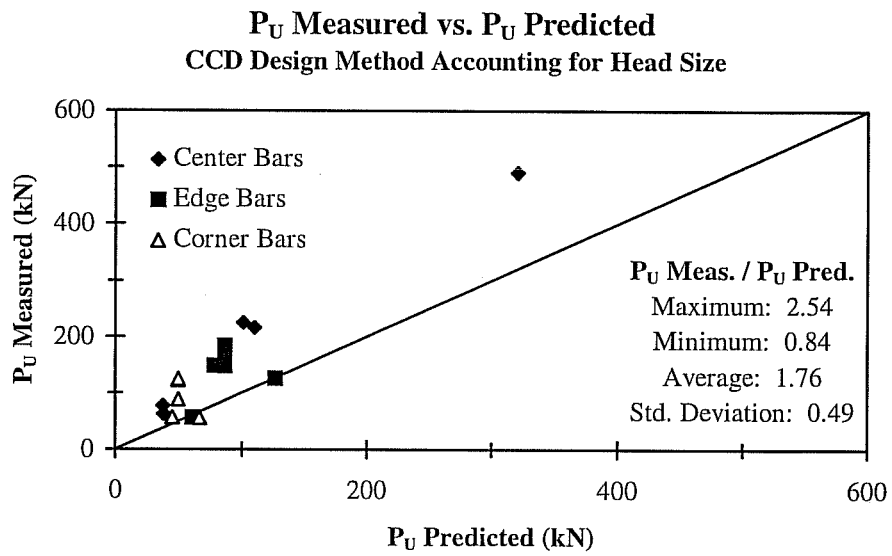


Figure 4.12 - Comparison of Predicted Capacities with CCD Design Method with Head Area with Measured Capacities of Shallow-Embedment Tests

	Test ID - Center Bars				
	T1B1	T1B2	T1B5	T1B6	T1B7
d_b (mm)	20	20	35	35	35
h_1 (mm)	50	70	90	100	90
h_2 (mm)	50	35	90	55	90
t (mm)	12	16	20	25	20
C_1 (mm)	457	457	457	457	457
C_2 (mm)	457	457	457	457	457
h_d (mm)	36	36	80	80	209
l_d (mm)	0	0	0	0	0
Trans. Reinf.	None	None	None	None	None
f'_c (MPa)	83	83	83	83	83
P_{UO} (kN)	18	18	58	58	246
A_n (mm ²)	24964	25454	108900	100300	514089
A_{no} (mm ²)	11664	11664	57600	57600	393129
A_n/A_{no}	2.14	2.18	1.89	1.74	1.31
PSI	1.00	1.00	1.00	1.00	1.00
P_{UCCD} (kN)	38	38	110	101	321
P_U (kN)	77	62	215	225	490
P_U/P_{UCCD}	2.05	1.62	1.95	2.22	1.52

Table 4.4a - Calculations of CCD Design Capacities with Head Area for Shallow-Embedment Tests on Center Bars

	Test ID - Edge Bars						
	T1B8	T1B10	T2B1	T2B2	T2B3	T2B4	T3B4
d_b (mm)	20	35	20	20	20	20	20
h_1 (mm)	35	90	50	50	50	50	50
h_2 (mm)	70	90	50	50	50	50	50
t (mm)	16	20	12	12	12	12	12
C_1 (mm)	43	65	51	51	51	51	51
C_2 (mm)	457	457	457	457	457	457	457
h_d (mm)	111	183	229	229	229	229	229
l_d (mm)	0	0	0	229	0	229	0
Trans. Reinf.	None	None	None	None	STE-1	STE-1	None
f'_c (MPa)	83	83	33	33	33	33	27
P_{UO} (kN)	95	201	178	178	178	178	161
A_n (mm ²)	91481	245696	309172	309172	309172	309172	309172
A_{no} (mm ²)	110889	301401	471969	471969	471969	471969	471969
A_n/A_{no}	0.82	0.82	0.66	0.66	0.66	0.66	0.66
PSI	0.78	0.77	0.74	0.74	0.74	0.74	0.74
P_{UCCD} (kN)	61	127	87	87	87	87	78
P_U (kN)	57	126	184	148	160	172	149
P_U/P_{UCCD}	0.93	1.00	2.12	1.71	1.85	1.98	1.90

Table 4.4b - Calculations of CCD Design Capacities with Head Area for Shallow-Embedment Tests on Edge Bars

	Test ID - Corner Bars					
	T1B9	T2B5	T2B6	T2B7	T2B8	T3B8
d_b (mm)	25	20	20	20	20	20
h_1 (mm)	70	50	50	50	50	50
h_2 (mm)	70	50	50	50	50	50
t (mm)	16	12	12	12	12	12
C_1 (mm)	84	51	51	51	51	51
C_2 (mm)	84	51	51	51	51	51
h_d (mm)	136	229	229	229	229	229
l_d (mm)	0	0	229	0	229	229
Trans. Reinf.	None	None	None	STE-1	STE-1	None
f'_c (MPa)	83	33	33	33	33	27
P_{UO} (kN)	129	178	178	178	178	161
A_n (mm ²)	104329	175980	175980	175980	175980	175980
A_{no} (mm ²)	166464	471969	471969	471969	471969	471969
A_n/A_{no}	0.63	0.37	0.37	0.37	0.37	0.37
PSI	0.82	0.74	0.74	0.74	0.74	0.74
P_{UCCD} (kN)	67	49	49	49	49	45
P_U (kN)	56	88	122	89	125	57
P_U/P_{UCCD}	0.84	1.78	2.47	1.80	2.53	1.28

Table 4.4c - Calculations of CCD Design Capacities with Head Area for Shallow-Embedment Tests on Corner Bars

Chapter 5

Deep-Embedment Pullout Tests Effect of Variables on Anchorage

5.1 Overview of Results

The deep-embedment test specimens were expected to fail in one of two modes, a side-blowout failure with spalling of the concrete cover over the head or bar fracture. No bar fractures of headed reinforcement were observed though many tests reached bar stresses well into the strain hardening range. 108 of the tests on single bars and all six tests on closely spaced paired bars resulted in side-blowout failures. The results of the 108 single bar tests are summarized in Table 5.1 and the results of the 6 tests on closely spaced bars are summarized in Table 5.2. In these tables, P_U is the measured capacity (ultimate load) of the anchorage and f'_c denotes the concrete strength on the day of testing.

Test ID	d_b (mm)	Nominal Head (mm)	C_1 (mm)	C_2 (mm)	l_d (mm)	Trans. Reinf.	f'_c (MPa)	P_U (kN)
C1B1	25	70x70x16	35	457	0	None	25	239
C1B2	25	70x70x16	48	457	0	None	25	283
C1B3	25	70x70x16	48	457	0	None	25	272
C2B1	25	70x70x16	35	35	0	None	25	97
C2B2	25	70x70x16	48	48	0	None	25	179
C2B3	25	70x70x16	48	48	0	None	25	157
C2B4	25	70x70x16	60	60	0	None	25	197
C3B1	35	100x55x25	51	457	0	None	29	285
C3B2	35	55x100x25	51	457	0	None	29	284
C3B3	35	100x55x25	64	457	0	None	29	330
C3B4	35	55x100x25	64	457	0	None	29	335
C3B6	20	35x70x16	18	48	0	None	29	55
C3B7	20	35x70x16	30	35	0	None	29	64
C4B1	35	90x90x20	45	457	0	None	29	403
C4B2	35	90x90x20	51	457	0	None	29	476
C4B3	35	90x90x20	64	457	0	None	29	491
C4B4	35	90x90x20	76	457	0	None	29	512
C4B6	25	40x80x18	33	53	0	None	29	59
C4B7	25	40x80x18	45	65	0	None	29	106
C5B1	35	100x55x25	64	457	305	None	21	474
C5B2	35	55x100x25	64	457	305	None	21	477
C5B3	35	100x55x25	64	457	610	None	21	526
C5B4	35	55x100x25	64	457	610	None	21	496
C5B5	20	50x50x12	38	38	0	None	21	67
C5B6	20	50x50x12	38	38	152	None	21	105
C6B3	35	90x90x20	76	457	305	None	21	562
C6B4	35	90x90x20	76	457	610	None	21	613
C6B5	25	40x80x18	45	66	152	None	21	147
C6B6	25	40x80x18	45	66	305	None	21	192
C6B7	25	40x80x18	45	66	457	None	21	179

Table 5.1 - Parameters and Results of Deep-Embedment Tests

Test ID	d_b (mm)	Nominal Head (mm)	C_1 (mm)	C_2 (mm)	l_d (mm)	Trans. Reinf.	f'_c (MPa)	P_U (kN)
C7B1	35	90x90x20	89	457	0	None	24	589
C7B2	35	90x90x20	102	457	0	None	24	609
C7B3	35	100x55x25	102	457	0	None	24	460
C7B4	35	55x100x25	102	457	0	None	24	464
C7B5	25	40x80x18	58	78	0	None	24	158
C7B6	25	40x80x18	71	91	0	None	24	193
C7B7	25	40x80x18	46	91	0	None	24	87
C8B1	35	90x90x20	89	89	0	None	24	355
C8B2	35	90x90x20	127	127	0	None	24	502
C8B3	35	100x55x25	89	89	0	None	24	283
C8B4	35	100x55x25	127	127	0	None	24	411
C8B5	20	35x70x16	30	457	0	None	24	127
C8B6	20	70x35x16	45	457	0	None	24	177
C8B7	20	35x70x16	45	457	0	None	24	155
C9B1	35	55x100x25	64	457	305	TE-1	27	591
C9B2	35	55x100x25	64	457	305	TE-1	27	604
C9B3	35	55x100x25	64	457	305	TE-1	27	621
C9B4	35	55x100x25	64	457	305	TE-1a	27	598
C9B5	25	70x70x16	61	61	305	None	27	263
C9B6	25	70x70x16	61	61	305	TC-1	27	301
C9B7	25	70x70x16	61	61	305	TC-1	27	298
C10B1	35	55x100x25	64	457	305	None	27	581
C10B2	35	55x100x25	64	457	305	TE-2	27	581
C10B3	35	55x100x25	64	457	305	TE-2	27	583
C10B4	35	55x100x25	64	457	305	TE-2	27	564
C10B6	20	50x50x12	38	76	305	None	27	185
C10B7	20	50x50x12	38	114	305	None	27	178
C11B3	35	90x90x20	64	457	305	TE-1a	27	660
C11B4	35	90x90x20	64	457	305	TE-2	27	632
C11B7	20	70x35x16	38	114	305	None	27	196

Table 5.1 - Continued

Test ID	d_b (mm)	Nominal Head (mm)	C_1 (mm)	C_2 (mm)	l_d (mm)	Trans. Reinf.	f'_c (MPa)	P_U (kN)
C12B1	35	90x90x20	64	64	305	TC-1	21	404
C12B3	35	90x90x20	64	127	305	TC-1	21	496
C13B1	35	55x100x25	64	457	305	TE-3	21	517
C13B2	35	55x100x25	64	457	305	TE-3	21	553
C13B3	35	55x100x25	64	457	305	TE-3	21	549
C13B4	35	90x90x20	64	457	305	TE-3	21	581
C13B5	25	40x80x18	61	61	305	TC-1	21	234
C13B6	25	40x80x18	61	61	305	TC-1	21	273
C13B7	25	70x70x16	61	61	305	TC-1	21	278
C15B1	35	57x57x16	45	305	0	None	19	162
C15B2	35	40x80x16	45	305	0	None	19	185
C15B3	35	70x70x16	45	305	0	None	19	221
C15B4	35	49x99x16	45	305	0	None	19	217
C15B5	35	55x100x25	45	305	0	None	19	194
C15B6	35	80x80x16	45	305	0	None	19	283
C15B7	35	90x90x16	45	305	0	None	19	374
C16B1	25	33x33x16	45	305	0	None	19	93
C16B2	25	57x57x12	45	305	0	None	19	154
C16B3	25	57x57x16	45	305	0	None	19	168
C16B4	25	57x57x20	45	305	0	None	19	176
C16B5	25	40x80x12	45	305	0	None	19	162
C16B6	25	40x80x16	45	305	0	None	19	163
C16B7	25	40x80x18	45	305	0	None	19	180
C16B8	25	40x80x20	45	305	0	None	19	149

Table 5.1 - Continued

Test ID	d_b (mm)	Nominal Head (mm)	C_1 (mm)	C_2 (mm)	l_d (mm)	Trans. Reinf.	f'_c (MPa)	P_U (kN)
C17B1	25	33x98x12	45	305	0	None	19	144
C17B2	25	33x98x16	45	305	0	None	19	165
C17B3	25	33x98x20	45	305	0	None	19	199
C17B4	25	70x70x12	45	305	0	None	19	238
C17B5	25	70x70x16	45	305	0	None	19	235
C17B6	25	70x70x20	45	305	0	None	19	222
C17B7	25	49x99x16	45	305	0	None	19	222
C17B8	25	55x100x25	45	305	0	None	19	233
C17B9	25	80x80x12	45	305	0	None	19	285
C17B10	25	80x80x16	45	305	0	None	19	331
C17B11	25	70x70x16	45	305	0	None	19	183
C17B12	25	77x77x16	45	305	0	None	19	193
C18B1	35	55x100x25	45	305	0	None	44	411
C18B2	35	55x100x25	51	305	0	None	44	432
C18B3	35	55x100x25	64	305	0	None	44	517
C18B4	35	90x90x20	45	305	0	None	44	555
C18B5	35	40x80x25	45	305	0	None	44	238
C18B6	35	40x80x25	64	305	0	None	44	330
C19B1	35	70x70x20	45	305	0	None	44	360
C19B2	35	70x70x20	64	305	0	None	44	470
C19B3	25	40x80x25	45	305	0	None	44	287
C19B4	25	40x80x25	25	305	0	None	44	196
C19B5	25	57x57x16	45	305	0	None	44	295
C19B6	25	57x57x16	30	305	0	None	44	261

Table 5.1 - Continued

Test ID	d_b (mm)	Nominal Head (mm)	C_1 (mm)	C_2 (mm)	C_{SP2} (mm)	l_d (mm)	Trans. Reinf.	f'_c (MPa)	P_U (kN)
C12B5	25	40x80x18	25	457	102	0	None	25	135
C12B6	25	40x80x18	25	457	152	0	None	25	182
C12B7	25	40x80x18	38	457	102	0	None	25	167
C12B8	25	40x80x18	38	457	152	0	None	25	188
C18B7	25	40x80x18	25	457	102	0	None	44	204
C19B7	25	40x80x18	25	457	152	0	None	44	224

Table 5.2 - Parameters and Results of Deep-Embedment Tests on Paired Bars

Fifteen tests resulted in an unexpected failure of the top bearing, or loaded, surface (Figure 5.1). This failure was characterized by a spalling of the top edge of concrete directly under the applied load. When a bearing failure occurred the test was stopped. If the damage to the concrete was not too severe, attempts were made to retest the bar by creating a reaction frame with steel beams on top of plates placed on sound concrete and tied down to the specimen using the lifting

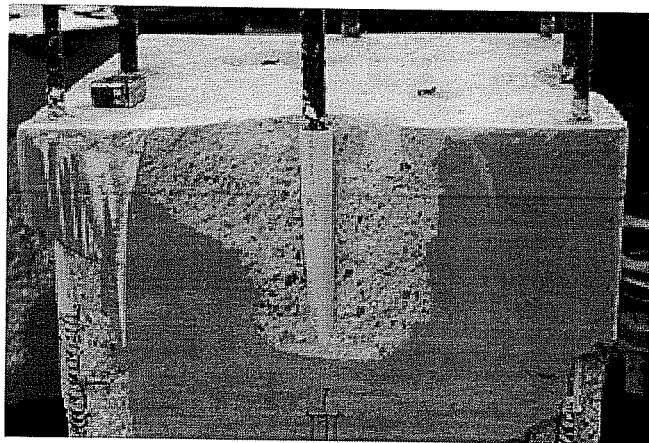


Figure 5.1 - Bearing Failure of Loaded Surface

inserts (Figure 5.2 and 5.3). During retesting either a side blowout would occur or the lifting inserts would fail. The parameters and results of the 15 tests with bearing failures are summarized in Table 5.3. In Table 5.3, P_{U1} is the highest load reached during the first test which resulted in the bearing failure and P_{U2} is the highest load reached during retesting. Since it was not possible to gauge what damage was done to the anchorage during the first loading sequence, the capacities of these 15 tests will not be compared with the other tests that resulted in blowout failures.

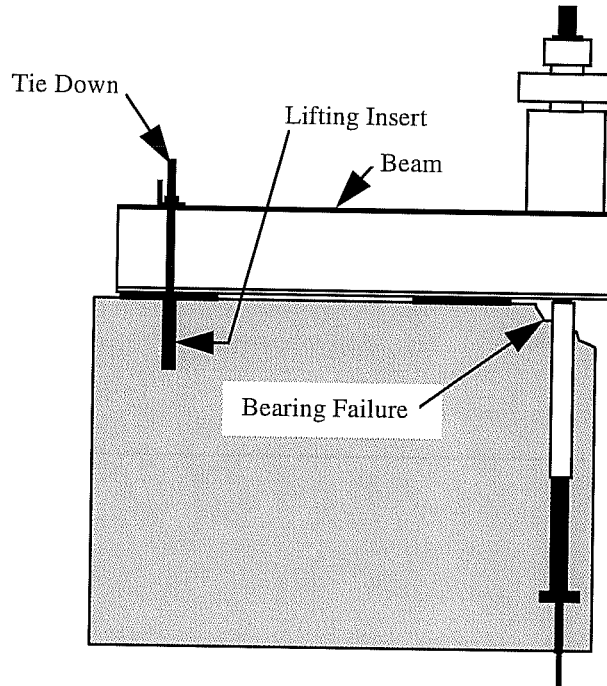


Figure 5.2 - Setup for Retesting after Bearing Failure

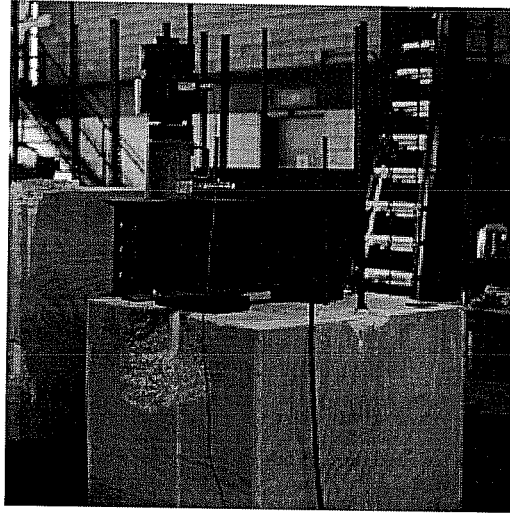


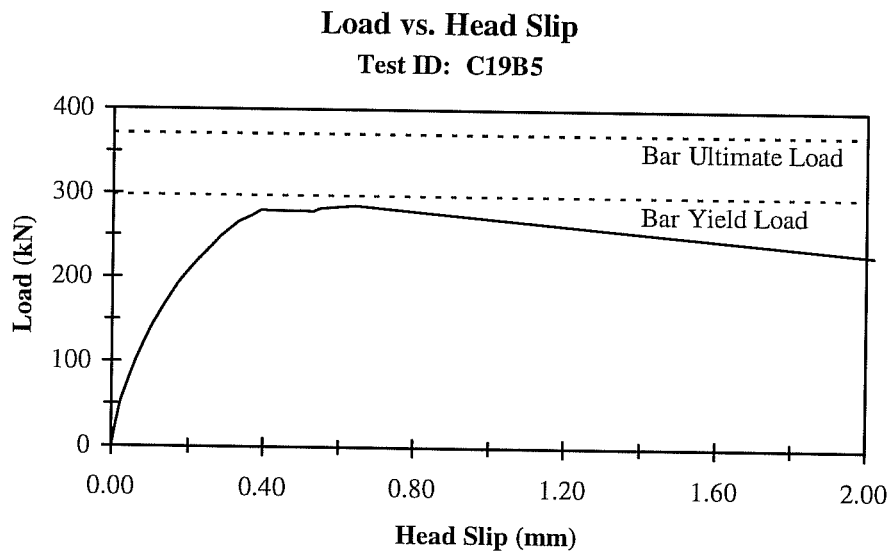
Figure 5.3 - Setup for Retesting after Bearing Failure

Test ID	d_b (mm)	Nominal Head (mm)	C_1 (mm)	C_2 (mm)	l_d (mm)	Trans. Reinf.	f'_c (MPa)	P_{U1} (kN)	P_{U2} (kN)
C1B4	25	70x70x16	60	457	0	None	25	177	247
C3B5	20	35x70x16	18	35	0	None	29	35	56
C4B5	25	40x80x18	20	40	0	None	29	53	72
C5B7	20	50x50x12	38	38	305	None	21	105	95
C6B1	35	90x90x20	45	457	305	None	21	481	#N/A
C6B2	35	90x90x20	45	457	610	None	21	460	#N/A
C9B8	25	70x70x16	61	61	305	None	27	123	290
C10B5	20	50x50x12	38	38	305	None	27	100	134
C11B1	35	90x90x20	45	457	305	None	27	#N/A	#N/A
C11B2	35	90x90x20	45	457	610	None	27	402	#N/A
C11B5	20	70x35x16	38	38	305	None	27	43	128
C11B6	20	70x35x16	38	76	305	None	27	153	147
C12B2	35	90x90x20	64	64	305	None	21	320	340
C12B4	35	90x90x20	64	64	305	None	21	370	#N/A
C15B8	35	90x90x20	45	305	0	None	19	360	394

Table 5.3 - Parameters and Results of Deep-Embedment Tests with Bearing Failures

5.2 General Behavior Under Load

A typical load-slip response of a deeply embedded headed bar with no development length is shown in Figure 5.4. The slip was measured at the head. In general, head deflection was observed immediately on the application of load. As the load neared the peak or ultimate load the slip increased rapidly. At failure, the side cover spalled in a sudden brittle fashion and the load dropped significantly with a large increase in displacement. For bars with no development



Test ID	d_b (mm)	Nominal Head (mm)	C_1 (mm)	C_2 (mm)	l_d (mm)	Trans. Reinf.	f'_c (MPa)	P_U (kN)
C19B5	25	57x57x16	45	305	0	None	44	295

Figure 5.4 - Deflection at Head for Bar without Development Length

length or transverse reinforcement in the anchorage zone, there was no cracking until failure was imminent. Cracks were observed in some tests forming around the head just before failure.

The amount of spalled concrete varied from test to test. After failure, any loose cover was removed. A wedge of concrete was observed to have formed at the head (Figure 5.5). This observation is similar to behavior reported by Hasselwander [21]. The size and shape of the wedge varied with the size and aspect ratio of the head. For many of the tests, the wedge did not remain intact after failure. It was observed in some tests that when additional deformation was

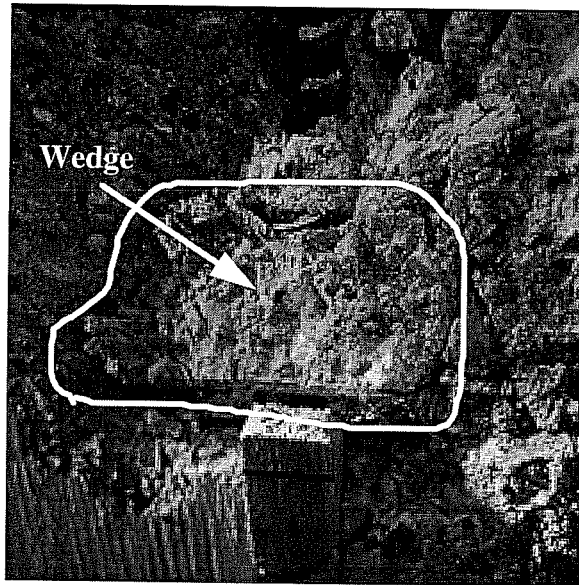


Figure 5.5 - Wedge of Concrete Observed on Head after Failure

applied after failure, the wedge of concrete bore against the inside face of concrete and forced the head outward with sufficient force to permanently bend the bar near the head (Figure 5.6).

In several tests, the bar yielded, went through the yield plateau and entered strain hardening. Yielding was characterized by a large displacement of the ram with no increase in measured load. During yielding there was no marked increase in deflection of the head. There was also no change in the cracking behavior of the concrete around the yielded bar. Based on these observations it appears that yielding of the bar had no impact on the ultimate blowout capacity or behavior of the anchorage.



Figure 5.6 - Head Movement after Failure

For bars with development length, a crack formed at the start of the development length and propagated down to the head as load increased (Figure 5.7). However, this crack was not directly involved with the final blowout failure. When the cover was removed, it was observed that concrete was sheared at the lugs along the development length (Figure 5.8).

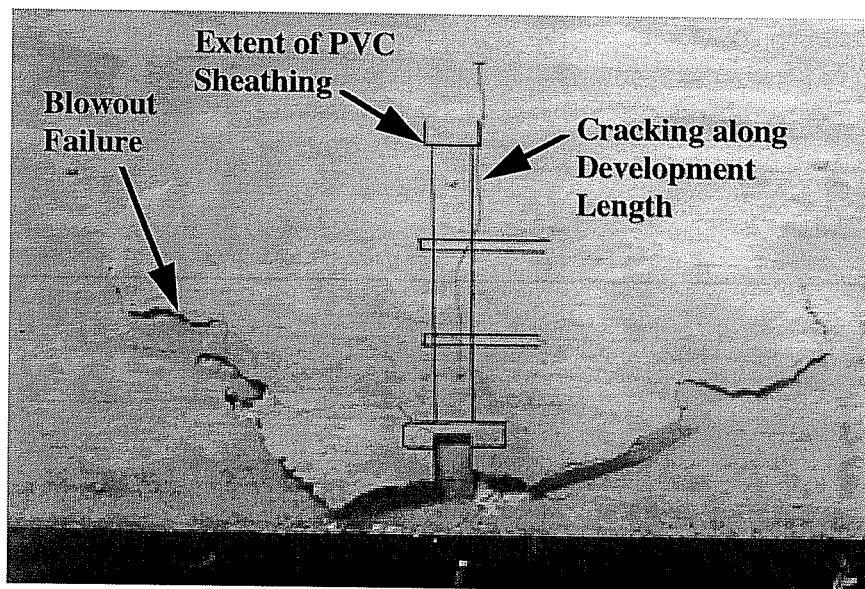


Figure 5.7 - Cracking along Development Length during Testing

When substantial transverse reinforcement was present in the anchorage zone, the headed bar maintained a larger portion of the ultimate load after failure through large deflections. All tests with transverse reinforcement had some development length and exhibited the same cracking behavior as bars with similar development length and no transverse reinforcement.

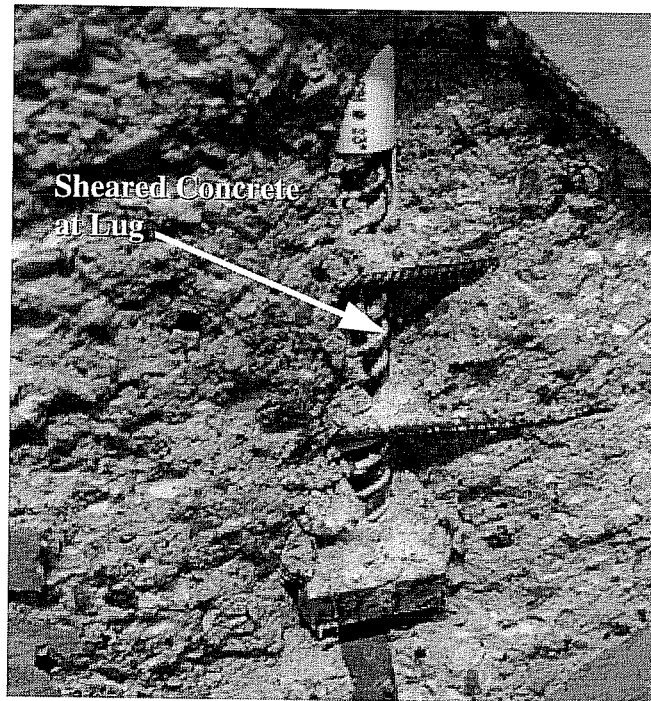
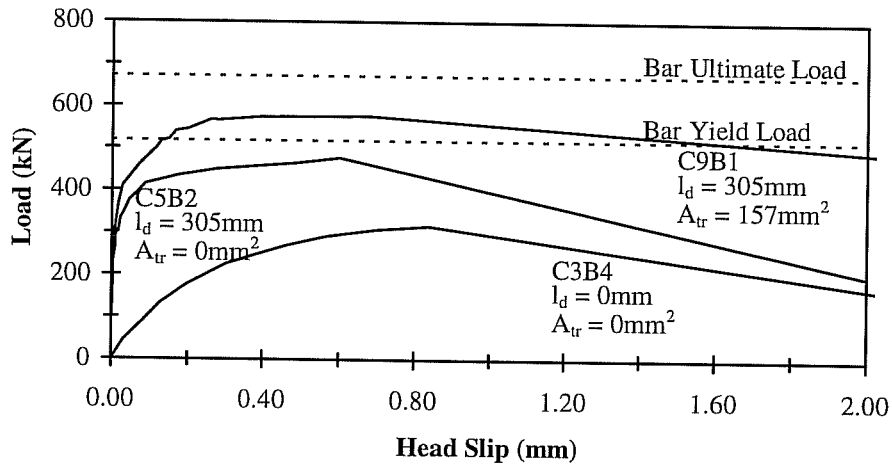


Figure 5.8 - Shearing of Concrete at Lugs

5.3 Deflections

In Figure 5.9, the deflection curves for three tests: C3B4 with no development length or transverse reinforcement; C5B2 with 305mm of development length and no transverse reinforcement and C9B1 with 305mm of development length and transverse reinforcement, are compared. All three tests were edge bars with identical edge distance, C_1 ; bar diameter, d_b ; head, $h_1 \times h_2 \times t$; and nominal concrete strength, f'_c . The addition of development length significantly increased the load at which initial slip was noted.

Load vs. Head Slip

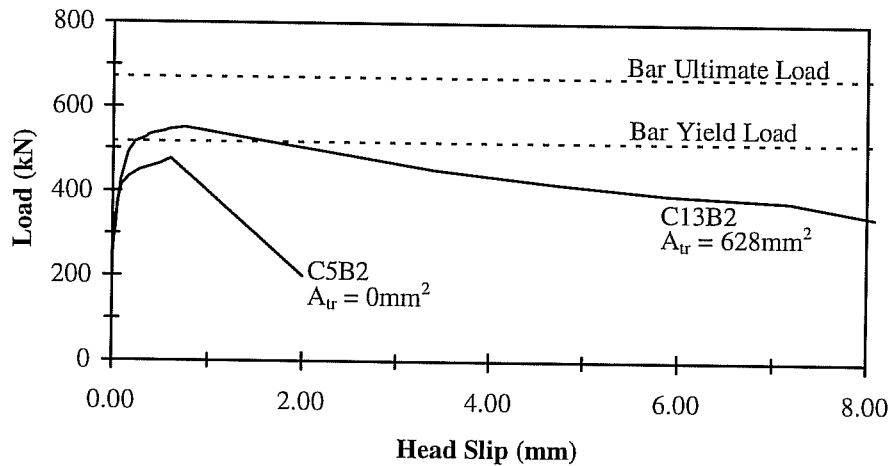


Test ID	d_b (mm)	Nominal Head (mm)	C_1 (mm)	C_2 (mm)	l_d (mm)	Trans. Reinf.	f'_c (MPa)	P_U (kN)
C3B4	35	55x100x25	64	457	0	None	29	335
C5B2	35	55x100x25	64	457	305	None	21	477
C9B1	35	55x100x25	64	457	305	TE-1	27	591

Figure 5.9 - Comparison of Head Slips for Various Deep-Embedment Tests

In Figure 5.10 the head slips for two tests are compared. The two tests were identical except one test, C5B2, had no transverse reinforcement, and C13B4 had a large amount of transverse reinforcement near the head. The large amount of transverse reinforcement near the head made little difference in the ultimate capacity but substantially increased the level of load maintained at any given slip after the peak load was reached. C5B2 with no transverse reinforcement had essentially no reserve while C13B4 with transverse reinforcement maintained a

Load vs. Head Slip



Test ID	d_b (mm)	Nominal Head (mm)	C_1 (mm)	C_2 (mm)	l_d (mm)	Trans. Reinf.	f'_c (MPa)	P_U (kN)
C5B2	35	55x100x25	64	457	305	None	21	477
C13B2	35	55x100x25	64	457	305	TE-3	21	553

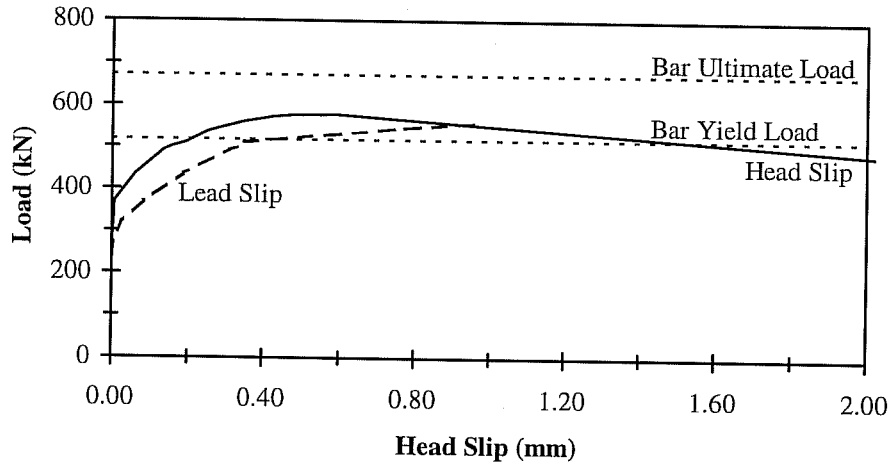
Figure 5.10 - Effect of Transverse Reinforcement on Head Slip

load approximately equal to the capacity of C5B2 through a deflection 4 to 10 times greater than the head slip at the peak load.

In Figure 5.11, the head and lead slip are compared for one test. The lead slip was measured at the beginning of the development length. Initially the lead slip was greater than the head slip at all loads before ultimate but after ultimate was reached and the concrete cover had spalled off, the values were approximately equal.

Load vs. Head and Lead Slip

Test ID: C13B4



Test ID	d_b (mm)	Nominal Head (mm)	C_1 (mm)	C_2 (mm)	l_d (mm)	Trans. Reinf.	f'_c (MPa)	P_U (kN)
C13B4	35	90x90x20	64	457	305	TE-3	21	581

Figure 5.11 - Comparison of Head and Lead Slip

5.4 Embedment Depth

For headed bars with deep embedments, it was assumed that an embedment depth of 762mm would be sufficient to cause a side blowout failure for the range of edge distances tested. It was also assumed that if the embedment depth was deep enough to cause a blowout, increasing the depth would not change the capacity of the anchorage. This was supported by results reported by Hasselwander [20]. Further, it was assumed that the bearing reaction from the loading on the top surface of the concrete block would have little or no effect on

the anchorage capacity. To verify these assumptions two pairs of tests were conducted with the only variable being the embedment depth. For a pair of edge bars and a pair of corner bars, one bar had an embedment depth of 762mm and the other 508mm. All four bars were 25mm diameter with a 70x70x16mm head and no development length or transverse reinforcement. The edge distance, C_1 , for the edge bars was 48mm. The edge distance in both directions, C_1 and C_2 , was 48mm for the corner bars. The parameters for this series of tests are summarized in Table 5.4.

The capacities from the four tests are summarized in Figure 5.12. All four bars resulted in side blowout failures. For both pairs of tests the bar with the deeper embedment had a higher capacity. The edge bar with the larger embedment had 4% more capacity and the corner bar with the larger embedment had 14% more capacity. These differences can be attributed to experimental scatter.

Test ID	d_b (mm)	Nominal Head (mm)	C_1 (mm)	C_2 (mm)	h_d (mm)	f'_c (MPa)	P_U (kN)
C1B2	25	70x70x16	48	457	762	25	283
C1B3	25	70x70x16	48	457	508	25	272
C2B2	25	70x70x16	48	48	762	25	179
C2B4	25	70x70x16	48	48	508	25	157

Table 5.4 - Parameters and Results for Tests on Embedment Depth

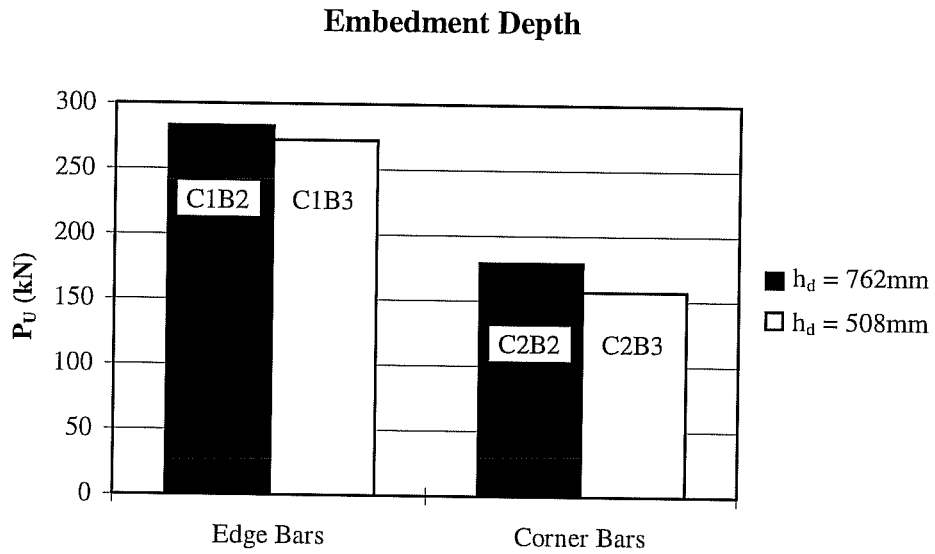


Figure 5.12 - Comparison of Capacities for Tests with Different Embedment Depths

5.5 Head Orientation

One of the major differences between the headed reinforcing bars in this study and anchor bolt tests reported in the literature was the shape of the head. The head on a cast-in-place headed anchor bolt is usually round. For the headed reinforcing bars of this study, the heads were square or rectangular. Since the shape of the head for anchor bolts was not a variable there is no data on effects of head shape and head orientation. To measure the effect of head orientation a series of tests was conducted on edge bars with rectangular heads. The series consisted of 6 pairs of tests with the only variable between the bars in each pair being the head orientation. The parameters for these tests are summarized in Table 5.5. All twelve tests resulted in side blowout failures.

The capacities from these pairs of tests are compared in Figure 5.13. For four of the six pairs there was less than 2% difference in the capacity of the anchorage. The maximum difference in capacity of 14% was observed in the pair of 20mm bars, C8B6 and C8B7. From these observations it was concluded that the head orientation had no effect on the capacity of the anchorage. All subsequent tests with rectangular heads were placed with the long side parallel with the face of the concrete ($h_1 < h_2$).

Test ID	d_b (mm)	Nominal Head (mm)	C_1 (mm)	C_2 (mm)	l_d (mm)	f'_c (MPa)	P_U (kN)
C3B1	35	100x55x25	51	457	0	29	285
C3B2	35	55x100x25	51	457	0	29	284
C3B3	35	100x55x25	64	457	0	29	330
C3B4	35	55x100x25	64	457	0	29	335
C5B1	35	100x55x25	64	457	305	21	474
C5B2	35	55x100x25	64	457	305	21	477
C5B3	35	100x55x25	64	457	610	21	526
C5B4	35	55x100x25	64	457	610	21	496
C7B3	35	100x55x25	102	457	0	24	460
C7B4	35	55x100x25	102	457	0	24	464
C8B6	20	70x35x16	45	457	0	24	177
C8B7	20	35x70x16	45	457	0	24	155

Table 5.5 - Parameters and Results of Tests with Different Head Orientation

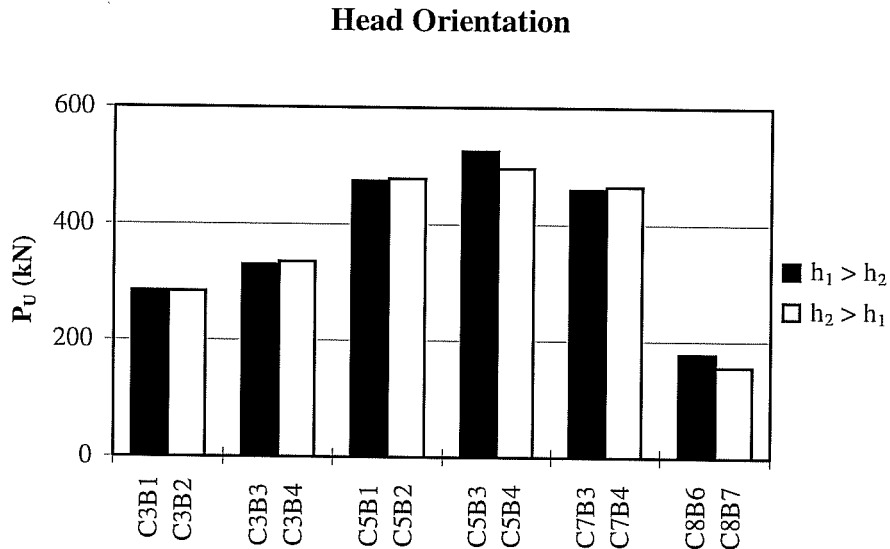


Figure 5.13 - Comparison of Capacities of Tests with Different Head Orientations

5.6 Transverse Reinforcement

In most applications of headed reinforcement in concrete members, it is likely there will be transverse reinforcement near the head. Since side blowout failure involves the tensile capacity of the concrete cover, transverse reinforcement should provide additional tensile strength and increase the capacity of the anchorage. Hasselwander [20] made a preliminary conclusion on the basis of two tests that transverse reinforcement did increase the side blowout strength of anchorage of anchor bolts with washers. Cote and Wallace [15] also concluded that transverse reinforcement would increase the side blowout anchorage capacity of headed reinforcement based on the results of three knee-joint tests.

Six different types of transverse ties were used to model different configurations of transverse reinforcement. The four types of ties tested for edge bars are shown in Figure 5.14 and the two types of ties used for corner bars are shown in Figure 5.15. The number of legs which provide a component (parallel to C_1 for edge bars or to C_1 or C_2 for corner bars) of tensile resistance across the concrete splitting failure plane are included in the figures. All tests in the series for transverse reinforcement had 305mm of development length and the ties were all located along this development length. The total area of transverse reinforcement

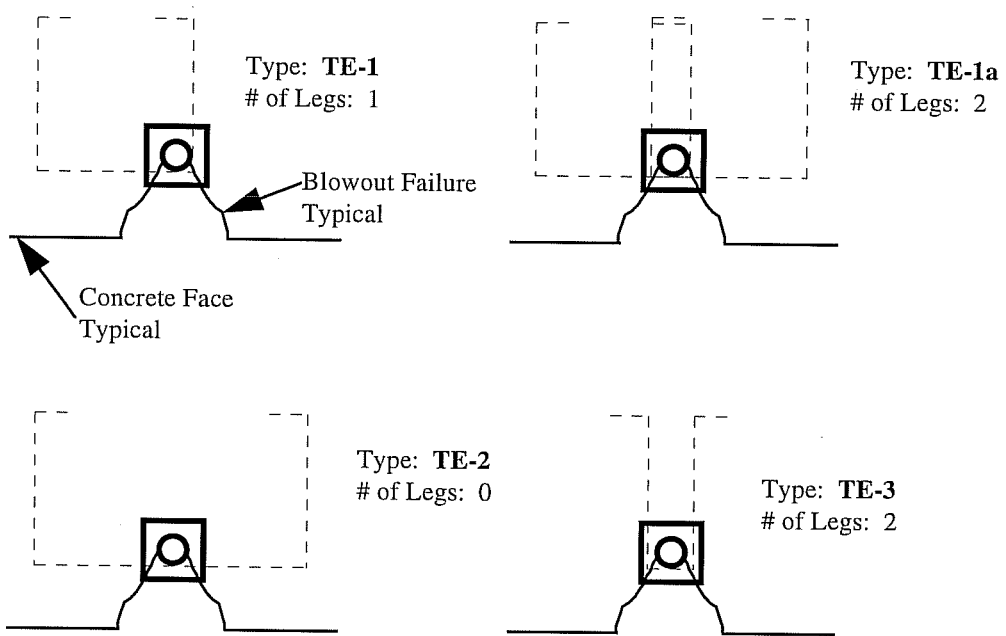


Figure 5.14 - Tie Configurations for Edge Bars

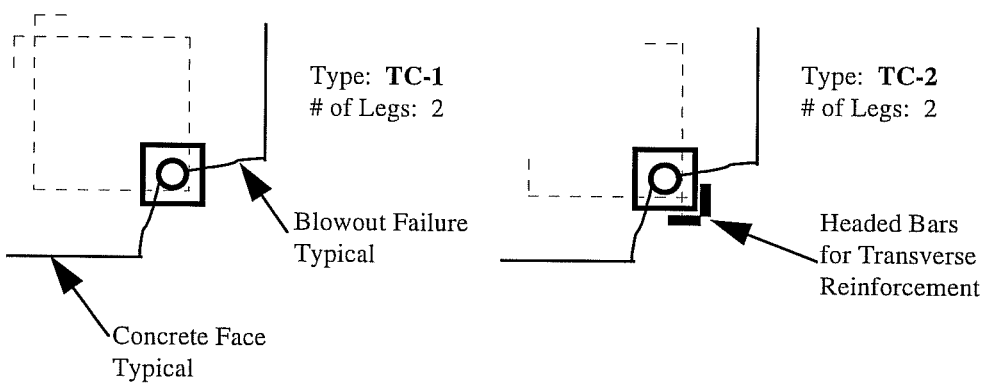


Figure 5.15 - Tie Configurations for Corner Bars

along the development length, A_{tr} , is calculated by multiplying the cross-sectional area of the tie bar by the number of legs and the number of ties.

A total of 27 bars, fourteen edge bars and thirteen corner bars, arranged in seven groups were tested. The type and amount of transverse reinforcement was varied. The parameters for these tests are summarized in Table 5.6. Three of the tests resulted in bearing failures, the parameters of these tests (C9B8, C12B2 and C12B4) are included in Table 5.6 for completeness. The results of the 24 tests resulting in blowout failures are summarized in Table 5.7. Included in Table 5.7 is a normalized capacity for each test, P_{UNI} , which takes into account variations in concrete strength, f'_c . The measured capacities, P_U , were normalized by:

$$P_{UNI} = P_U \left(\frac{\sqrt{27}}{\sqrt{f'_c}} \right) \quad \text{eq. 5.1}$$

where f'_c was the measured concrete strength on the day of testing.

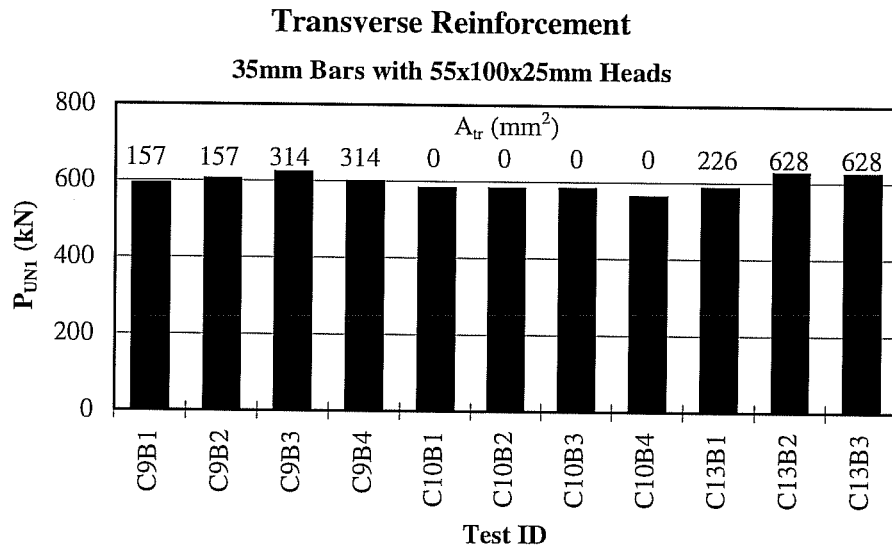
In Figure 5.16, the normalized results from 11 edge bar tests on 35mm bars with 55x100x25mm heads are compared. The transverse reinforcement provided had essentially no affect on the ultimate capacity in these tests. Results from the other tests with transverse reinforcement showed similar results. Neither the types or amount of transverse reinforcement significantly affected the ultimate capacity.

Test ID	d _b (mm)	Nominal Head (mm)	C ₁ (mm)	C ₂ (mm)	Transverse Reinforcement					
					Type	d _{btr} (mm)	Num.	S _{p1} (mm)	S _p (mm)	A _{tr} (mm ²)
C9B1	35	55x100x25	64	457	TE-1	10	2	102	102	157
C9B2	35	55x100x25	64	457	TE-1	10	2	51	102	157
C9B3	35	55x100x25	64	457	TE-1	10	4	51	51	314
C9B4	35	55x100x25	64	457	TE-1a	10	2	51	51	314
C10B1	35	55x100x25	64	457	None	0	0	0	0	0
C10B2	35	55x100x25	64	457	TE-2	10	2	102	102	0
C10B3	35	55x100x25	64	457	TE-2	10	2	51	102	0
C10B4	35	55x100x25	64	457	TE-2	10	2	51	51	0
C11B3	35	90x90x20	64	457	TE-1a	10	2	51	102	314
C11B4	35	90x90x20	64	457	TE-2	10	2	51	102	0
C13B1	35	55x100x25	64	457	TE-3	12	1	0	0	226
C13B2	35	55x100x25	64	457	TE-3	20	1	51	0	628
C13B3	35	55x100x25	64	457	TE-3	20	1	0	0	628
C13B4	35	90x90x20	64	457	TE-3	12	1	0	0	226
C9B5	25	70x70x16	61	61	None	0	0	0	0	0
C9B6	25	70x70x16	61	61	TC-1	10	2	102	102	314
C9B7	25	70x70x16	61	61	TC-1	10	2	51	102	314
C9B8	25	70x70x16	61	61	TC-1	10	4	51	51	628
C12B1	35	90x90x20	64	64	TC-1	12	1	0	0	226
C12B2	35	90x90x20	64	64	TC-1	20	1	0	0	628
C12B3	35	90x90x20	64	127	TC-1	20	1	0	0	628
C12B4	35	90x90x20	64	64	TC-2	20	1	0	0	628
C13B5	25	40x80x18	61	61	TC-1	20	1	51	0	628
C13B6	25	40x80x18	61	61	TC-1	20	1	0	0	628
C13B7	25	70x70x16	61	61	TC-1	20	1	0	0	628

Table 5.6 - Parameters for Tests with Transverse Reinforcement

Test ID	d_b (mm)	Nominal Head (mm)	C_1 (mm)	C_2 (mm)	Type	A_{tr} (mm ²)	f'_c (MPa)	P_U (kN)	P_{UN1} (kN)
C9B1	35	55x100x25	64	457	TE-1	157	27	591	591
C9B2	35	55x100x25	64	457	TE-1	157	27	604	604
C9B3	35	55x100x25	64	457	TE-1	314	27	621	621
C9B4	35	55x100x25	64	457	TE-1a	314	27	598	598
C10B1	35	55x100x25	64	457	None	0	27	581	581
C10B2	35	55x100x25	64	457	TE-2	0	27	581	581
C10B3	35	55x100x25	64	457	TE-2	0	27	583	583
C10B4	35	55x100x25	64	457	TE-2	0	27	564	564
C11B3	35	90x90x20	64	457	TE-1a	314	27	660	660
C11B4	35	90x90x20	64	457	TE-2	0	27	632	632
C13B1	35	55x100x25	64	457	TE-3	226	21	517	456
C13B2	35	55x100x25	64	457	TE-3	628	21	553	488
C13B3	35	55x100x25	64	457	TE-3	628	21	549	484
C13B4	35	90x90x20	64	457	TE-3	226	21	581	512
C9B5	25	70x70x16	61	61	None	0	27	263	263
C9B6	25	70x70x16	61	61	TC-1	314	27	301	301
C9B7	25	70x70x16	61	61	TC-1	314	27	298	298
C12B1	35	90x90x20	64	64	TC-1	226	21	404	356
C12B3	35	90x90x20	64	127	TC-1	628	21	496	437
C13B5	25	40x80x18	61	61	TC-1	628	21	234	206
C13B6	25	40x80x18	61	61	TC-1	628	21	273	241
C13B7	25	70x70x16	61	61	TC-1	628	21	278	245

Table 5.7 - Results from Tests with Transverse Reinforcement

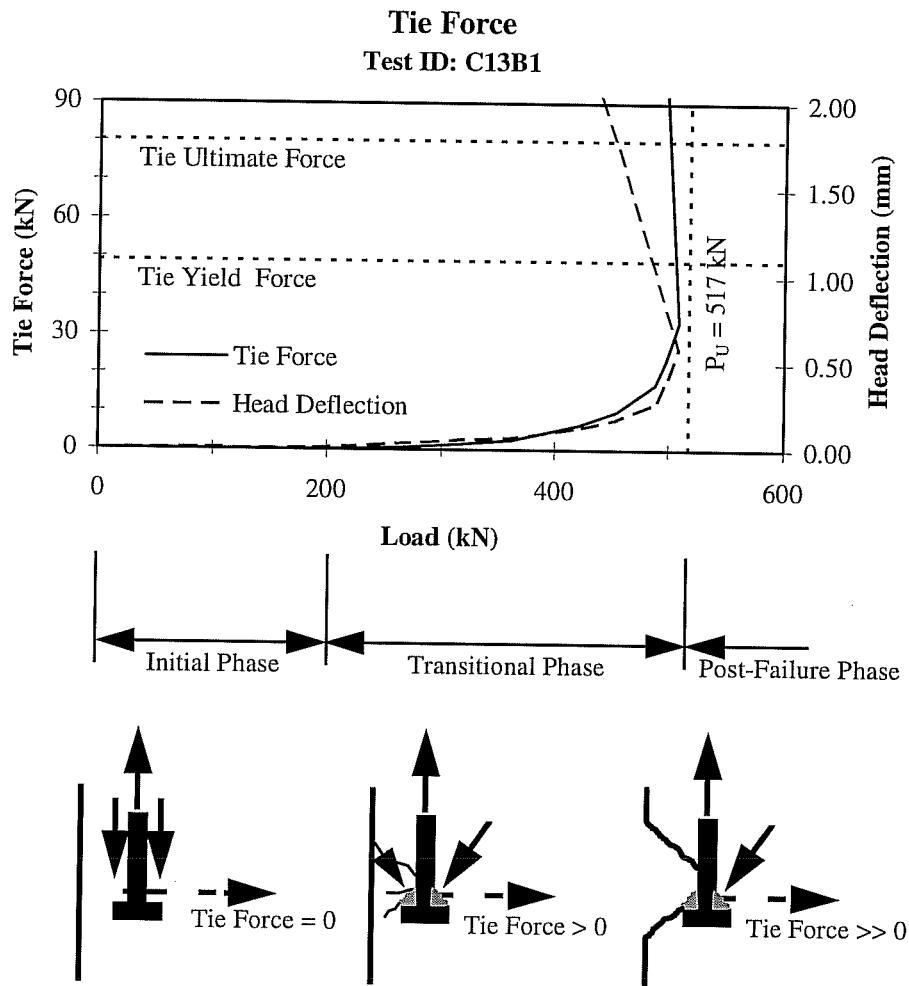


Test ID	d_b (mm)	Nominal Head (mm)	C_1 (mm)	C_2 (mm)	l_d (mm)	Trans. Reinf.	f'_c (MPa)	P_U (kN)	P_{U1} (kN)
C9B1	35	55x100x25	64	457	305	TE-1	27	591	591
C9B2	35	55x100x25	64	457	305	TE-1	27	604	604
C9B3	35	55x100x25	64	457	305	TE-1	27	621	621
C9B4	35	55x100x25	64	457	305	TE-1a	27	598	598
C10B1	35	55x100x25	64	457	305	None	27	581	581
C10B2	35	55x100x25	64	457	305	TE-2	27	581	581
C10B3	35	55x100x25	64	457	305	TE-2	27	583	583
C10B4	35	55x100x25	64	457	305	TE-2	27	564	564
C13B1	35	55x100x25	64	457	305	TE-3	21	517	586
C13B2	35	55x100x25	64	457	305	TE-3	21	553	627
C13B3	35	55x100x25	64	457	305	TE-3	21	549	623

Figure 5.16 - Comparison of Capacities of Tests with Transverse Reinforcement

The main influence of transverse reinforcement was on the residual strength after failure. For bars with no transverse reinforcement, the capacity of the anchorage dropped to less than 30% of the ultimate capacity after blowout failure occurred and continued to decline with increased displacement. Similar behavior was observed for bars with transverse reinforcement placed away from the head. For bars with a large amount of transverse reinforcement placed near the head, the strength of the anchorage did not decrease as precipitously at failure and dropped only after large head displacements. A few of the tests retained 80% of the ultimate capacity at very large amounts of head slip. The residual strength was maintained until the ties fractured.

Strain gauges were placed on several transverse ties. In Figure 5.17, the tie force calculated from the measured strains using a modulus of 200,000 MPa for one test is shown along with the head deflection of the test. During the initial loading both the tie force and head deflection were essentially zero, suggesting that the compression and tension struts were parallel making the perpendicular tie force zero. As the loading increased both the tie force and head deflection began to increase. Based on this observation, as the wedge of concrete formed on the head, cracks may have begun to form in the cover around the head and the head moved outward due to the bearing of the wedge on the interior concrete, mobilizing the tie. As the load neared ultimate, both the head deflection and tie



Test ID	d_b (mm)	Nominal Head (mm)	C_1 (mm)	C_2 (mm)	l_d (mm)	Trans. Reinf.	f'_c (MPa)	P_U (kN)
C13B1	35	55x100x25	64	457	305	TE-3	21	517

Figure 5.17 - Comparison of Tie Force with Head Deflection

force increased rapidly. Also at ultimate, the cover spalled off and the head moved outward with only the tie restraining it, mobilizing the tie further. After failure the tie force held the head and wedge against the remaining concrete, providing anchorage until the tie fractured.

Based on results from these tests, transverse reinforcement did not contribute to the ultimate capacity of the anchorage. The ductility (maintaining load after failure through large deflections) of the anchorage was increased by placing a large amount of transverse reinforcement (A_{tr} approximately 50% of the bar area) near the head.

5.7 Development Length

One major difference between headed reinforcement and anchor bolts is the presence of deformations along the length of the headed reinforcing bar. Bearing of the lugs on the surrounding concrete along the available development length may provide additional capacity. It is unclear how the two modes, head bearing and lug bearing, will interact. A total of eleven tests resulting in blowout failures were conducted with varying development lengths. In addition to these tests, all the tests with transverse reinforcement included development length.

The eleven bars, six edge bars and five corner bars, were divided into five groups with the only variable among bars within a group being development

length. The parameters for these tests are summarized in Table 5.8. The capacities of the 11 tests are compared in Figure 5.18. In general, the results of these tests show a slight increase in capacity with increased development length.

Six tests with development length and transverse reinforcement were instrumented with strain gauges located on the bar near the head. The forces in a bar determined from strain measurements are plotted against the applied load in Figure 5.19. Since the gauge is located near the head, the vertical axis represents the portion of the total load carried by the head. The diagonal line represents the force carried by the head if there were no development length, that is, the total load on the bar. Under initial loading, the force carried by the head is very small and nearly all the force is being transferred along the development length. As the load increases the head carries an increasing portion of the load. The cracking behavior observed indicates that radial stresses develop along the development length. During loading, a single crack formed at the beginning of the development length and propagated down to the head. As this crack opened, the development strength along the bar degraded and the portion of bar force carried by the head increased. At failure the development length carried approximately 33% of the total load based on data from six tests with strain gauges near the head.

Test ID	d_b (mm)	Nominal Head (mm)	C_1 (mm)	C_2 (mm)	l_d (mm)	f'_c (MPa)	P_U (kN)
C5B1	35	100x55x25	64	457	305	21	474
C5B3	35	100x55x25	64	457	610	21	526
C5B2	35	55x100x25	64	457	305	21	477
C5B4	35	55x100x25	64	457	610	21	496
C6B3	35	90x90x20	76	457	305	21	562
C6B4	35	90x90x20	76	457	610	21	613
C5B5	20	50x50x12	38	38	0	21	67
C5B6	20	50x50x12	38	38	152	21	105
C6B5	25	40x80x18	45	66	152	21	147
C6B6	25	40x80x18	45	66	305	21	192
C6B7	25	40x80x18	45	66	457	21	179

Table 5.8 - Parameters and Results of Tests with Development Length

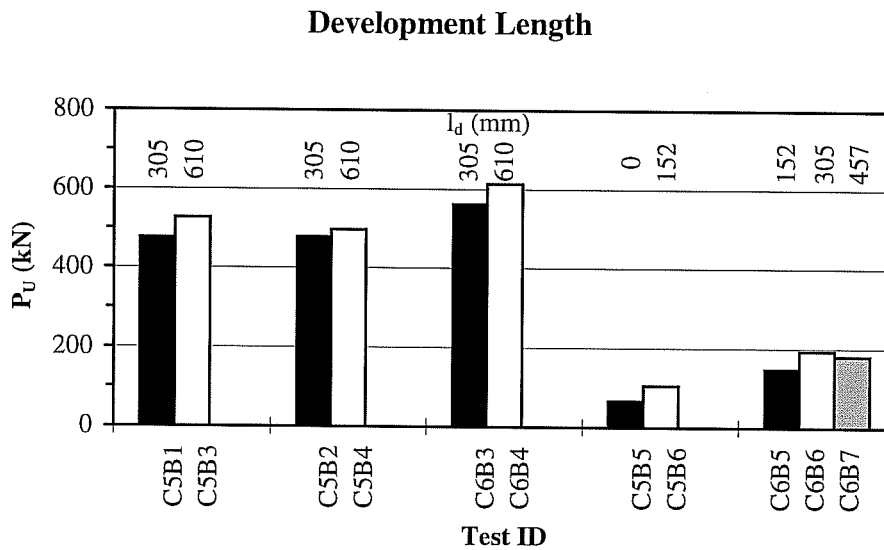
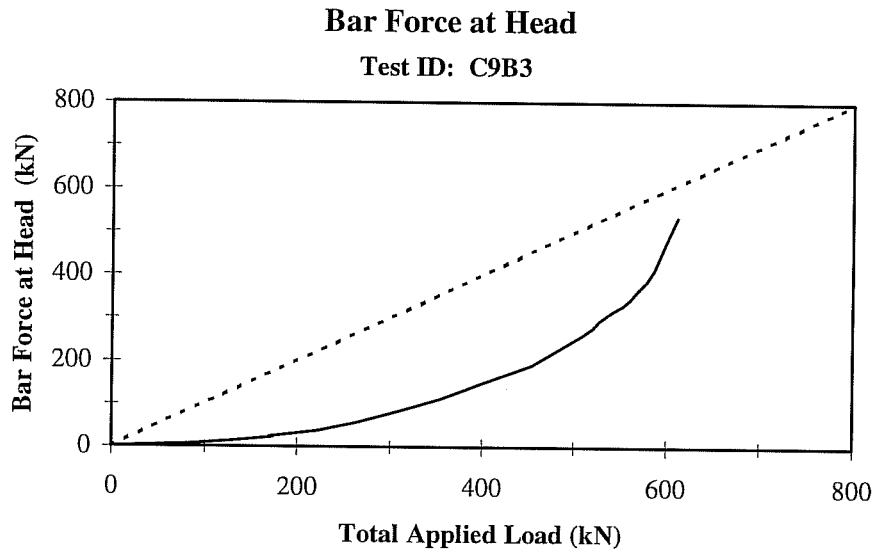


Figure 5.18 - Comparison of Capacities of Tests with Development Length



Test ID	d_b (mm)	Nominal Head (mm)	C_1 (mm)	C_2 (mm)	l_d (mm)	Trans. Reinf.	f'_c (MPa)	P_U (kN)
C9B3	35	55x100x25	64	457	305	TE-1	27	621

Figure 5.19 - Bar Force at Head versus Total Bar Load

After reviewing many studies on development length, Orangun [39] proposed the following equation for average bond stress along development length with all terms in customary US units:

$$\mu = \left[1.2 + \frac{3C_{C1}}{d_b} + \frac{50d_b}{l_d} + \frac{A_{tr}f_{yt}}{500sd_b} \right] \sqrt{f'_c} \quad \text{eq. 5.2}$$

where d_b is the bar diameter, C_{C1} the minimum clear cover, l_d the development length, A_{tr} the area of transverse reinforcement, f_{yt} the yield stress of the transverse reinforcement, s the spacing of transverse reinforcement and f'_c the concrete compressive strength. Orangun's equation takes into account the effect

of spacing, cover and transverse reinforcement. Once the average bond stress is known the development force can be calculated by multiplying the average bond stress by the surface area of the bar along the development length.

$$F_{ld} = \mu l_d \pi d_b \quad \text{eq. 5.3}$$

The measured ultimate capacity and the predicted bond force from Equation 5.3 for pairs of tests with the only variable being development length or amount of transverse reinforcement are tabulated in Table 5.9. The differences between the measured loads and predicted bond force are also listed. To calculate the predicted bond force for tests with transverse reinforcement, the spacing of the ties was taken to be the development length divided by the number of ties. For each pair a predicted capacity, P_{UP1} , was calculated by adding the difference between the two predicted development forces to the measured capacity of the first test:

$$P_{UP1} = P_{U1} + (F_{ld2} - F_{ld1}) \quad \text{eq. 5.4}$$

This value, P_{UP1} , was compared with the measured capacity of the second test. Statistical measures of the comparison are included on Table 5.9. The Orangun equation accurately predicted the increase in capacity for tests with varying development length.

Test ID 1	P _{U1}	F _{ld1}	Test ID 2	P _{U2}	F _{ld2}	P _{U2} -P _{U1}	F _{ld2} -F _{ld1}	P _{UP1}	P _{U2} /P _{UP1}
	(kN)	(kN)		(kN)	(kN)	(kN)	(kN)	(kN)	
C5B1	474	139	C5B3	526	206	52	66	540	0.97
C5B1	474	139	C5B4	496	206	22	66	540	0.92
C5B2	477	139	C5B3	526	206	49	66	543	0.97
C5B2	477	139	C5B4	496	206	19	66	543	0.91
C6B3	562	153	C6B4	613	232	51	79	641	0.96
C9B1	591	209	C9B2	604	209	13	0	591	1.02
C9B1	591	209	C9B3	621	363	30	153	744	0.83
C9B1	591	209	C9B4	598	260	7	51	642	0.93
C9B2	604	209	C9B3	621	363	17	153	757	0.82
C9B4	598	260	C9B2	604	209	6	-51	547	1.10
C9B4	598	260	C9B3	621	363	23	102	700	0.89
C10B1	581	158	C10B2	581	158	0	0	581	1.00
C10B1	581	158	C10B3	583	158	2	0	581	1.00
C10B2	581	158	C10B3	583	158	2	0	581	1.00
C10B4	564	158	C10B1	581	158	17	0	564	1.03
C10B4	564	158	C10B2	581	158	17	0	564	1.03
C10B4	564	158	C10B3	583	158	19	0	564	1.03
C11B4	632	158	C11B3	660	260	28	102	734	0.90
C13B1	517	172	C13B2	553	230	36	58	575	0.96
C13B1	517	172	C13B3	549	230	32	58	575	0.96
C13B1	517	172	C13B4	581	172	64	0	517	1.12
C13B2	553	230	C13B4	581	172	28	-58	495	1.17
C13B3	549	230	C13B2	553	230	4	0	549	1.01
C13B3	549	230	C13B4	581	172	32	-58	491	1.18
C5B5	67	0	C5B6	105	44	38	44	111	0.95
C6B5	147	61	C6B6	192	84	45	23	170	1.13
C6B5	147	61	C6B7	179	107	32	47	194	0.92
C6B7	179	107	C6B6	192	84	13	-23	156	1.23

Table 5.9 - Predicted Anchorage Capacity based on Orangun's Equation

Test ID 1	P _{U1}	F _{ld1}	Test ID 2	P _{U2}	F _{ld2}	P _{U2} -P _{U1}	F _{ld2} -F _{ld1}	P _{UP1}	P _{U2} /P _{UP1}
	(kN)	(kN)		(kN)	(kN)	(kN)	(kN)	(kN)	
C9B5	263	115	C9B6	301	217	38	102	365	0.82
C9B5	263	115	C9B7	298	217	35	102	365	0.82
C9B7	298	217	C9B6	301	217	3	0	298	1.01
C12B1	404	195	C12B3	496	260	92	65	469	1.06
C13B5	234	192	C13B6	273	192	39	0	234	1.17
C13B5	234	192	C13B7	278	192	44	0	234	1.19
C13B6	273	192	C13B7	278	192	5	0	273	1.02

Maximum	1.23
Minimum	0.82
Average	1.00
Standard Deviation	0.11

Table 5.9 - Continued

The current ACI 318-95 [1] provisions for development length reflect the approach of Orangun's equation. Section 12.2.3 contains Equation 12-1 with all terms in customary US units:

$$\frac{l_d}{d_b} = \frac{3 f_y}{40 \sqrt{f'_c}} \frac{\alpha\beta\gamma\lambda}{\left(\frac{c + K_{tr}}{d_b} \right)} \quad \text{eq. 5.5}$$

where l_d is the development length, d_b the bar diameter, f_y the yield stress of the reinforcing, f'_c the concrete strength and c the smallest clear cover. The terms α , β , γ and λ are factors for reinforcement location, bar coating, reinforcement size and lightweight aggregate concrete, respectively. For this study of headed reinforcement all four factors are 1.0. K_{tr} is a transverse reinforcement index. The development length from Equation 5.5 is the length required to reach the

Test ID 1	P _{U1}	F _{ld1}	Test ID 2	P _{U2}	F _{ld2}	P _{U2} -P _{U1}	F _{ld2} -F _{ld1}	P _{UP1}	P _{U2} /P _{UP1}
	(kN)	(kN)		(kN)	(kN)	(kN)	(kN)	(kN)	
C5B1	474	57	C5B3	526	113	52	57	531	0.99
C5B1	474	57	C5B4	496	113	22	57	531	0.93
C5B2	477	57	C5B3	526	113	49	57	534	0.99
C5B2	477	57	C5B4	496	113	19	57	534	0.93
C6B3	562	71	C6B4	613	142	51	71	633	0.97
C9B1	591	93	C9B2	604	93	13	0	591	1.02
C9B1	591	93	C9B3	621	121	30	28	619	1.00
C9B1	591	93	C9B4	598	121	7	28	619	0.97
C9B2	604	93	C9B3	621	121	17	28	632	0.98
C9B4	598	121	C9B2	604	93	6	-28	570	1.06
C9B4	598	121	C9B3	621	121	23	0	598	1.04
C10B1	581	64	C10B2	581	64	0	0	581	1.00
C10B1	581	64	C10B3	583	64	2	0	581	1.00
C10B2	581	64	C10B3	583	64	2	0	581	1.00
C10B4	564	64	C10B1	581	64	17	0	564	1.03
C10B4	564	64	C10B2	581	64	17	0	564	1.03
C10B4	564	64	C10B3	583	64	19	0	564	1.03
C11B4	632	64	C11B3	660	121	28	57	689	0.96
C13B1	517	93	C13B2	553	106	36	14	531	1.04
C13B1	517	93	C13B3	549	106	32	14	531	1.03
C13B1	517	93	C13B4	581	93	64	0	517	1.12
C13B2	553	106	C13B4	581	93	28	-14	539	1.08
C13B3	549	106	C13B2	553	106	4	0	549	1.01
C13B3	549	106	C13B4	581	93	32	-14	535	1.09
C5B5	67	0	C5B6	105	17	38	17	84	1.25
C6B5	147	20	C6B6	192	40	45	20	167	1.15
C6B5	147	20	C6B7	179	59	32	40	187	0.96
C6B7	179	59	C6B6	192	40	13	-20	159	1.21

Table 5.10 - Predicted Anchorage Capacities based on ACI Provisions for Development Length

yield force in the bar. Assuming a linear relationship, the bond force for other development lengths can be calculated by:

$$F_{ld} = \frac{l_d}{l_{dACI}} F_y \quad \text{eq 5.6}$$

where l_d is the development length provided, l_{dACI} the development length from Equation 5.5 and F_y the yield force of the bar.

The analysis that led to Table 5.9 was repeated except the predicted bond force is based on the ACI provisions and Equation 5.6. The results are listed in Table 5.10. As with the Orangun equation, the ACI provisions accurately predict the increase in capacity from development length.

5.8 Head Geometry

The heads on studs and anchor bolts are usually made by upsetting the end of the bar. Because of the manufacturing process, the head is circular or hexagonal and the total area of the head is limited to approximately three times the bolt area. The manufacturing process for headed reinforcement allows many different shapes or sizes of heads to be attached to a reinforcing bar. Flexibility in the shape and size can be useful during construction. For example, if only round heads are available then the closest possible spacing is controlled by the diameter of the head. Using rectangular heads allow closer spacing while providing the

Test ID 1	P_{U1}	F_{ld1}	Test ID 2	P_{U2}	F_{ld2}	$P_{U2}-P_{U1}$	$F_{ld2}-F_{ld1}$	P_{UP1}	P_{U2}/P_{UP1}
	(kN)	(kN)		(kN)	(kN)	(kN)	(kN)	(kN)	
C9B5	263	67	C9B6	301	86	38	19	282	1.07
C9B5	263	67	C9B7	298	86	35	19	282	1.06
C9B7	298	86	C9B6	301	86	3	0	298	1.01
C12B1	404	105	C12B3	496	121	92	16	420	1.18
C13B5	234	76	C13B6	273	76	39	0	234	1.17
C13B5	234	76	C13B7	278	76	44	0	234	1.19
C13B6	273	76	C13B7	278	76	5	0	273	1.02

Maximum 1.25
Minimum 0.93
Average 1.05
Standard Deviation 0.08

Table 5.10 - Continued

same bearing area. In the construction of offshore platforms, reinforcing bars with rectangular heads are used because of the close spacing required between bars. In typical concrete members, rectangular heads can be used to place bars near a face to help control cracking and still provide cover over the head (Figure 5.20). Also, the thickness of the head can be adjusted for headed reinforcement. The head can be between a thin flexible or a thick rigid plate. The optimum thickness provides the desired performance using the least material.

Since previous studies on studs and anchor bolts have not reported effects of head geometry, a series of tests was conducted in which head geometry (head area, head aspect ratio, head shape and head thickness) was varied. A total of 28 tests were conducted on edge bars. All tests in this series had no development length or transverse reinforcement. The specimens were constructed and tested at

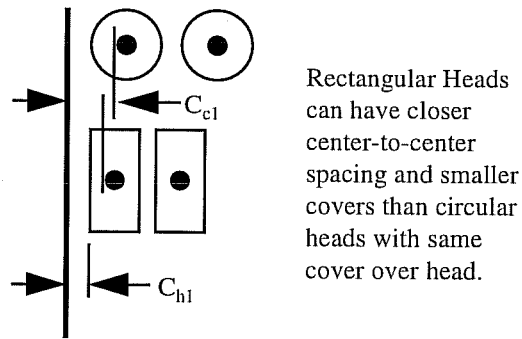


Figure 5.20 - Comparison of Spacing for Circular and Rectangular Heads

the same time so the concrete strength was the same for all tests. Both 25mm and 35mm diameter bars were tested and the edge distance, C_1 , was constant. The parameters and results for the 28 tests are summarized in Table 5.11. All but one test resulted in a side-blowout failure.

The head sizes and shapes were altered by using band saws to cut the length and width of the heads to the desired size. A lathe and cutting tool were used to cut the thickness down to the desired size. These methods were not perfectly accurate so the final head dimensions were measured before placing the bars in concrete. In Table 5.12, the nominal and actual head dimensions and geometric properties are listed. Two tests, C17B11 and C17B12, had octagonal heads to simulate circular heads and are denoted with an asterisk. The head dimensions listed for these two tests represent the out-to-out dimension of the head, L . The listed dimensions and equations for the various geometric properties are shown in Figure 5.21.

4.7 Conclusion

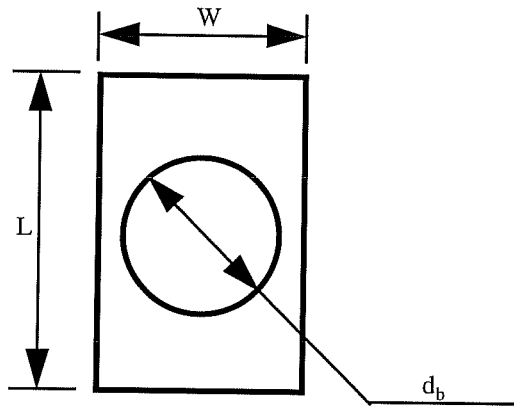
The Concrete Capacity Design method for the pullout capacity of anchor bolts can also be used to predict the pullout capacity of headed reinforcement. The CCD method is based on tests of anchor bolts. To take into account the larger heads typical of headed reinforcement, the assumed failure area should be based on the perimeter of the head, assuming the head has adequate stiffness.

Test ID	d_b (mm)	Nominal Head (mm)	C_1 (mm)	C_2 (mm)	l_d (mm)	f_c (MPa)	P_U (kN)
C15B1	35	57x57x16	45	305	0	19	162
C15B2	35	40x80x16	45	305	0	19	185
C15B3	35	70x70x16	45	305	0	19	221
C15B4	35	49x99x16	45	305	0	19	217
C15B5	35	55x100x25	45	305	0	19	194
C15B6	35	80x80x16	45	305	0	19	283
C15B7	35	90x90x16	45	305	0	19	374
C15B8	35	90x90x20	45	305	0	19	#N/A
C16B1	25	33x33x16	45	305	0	19	93
C16B2	25	57x57x12	45	305	0	19	154
C16B3	25	57x57x16	45	305	0	19	168
C16B4	25	57x57x20	45	305	0	19	176
C16B5	25	40x80x12	45	305	0	19	162
C16B6	25	40x80x16	45	305	0	19	163
C16B7	25	40x80x18	45	305	0	19	180
C16B8	25	40x80x20	45	305	0	19	149
C17B1	25	33x98x12	45	305	0	19	144
C17B2	25	33x98x16	45	305	0	19	165
C17B3	25	33x98x20	45	305	0	19	199
C17B4	25	70x70x12	45	305	0	19	238
C17B5	25	70x70x16	45	305	0	19	235
C17B6	25	70x70x20	45	305	0	19	222
C17B7	25	49x99x16	45	305	0	19	222
C17B8	25	55x100x25	45	305	0	19	233
C17B9	25	80x80x12	45	305	0	19	285
C17B10	25	80x80x16	45	305	0	19	331
C17B11*	25	70x70x16	45	305	0	19	183
C17B12*	25	77x77x16	45	305	0	19	193

Table 5.11 - Parameters and Results of Tests on Head Geometry

Test ID	d _b (mm)	Nominal Head (mm)	Actual Head (mm)	Nominal			Actual		
				A _h (mm ²)	S _x (mm ³)	I _x (mm ⁴)	A _h (mm ²)	S _x (mm ³)	I _x (mm ⁴)
C15B1	35	57x57x16	54x54x16	3200	2432	19456	2916	2304	18432
C15B2	35	40x80x16	38x78x16	3200	1707	13653	2964	1621	12971
C15B3	35	70x70x16	68x68x16	4900	2987	23893	4624	2901	23211
C15B4	35	49x99x16	46x100x16	4900	2091	16725	4600	1963	15701
C15B5	35	55x100x25	55x100x25	5500	5729	71615	5500	5729	71615
C15B6	35	80x80x16	78x77x16	6400	3413	27307	6006	3285	26283
C15B7	35	90x90x16	90x90x16	8100	3840	30720	8100	3840	30720
C15B8	35	90x90x20	90x90x20	8100	6000	60000	8100	6000	60000
C16B1	25	33x33x16	32x30x19	1100	1408	11264	960	1805	17148
C16B2	25	57x57x12	55x54x11	3200	1368	8208	2970	1089	5990
C16B3	25	57x57x16	55x54x16	3200	2432	19456	2970	2304	18432
C16B4	25	57x57x20	56x55x20	3200	3800	38000	3080	3667	36667
C16B5	25	40x80x12	40x80x12	3200	960	5760	3200	960	5760
C16B6	25	40x80x16	40x80x17	3200	1707	13653	3200	1927	16377
C16B7	25	40x80x18	40x80x18	3200	2160	19440	3200	2160	19440
C16B8	25	40x80x20	38x78x20	3200	2667	26667	2964	2533	25333
C17B1	25	33x98x12	31x100x13	3200	792	4752	3100	873	5676
C17B2	25	33x98x16	34x100x16	3200	1408	11264	3400	1451	11605
C17B3	25	33x98x20	32x100x19	3200	2200	22000	3200	1925	18291
C17B4	25	70x70x12	70x70x12	4900	1680	10080	4900	1680	10080
C17B5	25	70x70x16	70x70x16	4900	2987	23893	4900	2987	23893
C17B6	25	70x70x20	69x66x20	4900	4667	46667	4554	4400	44000
C17B7	25	49x99x16	49x100x16	4900	2091	16725	4900	2091	16725
C17B8	25	55x100x25	55x100x25	5500	5729	71615	5500	5729	71615
C17B9	25	80x80x12	79x79x12	6400	1920	11520	6241	1896	11376
C17B10	25	80x80x16	78x78x15	6400	3413	27307	6084	2925	21938
C17B11*	25	70x70x16	67x67x16	4100	2987	23893	3719	2859	22869
C17B12*	25	77x77x16	75x75x16	4900	3285	26283	4660	3200	25600

Table 5.12 - Nominal and Actual Head Sizes for Tests on Head Geometry

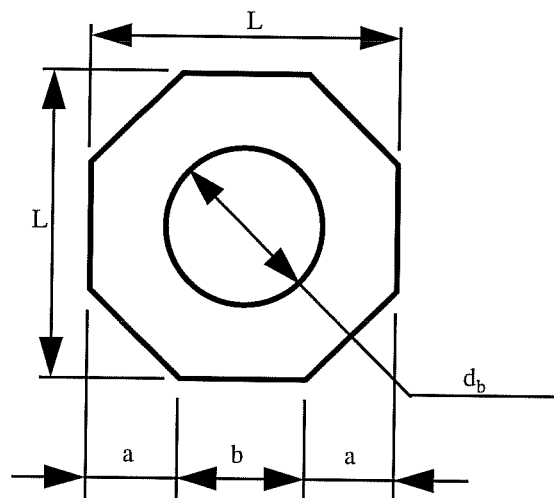


$$L > W$$

$$A_h = LW$$

$$S_x = \frac{Wt^2}{6}$$

$$I_x = \frac{Wt^3}{12}$$



$$b + 2a = L$$

$$\sqrt{2}a = b$$

$$a = \frac{L}{2 + \sqrt{2}}$$

$$b = \frac{L}{1 + \sqrt{2}}$$

$$A_h = \left(\frac{2 + 2\sqrt{2}}{3 + 2\sqrt{2}} \right) L^2$$

$$S_x = \frac{Lt^2}{6}$$

$$I_x = \frac{Lt^3}{12}$$

Figure 5.21 - Head Dimensions and Geometric Properties

Head Area

The total head area was varied from a minimum of two times the bar area to a maximum of thirteen times the bar area. The minimum head size is typical of a headed stud while the maximum size represents an upper limit of the expected sizes for headed reinforcement. The measured capacities of the tests are plotted against the actual total head area in Figure 5.22 for the 27 tests resulting in side-blowout failures. The general trend is for increasing load with increasing head area. The relationship between capacity and head area for these tests appears to be linear with the capacity being in direct proportion to the head area.

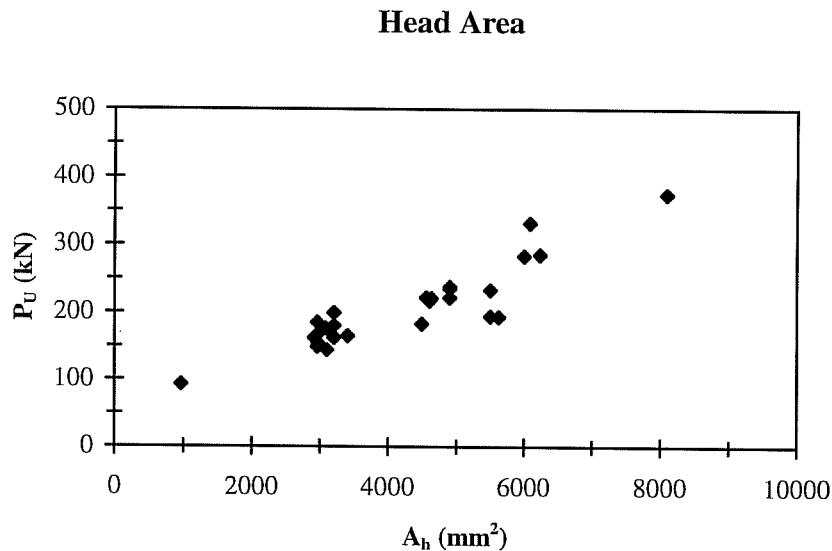


Figure 5.22 - Comparison of Capacities with Head Area

Head Aspect Ratio

Fifteen of the 27 tests in this series were arranged into six groups with the only variable between tests in each group being the aspect ratio of the head. The parameters and results for these 15 tests are listed in Table 5.13. Included in this table is a normalized capacity, P_{UN2} , to account for slight differences in head area among the tests of each group. P_{UN2} is calculated by dividing the measured capacity, P_U , by the actual head area and multiplying by the nominal head area:

$$P_{UN2} = P_U \left(\frac{A_{h(Nominal)}}{A_{h(Actual)}} \right) \quad \text{eq. 5.7}$$

this equation is based on the previous observation that the capacity seems to be directly proportional with head area. The normalized capacities of these tests are compared in Figure 5.23 and show no clear relationship between aspect ratio and capacity.

Head Shape

To compare the efficiency of square and rectangular heads with circular heads two octagonal heads were tested. It is possible the corners of square heads may not be utilized in bearing and be wasted material. Results from the tests with rectangular heads showed the concrete wedge forming on the entire head and not on a circle inscribed within the perimeter of the head which suggested that the corners were utilized and the head shape did not matter.

Nominal A_h (mm ²)	Test ID	Nominal Head (mm)	Nominal Aspect Ratio	P_U (kN)	P_{UN2} (kN)
3200	C15B1	57x57x16	1:1	162	178
	C15B2	40x80x16	2:1	185	200
3200	C16B2	57x57x12	1:1	154	166
	C16B5	40x80x12	2:1	162	162
	C17B1	33x98x12	3:1	144	149
3200	C16B3	57x57x16	1:1	168	181
	C16B6	40x80x16	2:1	163	163
	C17B2	33x98x16	3:1	165	155
3200	C16B4	57x57x20	1:1	176	183
	C16B7	40x80x20	2:1	149	149
	C17B3	33x98x20	3:1	199	199
4900	C15B3	70x70x16	1:1	221	221
	C15B4	49x99x16	2:1	217	231
4900	C17B5	70x70x16	1:1	235	235
	C17B7	49x99x16	2:1	222	222

Table 5.13 - Parameters and Results for Tests on Head Aspect Ratio

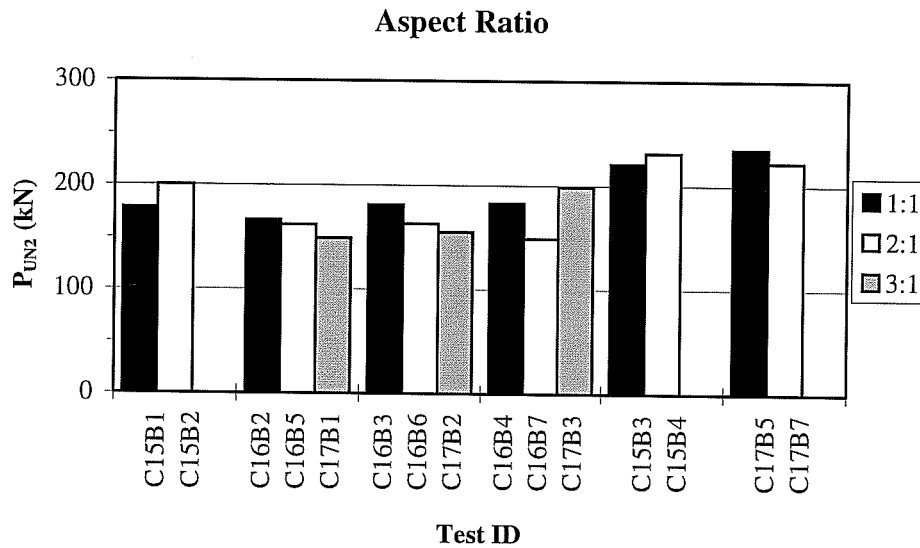


Figure 5.23 - Comparison of Capacities for Tests on Head Aspect Ratio

To determine the effect of head shape, the results of three tests were compared; one test with a square head and two tests with octagonal heads. The octagon was chosen, since it was an easily fabricated shape that approximated a circle. One octagonal head was designed so that it would have the same out-to-out dimensions as the square head and the second so it would have the same area as the square head. The parameters and results are summarized in Table 5.14. Listed in this table are the measured ultimate capacity, P_U , and a normalized capacity P_{UN3} . P_{UN3} is a normalization of the measured capacities with respect to the actual head area and the head area of the square head, 4900mm²:

$$P_{UN3} = P_U \left(\frac{4900}{A_{h(Actual)}} \right) \quad \text{eq 5.8}$$

In Figure 5.24, the normalized capacities for these three tests are compared. There appears to be no effect on capacity due to head shape. There is a 15% difference between the high and low normalized capacities, but this is within normal scatter for concrete testing.

Test ID	d_b (mm)	Nominal Head (mm)	Actual Head (mm)	Nominal A_h (mm ²)	Actual A_h (mm ²)	P_U (kN)	P_{UN3} (kN)
C17B5	25	70x70x16	70x70x16	4900	4900	235	235
C17B11*	25	70x70x16	67x67x16	4100	3719	183	241
C17B12*	25	77x77x16	75x75x16	4900	4660	193	203

Table 5.14 - Parameters and Results for Tests on Head Shape

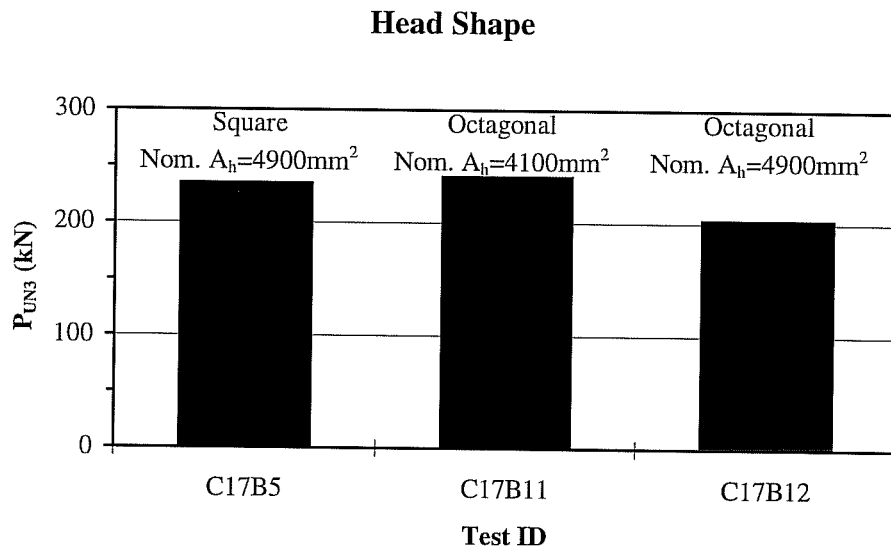


Figure 5.24 - Comparison of Capacities of Tests on Head Shape

Head Thickness

Providing a head with more thickness than necessary results in a waste of material. Also attaching a very large head with inadequate thickness may produce a head where only a small portion of the head area effectively resists the load. Before testing it was assumed that the head thickness should be designed to avoid yielding of the head steel. It was also assumed that once a head thickness was determined to avoid yielding, further increase in the thickness would not increase the capacity of the anchorage.

Fifteen of the 27 tests can be arranged into five groups, with two to four tests in each group where the only variable between tests in a group is the head thickness. The parameters, results and results normalized with respect to the nominal area, P_{UN2} (see Equation 5.7), for the 15 tests are summarized in Table 5.15. The normalized capacities are compared in Figure 5.25. In general there is very little difference in the normalized capacities with respect to head thickness for each group.

In addition to measuring the load and deflection of the headed reinforcement, gauges were placed on the heads to measure the strain in the heads. Gauges were on the bottom of the heads at one, two or four of the positions shown in Figure 5.26. The gauges were meant to be placed at the face of the bar; however, accurate placement was difficult when attaching the gauges. The final

Test ID	d _b (mm)	Nominal Head (mm)	Actual			P _U (kN)	P _{UN2} (kN)
			Head (mm)	A _h (mm ²)	S _x (mm ³)		
C16B2	25	57x57x12	55x54x11	2970	1089	154	166
C16B3	25	57x57x16	55x54x16	2970	2304	168	181
C16B4	25	57x57x20	56x55x20	3080	3667	176	183
C16B5	25	40x80x12	40x80x12	3200	960	162	162
C16B6	25	40x80x16	40x80x17	3200	1927	163	163
C16B7	25	40x80x18	40x80x18	3200	2160	180	180
C16B8	25	40x80x20	38x78x20	2964	2533	149	161
C17B1	25	33x98x12	31x100x13	3100	873	144	149
C17B2	25	33x98x16	34x100x16	3400	1451	165	155
C17B3	25	33x98x20	32x100x19	3200	1925	199	199
C17B4	25	70x70x12	70x70x12	4900	1680	238	238
C17B5	25	70x70x16	70x70x16	4900	2987	235	235
C17B6	25	70x70x20	69x66x20	4554	4400	222	239
C17B9	25	80x80x12	79x79x12	6241	1896	285	292
C17B10	25	80x80x16	78x78x15	6084	2925	331	348

Table 5.15 - Parameters and Results for Tests on Head Thickness

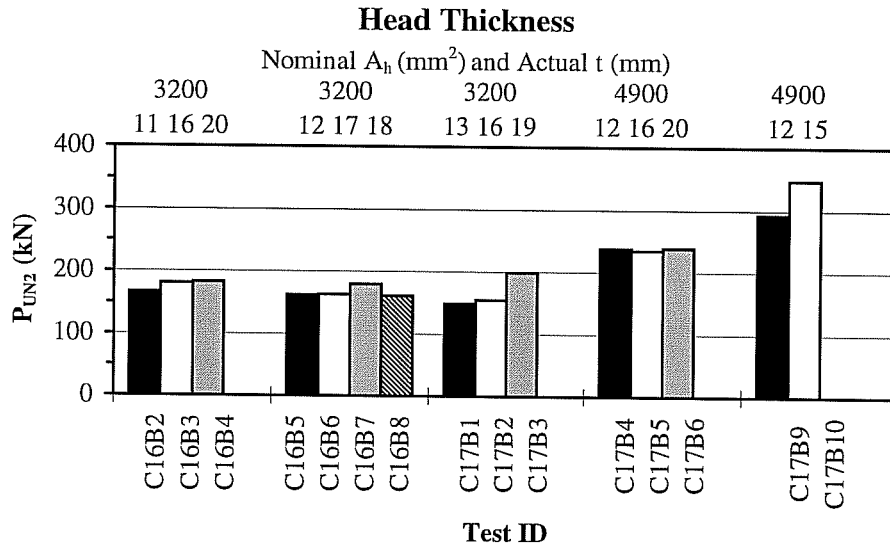


Figure 5.25 - Comparison of Capacities for Tests on Head Thickness

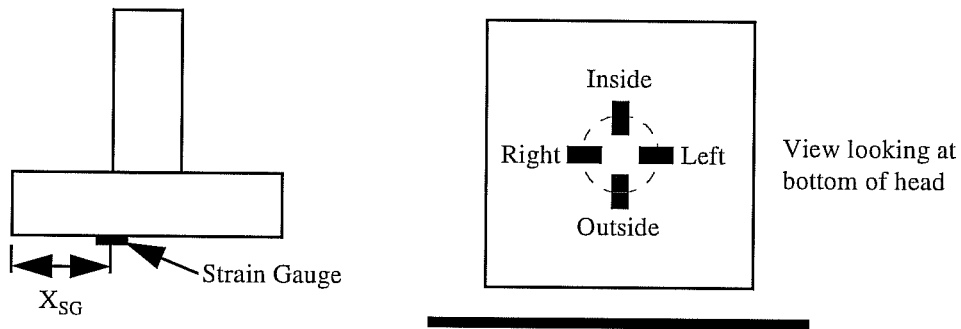
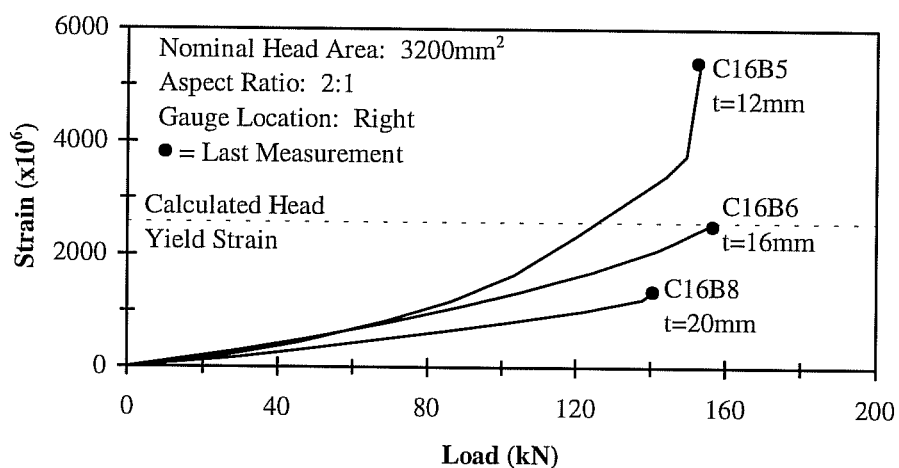


Figure 5.26 - Strain Gauge Locations

location, X_{SG} , was measured from the outside of the head to the center of the gauge.

The measured strains in the heads for three tests are shown in Figure 5.27. The three tests had a nominal head area of 3200mm^2 and a 2:1 aspect ratio. The yield strain shown on the graph was calculated from the actual yield stress of the heads and a modulus of 200,000 MPa. At a given load the strains decrease with increasing thickness, as expected. The curves are nearly linearly until failure is imminent at which point the strains increase rapidly. The head for test C16B5 reached strains higher than the calculated yield strain before the ultimate load was reached. However, these strains did not reduce the anchorage capacity.

Head Strain vs Load



Test ID	d_b (mm)	Nominal Head (mm)	C_1 (mm)	C_2 (mm)	l_d (mm)	Trans. Reinf.	f'_c (MPa)	P_U (kN)
C16B5	25	40x80x12	45	305	0	None	19	162
C16B6	25	40x80x16	45	305	0	None	19	163
C16B8	25	40x80x20	45	305	0	None	19	149

Figure 5.27 - Comparison of Head Strains

The head can be modeled as a cantilever beam with a distributed load by assuming the head is fixed at the bar and assuming a uniform distribution of bearing stress over the head. With this model it is possible to predict the moment, stress and strain at sections in the head for a given load (Figure 5.28). This model is very similar to the approach used for the design of footings. A total of 77 gauges were attached to heads of 52 tests. For each gauge, the head strain was calculated at the location of the gauge for the highest measured load with a corresponding strain measurement below the calculated head yield strain. The

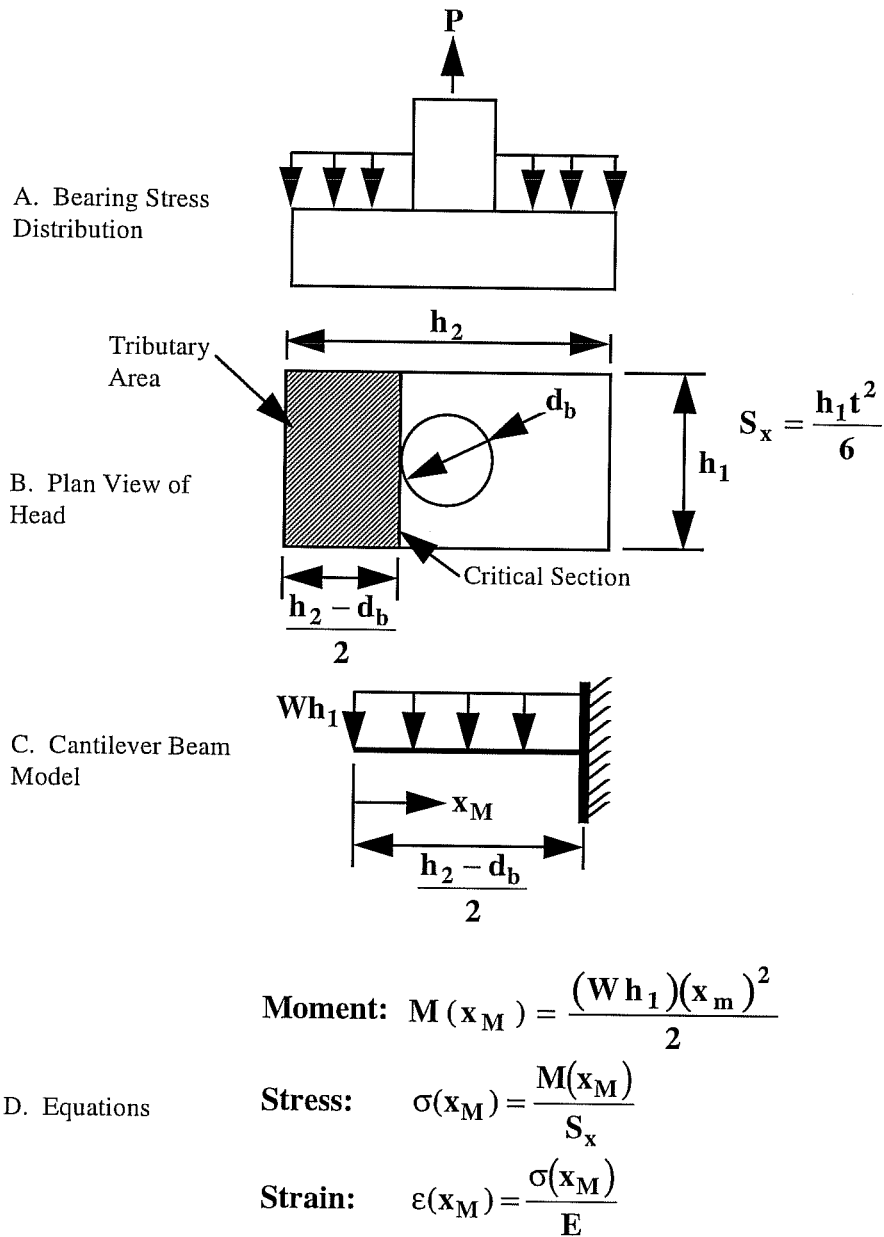


Figure 5.28 - Head Thickness Design Parameters and Equations

calculated strains are compared with the measured strains in Table 5.16. The measured strains were on average 88% of the predicted strains with a 48% standard deviation. The calculated strains were not consistently higher or lower than the measured strains. There appears to be no pattern in the variation with respect to development length, head thickness or ratio of bearing stress to concrete compressive strength.

In Table 5.17, the predicted strains are compared with the measured strains for readings from one test. At low loads the calculated strains are much higher than measured. As the load increases the calculated strains get closer to the measured values. From these results it would appear that at low loads the distribution of bearing stress on the head is higher at the bar than at the edges with a resultant force closer to the bar than the assumed uniform distribution. If the resultant of the distribution is closer to the bar, the calculated moment, stress and strain would be lower than predicted by a uniform distribution of bearing stress. It also would appear from these results, that as the load is increased the distribution becomes more uniform. Since only one gauge was placed on each side of the head, it is not possible to verify changes in the distribution of bearing stress as load increased, however; assuming uniform bearing stress at failure appears to be a reasonable model.

Test ID	d _b (mm)	Actual Head (mm)	Gauge Location	x _M (mm)	P (kN)	Measured Strain x10 ⁶	Predicted Strain x10 ⁶	Meas./Pred. Strain
C3B1	35	100x55x25	Inside	32.5	222	1060	1251	0.85
C3B1	35	100x55x25	Outside	32.5	222	1110	1251	0.89
C3B2	35	55x100x25	Left	32.5	267	1405	1504	0.93
C3B2	35	55x100x25	Right	32.5	267	1515	1504	1.01
C3B3	35	100x55x25	Inside	32.5	306	2500	1724	1.45
C3B3	35	100x55x25	Outside	32.5	306	1215	1724	0.70
C3B4	35	55x100x25	Left	32.5	316	1905	1780	1.07
C3B4	35	55x100x25	Right	32.5	316	1910	1780	1.07
C9B1	35	55x100x25	Left	32.5	577	1575	3250	0.48
C9B1	35	55x100x25	Right	32.5	577	1520	3250	0.47
C9B2	35	55x100x25	Left	32.5	575	1160	3239	0.36
C9B3	35	55x100x25	Right	32.5	578	1165	3256	0.36
C9B4	35	55x100x25	Right	32.5	580	1430	3267	0.44
C9B5	25	70x70x16	Right	22.5	254	1760	1712	1.03
C9B6	25	70x70x16	Left	22.5	294	775	1982	0.39
C9B6	25	70x70x16	Right	22.5	294	865	1982	0.44
C9B7	25	70x70x16	Left	22.5	288	670	1942	0.35
C9B7	25	70x70x16	Right	22.5	288	575	1942	0.30
C10B1	35	55x100x25	Left	32.5	532	1000	2997	0.33
C10B1	35	55x100x25	Right	32.5	532	1140	2997	0.38
C10B2	35	55x100x25	Right	32.5	548	1060	3087	0.34
C10B3	35	55x100x25	Right	32.5	566	1430	3188	0.45
C10B4	35	55x100x25	Right	32.5	542	1460	3053	0.48
C11B3	35	90x90x20	Inside	27.5	607	665	2425	0.27
C11B3	35	90x90x20	Outside	27.5	607	490	2425	0.20
C11B4	35	90x90x20	Left	27.5	606	1440	2421	0.59
C11B4	35	90x90x20	Right	27.5	606	1240	2421	0.51
C15B1	35	54x54x16	Inside	9.4	150	70	405	0.17
C15B1	35	54x54x16	Ouside	15.7	150	215	1131	0.19
C15B2	35	38x78x16	Left	20.3	177	2240	2176	1.03
C15B2	35	38x78x16	Right	17.3	177	1760	1580	1.11
C15B3	35	68x68x16	Left	16.8	207	965	945	1.02
C15B3	35	68x68x16	Right	18.0	207	660	1084	0.61

Table 5.16 - Comparison of Measured and Predicted Head Strains

Test ID	d _b (mm)	Actual Head (mm)	Gauge Location	x _M (mm)	P (kN)	Measured Strain x10 ⁶	Predicted Strain x10 ⁶	Meas./Pred. Strain
C15B4	35	46x100x16	Left	32.5	193	2865	3318	0.86
C15B5	35	55x100x25	Left	30.7	175	1150	880	1.31
C15B5	35	55x100x25	Right	33.8	175	1035	1066	0.97
C15B6	35	78x77x16	Left	26.4	264	1675	2154	0.78
C15B6	35	78x77x16	Right	23.1	264	1675	1649	1.02
C15B7	35	90x90x16	Outside	29.2	333	2005	2343	0.86
C16B2	25	55x54x11	Inside	10.9	180	900	1073	0.84
C16B3	25	55x54x16	Inside	15.5	156	780	889	0.88
C16B3	25	55x54x16	Outside	10.9	156	90	440	0.20
C16B5	25	40x80x12	Right	21.6	120	2325	2160	1.08
C16B6	25	40x80x17	Left	19.8	157	2070	1183	1.75
C16B6	25	40x80x17	Right	23.6	157	2580	1681	1.53
C16B7	25	40x80x18	Right	18.5	170	1480	998	1.48
C16B8	25	38x78x20	Right	21.3	141	1370	974	1.41
C17B1	25	31x100x13	Left	38.6	87	2320	4425	0.52
C17B2	25	34x100x16	Left	33.8	131	2830	3024	0.94
C17B2	25	34x100x16	Right	36.1	131	2930	3449	0.85
C17B3	25	32x100x19	Right	35.3	167	2835	3202	0.89
C17B4	25	70x70x12	Inside	19.1	179	2380	1546	1.54
C17B4	25	70x70x12	Outside	21.6	179	1965	1977	0.99
C17B5	25	70x70x16	Left	17.8	225	1515	949	1.60
C17B5	25	70x70x16	Right	17.5	225	1265	918	1.38
C17B5	25	70x70x16	Inside	19.8	225	1385	1175	1.18
C17B5	25	70x70x16	Outside	19.8	225	735	1175	0.63
C17B6	25	69x66x20	Left	16.8	207	615	540	1.14
C17B6	25	69x66x20	Right	20.6	207	830	813	1.02
C17B7	25	49x100x16	Right	31.2	209	2570	2709	0.95
C17B8	25	55x100x25	Left	34.3	219	1420	1237	1.15
C17B8	25	55x100x25	Right	28.4	219	995	848	1.17
C17B9	25	79x79x12	Left	25.4	67	2540	784	3.24
C17B10	25	78x78x15	Left	22.4	283	2390	1695	1.41
C17B10	25	78x78x15	Right	25.1	283	1610	2129	0.76

Table 5.16 - Continued

Test ID	d_b (mm)	Actual Head (mm)	Gauge Location	x_M (mm)	P (kN)	Measured Strain $\times 10^6$	Predicted Strain $\times 10^6$	Meas./Pred. Strain
C18B1	35	55x100x25	Right	30.0	396	1670	1901	0.88
C18B2	35	55x100x25	Right	30.0	423	1900	2030	0.94
C18B3	35	55x100x25	Right	30.0	502	1870	2410	0.78
C18B4	35	90x90x20	Right	21.5	543	1745	1326	1.32
C18B5	35	33x82x25	Right	16.5	232	1000	889	1.13
C18B6	35	33x82x25	Right	16.5	322	1205	1233	0.98
C19B1	35	68x66x20	Right	10.0	348	670	374	1.79
C19B2	35	68x68x20	Right	10.0	447	170	463	0.37
C19B3	25	31x80x25	Right	24.0	272	840	1899	0.44
C19B4	25	31x80x25	Right	24.0	191	1420	1334	1.06
C19B5	25	54x53x16	Right	11.5	283	960	928	1.03
C19B6	25	55x53x16	Right	11.5	251	670	805	0.83

Maximum **3.24**
Minimum **0.17**
Average **0.88**
Standard Deviation **0.48**

Table 5.16 - Continued

C17B7 Gauge on Right Side of Head $x_M = 31\text{mm}$			
Load (kN)	Measured Strain	Predicted Strain	Meas./Pred. Strain
0	0	0	
27	99	349	0.28
45	205	583	0.35
68	389	889	0.44
85	553	1109	0.50
102	739	1329	0.56
120	949	1556	0.61
136	1201	1766	0.68
155	1476	2018	0.73
173	1816	2254	0.81
184	2059	2385	0.86
194	2296	2517	0.91
200	2421	2593	0.93
205	2516	2659	0.95
209	2570	2720	0.95
205	2737	2670	1.03

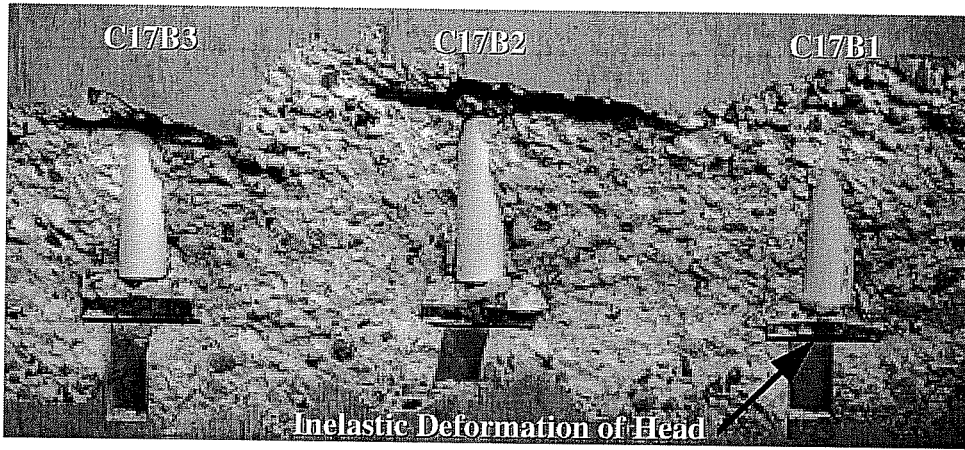
Test ID	d_b (mm)	Nominal Head (mm)	C_1 (mm)	C_2 (mm)	l_d (mm)	Trans. Reinf.	f'_c (MPa)	P_U (kN)
C17B7	25	49x99x16	45	305	0	None	19	222

Table 5.17 - Comparison of Measured and Predicted Head Strains

Eight of the 27 tests on head geometry reached strains higher than the calculated yield strain and are summarized in Table 5.18. The readings were verified by observing the head after failure. The inelastic deformations of the heads for three tests (C17B1, C17B2 and C17B3) with measured strains higher than the yield strain can be seen in Figure 5.29. In Figure 5.30, the measured capacities normalized with respect to nominal head area, P_{UN2} (see Equation 5.7), for the 27 tests are plotted against head area, A_h . The tests with head yielding are differentiated by symbol from the tests without head yielding. It appears that head yielding did not affect the ultimate capacity.

Test ID	d_b (mm)	Actual Head (mm)	Calc. Yield Strain $\times 10^6$	Maximum Strain $\times 10^6$	% of Yield Strain
C15B4	35	46x100x16	2540	2865	113%
C16B5	25	40x80x12	2575	5425	211%
C17B1	25	31x100x13	2540	9080	357%
C17B2	25	34x100x16	2540	5370	211%
C17B3	25	32x100x19	2540	4940	194%
C17B4	25	70x70x12	2525	7425	294%
C17B9	25	79x79x12	2470	13455	545%
C17B10	25	78x78x15	2470	3415	138%

Table 5.18 - Summary of Tests with Head Yielding



Test ID	d_b (mm)	Nominal Head (mm)	C_1 (mm)	C_2 (mm)	l_d (mm)	Trans. Reinf.	f'_c (MPa)	P_U (kN)
C17B1	25	33x98x12	45	305	0	None	19	144
C17B2	25	33x98x16	45	305	0	None	19	165
C17B3	25	33x98x20	45	305	0	None	19	199

Figure 5.29 - Inelastic Deformations of Thin Heads

Head Yielding

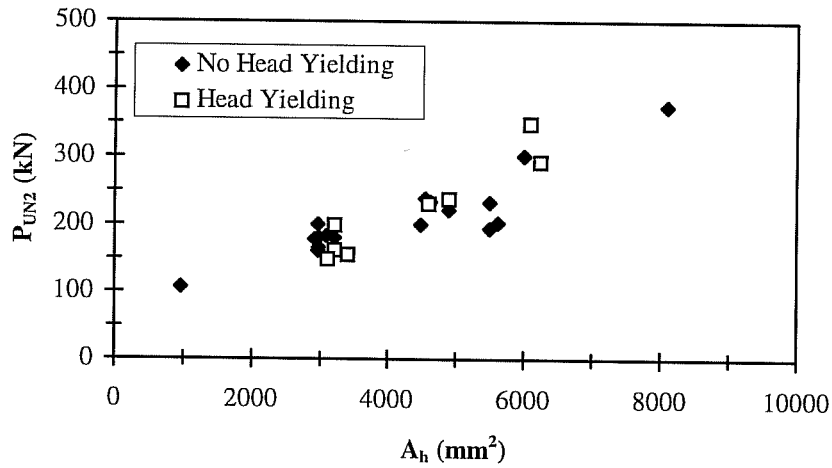


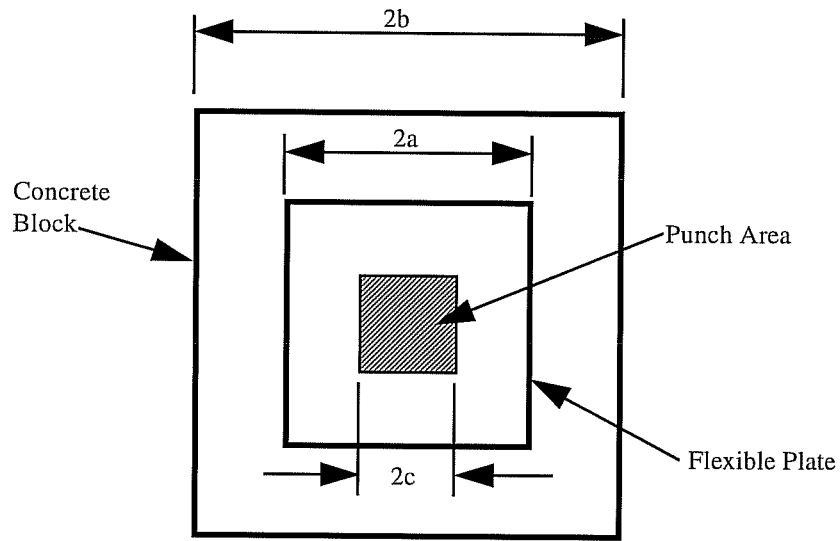
Figure 5.30 - Comparison of Capacities for Tests with and without Head Yielding

Hawkins [24] conducted tests on the bearing capacity of concrete prisms by applying a load with a punch through flexible plates. Hawkins concluded that the flexibility of the plates did decrease the bearing capacity compared to rigid plates and presented an equation, in customary US units, for minimum thickness for a square rigid plate:

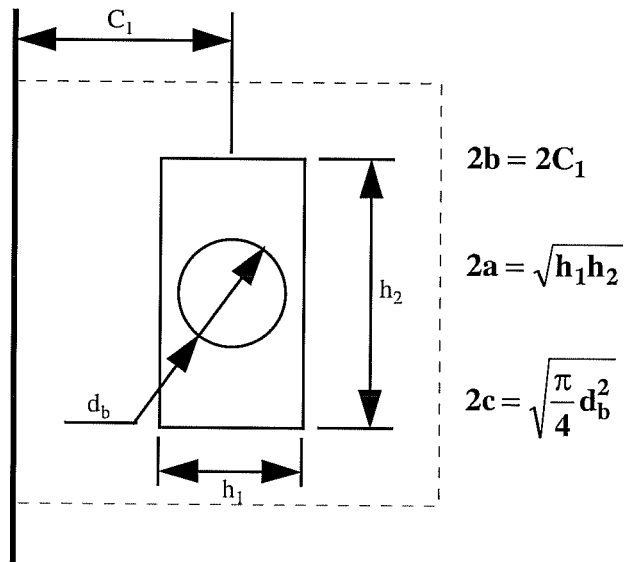
$$t^2 > \frac{4}{f_y} \left[f'_c + K \sqrt{f'_c} \left(\frac{b}{a} - 1 \right) \right] \left(4c(a-c) + \frac{\pi}{2} (a-c)^2 \right) \quad \text{eq. 5.9}$$

$$2\pi + \frac{8c}{a-c}$$

where t is the plate thickness, f_y is the plate yield stress, f'_c is the compressive strength of concrete, K is a factor for the concrete internal angle of friction - assumed to be 50, c is one-half the side dimension of the load application or punch area, a is one-half the side dimension of the square plate and b is one-half the side dimension of the concrete prism. In Figure 5.31, these variables and the equivalents assumed for headed reinforcement are illustrated. In Table 5.19, the minimum thickness using Equation 5.9 for the heads tested in this series are listed. All plates were rigid according to Equation 5.9 even though yielding was observed in eight plates.



A. Variables from Hawkins



B. Headed Reinforcement Equivalents

Figure 5.31 - Hawkins' Variables for Flexible Plates and Headed Reinforcement Equivalents

Test ID	d_b (mm)	Nominal Head (mm)	C_1 (mm)	f_c (MPa)	Head f_y (MPa)	t_{min} (mm)	Rigid?
C15B1	35	57x57x16	45	19	494	4	Yes
C15B2	35	40x80x16	45	19	508	4	Yes
C15B3	35	70x70x16	45	19	494	5	Yes
C15B4	35	49x99x16	45	19	508	5	Yes
C15B5	35	55x100x25	45	19	508	6	Yes
C15B6	35	80x80x16	45	19	494	6	Yes
C15B7	35	90x90x16	45	19	494	7	Yes
C15B8	35	90x90x20	45	19	494	7	Yes
C16B1	25	33x33x16	45	19	508	2	Yes
C16B2	25	57x57x12	45	19	505	5	Yes
C16B3	25	57x57x16	45	19	505	5	Yes
C16B4	25	57x57x20	45	19	505	5	Yes
C16B5	25	40x80x12	45	19	515	5	Yes
C16B6	25	40x80x16	45	19	515	5	Yes
C16B7	25	40x80x18	45	19	515	5	Yes
C16B8	25	40x80x20	45	19	494	5	Yes
C17B1	25	33x98x12	45	19	508	5	Yes
C17B2	25	33x98x16	45	19	508	5	Yes
C17B3	25	33x98x20	45	19	508	5	Yes
C17B4	25	70x70x12	45	19	505	6	Yes
C17B5	25	70x70x16	45	19	505	6	Yes
C17B6	25	70x70x20	45	19	494	6	Yes
C17B7	25	49x99x16	45	19	508	6	Yes
C17B8	25	55x100x25	45	19	508	6	Yes
C17B9	25	80x80x12	45	19	494	7	Yes
C17B10	25	80x80x16	45	19	494	7	Yes
C17B11*	25	70x70x16	45	19	505	6	Yes
C17B12*	25	77x77x16	45	19	494	7	Yes

Table 5.19 - Minimum Thicknesses of Heads Based on Hawkins' Equation

Based on studies of anchorage zones for post-tensioned concrete members, Roberts [40] proposed a criteria for rigid bearing plates limiting the slenderness and deflections of the plate:

$$\frac{n}{t} \leq 0.073 \sqrt{\frac{E_s}{f_b}} \quad \text{eq. 5.10}$$

where n is the maximum distance from the face of the bar to the edge of the plate, t the thickness of the plate, E_s the modulus of elasticity of the plate and f_b the bearing stress at the plate at the failure load (or design load). Roberts also proposed that the bending stress in the plate, f_s , be less than the yield stress of the plate. The minimum thicknesses using these criteria are listed in Table 5.20 for the 27 tests in this series resulting in blowout failures. The measured ultimate load was used to calculate the bearing stress. The slenderness limit (Equation 5.10) controlled for all 27 tests. Only 5 of the 27 heads were rigid by this criteria.

Test ID	d_b (mm)	Nominal Head (mm)	P_U (MPa)	Head f_y (MPa)	t_{min} (mm)	Rigid?
C15B1	35	57x57x16	162	494	11	Yes
C15B2	35	40x80x16	185	508	24	No
C15B3	35	70x70x16	221	494	16	No
C15B4	35	49x99x16	217	508	30	No
C15B5	35	55x100x25	194	508	28	No
C15B6	35	80x80x16	283	494	21	No
C15B7	35	90x90x16	374	494	25	No
C15B8	35	90x90x20	93	494	16	Yes
C16B1	25	33x33x16	154	508	6	Yes
C16B2	25	57x57x12	168	505	15	No
C16B3	25	57x57x16	176	505	16	Yes
C16B4	25	57x57x20	162	505	15	Yes
C16B5	25	40x80x12	163	515	26	No
C16B6	25	40x80x16	180	515	27	No
C16B7	25	40x80x18	149	515	26	No
C16B8	25	40x80x20	144	494	25	No
C17B1	25	33x98x12	165	508	35	No
C17B2	25	33x98x16	199	508	37	No
C17B3	25	33x98x20	238	508	40	No
C17B4	25	70x70x12	235	505	21	No
C17B5	25	70x70x16	222	505	20	No
C17B6	25	70x70x20	222	494	20	No
C17B7	25	49x99x16	233	508	34	No
C17B8	25	55x100x25	285	508	35	No
C17B9	25	80x80x12	331	494	26	No
C17B10	25	80x80x16	183	494	21	No
C17B11*	25	70x70x16	193	505	19	No
C17B12*	25	77x77x16	571	494	30	No

Table 5.20 - Minimum Thicknesses for Rigid Heads Based on Roberts' Criteria

There is insufficient evidence from these test results to show that yielding or deflections of the head is detrimental to the anchorage capacity. It seems conservative to design the thickness of the head to resist yielding by using the cantilever beam or footing model described above. Using this method, the minimum thicknesses to prevent yielding in the head before bar yield for the standard heads supplied for this research are listed in Table 5.21. According to these assumptions, the standard square heads were all supplied with sufficient thickness, while the two larger standard rectangular heads were undersized.

5.9 Concrete Strength

The mode of failure observed in the deep-embedment tests involved the splitting of the concrete cover so that the capacity of the anchorage should be a function of the tensile strength of the concrete. Concrete tensile strength is generally assumed to be a function of the compressive strength. Therefore, the

d_b (mm)	Head (mm)	Bar f_y (MPa)	P_y (kN)	Head f_y (MPa)	t_{min} (mm)	Head (mm)
35	100x55	500	500	500	27	100x55x27
35	90x90	500	500	500	18	90x90x18
25	80x40	500	250	500	20	80x40x20
25	70x70	500	250	500	13	70x70x13
20	70x35	500	150	500	16	70x35x16
20	50x50	500	150	500	10	50x50x10

Table 5.21 - Minimum Head Thicknesses for Rigid Heads based on Cantilever Beam Model

compressive strength of concrete would seem to be an important factor in the anchorage capacity of headed reinforcement. The majority of tests conducted had concrete compressive strengths between 21 and 29 MPa. To investigate the effect of concrete strength on the anchorage, a series of tests were conducted with a nominal concrete strength of 49 MPa. The parameters and results for the 12 tests of this series are listed in Table 5.22. The sizes of several of the heads tested in this series were reduced; the actual head sizes and geometrical properties for these tests are listed Table 5.23. The results from eight pairs of tests where the only variable between each pair is the concrete strength are compared in Table 5.24. The ratios of the measured ultimate capacities, concrete strength and square root of the concrete strengths are compared. The value x in Table 5.24 is the exponent for the concrete strengths that would predict the increase in capacity and is calculated for each pair from:

$$\frac{P_{U1}}{P_{U2}} = \left(\frac{f'_{c1}}{f'_{c2}} \right)^x \quad \text{eq. 5.11}$$

From the results of these tests, the capacity of the anchorage increases with increasing concrete compressive strength. The values of x suggest that the increase in anchorage capacity is less than the increase in concrete strength, in other words, doubling the concrete strength will result in less than a doubling of anchorage capacity.

Test ID	d_b (mm)	Nominal Head (mm)	C_1 (mm)	C_2 (mm)	I_d (mm)	f'_c (MPa)	P_U (kN)
C18B1	35	55x100x25	45	305	0	44	411
C18B2	35	55x100x25	51	305	0	44	432
C18B3	35	55x100x25	64	305	0	44	517
C18B4	35	90x90x20	45	305	0	44	555
C18B5	35	40x80x25	45	305	0	44	238
C18B6	35	40x80x25	64	305	0	44	330
C19B1	35	70x70x20	45	305	0	44	360
C19B2	35	70x70x20	64	305	0	44	470
C19B3	25	40x80x25	45	305	0	44	287
C19B4	25	40x80x25	25	305	0	44	196
C19B5	25	57x57x16	45	305	0	44	295
C19B6	25	57x57x16	30	305	0	44	261

Table 5.22 - Parameters and Results for Tests on Concrete Strength

Test ID	d_b (mm)	Nominal Head (mm)	Actual Head (mm)	Nominal			Actual		
				A_h (mm ²)	S_x (mm ³)	I_x (mm ⁴)	A_h (mm ²)	S_x (mm ³)	I_x (mm ⁴)
C18B5	35	40x80x25	33x82x25	3200	4167	52083	2706	3438	42969
C18B6	35	40x80x25	33x82x25	3200	4167	52083	2706	3438	42969
C19B1	35	70x70x20	68x66x20	4900	4667	46667	4488	4400	44000
C19B2	35	70x70x20	68x68x20	4900	4667	46667	4624	4533	45333
C19B3	25	40x80x25	31x80x25	3200	4167	52083	2480	3229	40365
C19B4	25	40x80x25	31x80x25	3200	4167	52083	2480	3229	40365
C19B5	25	57x57x16	54x53x16	3200	2432	19456	2862	2261	18091
C19B6	25	57x57x16	55x55x16	3200	2432	19456	3025	2347	18773

Table 5.23 - Nominal and Actual Head Sizes for Tests on Concrete Strength

Test ID 1	P_{U1}	f'_{c1}	Test ID 2	P_{U2}	f'_{c2}	P_{U1}/P_{U2}	f'_{c1}/f'_{c2}	$(f'_{c1}/f'_{c2})^{0.5}$	x
	(kN)	(MPa)		(kN)	(MPa)				
C18B1	411	44	C15B5	194	19	2.12	2.32	1.52	0.89
C18B2	432	44	C3B2	284	29	1.52	1.52	1.23	1.01
C18B3	517	44	C3B4	335	29	1.54	1.52	1.23	1.04
C18B4	555	44	C4B2	476	29	1.17	1.52	1.23	0.37
C18B5	238	44	C15B2	185	19	1.29	2.32	1.52	0.30
C19B1	360	44	C15B3	221	19	1.63	2.32	1.52	0.58
C19B3	287	44	C16B7	180	19	1.59	2.32	1.52	0.56
C19B5	295	44	C16B3	168	19	1.76	2.32	1.52	0.67

Maximum **1.04**
Minimum **0.30**
Average **0.68**
Std. Dev. **0.28**

Table 5.24 - Comparison of Capacities for Tests with Different Concrete Strengths

5.10 Cover

The distance from the edge of concrete to the center of the bar was varied from a minimum of 25mm to a maximum of 102mm. The clear cover over the bars varied from 13mm to 84mm. The minimum clear cover tested represents an extreme case where there is no cover over the head and is less than allowed by the ACI Building Code. A clear cover of 84mm is at the upper end of values routinely used in construction and would be required where durability concerns are high or large members are used.

A side blowout failure results in a cone of concrete being pushed away from the surrounding concrete. Increasing the size of the cone by increasing the amount of cover should result in increased capacity. The measured capacities for 114 deep-embedment pullout tests, 77 edge bars, 31 corner bars and 6 paired bars

with close spacing, which resulted in blowout failures are plotted against increasing edge distance, C_1 , in Figure 5.32. The general trend is one of increased capacity with increased edge distance. The large number of values at edge distances of 45mm and 64mm are from series where only head geometry or transverse reinforcement were varied. There is considerable scatter in the data and the relationship between edge distance and capacity is not obvious.

The parameters and results for several groups of tests where the only variable was the edge distance are listed in Table 5.25. Assuming that the capacity varies as a function of clear cover, specifically C_1^z , then the exponent, z , can be determined by comparing similar tests. Fifteen pairs of tests are compared

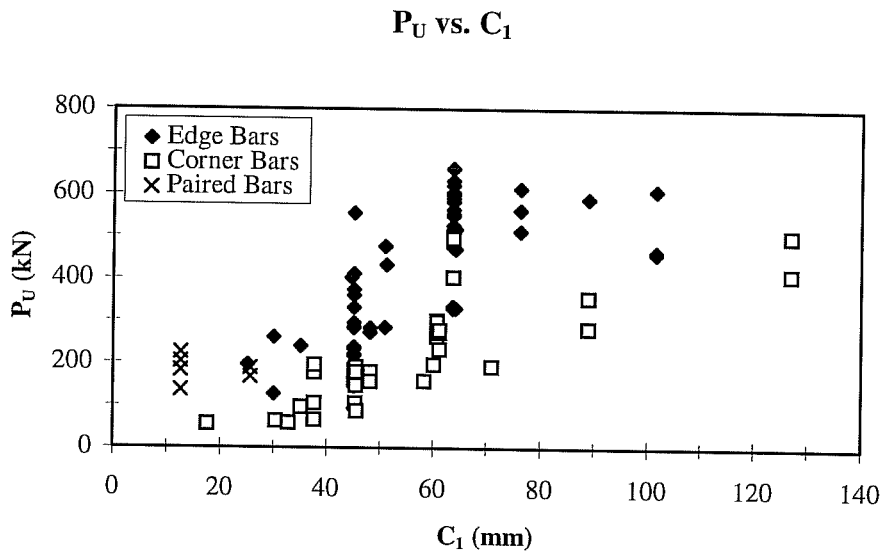


Figure 5.32 - Measured Capacities versus Edge Distance

in Table 5.26 and values for z are listed. To account for slight variations in head area with the groups, the capacities were normalized by the nominal head area, P_{UN2} (see Equation 5.7). Based on these observations it appears that the capacity varies with the cover raised to approximately the 0.5 to the 0.6 power. This preliminary analysis assumes that a headed reinforcing bar with no cover has no anchorage capacity. Other functions may better describe the relationship between the edge distance and capacity.

Test ID	d_b (mm)	Nominal Head (mm)	C_1 (mm)	f'_c (MPa)	P_U (kN)	Nominal A_h (mm ²)	Actual A_h (mm ²)	P_{UN2} (kN)
C4B1	35	90x90x20	45	29	403	8100	8100	403
C4B2	35	90x90x20	51	29	476	8100	8100	476
C4B3	35	90x90x20	64	29	491	8100	8100	491
C4B4	35	90x90x20	76	29	512	8100	8100	512
C18B1	35	55x100x25	45	44	411	5500	5500	411
C18B2	35	55x100x25	51	44	432	5500	5500	432
C18B3	35	55x100x25	64	44	517	5500	5500	517
C1B1	25	70x70x16	35	25	239	4900	4900	239
C1B2	25	70x70x16	48	25	283	4900	4900	283
C7B1	35	90x90x20	89	24	589	8100	8100	589
C7B2	35	90x90x20	102	24	609	8100	8100	609
C18B5	35	40x80x25	45	44	238	3200	2706	281
C18B6	35	40x80x25	64	44	330	3200	2706	390
C19B1	35	70x70x20	45	44	360	4900	4488	393
C19B2	35	70x70x20	64	44	470	4900	4624	498
C19B3	25	40x80x25	45	44	287	3200	2480	370
C19B4	25	40x80x25	25	44	196	3200	2480	253
C19B5	25	57x57x16	45	44	295	3249	2862	335
C19B6	25	57x57x16	30	44	261	3249	3025	280

Table 5.25 - Parameters and Results for Tests on Edge Distance

Test ID 1	C ₁₁	P _{UN21}	Test ID 2	C ₁₂	P _{UN22}	P _{UN22} /P _{UN21}	C ₁₂ /C ₁₁	z
	(mm)	(kN)		(mm)	(kN)			
C4B1	45	403	C4B2	51	476	1.18	1.13	1.33
C4B1	45	403	C4B3	64	491	1.22	1.42	0.56
C4B1	45	403	C4B4	76	512	1.27	1.69	0.46
C4B2	51	476	C4B3	64	491	1.03	1.25	0.14
C4B2	51	476	C4B4	76	512	1.08	1.49	0.18
C4B3	64	491	C4B4	76	512	1.04	1.19	0.24
C18B1	45	411	C18B2	51	432	1.05	1.13	0.40
C18B1	45	411	C18B3	64	517	1.26	1.42	0.65
C18B2	51	432	C18B3	64	517	1.20	1.25	0.79
C1B1	35	239	C1B2	48	283	1.18	1.37	0.54
C7B1	89	589	C7B2	102	609	1.03	1.15	0.24
C18B5	45	281	C18B6	64	390	1.39	1.42	0.93
C19B1	45	393	C19B2	64	498	1.27	1.42	0.67
C19B4	25	253	C19B3	45	370	1.46	1.80	0.65
C19B6	30	276	C19B5	45	330	1.19	1.50	0.44

Maximum 1.33
Minimum 0.14
Average 0.55
Standard Deviation 0.31

Table 5.26 - Comparison of Effect of Edge Distance on Capacity

Corner Bars

Corner placement of the headed reinforcing bar reduced the size of the blowout failure and the anchorage capacity. A typical failure for a corner bar is shown in Figure 5.33. The effect on capacity from corner placement can be seen in Figure 5.32, where the capacity of corner bars were in general less than edge bars with identical edge distance. The capacities from five pairs of tests in which the only variable between pairs is bar position are compared in Table 5.27. The

corner bars had equal edge distances, C_1 and C_2 . On average, corner bars had approximately 60% the capacity of an edge bar with the same minimum clear cover. Because of the number of variables and wide range of results it is difficult to determine how large the second edge distance, C_2 , has to be for a bar to have the capacity of an edge bar. It appears that a value of C_2 three to five times larger than C_1 is a reasonable estimate.

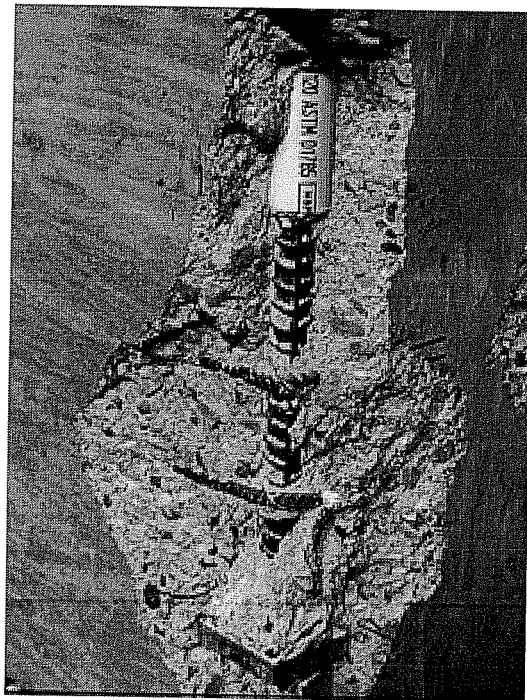


Figure 5.33 - Typical Failure Surface for Corner Bar

d_b (mm)	Nominal Head (mm)	C_1 & C_2 (mm)	Edge Bar		Corner Bar		P_{U2}/P_{U1}
			Test ID 1	P_{U1} (kN)	Test ID 2	P_{U2} (kN)	
25	70x70x16	35	C1B1	239	C2B1	97	0.41
25	70x70x16	48	C1B2	283	C2B2	179	0.63
25	70x70x16	48	C1B3	272	C2B3	157	0.58
35	90x90x20	89	C7B1	589	C8B1	355	0.60
35	90x90x20	64	C13B4	581	C12B1	404	0.70

Maximum	0.70
Minimum	0.41
Average	0.58
Standard Deviation	0.11

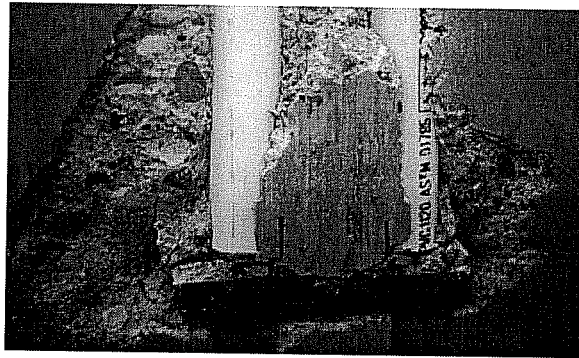
Table 5.27 - Comparison of Capacities of Edge and Corner Bar Tests

Close Spacing

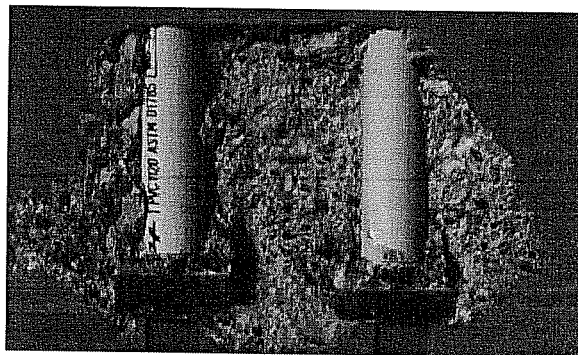
Results from the six tests on paired bars are summarized in Table 5.28. The ultimate load, P_U , is the load on each bar. In general the paired bars followed the same trends observed with single edge bars: increased capacity with increased edge distance or concrete strength. The failure surfaces for tests C12B5 and C12B6 are shown in Figure 5.34. The blowout cones for the test with the closest spacing, C12B5, overlapped and created one cone while the test with larger spacing, C12B6, had two distinct cones. In general it appeared that close spacing had an effect on the capacity similar to corner placement.

Test ID	d_b (mm)	Nominal Head (mm)	C_1 (mm)	C_{SP2} (mm)	f'_c (MPa)	P_U (kN)
C12B5	25	40x80x18	25	102	25	135
C12B6	25	40x80x18	25	152	25	182
C12B7	25	40x80x18	38	102	25	167
C12B8	25	40x80x18	38	152	25	188
C18B7	25	40x80x18	25	102	44	204
C19B7	25	40x80x18	25	152	44	224

Table 5.28 - Parameters and Results of Tests on Closely Spaced Bars



A. Failure Surface of C12B5 - $C_{SP2} = 102\text{mm}$ Note Overlapping Cone on Heads



B. Failure Surface of C12B6 - $C_{SP2} = 152\text{mm}$ Note Separate Cones on Heads

Figure 5.34 - Failure Surfaces of Tests on Closely Spaced Paired Bars

5.11 Summary

Based on results of 114 deep-embedment pullout tests on headed reinforcement, clear cover, concrete strength and head area were the primary factors affecting the anchorage capacity. Development length increased the capacity and the increase could be predicted using existing equations for straight bar anchorage capacities. Corner placement or close spacing of bars reduced the anchorage capacity compared to a single edge bar.

Transverse reinforcement did not affect the ultimate strength but did increase the level of load maintained and the deformations reached after failure when large amounts of transverse reinforcement were placed near the head.

Head orientation did not affect the capacity, nor did head aspect ratio or head shape provided the head had sufficient stiffness. The results indicated that the thickness could be designed conservatively using a simple cantilever beam model of the head. Finally, if the embedment depth was large enough to cause a side blowout failure, additional depth did not increase the capacity of the anchorage.

Chapter 6

Deep-Embedment Pullout Tests Comparison with Previous Research and Design Methods

6.1 Introduction

The basic mechanism for transferring force between headed reinforcement and surrounding concrete is the bearing of the head on the concrete. This behavior is similar to anchor bolts and anchorages for prestressing steel, as well as the bearing capacity of concrete. Several studies have reported the behavior of bearing loads on concrete, anchor bolts and prestressing anchors leading to code provisions for these applications.

Before formulating design provisions for deeply embedded headed reinforcement, the measured capacities from the 108 deep-embedment tests on edge and corner bars (paired bars are not included) which resulted in blowout failures will be compared with the equations and methods previously developed for similar phenomena.

6.2 Bearing Strength of Concrete

Experimental Studies

Hawkins [23] conducted a series of tests measuring the bearing capacity of cubic and cylindrical concrete specimens. Hawkins monotonically loaded the specimens through rigid steel plates until failure. From the results of 38 tests, Hawkins proposed a failure model and equation predicting the bearing capacity. A continuation of this research led to the equation for minimum thickness of a rigid plate previously mentioned. The failure model proposed by Hawkins consists of a pyramid of concrete forming under the plate and splitting away the surrounding concrete (Figure 6.1). The proposed failure model is very similar to the failure mode observed in the deep-embedment pullout tests.

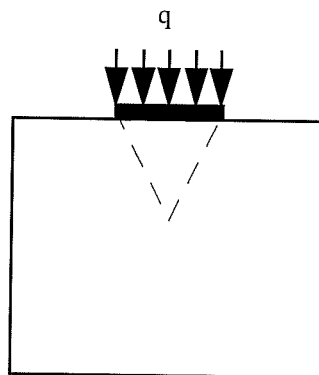


Figure 6.1 - Failure Mechanism Proposed by Hawkins

In Hawkins' tests the concrete strength varied from 21 to 50 MPa which is a similar range of strengths for the deep-embedment pullout tests on headed reinforcement. The steel plates and covers Hawkins used were larger than those used in the tests in this program. Variables from the deep-embedment tests not considered by Hawkins include: transverse reinforcement, development length, and head (or plate) orientation.

Based on the variables in Figure 6.2, Hawkins proposed the following equation for a bearing load through a rectangular plate near an edge with all variables in standard US units:

$$\frac{q}{f'_c} = 1 + \frac{K}{2\sqrt{f'_c}} \left[\frac{c}{b} \left(3 - \frac{a}{b} \right) - 1 \right] \quad \text{eq. 6.1}$$

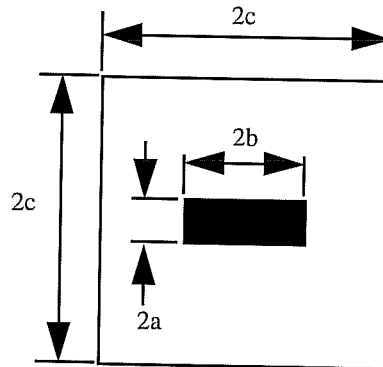


Figure 6.2 - Variables for Equation 6.1 by Hawkins

where q is the bearing pressure under the plate. The value K is a constant representative of the internal angle of friction for concrete. K is to be determined experimentally and is a function of the coarse aggregate size and type. Hawkins proposed a practical value for K of 50.

Hawkins' equation can be rearranged to calculate the ultimate load of a headed reinforcing bar using the variables for headed reinforcement shown in Figure 6.3. Rearranging the terms (using US standard units) the equation becomes:

$$P_U = A_h f_c' \left(1 + \frac{K}{2\sqrt{f_c'}} \left[\frac{2C_1}{h_{\max}} \left(3 - \frac{h_{\min}}{h_{\max}} \right) - 1 \right] \right) \quad \text{eq. 6.2}$$

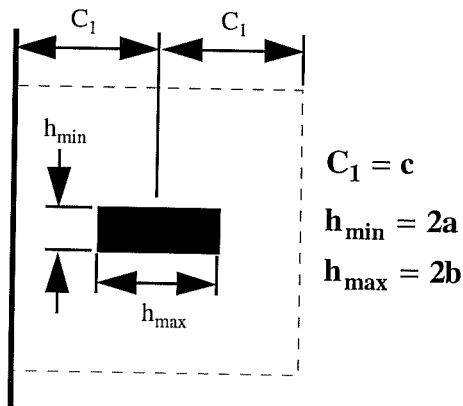


Figure 6.3 - Headed Reinforcement Variables for Equation 6.2

The measured capacities from the deep-embedment pullout tests are plotted against the predicted values from Equation 6.2 in Figure 6.4. Equation 6.2 correlates reasonably well with the measured values, though it underestimates the capacity of all the edge bar tests and overestimates the capacity (is unconservative) for many of the corner bars tests.

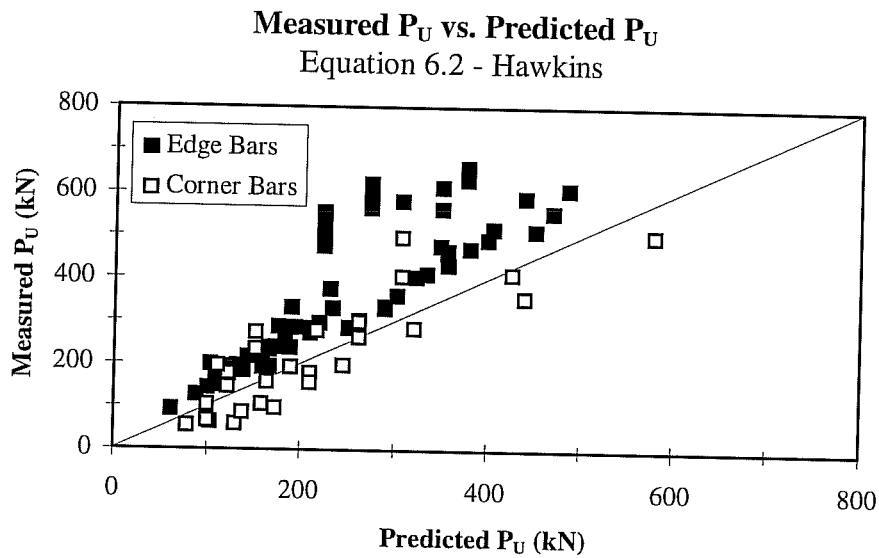


Figure 6.4 - Comparison of Measured and Predicted Capacities using Equation 6.2 by Hawkins

Code Provisions: ACI 318 Section 10.17

The studies by Hawkins form the basis for Section 10.17 in the ACI Building Code [1] which governs the bearing strength of concrete. The equation for bearing capacity of concrete in customary US units is given as:

$$P_n = \phi(0.85f'_c A_1) \quad \text{eq. 6.3}$$

where A_1 is the loaded area. When the supporting area is larger than the loaded area the capacity can be increased by the square root of the ratio of the supporting area divided by the loaded area. The capacity though cannot be increased by more than 2. The capacity reduction factor, ϕ , is equal to 0.70. Since there are no uncertainties in the variables for the 108 deep-embedment tests, the capacity reduction factor is not used for this comparison.

Using Equation 6.3, the measured capacities from the 108 deep-embedment pullout tests are plotted against the predicted values in Figure 6.5. The ACI Code equation is very conservative for both edge and corner bars since it only allows a doubling of the compressive strength of concrete in bearing. The bearing stress at the head for the 108 pullout tests averaged 2.7 times the concrete compressive strength with a maximum value of 5.1 times the compressive strength.

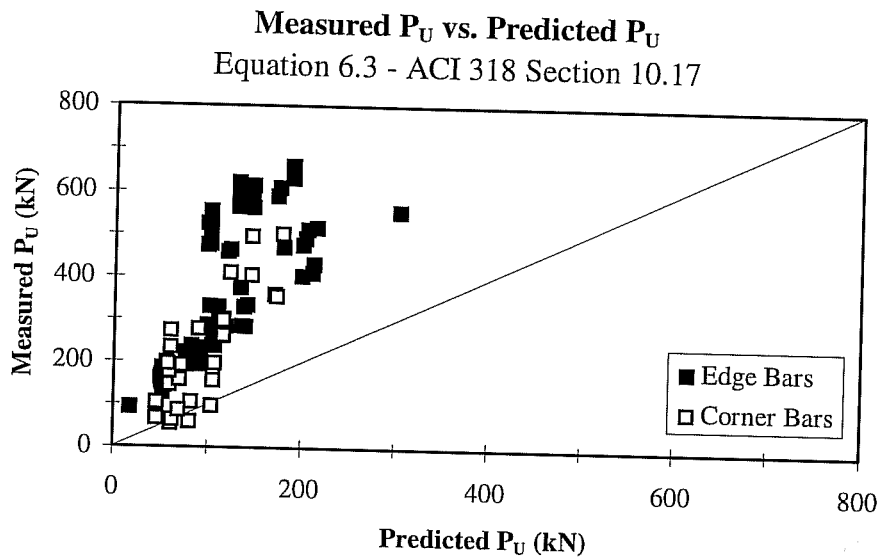


Figure 6.5 - Comparison of Measured and Predicted Capacities using Equation 6.3 from ACI 318 Section 10.17

6.3 Prestress Anchorage

Experimental Studies

Many of the studies of anchorage of prestressing steel were similar to studies for bearing capacity of concrete. One major difference is the addition of transverse or confining reinforcement. In the 1970's, Williams [54] conducted a comprehensive program on anchorages. He tested both unreinforced and reinforced specimens and proposed the following best-fit formula for the ultimate bearing stress in standard US units:

$$f_b = 6.92f_t \left(\frac{A_b}{A} \right)^{-0.47} \quad \text{eq. 6.4}$$

where f_t is the tensile capacity of concrete, A_b the loaded area and A the unloaded area. Equation 6.4 is one of the few equations that is based explicitly on the tensile capacity of concrete. Most approaches use the square root or other function of the compressive strength.

Using the head area, A_h , for A_b , assuming the unloaded area is:

$$A = 4C_1^2 \quad \text{eq 6.5}$$

and assuming the tensile strength of concrete is:

$$f_t = 6\sqrt{f'_c} \quad \text{eq. 6.6}$$

Equation 6.4 can be rewritten for the ultimate capacity of headed reinforcement, in customary US units, as:

$$P_U = 41.52A_h \sqrt{f'_c} \left(\frac{A_h}{4C_1^2} \right)^{-0.47} \quad \text{eq. 6.7}$$

The measured capacities for the 108 deep-embedment pullout tests are compared with the predicted capacities of Equation 6.7 in Figure 6.6. The equation seems to somewhat model the behavior but is very conservative in predicting the capacity.

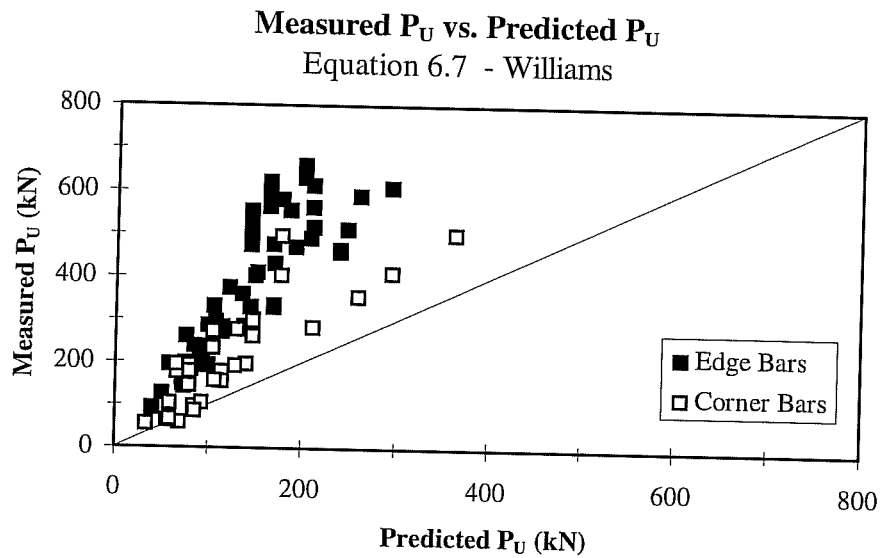


Figure 6.6 - Comparison of Measured and Predicted Capacities using Equation 6.7 by Williams

Based on a study of local anchorage zones of post-tensioned concrete members, Roberts [40] proposed the following equation, in customary US units, for the bearing capacity:

$$P_U = \Gamma f'_c \sqrt{\frac{A}{A_b}} A_b + 4f_{lat} A_{core} \left(1 - \frac{s}{D}\right)^2 \quad \text{eq. 6.8}$$

where A is the unloaded area and can be calculated for headed reinforcement from Equation 6.5 and A_b is the bearing area (the head area, A_h , for headed reinforcement). The second term of Equation 6.8 takes into account confinement from transverse reinforcement and is taken as 0 for the deep-embedment tests of

headed reinforcement. The value Γ takes into account higher strength concrete and is equal to 0.80 for concrete strengths of 4000 psi and lower and is decreased by 0.05 for every 2000 psi increase in concrete strength over 4000 psi. The value Γ is 0.65 for concrete strengths of 10000 psi and higher. Rearranging Equation 6.8 for variables associated with headed reinforcement gives:

$$P_U = \Gamma f'_c \sqrt{\frac{4C_1^2}{A_h}} A_h \quad \text{eq. 6.9}$$

The measured capacities for the 108 deep-embedment tests are compared with the predicted capacities from Equation 6.9 in Figure 6.7. As with Equation 6.7, Equation 6.9 models the behavior somewhat and is conservative.

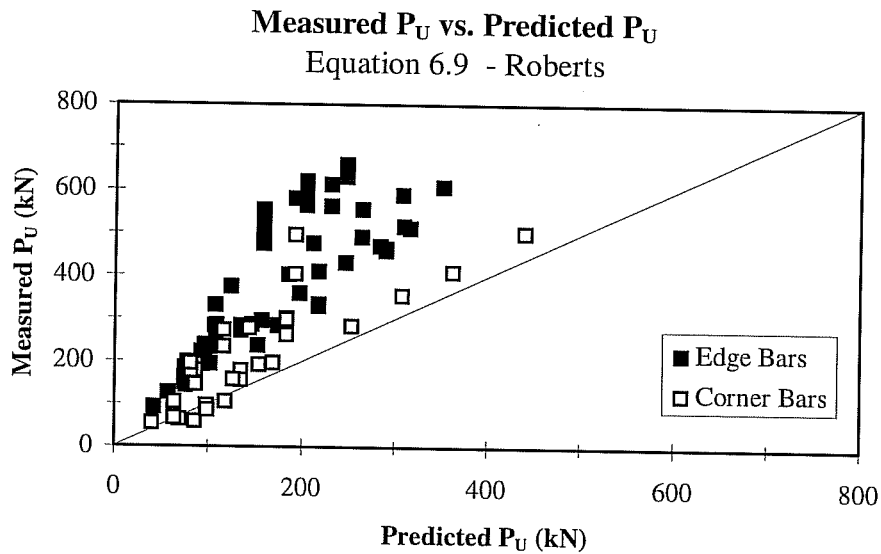


Figure 6.7 - Comparison of Measured and Predicted Capacities using Equation 6.9 by Roberts

Code Provisions

A model code proposed by the Comite Euro-International du Beton (CEB) [11] gave the following equation for ultimate bearing stress for prestressing anchors in SI units:

$$f_b = \frac{f_{ck}}{1.5} \sqrt{\frac{A}{A_b}} \leq 3.3 \frac{f_{ck}}{1.5} \quad \text{eq. 6.10}$$

where f_{ck} is the compressive strength and A and A_b are the same as for Equation 6.4. Using Equation 6.5 for A , and A_h for A_b , Equation 6.10 can be rewritten for the ultimate capacity for headed reinforcement in SI units as:

$$P_U = A_h \frac{f'_c}{1.5} \sqrt{\frac{4C^2}{A_h}} \leq 3.3 A_h \frac{f'_c}{1.5} \quad \text{eq. 6.11}$$

The capacities predicted by Equation 6.11 are compared with the measured capacities for the 108 deep-embedment pullout tests in Figure 6.8. As with the equations by Williams and Roberts, Equation 6.11 conservatively models the behavior of headed reinforcement.

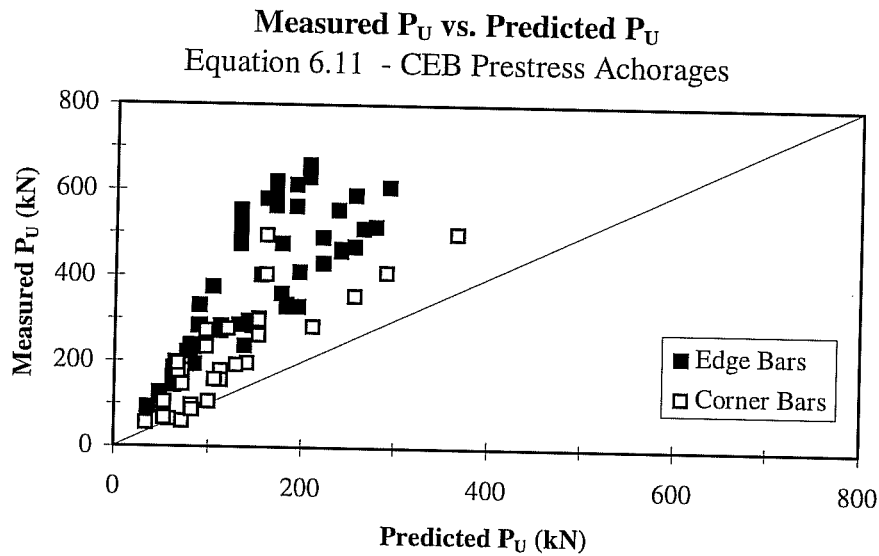


Figure 6.8 - Comparison of Measured and Predicted Capacities using Equation 6.11 based on CEB Model Code

6.4 Anchor Bolts

Experimental Studies: University of Texas

Hasselwander [20] studied the behavior of anchor bolts near the edges of concrete piers. Variables considered in this test program included embedment depth, clear cover and bearing area. To change the bearing area of the anchor bolts, washers of various sizes were attached to the anchor bolts. The range of bearing area sizes tested was similar to the range tested in the deep-embedment tests reported herein. The clear covers and concrete strengths were also similar to the deep-embedment tests. Variables from the deep-embedment tests not included

in Hasselwander's study include head shape, head aspect ratio, head thickness, development length and corner placement.

Hasselwander used a test setup that placed the anchor bolts in tension by simulating a moment on the pier. Unlike the deep-embedment pullout tests, the bearing reaction was not directly above the anchorage zone. For most of the tests longitudinal and transverse reinforcement was placed in the anchorage area to model typical details found in piers. Hasselwander, however, found very little difference in load-deflection behavior or ultimate capacity with different amounts, types and locations of pier reinforcement. Increases in ultimate capacity for two tests with hairpin transverse reinforcement placed near the head were measured. A wedge of concrete formed on the head at failure and was identical to that observed in the deep-embedment tests.

Based on the statistical regression analysis of his data, Hasselwander proposed the following best fit equation with all variables in standard US units:

$$P_U = A_b \sqrt{f'_c} \left[96 + 142 \ln \left(\frac{1}{1 - \frac{C_w}{C'}} \right) \right] \quad \text{eq. 6.12}$$

where A_b is the net bearing area, C_w is the clear cover over the washer (corresponding to C_h), C' is the clear cover over the bolt (corresponding to C_{cl}) and \ln is the natural log function.

Equation 6.12 is the only equation found that takes into account the effect of cover over the head. However, since Hasselwander used only circular heads, there was always some cover over the bar and the C_w/C' term never approached unity which would result in a division by zero. In the deep-embedment tests, two 35mm diameter bars had heads with an average width of 33mm. In this case, the cover over the head was equal to the clear cover and Hasselwander's equation cannot be applied. Measured capacities from the 108 deep-embedment pullout tests on edge and corner bars that resulted in blowout failures are plotted against the values calculated using Equation 6.12 in Figure 6.9. There is a large amount of scatter between the predicted and measured values for both edge and corner bars.

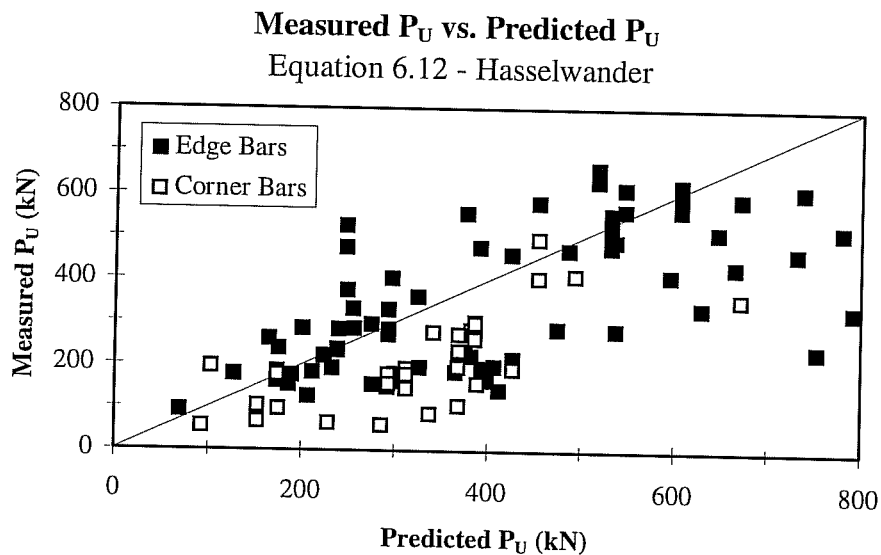


Figure 6.9 - Comparison of Measured and Predicted Capacities using Equation 6.12 by Hasselwander

Hasselwander modified Equation 6.12 to produce an equation better suited for design:

$$P_U = \phi 140 A_b \sqrt{f'_c} \left[0.7 + \ln \left(\frac{2C'}{D_w - D} \right) \right] \quad \text{eq. 6.13}$$

All the variables are in standard US units. D_w is the diameter of the circular head and D is the bolt diameter. In Figure 6.10, the measured capacities for the 108 deep-embedment tests are compared with predicted capacities using Equation 6.13. The term D_w was calculated for square and rectangular heads as an equivalent diameter:

$$D_w = \sqrt{\frac{4(h_1 h_2)}{\pi}} \quad \text{eq. 6.14}$$

The design equation, Equation 6.13, has less scatter than Equation 6.12, but scatter is still significant.

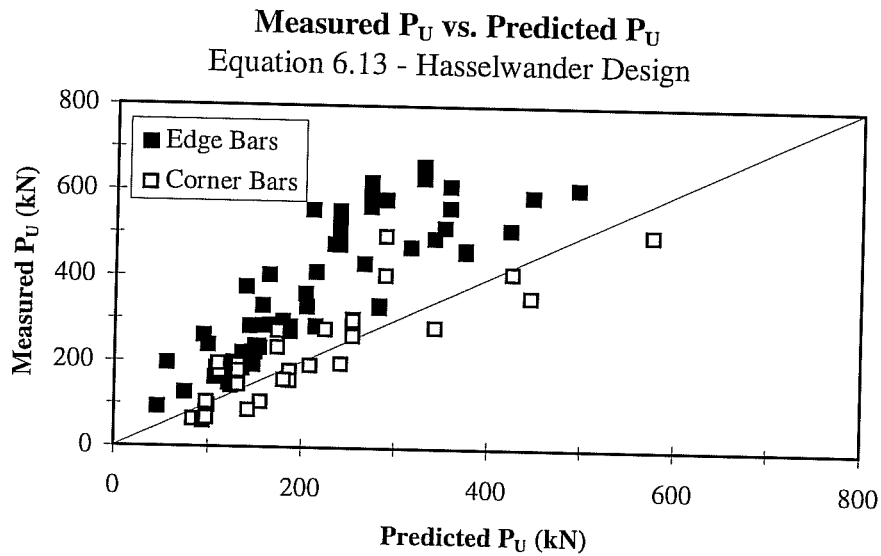


Figure 6.10 - Comparison of Measured and Predicted Capacities using Equation 6.13 by Hasselwander

Experimental Studies: University of Stuttgart

Furche and Eligehausen [18] conducted pullout tests on deeply embedded anchors near an edge of concrete to predict the side blowout capacity of the bolts. The test setup used by Furche and Eligehausen removed the bearing reaction from the anchorage zone. The head areas were less than most of the head areas for the deep-embedment pullout tests. The edge distances tested by Furche and Eligehausen were within the range used in the deep-embedment tests. Variables included in the deep-embedment tests on headed reinforcement not considered by

Furche and Eligehausen include: development length, transverse reinforcement, corner position and head geometry.

Based on a total of 51 tests with side blowout failures, Furche and Eligehausen proposed the following equation with all variables in SI units:

$$\mathbf{P_U} = 16.8\mathbf{m}\sqrt{\mathbf{A_b f'_c}} \quad \text{eq. 6.15}$$

where $\mathbf{P_U}$ is in N, \mathbf{m} is the distance from the edge to the center of the bolt (corresponding to $\mathbf{C_1}$) and $\mathbf{A_b}$ is the net bearing area ($\mathbf{A_n}$). The measured capacities from the 108 deep-embedment pullout tests are compared with the predicted values from Equation 6.15 in Figure 6.11. There is reasonable correlation between Equation 6.15 and the measured capacities of edge bars. The equation significantly overestimates the capacity of corner bars.

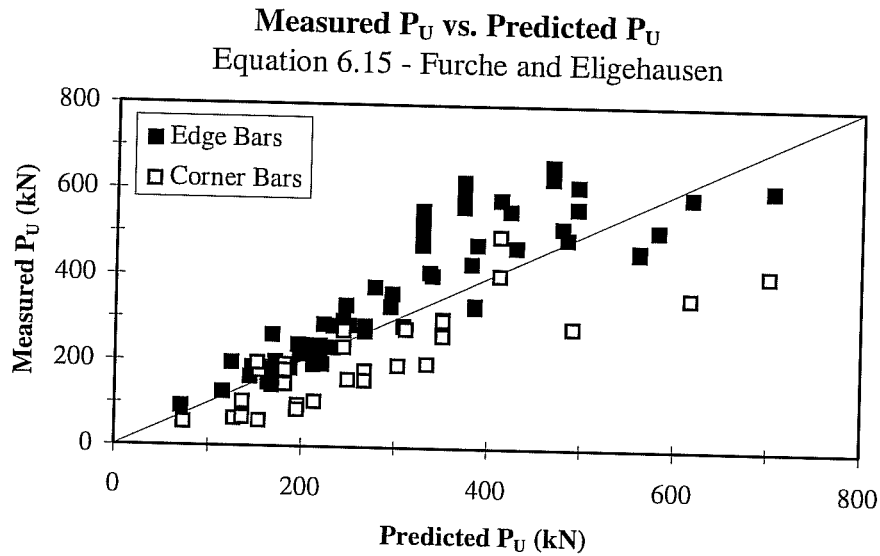


Figure 6.11 - Comparison of Measured and Predicted Capacities using Equation 6.15 by Furche and Eligehausen

Code Provisions: Proposed ACI 318 Section 23.11

Equation 6.15 by Furche and Eligehausen was adapted into a design equation in the recently proposed Chapter 23 governing anchorage to concrete for the ACI 318 (-98 or -01) Building Code [3].

The proposed design equation in customary US units is of the form:

$$P_U = 160c\sqrt{A_b f'_c} \quad \text{eq. 6.16}$$

where c is the edge distance (C_1) and A_b the net bearing area of the head (A_n). The measured values from the 108 deep-embedment pullout tests are compared with the predicted values from Equation 6.16 in Figure 6.12. The correlation

between this equation and the results is similar to the Furche and Eligehausen equation. Since it is a design equation it is more conservative. Neither Equation 6.15 or Equation 6.16 takes into account corner placement nor effects of close spacing.

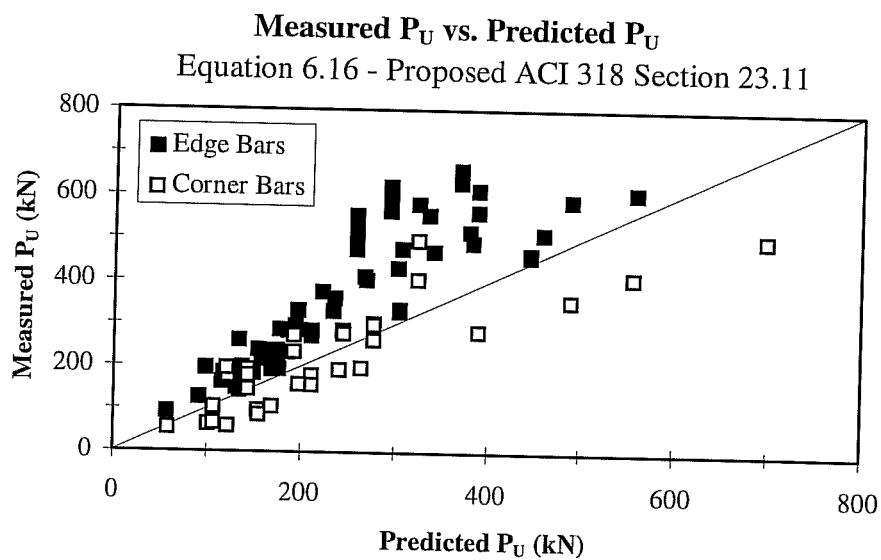


Figure 6.12 - Comparison of Measured and Predicted Capacities using Equation 6.14 from Proposed ACI 318 Section 23.11

Code Provisions: CEB Method

In the CEB Information Bulletin #226, “Design of Fastenings in Concrete - State-of-Art Report on Design and Application” [13], a method is outlined for determining the side blowout capacity of an anchor bolt. This method takes into

account close spacings, corner placement and head area. Some factors not included are development length, transverse reinforcement and head aspect ratio or thickness.

The CEB method begins with a characteristic equation for a single deeply embedded bolt near an edge with no influences from a second edge or other bolts.

The characteristic equation, in SI units, is of the form:

$$P_{U0} = k_5 C_1 d_b \sqrt{f'_c} \quad \text{eq. 6.17}$$

where P_{U0} is in N, C_1 is the edge distance and d_b is the bolt diameter. The value k_5 takes into account the head area and is calculated by:

$$k_5 = 7.2 \sqrt{\frac{d_h^2}{d_b^2} - 1} \quad \text{eq. 6.18}$$

where d_h is the diameter of the head.

The characteristic capacity, P_{U0} , is then modified for corner placement or close spacing by taking into account the changes in the area of the failure surface. This step is very similar in approach to that used in the Concrete Capacity Design method for pullout failures of anchor bolts. The CEB method assumes the blowout failure will be a pyramid with the size of the base of the pyramid being six times the edge distance on each side of the bolt (Figure 6.13). When the bolt is near an edge the full pyramid cannot form and the size of the pyramid is controlled by the second edge distance, C_2 (Figure 6.14). When bolts are closely

spaced the resulting failure surface is smaller than the combined failure surfaces for two individual bolts (Figure 6.15). To take these effects into account the characteristic capacity, P_{U0} , is multiplied by:

$$\frac{A_c}{A_c^0} \quad \text{eq. 6.19}$$

with

$$A_c^0 = 36C_1^2 \quad \text{eq. 6.20}$$

and A_c is the available area for the failure surface.

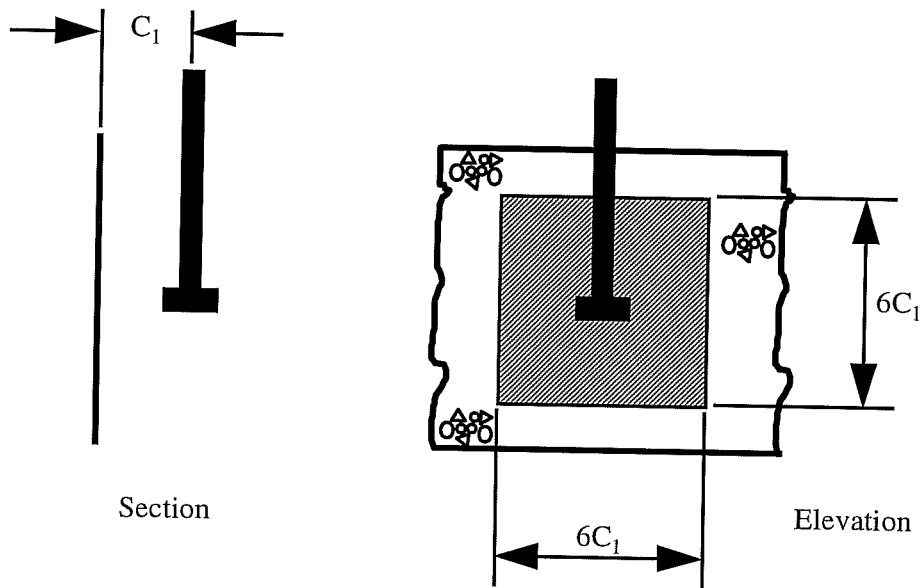


Figure 6.13 - Basic Blowout Failure Area for CEB Method

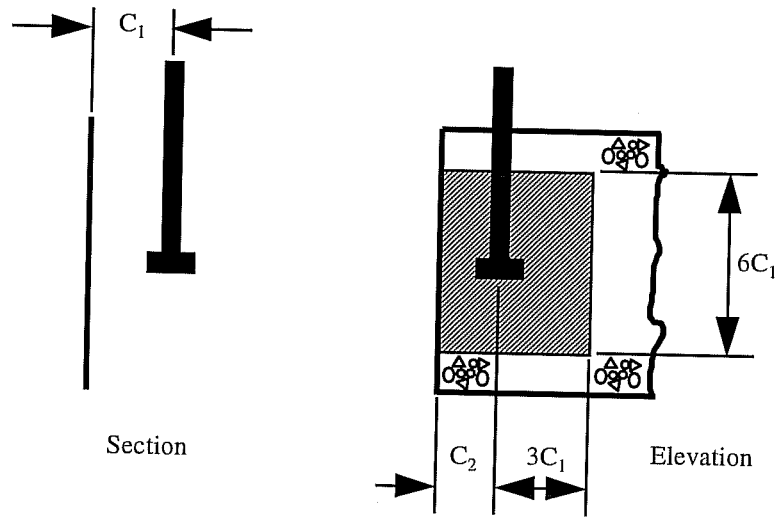


Figure 6.14 - CEB Blowout Failure Area for Corner Placement

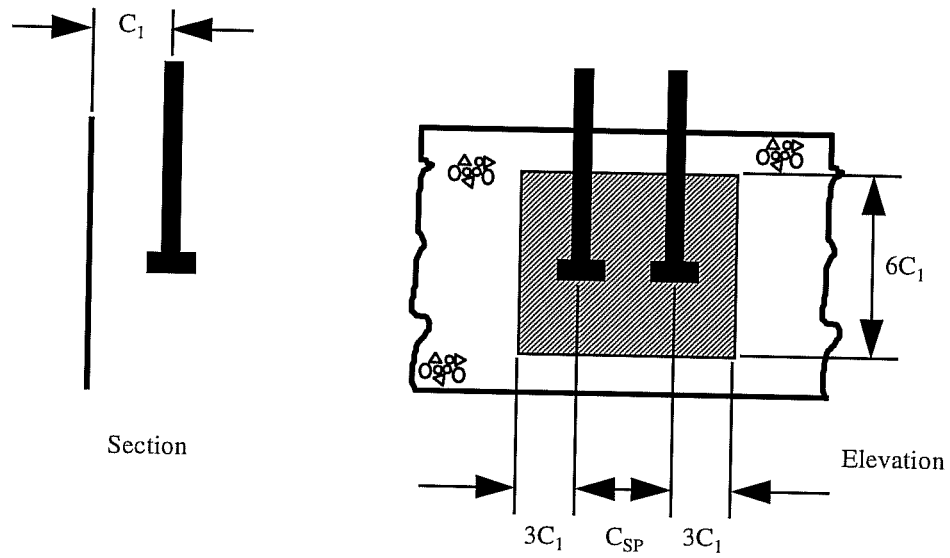


Figure 6.15 - CEB Blowout Failure Area for Close Spacing

In addition, the influence of the corner on the assumed distribution of stresses is taken into account by multiplying the characteristic value, P_{U0} , by a reduction factor:

$$\Psi = 0.7 + 0.3 \frac{C_2}{3C_1} \leq 1 \quad \text{eq. 6.21}$$

The characteristic equation with the two reduction factors provides the blowout capacity. The capacities predicted by this method are compared with the measured capacities from the 108 deep-embedment pullout tests in Figure 6.16. Since this method is valid for closely spaced bars, the results from the six tests on paired bars are included in Figure 6.16. There is little scatter in the data points,

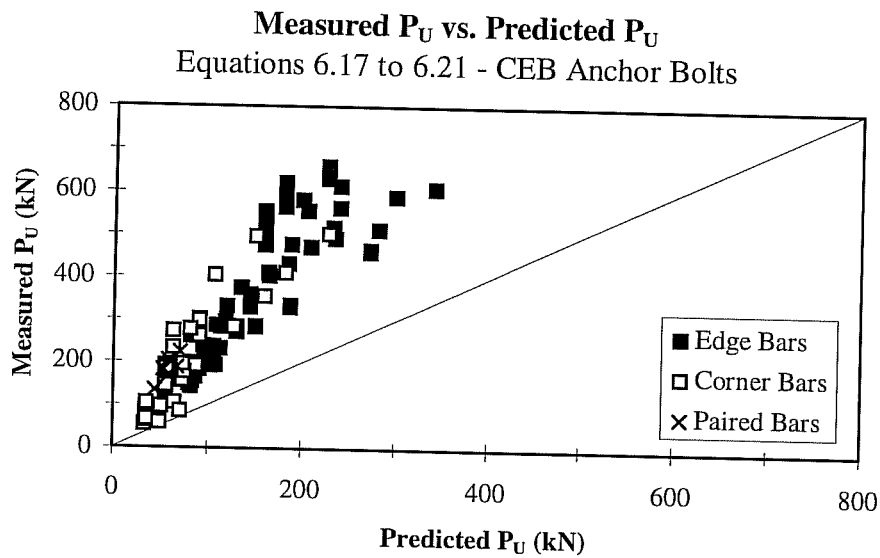


Figure 6.16 - Comparison of Measured and Predicted Capacities using CEB Method - Equations 6.17 through 6.21

which suggests that the variables included in this approach are valid, but the method is very conservative.

6.5 Summary

To compare the effectiveness of the various methods for predicting the capacity of deeply embedded headed reinforcement, statistical measures of the measured capacities divided by the predicted capacities were calculated. Since most methods did not take into account corner effects, the results from the deep-embedments tests on edge bars provide the best comparison. In Table 6.1 the standard deviation, average, maximum and minimum of the measured ultimate capacities divided by the predicted capacities from the various equations discussed for the 77 deep-embedment tests on edge bars are summarized. The methods are listed in the order that best model the behavior of headed reinforcement. The best approach should have good correlation with the measured data by minimizing the standard deviation or scatter. A small standard deviation would suggest that the method modeled the observed behavior well. Also, the average, maximum and minimum of the measured capacities divided by the predicted capacities should be close to unity. If these three values equal 1, then the method perfectly predicted the capacities of the tests.

		Edge Bars P_U Measured / P_U Predicted			
Method	Eq.	Standard Deviation	Average	Maximum	Minimum
Furche and Eligehausen	6.15	0.25	1.19	1.69	0.82
ACI 318 Proposed Section 23.11	6.16	0.32	1.50	2.15	1.03
Hasselwander	6.12	0.35	0.93	2.13	0.32
Hawkins	6.2	0.37	1.57	2.47	1.13
Hasselwander Design	6.13	0.46	1.75	3.57	1.16
Roberts	6.9	0.51	2.32	3.49	1.52
CEB Method (Anchor Bolts)	6.17...	0.52	2.45	3.47	1.69
Williams	6.7	0.56	2.70	3.84	1.92
CEB Model Code (Prestress)	6.11	0.64	2.76	4.19	1.69
ACI 318 Section 10.17	6.3	0.98	3.26	5.50	1.83

Table 6.1 - Summary of Statistical Measures for Comparisons of Edge Bar Capacities

Equation 6.15 by Furche and Eligehausen had the best correlation (lowest standard deviation) with the measured data. The proposed ACI design equation, Equation 6.16, based on Equation 6.15 also performed well. The two equations by Hasselwander, Equation 6.12 and 6.13, had good correlation but a wider range of values for average, maximum and minimum. The equation by Hawkins, Equation 6.2, modeled the behavior surprisingly well given the differences in test setups and variables. The CEB design method for anchor bolts, Equations 6.17 through 6.21, was quite conservative as were the prestress anchorage methods, Equation 6.7 by Williams, Equation 6.9 by Roberts and Equation 6.11 from the CEB Model Code. The ACI equation, Equation 6.3, for bearing capacity of concrete was very conservative and had the poorest correlation with the data.

The statistical measures of the methods for the 31 deep-embedment corner bar tests are listed in Table 6.2. The general trends are the same as for the edge bar results. The statistical measures for the 108 deep-embedment tests on single bars are listed in Table 6.3

		Corner Bars P_U Measured / P_U Predicted			
Method	Eq.	Standard Deviation	Average	Maximum	Minimum
Furche and Eligehausen	6.15	0.26	0.77	1.29	0.38
ACI 318 Proposed Section 23.11	6.16	0.33	0.98	1.63	0.49
Hasselwander	6.12	0.32	0.67	1.92	0.21
Hawkins	6.2	0.38	1.07	1.81	0.45
Hasselwander Design	6.13	0.34	1.10	1.78	0.61
Roberts	6.9	0.54	1.54	2.58	0.69
CEB Method (Anchor Bolts)	6.17...	0.78	2.61	4.33	1.20
Williams	6.7	0.60	1.80	3.01	0.87
CEB Model Code (Prestress)	6.11	0.65	1.85	3.10	0.82
ACI 318 Section 10.17	6.3	0.96	2.41	4.57	0.73

Table 6.2 - Summary of Statistical Measures for Comparisons of Corner Bar Capacities

		All Bars P_U Measured / P_U Predicted			
Method	Eq.	Standard Deviation	Average	Maximum	Minimum
Furche and Eligehausen	6.15	0.32	1.07	1.69	0.38
ACI 318 Proposed Section 23.11	6.16	0.40	1.35	2.15	0.49
Hasselwander	6.12	0.36	0.87	2.13	0.21
Hawkins	6.2	0.43	1.42	2.47	0.45
Hasselwander Design	6.13	0.52	1.57	3.57	0.61
Roberts	6.9	0.52	1.57	3.57	0.61
CEB Method (Anchor Bolts)	6.17...	0.60	2.50	4.33	1.20
Williams	6.7	0.70	2.44	3.84	0.87
CEB Model Code (Prestress)	6.11	0.76	2.50	4.19	0.82
ACI 318 Section 10.17	6.3	1.04	3.02	5.50	0.73

Table 6.3 - Summary of Statistical Measures for Comparison of All Deep-Embedment Test Capacities

Chapter 7

Deep-Embedment Pullout Tests Regression Analysis

7.1 Introduction

After reviewing the effects of the individual variables tested in the deep-embedment tests, the primary variables affecting the anchorage capacity of headed reinforcement were edge distance, head area and concrete strength. Development length added strength to the anchorage, while placing the reinforcing bar in a corner or closely spacing the bars reduced the capacity. Regression analyses were conducted on the results to determine the best description of these primary variables and to generate a “best-fit” equation for the blowout capacity of headed reinforcement.

7.2 Regression Analysis Procedure

To determine the best description of the main variables affecting the anchorage capacity, multi-variable non-linear regression analyses were conducted using the data generated from the deep embedment pullout tests. Based on the results of the tests, the influence of cover, head area and concrete strength were considered. It was assumed that the characteristic application of headed reinforcement would be an edge bar with no development length. Since the goal was to generate a design equation, the simplicity of the “best-fit” equation was considered in choosing variables and equations.

The non-linear multi-variable regression analyses were conducted using a PC-based computer program, NLREG 3.3. NLREG is a program for curve fitting with virtually no limit on the number of variables or parameters. NLREG uses a model/trust-region technique for an adaptive algorithm which combines the Gauss-Newton and Levenberg-Marquardt methods [41].

The output from NLREG includes several statistical measures of the curve fit in addition to the calculated parameters for the curve fit equation. Four statistical measures of the regressions will be presented to gauge which variables and equations provide the best description of the data. These four measures are the maximum deviation, average deviation, standard error and proportion of variance explained.

The maximum deviation represents the maximum absolute value of the difference between the measured value and the predicted value. The average deviation is the average of the absolute values of the differences. The standard error measures the variation or scatter of the deviations between the measured and predicted values. Finally the “proportion of variance explained” or the “coefficient of multiple determination”, R^2 , is presented. R^2 is a measure of how well the curve fit predicts the values and is presented as a percentage. A value of 100% means the curve fit perfectly predicts the measured values while a value of 0% means that the curve fit does no better in predicting the measured values than using the mean of the measured values. To choose the best equation or description of a variable for the data, the maximum deviation, average deviation and standard error should be minimized, while R^2 should be maximized.

Although there was no restriction on the analysis from NLREG, the regressions all used power functions for the analyses. Choosing one equation type reduced the number of regressions performed. Power functions were chosen over such functions as log and natural log because power functions are usually more transparent (the results are easier to predict without a calculator) than the log functions and are traditionally used for equations describing the behavior of concrete members and have proven to be effective in modeling behavior of concrete.

7.3 Head Area

The first of the three primary variables analyzed was head area. To determine the best description of the effect of head area, regression analyses were performed using results from the series of 27 tests on head geometry discussed in Section 5.10 (See Table 5.17 for the parameters and results of these tests). Head yielding was measured in several of these 27 tests. Since it was unclear how head yielding affected the capacity, the regression analyses were repeated using results from 18 tests in which the head did not yield. The results from these regressions were not significantly different from the results using all 27 tests.

Four different descriptions were considered for head area: the total head area, A_h ; the net bearing area, A_n ; and these two values divided by the bar area, A_b , A_h/A_b and A_n/A_b . The basic equation for the regression analyses was:

$$P_U = kV^x + B \quad \text{eq. 7.1}$$

where P_U is the ultimate capacity, V is one of the four descriptions of head area and k , x and B are curve fit parameters. Four forms of Equation 7.1 were analyzed: a linear form with x equal to unity and B equal to 0; a linear form with x equal to unity and no restraint on B ; a power function with no restraint on x and B equal to 0; and a power function with no restraint on x or B . The results from 16 analyses are summarized in Table 7.1.

Reg.	$P_U = kV^x + B$ V	k	x	B	Deviation		Std. Error	R ²
					Max.	Avg.		
1	A_h	0.294	0.786	0.000	63.0	15.5	22.7	86%
2	A_n	0.805	0.680	0.000	50.9	19.8	25.7	82%
3	A_h/A_b	85.9	0.455	0.000	152	35.8	48.4	37%
4	A_n/A_b	109	0.365	0.000	151	36.1	48.7	37%
5	A_h	0.00115	1.38	88.6	59.9	13.5	21.0	89%
6	A_n	0.000395	1.51	110	44.7	16.4	21.6	88%
7	A_h/A_b	2.81	1.58	140	158	33.5	48.6	39%
8	A_n/A_b	4.35	1.44	143	157	33.6	48.7	39%
9	A_h	0.0480	1.00	0.000	69.9	19.0	26.3	81%
10	A_n	0.0554	1.00	0.000	76.1	25.9	33.6	69%
11	A_h/A_b	27.3	1.00	0.000	153	44.4	60.3	
12	A_n/A_b	30.7	1.00	0.000	156	49.8	67.8	
13	A_h	0.0379	1.00	47.0	61.6	14.4	21.4	88%
14	A_n	0.0391	1.00	66.8	48.7	17.5	22.7	86%
15	A_h/A_b	14.0	1.00	106	154	34.6	47.8	39%
16	A_n/A_b	14.0	1.00	120	154	34.6	47.8	39%

Table 7.1 - Results of Regression Analyses for Head Area

Based on the results from these analyses, the two ratios, A_h/A_b and A_n/A_b , performed poorly and A_h performed slightly better than A_n . The power function with no restraint on x or B performed the best of the four equation forms. This is not surprising since this form has the most degrees of freedom.

The most accurate curve fit used the total head area, A_h , and was:

$$P_U = 0.00115A_h^{1.38} + 88.6 \quad \text{eq. 7.2}$$

This equation reasonably models the measured capacities for the 27 tests as shown in Figure 7.1.

P_u vs. Head Area

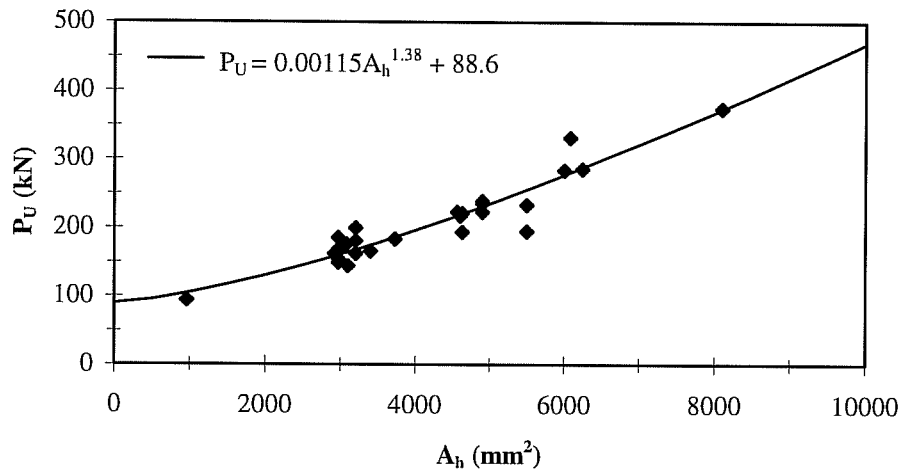


Figure 7.1 - Comparison of Best-Fit Equation for Head Area (Equation 7.2) with Test Results

There was little difference in the results of the regression analyses using the total head area and the net head bearing area. Normally the net bearing area is used in equations for anchor bolts. One mathematical advantage of using the net bearing is that it can conceivably equal zero while the total head area is limited to a minimum equal to the bar area. However, the total head area is easier to calculate in design.

The analyses that restricted the y-intercept, B , to 0 had results only slightly less accurate than Equation 7.2. It is intuitive that a headed reinforcing bar with no head area (and no development length) should have no capacity. However, it is

not necessarily true that an equation for the blowout capacity of headed reinforcement should predict no capacity with no head area.

If a bar is placed in concrete with no development length and no head then the pullout capacity is zero. If a small head, slightly larger than the bar is added, the pullout capacity would increase but a blowout failure would probably not occur. Instead a pullout failure characterized by a small cylinder of concrete being pulled out would occur. A pullout failure should not be confused with a pullout-cone failure. Blowout, pullout-cone and pullout modes of failure are compared in Figure 7.2. Only when the head reaches a certain size would a blowout or pullout-cone failure occur. The possibility of this switch in failure mode could lead to an equation for blowout capacity with a y-intercept greater than zero.

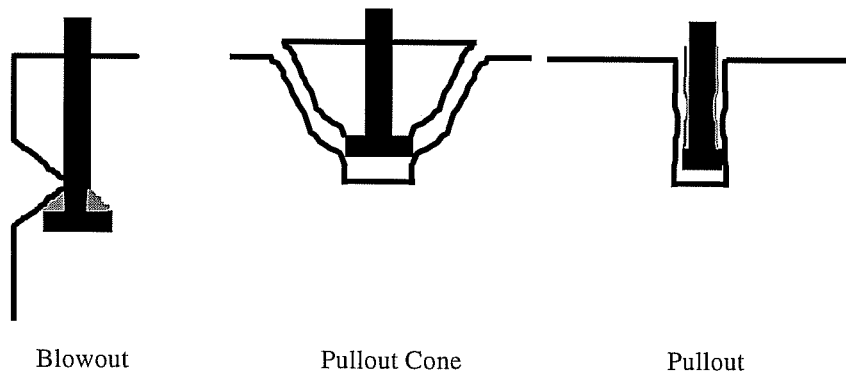


Figure 7.2 - Comparison of Possible Failure Modes

7.4 Concrete Strength

Since blowout failures involve the tensile capacity of concrete, the tensile strength of concrete may be the most appropriate material property to use in equations predicting the capacity. However, the tensile strength of concrete is usually described using the square root or other power function of the compressive strength. For this reason no regression analyses were conducted with concrete strength as the only variable and a power function of the compressive strength of concrete, $(f'_c)^x$, was used in the following regression analyses.

7.5 Edge Distance

The results from tests on 57 edge bars with no development length were used to analyze different descriptions of the edge distance. The parameters for these 57 tests are listed in Table 7.2. The edge distance, head area and concrete strength were variables for these tests. To account for the variation in head area and concrete strength the following equation was used for the regression analysis:

$$P_U = kV^x A_h^{1.38} \sqrt{f'_c} + B \quad \text{eq. 7.3}$$

where V is the variable describing edge distance. The value of 1.38 for the exponent of A_h is from Equation 7.2. The square root of the concrete strength was assumed since this is traditionally used to calculate the tensile strength of

Test ID	d _b (mm)	Nominal Head (mm)	C ₁ (mm)	C ₂ (mm)	l _d (mm)	f _c (MPa)	P _U (kN)
C1B1	25	70x70x16	35	457	0	25	239
C1B2	25	70x70x16	48	457	0	25	283
C1B3	25	70x70x16	48	457	0	25	272
C3B1	35	100x55x25	51	457	0	29	285
C3B2	35	55x100x25	51	457	0	29	284
C3B3	35	100x55x25	64	457	0	29	330
C3B4	35	55x100x25	64	457	0	29	335
C4B1	35	90x90x20	45	457	0	29	403
C4B2	35	90x90x20	51	457	0	29	476
C4B3	35	90x90x20	64	457	0	29	491
C4B4	35	90x90x20	76	457	0	29	512
C7B1	35	90x90x20	89	457	0	24	589
C7B2	35	90x90x20	102	457	0	24	609
C7B3	35	100x55x25	102	457	0	24	460
C7B4	35	55x100x25	102	457	0	24	464
C8B5	20	35x70x16	30	457	0	24	127
C8B6	20	70x35x16	45	457	0	24	177
C8B7	20	35x70x16	45	457	0	24	155
C15B1	35	57x57x16	45	305	0	19	162
C15B2	35	40x80x16	45	305	0	19	185
C15B3	35	70x70x16	45	305	0	19	221
C15B4	35	49x99x16	45	305	0	19	217
C15B5	35	55x100x25	45	305	0	19	194
C15B6	35	80x80x16	45	305	0	19	283
C15B7	35	90x90x16	45	305	0	19	374
C16B1	25	33x33x16	45	305	0	19	93
C16B2	25	57x57x12	45	305	0	19	154
C16B3	25	57x57x16	45	305	0	19	168
C16B4	25	57x57x20	45	305	0	19	176
C16B5	25	40x80x12	45	305	0	19	162
C16B6	25	40x80x16	45	305	0	19	163
C16B7	25	40x80x18	45	305	0	19	180
C16B8	25	40x80x20	45	305	0	19	149

Table 7.2 - Parameters and Results for Deep-Embedment Tests on Edge Bars with No Development Length

Test ID	d_b (mm)	Nominal Head (mm)	C_1 (mm)	C_2 (mm)	l_d (mm)	f_c (MPa)	P_U (kN)
C17B1	25	33x98x12	45	305	0	19	144
C17B2	25	33x98x16	45	305	0	19	165
C17B3	25	33x98x20	45	305	0	19	199
C17B4	25	70x70x12	45	305	0	19	238
C17B5	25	70x70x16	45	305	0	19	235
C17B6	25	70x70x20	45	305	0	19	222
C17B7	25	49x99x16	45	305	0	19	222
C17B8	25	55x100x25	45	305	0	19	233
C17B9	25	80x80x12	45	305	0	19	285
C17B10	25	80x80x16	45	305	0	19	331
C17B11*	25	70x70x16	45	305	0	19	183
C17B12*	25	77x77x16	45	305	0	19	193
C18B1	35	55x100x25	45	305	0	44	411
C18B2	35	55x100x25	51	305	0	44	432
C18B3	35	55x100x25	64	305	0	44	517
C18B4	35	90x90x20	45	305	0	44	555
C18B5	35	40x80x25	45	305	0	44	238
C18B6	35	40x80x25	64	305	0	44	330
C19B1	35	70x70x20	45	305	0	44	360
C19B2	35	70x70x20	64	305	0	44	470
C19B3	25	40x80x25	45	305	0	44	287
C19B4	25	40x80x25	25	305	0	44	196
C19B5	25	57x57x16	45	305	0	44	295
C19B6	25	57x57x16	30	305	0	44	261

Table 7.2 - Continued

concrete. The regression analyses for cover were conducted assuming that the y-intercept of the curve fit was greater than zero. In the development of straight bars, if the distance from the edge of the concrete to the center of the bar, C_1 , was equal to zero, or the clear cover equal to zero (Figure 7.3) then intuitively there should be essentially zero capacity. However, with headed reinforcement, there

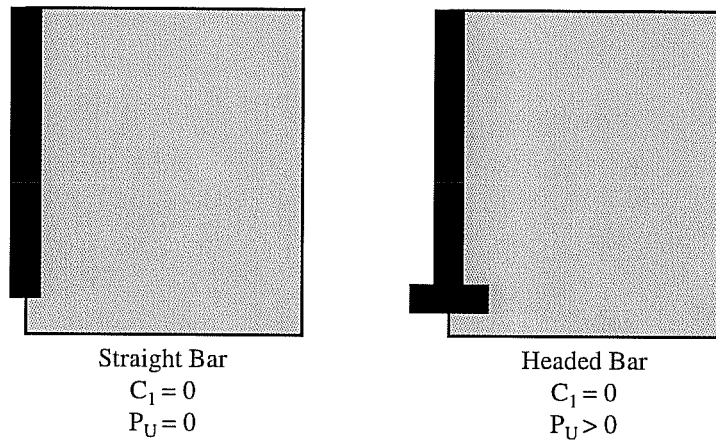


Figure 7.3 - Comparison of Straight and Headed Bars with No Cover

should still be a capacity when the edge distance or cover is zero, since half of the head still bears against the concrete.

As with head area, a variety of possible descriptions of edge distance were analyzed. A total of twenty-one were analyzed. The three main cover parameters, C_1 , C_{c1} , and C_{h1} , were considered as were each of these three parameters divided by d_b , h_1 , h_2 , h_{max} and h_{min} . These variables were chosen to determine if bar or head geometry affected the capacity. Also, three ratios of the cover parameters were analyzed, C_{c1}/C_1 , C_{h1}/C_1 and C_{h1}/C_{c1} . The results of the regression analyses are presented in Table 7.3.

Reg.	$P_U = kV^x A_h^{1.38} f_c^{0.5} + B$ V	k x10e6	x	B	Deviation		Std. Error	R ²
					Max.	Avg.		
1	C ₁	19.4	0.670	114	116	34.3	44.8	89%
2	C _{c1}	50.9	0.483	108	117	35.0	45.7	88%
3	C _{h1}	6.33	1.00	210	345	73.9	95.3	48%
4	C ₁ /d _b	231	0.604	90.3	128	36.8	48.5	87%
5	C _{c1} /d _b	297	0.431	89.5	125	37.3	48.9	86%
6	C _{h1} /d _b	288	0.312	155	400	67.2	93.3	50%
7	C ₁ /h ₁	409	0.520	61.2	108	30.0	43.3	89%
8	C _{c1} /h ₁	461	0.438	66.6	108	30.5	42.5	90%
9	C _{h1} /h ₁	334	0.196	147	408	67.0	95.2	48%
10	C ₁ /h ₂	387	0.481	91.0	125	35.8	48.0	87%
11	C _{c1} /h ₂	433	0.398	90.6	118	35.8	47.2	87%
12	C _{h1} /h ₂	412	0.372	158	397	64.7	91.1	53%
13	C ₁ /h _{min}	402	0.502	59.4	116	30.2	42.6	90%
14	C _{c1} /h _{min}	450	0.421	65.1	115	31.0	42.2	90%
15	C _{h1} /h _{min}	338	0.209	146	409	66.7	94.7	49%
16	C ₁ /h _{max}	413	0.637	96.2	121	34.7	45.0	88%
17	C _{c1} /h _{max}	462	0.477	94.3	113	35.5	45.4	88%
18	C _{h1} /h _{max}	419	0.378	158	397	65.5	91.4	52%
19	C _{c1} /C ₁	554	1.48	88.1	119	39.1	50.0	86%
20	C _{h1} /C ₁	344	0.256	148	406	68.2	95.9	48%
21	C _{h1} /C _{c1}	368	1.00	182	373	83.8	107	35%

Table 7.3 - Results of Regression Analyses for Edge Distance

From the results of the regression analyses, the edge distance, C₁, and the clear cover, C_{c1}, best describe the data. The ratios of bar or head dimensions with C₁ and C_{c1} also described the data very well. There was very little difference between the results from these twelve analyses. The clear cover over the head, C_{h1}, and the ratios of C_{h1} with bar or head dimensions did not perform as well as ratios of C₁ and C_{c1}. The three ratios of the cover parameters also did not perform

as well. It appears that the edge distance is important but the data is not sensitive to how this factor is described. For simplicity, the edge distance, C_1 , or the clear cover, C_{c1} , appear to be the best terms to use as variables. The most accurate equation using C_1 was:

$$P_U = 0.0000194C_1^{0.670} A_h^{1.38} \sqrt{f'_c} + 114 \quad \text{eq. 7.4}$$

The measured values for the 57 deep-embedment tests are compared with the predicted values from Equation 7.4 in Figure 7.4.

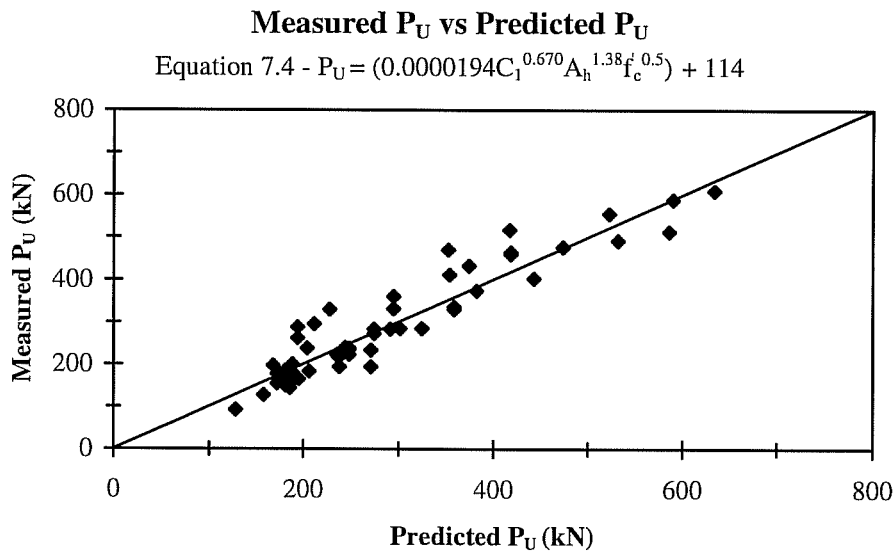


Figure 7.4 - Comparison of Best-Fit Equation for Edge Distance (Equation 7.4) with Test Results

In equations for anchor bolts it is common to use the edge distance. Anchor bolts are commonly placed after the concrete has been cast and hardened and often are drilled into place. For construction reasons it is easier to locate the center of the bolt. For longitudinal reinforcement, protection of the reinforcement is important and it is traditional to call out the required clear cover over the bar in construction documents, not the distance to the center of the bar. When headed reinforcement is to be used as the longitudinal reinforcement and not in anchor bolt type applications, the clear cover seems the most appropriate variable. However, both variables for cover can be used to accurately predict the capacity of the anchorage.

7.6 Best-Fit Equation

Following examples of equations for anchor bolts, the primary variables for the blowout capacity of headed reinforcement are: edge distance, C_1 ; net bearing area, A_n and concrete compressive strength, f'_c . When headed reinforcement is being used for main reinforcement of concrete members, the simplest variables are: clear cover, C_{cl} ; total head area, A_h and concrete compressive strength, f'_c . Both sets of variables can accurately predict the blowout capacity of headed reinforcement. However, since the Concrete Capacity Design method for the

pullout-cone capacity of headed reinforcement is calculated using “Anchor Bolt” variables, it seems simpler to also use these for the blowout capacity.

Though it is possible that a headed reinforcing bar could have a capacity with no cover and also possible that the best equation for blowout failures would predict a capacity if the bar has no head attached, it is not possible for there to be any capacity if the concrete strength is zero. It is very unusual to find design equations for reinforced concrete that predict capacities when one of the primary variables is equal to zero. With this in mind, it is best to use an equation with a y-intercept of zero.

A regression analysis was performed using the data from the 57 deep embedment pullout tests with no development length that resulted in blowout failures and the three primary “Anchor Bolt” variables to produce a best-fit equation. A power function was used for the curve fit:

$$P_U = kC_1^x A_n^y f_c^z \quad \text{eq. 7.5}$$

The regression produced the following equation:

$$P_U = 0.0252C_1^{0.609} A_n^{0.577} f_c^{0.671} \quad \text{eq. 7.6}$$

with P_U in kN, C_1 in mm, A_n in mm^2 and f_c in MPa. Equation 7.6 very accurately predicted the measured capacities. The maximum deviation between the predicted and measured capacities was 69.7 with an average of 20.6. The standard error from this regression was 28.2 and the value of R^2 was 96%. The

predicted capacities from Equation 7.6 are compared with the measured capacities of the 57 deep embedment tests in Figure 7.5.

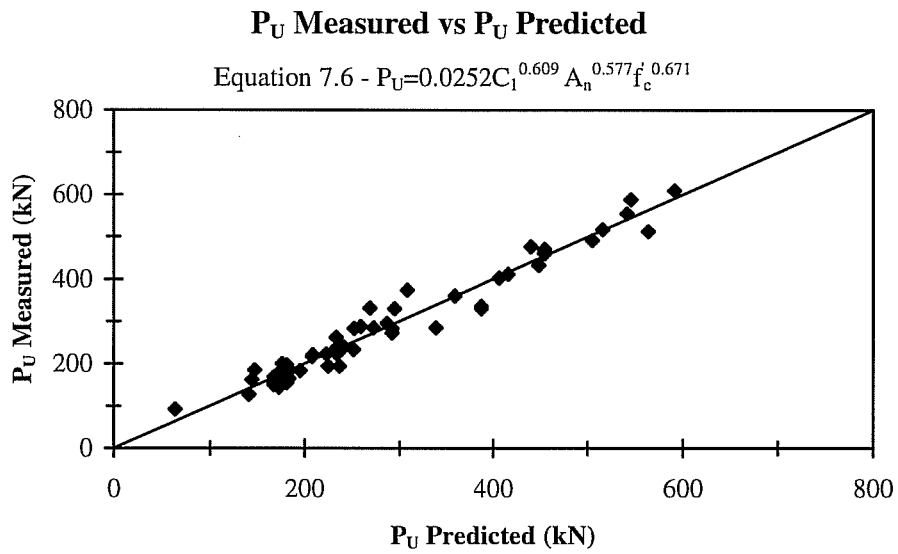


Figure 7.5 - Comparison of Measured Capacities with Capacities Predicted by Best-Fit Equation (Equation 7.6)

Chapter 8

Deep-Embedment Pullout Tests Physical Model

8.1 Introduction

In the previous chapter regression analyses were conducted on the results of the deep-embedment tests to determine the best description of the variables and to generate a “best-fit” equation for the blowout capacity of headed reinforcement. While the best-fit equation can accurately predict the capacity, there is no relationship between the equation and the physical behavior of concrete or headed reinforcement. One of the major advantages of the proposed Concrete Capacity Design method for anchorage to concrete is a relationship with a physical model to describe the behavior of anchor bolts.

In this chapter a physical model for a side blowout failure will be proposed. Equations predicting the blowout capacity of headed reinforcement will be generated from this model and compared with the measured capacities and the best-fit equation from the previous chapter.

8.2 Physical Model

The basic model for a pullout-cone failure of a headed stud or anchor bolt is that the bolt force is resisted by a distribution of tensile stress in the concrete surrounding the anchor. The tensile stress creates the failure plane of the pullout cone (Figure 8.1). In this model the driving force is the tension in the anchor and the resisting force is the tensile capacity of the pullout cone of concrete. Most models have used a circular cone to describe the failure surface. One of the advantages of the Concrete Capacity Design is the use of a pyramid to describe the failure surface, which simplifies the calculation of the cone area and the effects of corner placement or overlapping cones of anchor groups.

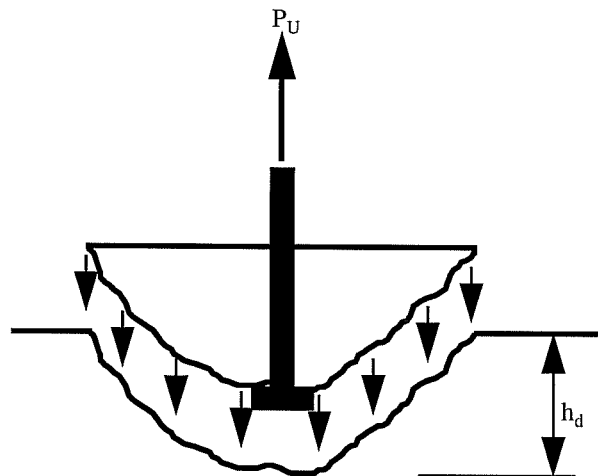


Figure 8.1 - Pullout-Cone Failure

The basic model used to describe a blowout failure is similar to the model for a pullout-cone but turned ninety degrees to the tension of the bar. In this model the edge distance replaces the embedment depth. This model was used by Furche and Eligehausen [18] in their study of blowout failures of anchor bolts.

As the load on an anchor or headed bar placed near an edge is increased, a cone or pyramid of compacted concrete forms on the head. The bearing of this pyramid of concrete on the surrounding concrete creates a quasi-hydrostatic state of stress in the surrounding concrete (Figure 8.2). The lateral force from this stress is resisted by tensile stress in the surrounding concrete. The failure surface is the blowout cone. For this model the driving force is proportional to the tensile load and the resisting force is the tensile capacity of the blowout cone.

8.3 Equations of the Physical Model

To generate an equation using this physical model the driving force or the relationship between the tension and lateral load, and the ultimate resisting force must be determined.

The ultimate resisting capacity, R_U , is equal to the ultimate tensile strength of the blowout cone which can be calculated by assuming a uniform tensile stress

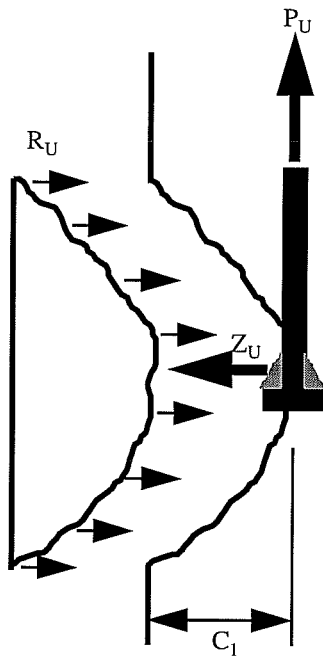


Figure 8.2 - Blowout Failure

equal to the tensile capacity of concrete distributed over the area of the failure surface:

$$\mathbf{R_U} = \mathbf{A_{bo}f_t} \quad \text{eq. 8.1}$$

where $\mathbf{R_U}$ is the ultimate resisting force, $\mathbf{A_{bo}}$ the area of the failure surface and $\mathbf{f_t}$ the tensile strength of concrete. Units of mm^2 for area and MPa for stress result in units of N for $\mathbf{R_U}$.

Assuming that the failure surface is a square based pyramid with height equal to the edge distance, C_1 , and the internal angle, θ , of the pyramid is constant, then the area of the base is proportional to C_1 and θ :

$$A_{bo} = 4C_1^2 \tan^2 \theta \quad \text{eq. 8.2}$$

or

$$A_{bo} = (2DC_1)^2 \quad \text{eq. 8.3}$$

where D is $\tan\theta$ as shown in Figure 8.3

The height and width of blowout failures were measured at the conclusion of each test. The failure surfaces were very rough and the height and widths were measured as the greatest overall horizontal and vertical distances as shown in Figure 8.4. Multiplying these two values results in A_{bo} . Table 8.1 lists statistical measures for measured values of A_{bo} , and calculated values of D and θ . In Figure 8.5, the measured blowout area, A_{bo} , is plotted against head area, A_h , for the series of 27 tests on head geometry discussed in Section 5.10. There is no obvious correlation between A_{bo} and A_h . The correlation between A_{bo} and the edge distance C_1 for the 57 deep embedment edge bar tests with no development length is shown in Figure 8.6. In Figures 8.7 and 8.8, θ is shown to be fairly constant with head area and edge distance.

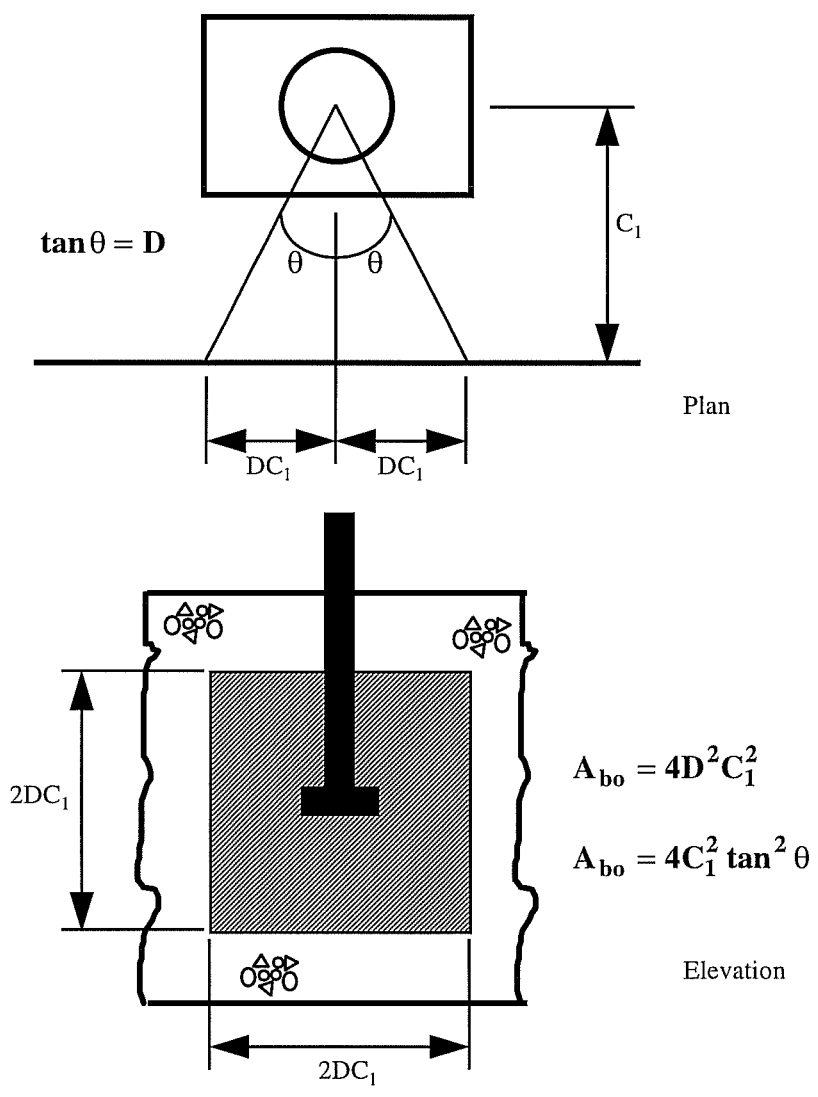


Figure 8.3 - Geometry of Blowout Failure

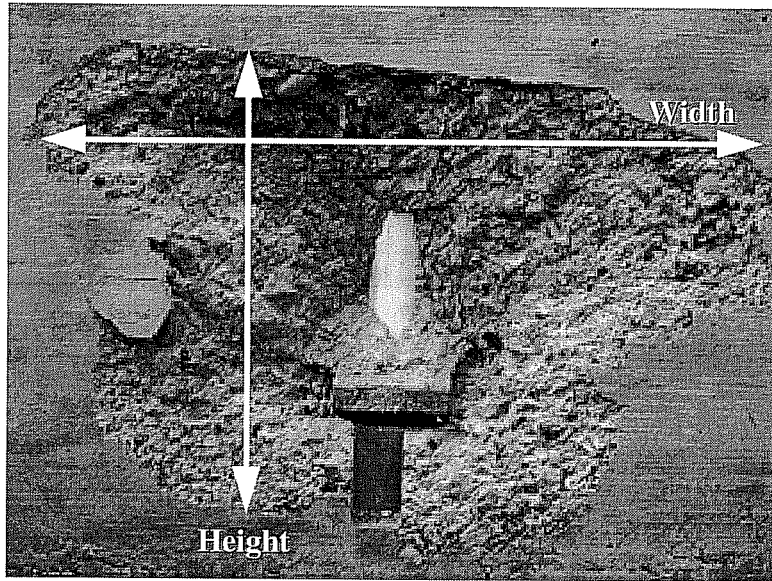


Figure 8.4 - Dimensions of Blowout Failures

	A_{bo} (mm ²)	D	θ
Maximum	411612	5.1	78.8
Minimum	10323	1.4	53.9
Average	130440	3.0	70.9
Standard Deviation	98476	0.7	4.8

Table 8.1 - Statistical Measures of Measured Sizes of Blowout Failures

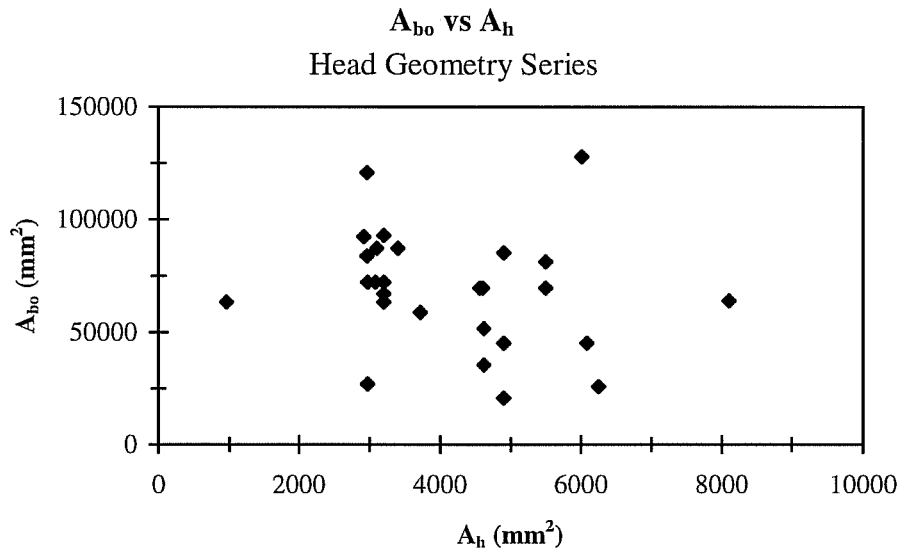


Figure 8.5 - Comparison of Blowout Area with Head Area

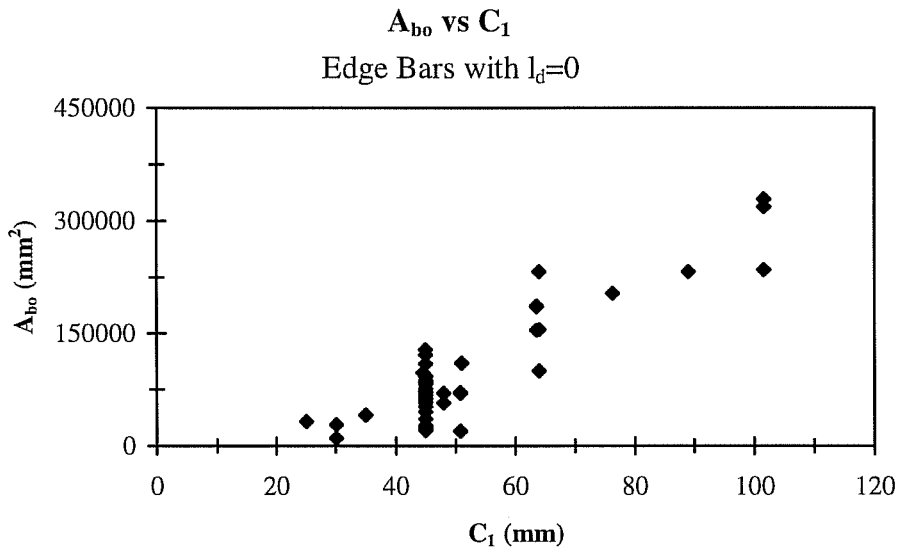


Figure 8.6 - Comparison of Blowout Area with Edge Distance

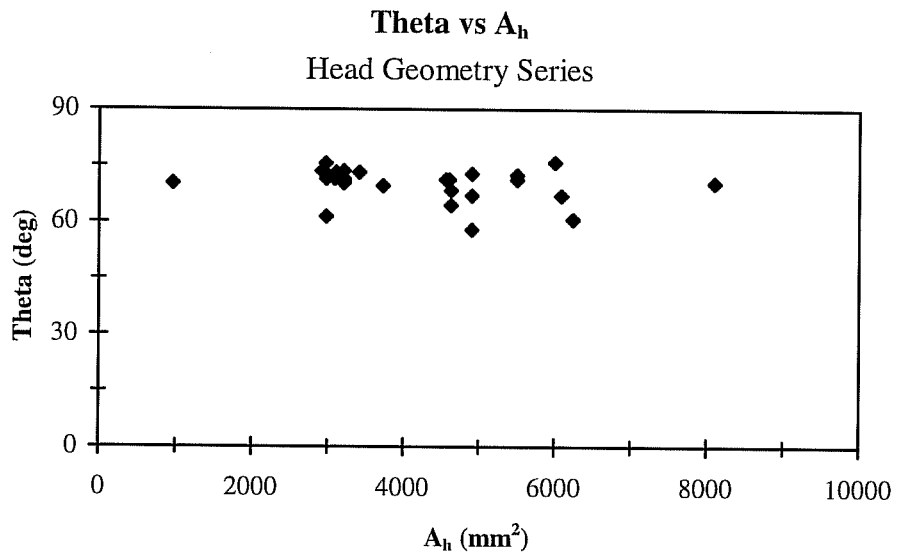


Figure 8.7 - Comparison of Theta with Head Area

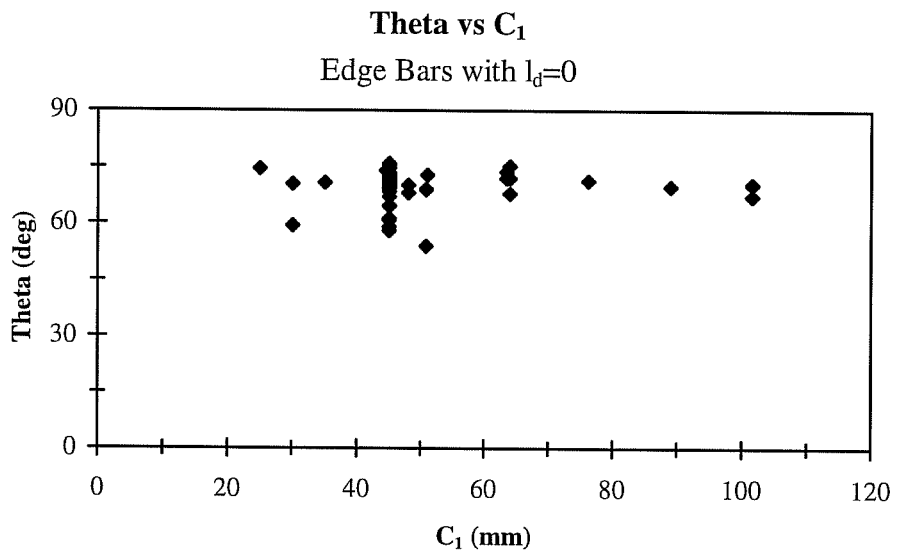


Figure 8.8 - Comparison of Theta with Edge Distance

From these results the average value for θ is 71° . The corresponding value assumed in the Concrete Capacity Design method for the pullout cone is 55° . The average value of D is 3, which corresponds well with the results of Furche and Eligehausen. In their tests the measured diameter of the blowout failure was 6 to 8 times the edge distance, which corresponds to D of 3 to 4.

Assuming D is 3, then Equation 8.3 for A_{bo} becomes:

$$A_{bo} = 36C_1^2 \quad \text{eq. 8.4}$$

This is the same equation used for the basic area of a blowout cone in the CEB method for anchor bolts discussed in Section 6.4. In Figure 8.9, the measured A_{bo} is plotted against C_1 with the solid line representing Equation 8.4.

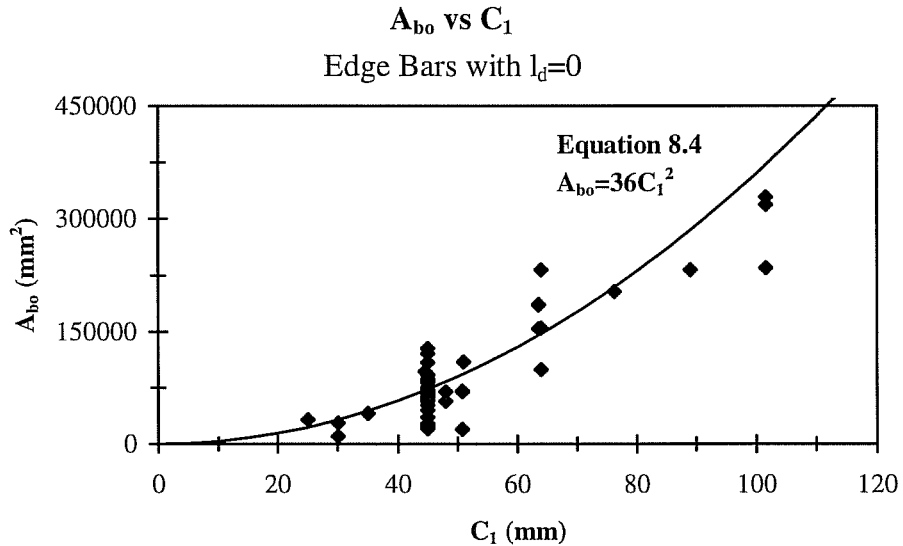


Figure 8.9 - Comparison of Blowout Area with Edge Distance and Predictive Equation

Once the size of the blowout failure is determined, the other half of the equation for the ultimate resisting force is the tensile strength of concrete. Concrete tensile strength varies from about 10% to 20% of the compressive strength and is traditionally specified as a function of the square root of the concrete strength. Values for the tensile capacity of concrete vary from 0.33 to 0.75 times the square root of the compressive strength ($4\sqrt{f'_c}$ to $9\sqrt{f'_c}$ in customary US units). An average value is $0.5\sqrt{f'_c}$ ($6\sqrt{f'_c}$ in customary US units). Using this value and converting to kN, the equation for the ultimate resistance, R_U , becomes:

$$R_U = \frac{(36C_1^2)(0.5\sqrt{f'_c})}{1000} = 0.018C_1^2\sqrt{f'_c} \quad \text{eq. 8.5}$$

The driving force, Z , is assumed to be a function of the tensile load on the bar, P :

$$Z = \alpha P \quad \text{eq. 8.6}$$

At ultimate the load is P_U , and Z_U is equal to R_U . Substituting these values into Equation 8.6 and solving for α leads to:

$$\alpha = \frac{R_U}{P_U} = \frac{0.018C_1^2\sqrt{f'_c}}{P_U} \quad \text{eq. 8.7}$$

Using an equation based on the pullout-cone capacity of anchor bolts for R_U , Furche and Eligehausen proposed a function for α based on the ratio of bearing stress at the head and concrete compressive strength:

$$\alpha = 0.1 \sqrt{\frac{f_b}{f'_c}} \quad \text{eq. 8.8}$$

where f_b is the bearing stress under the head at ultimate load and is equal to the ultimate load, P_U , divided by the net head area, A_n (note that α has no units). In Figure 8.10, α from Equation 8.7 is compared with α from Equation 8.8 for the 57 deep-embedment tests with no development length. Equation 8.8 does not fit the data and a better fit was obtained with the following function for α :

$$\alpha = 0.517 \sqrt{\frac{f_b}{f'_c}} \quad \text{eq. 8.9}$$

which is also shown in Figure 8.10.

Equation 8.9 can be rewritten as:

$$\alpha = 0.517 \sqrt{\frac{1000P_U / A_n}{f'_c}} \quad \text{eq. 8.10}$$

with P_U in kN, A_n in mm^2 and f'_c in MPa. Substituting Equation 8.10 into Equation 8.7 and rearranging yields:

$$P_U = 0.0107(C_1)^{1.33} (A_n)^{0.333} (f'_c)^{0.667} \quad \text{eq. 8.11}$$

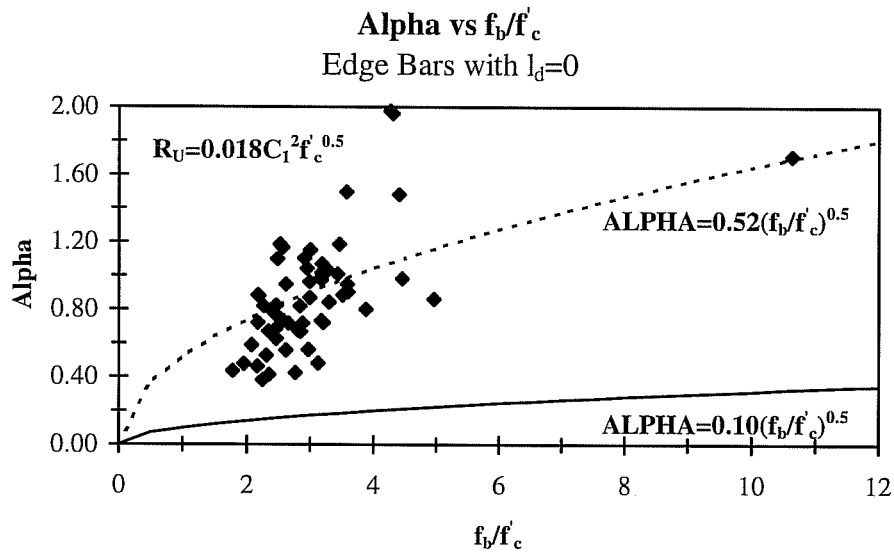


Figure 8.10 - Comparison of Alpha with f_b/f'_c

In Figure 8.11, the measured capacities for the 57 tests are compared with the predicted capacities from Equation 8.11. The physical model leads to an equation which has a reasonable fit with the data.

There are several aspects of the equation from the physical model that should be noted. First, the assumptions of the physical model naturally lead to an equation with the three primary variables and excludes factors that were found to not affect the capacity such as head orientation or aspect ratio. Second, the equation for α is based on the bearing stress at the head. The model suggests that if development length was present, tension in the bar would be transferred out of

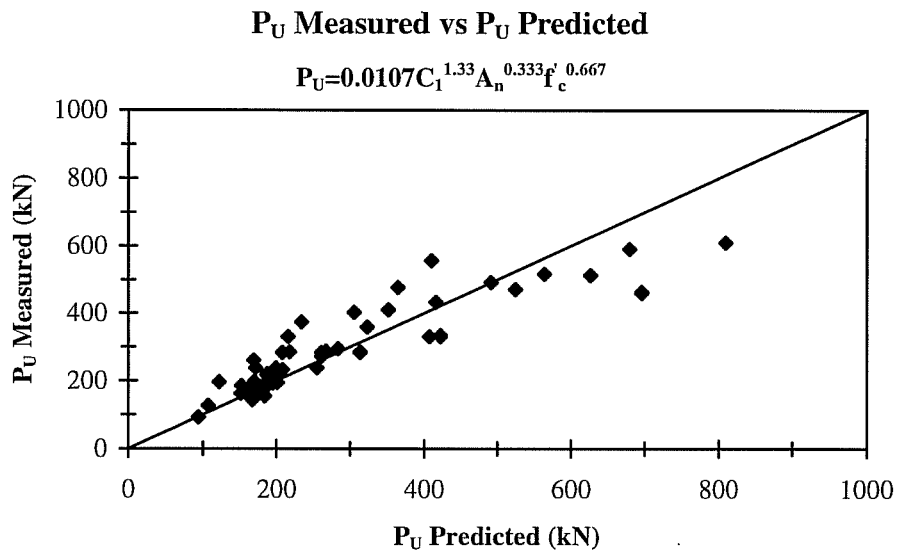


Figure 8.11 - Comparison of Measured Capacities with Capacities Predicted by Equation from Physical Model (Equation 8.11)

the bar along the development length decreasing the bearing stress at the head and increasing the blowout capacity. This matches the behavior observed during the tests. Finally, the physical model also leads to an equation with a y-intercept equal to zero and units which are algebraically consistent. It is generally accepted that functions of concrete strength represent stress and result in units of stress regardless of the exponent. The units of the edge distance are mm and the bearing area is in mm^2 . Raising edge distance to the 1.33 power and multiplying by the bearing area raised to the 0.333 power results in units of mm^2 . Multiplying

units of stress by units of area results in units of force. The units of the best-fit equation generated by the regression analysis are not algebraically consistent.

8.4 Equation from Physical Model and Regression

Another approach using the physical model is to determine the equations for the resistance and driving force algebraically from the best fit equation generated by a regression analysis of the results. Substituting a general equation for \mathbf{R}_U :

$$\mathbf{R}_U = k(C_1)^x m(f'_c)^y \quad \text{eq. 8.12}$$

and a general equation for α using the ratio of bearing stress at the head and the concrete compressive strength:

$$\alpha = n \left(\frac{P_U / A_n}{f'_c} \right)^z \quad \text{eq. 8.13}$$

into the general relationship of the physical model:

$$P_U = \frac{\mathbf{R}_U}{\alpha} \quad \text{eq. 8.14}$$

yields :

$$P_U = \frac{k(C_1)^x m(f'_c)^y}{n \left(\frac{P_U / A_n}{f'_c} \right)^z} \quad \text{eq. 8.15}$$

which can be rearranged:

$$P_U = \left(\frac{km}{n} \right)^{\frac{1}{1+z}} (C_1)^{\frac{x}{1+z}} (A_n)^{\frac{z}{1+z}} (f'_c)^{\frac{y+z}{1+z}} \quad \text{eq. 8.16}$$

Converting the best-fit equation from the regression analysis using the results of the 57 deep embedment pullout tests on edge bars with no development length so that P_U is in N yields:

$$P_U = 25.2(C_1)^{0.609} (A_n)^{0.577} (f'_c)^{0.671} \quad \text{eq. 8.17}$$

From which the exponents in Equation 8.16, x , y and z , can be calculated and substituted into Equation 8.15:

$$P_U = \frac{k(C_1)^{1.44} m(f'_c)^{0.222}}{n \left(\frac{P_U / A_n}{f'_c} \right)^{1.37}} \quad \text{eq. 8.18}$$

The exponent for edge distance, 1.44, is lower than the exponent from the physical model, 2. The exponent for concrete strength, 0.222, is less than half that assumed in the physical model which used the square root of concrete strength. Also the exponent on the ratio of bearing stress and concrete strength, 1.37, differs

greatly from the value assumed by the physical model which used the square root of this ratio.

8.5 Summary

Based on a physical model of the observed behavior of deeply-embedded headed reinforcement an equation was formulated to predict the blowout capacity. This equation predicted with reasonable accuracy the measured capacities from the deep-embedment tests. This equation also matched other observed behavior while using the primary variables. The equation from the physical model had different importance (or weight) for the variables than the equation resulting from the regression analysis. Finally, the equation from the physical model had consistent units and a y-intercept of zero.

Chapter 9

Deep-Embedment Pullout Tests Formulation of Design Procedures for Side Blowout Capacity

9.1 Introduction

In the previous chapters regression analyses and a physical model were used to form equations predicting the side-blowout anchorage capacity of headed reinforcement. While these equations accurately predict the capacity of a deeply embedded edge bar with no development length they are inappropriate as design equations. Adjustments for development length, corner placement and close spacing must be included. Also, design equations must conservatively predict the capacity for a wide variety of applications.

9.2 Review of Equations

The two equations that resulted from the regression analyses and physical model are functions of the edge distance, C_1 ; net bearing area, A_n ; and concrete strength, f'_c . The equation from the regression analysis was:

$$P_U = 0.0252(C_1)^{0.609} (A_n)^{0.577} (f'_c)^{0.671} \quad \text{eq. 9.1}$$

and the equation from the physical model was:

$$P_U = 0.0107(C_1)^{1.33} (A_n)^{0.333} (f'_c)^{0.667} \quad \text{eq. 9.2}$$

in both equations P_U is in kN, C_1 in mm, A_n in mm^2 and f'_c in MPa.

Both equations are based on the characteristic application of deeply embedded headed reinforcement: an edge bar with no development length. Both accurately predict the measured capacities for the 57 deep-embedment tests on edge bars with no development length. Statistical measures of the measured capacities divided by the predicted capacities are summarized in Table 9.1.

Equation	Measured P_U /Predicted P_U			
	Maximum	Minimum	Average	Standard Deviation
$P_U = 0.0252C_1^{0.609} A_n^{0.577} f'_c^{0.671}$	1.46	0.82	1.00	0.12
$P_U = 0.0107C_1^{1.33} A_n^{0.333} f'_c^{0.667}$	1.60	0.66	1.07	0.22

Table 9.1 - Statistical Measures of Equations from Regressions and Physical Model

However, neither equation is suitable for design. The equations are not transparent in the sense that the results are not easily predicted without the aid of a calculator nor are the effects of each variable obvious. To make these equations more transparent the exponents for the variables must be simplified. Common exponents that are easy to calculate manually include 0.5 (the square root), 1.0, 2.0 and 3.0. As long as the accuracy of the equation is not compromised, these exponents are preferable.

9.3 Simplification of Concrete Strength Term

Though the exponent for f'_c is approximately 0.67 in both equations the tensile strength of concrete, which controls the blowout capacity, is generally taken as a function of the square root of the concrete compressive strength. In Figure 9.1 normalized capacities for 57 deep-embedment pullout tests with no development length that resulted in side blowout failures (see Table 7.2 for the parameters and results of these 57 tests) are compared with three functions for concrete strength. Rearranging Equation 9.1 so that only the concrete strength is on one side results in the normalized capacities, P_{UNfc} , used for this comparison:

$$P_{UNfc} = \frac{P_{U(\text{Measured})}}{0.0252C_1^{0.609} A_n^{0.577}} \quad \text{eq. 9.3}$$

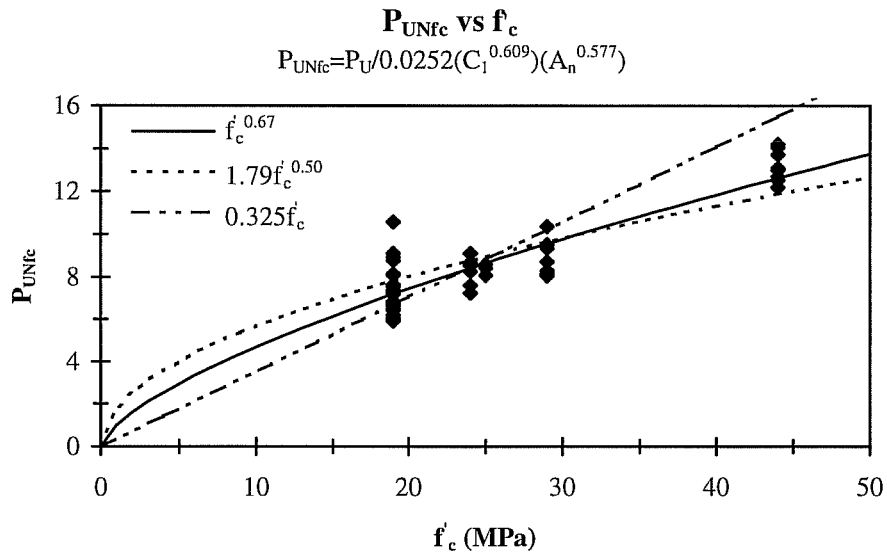


Figure 9.1 - Comparison of Functions for Concrete Strength

The coefficients for the functions of concrete strength are results of regression analyses. All three functions fit the normalized data well, though at higher concrete strengths the linear function overestimates the normalized capacities. Based on this comparison of normalized capacities, the use of the square root of concrete strength is an acceptable simplification.

9.4 Simplification of Net Bearing Area Term

In Equation 9.1 the exponent for net bearing area is 0.577, while for Equation 9.2 this exponent is 0.333. These values are close to the square root function. In the methods for bearing, prestress anchors and anchor bolts discussed in Chapter 6, the exponent for bearing area varied from 0.5 to 1.5. In Figure 9.2

the normalized capacities for the 57 edge bar tests are compared with functions of net bearing area. The normalized capacity, P_{UNAn} , results from rearranging Equation 9.1:

$$P_{UNAn} = \frac{P_{U(\text{Measured})}}{0.252C_1^{0.609}f_c^{0.671}} \quad \text{eq. 9.4}$$

Again, the coefficients for the functions of net bearing area are the results of regression analyses. The functions with exponents of 1.0 and 1.5 underestimate the normalized values for smaller head areas and overestimate the values at higher values of bearing area. The best function for simplifying the bearing area term is the square root.

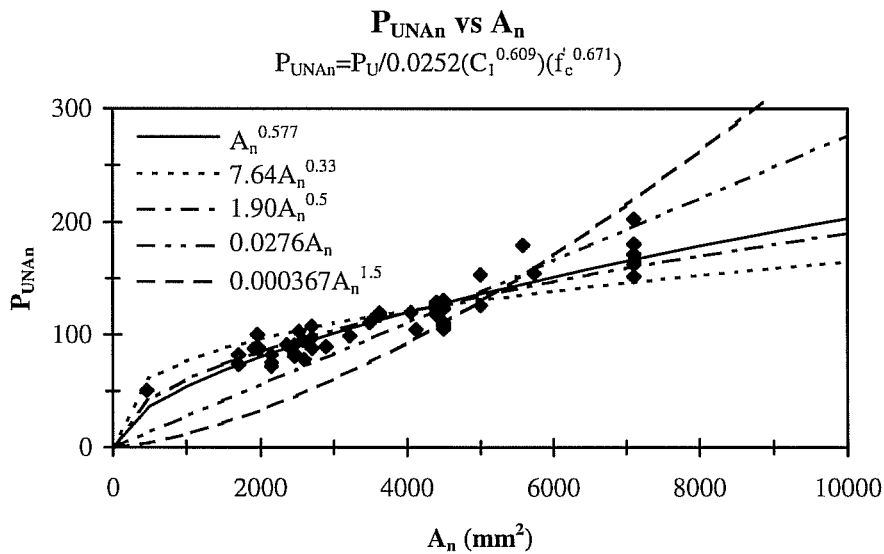


Figure 9.2 - Comparison of Functions for Net Bearing Area

9.5 Simplification of Edge Distance Term

The exponent for edge distance in Equation 9.1 is 0.609 and 1.33 in Equation 9.2. Design methods for similar phenomena included exponents between 1.0 and 2.0 for edge distance. In Figure 9.3 several functions for edge distance are compared with normalized capacities for the 57 edge bar tests. The normalized capacities, P_{UNCI} , were calculated by rearranging Equation 9.1:

$$P_{UNCI} = \frac{P_U}{0.252A_n^{0.577}f_c^{0.671}} \quad \text{eq. 9.5}$$

The functions for edge distance are the results of regression analyses. The functions with exponents higher than 1.0 underestimate the normalized capacities

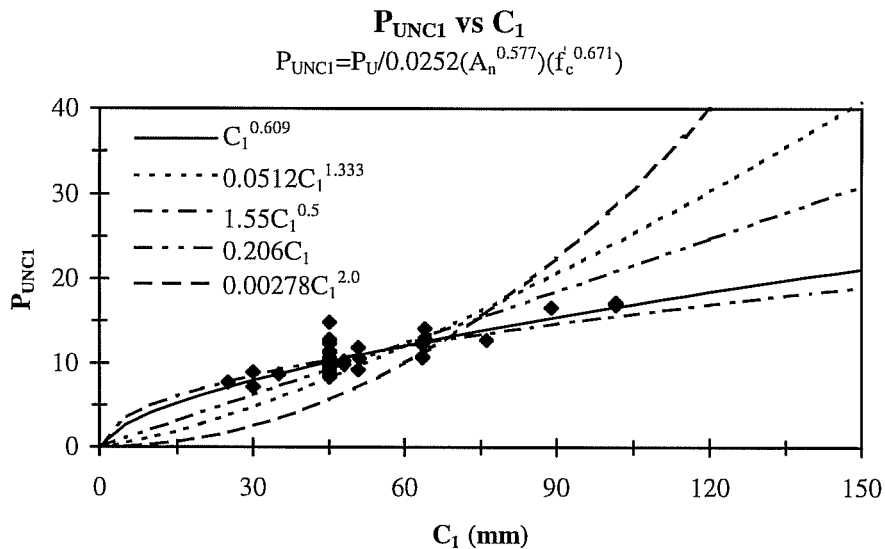


Figure 9.3 - Comparisons of Functions for Edge Distance

for small edge distances and overestimate the normalized values at higher values of edge distance. The function using the square root is very close to the original value in Equation 9.1. The linear function matches the data well for most of the range of edge distances tested. Since the square root of concrete strength describes the tensile capacity it is accepted that the units are MPa. The units resulting from the square root of the bearing area are mm. For the capacity equation to result in a unit of force, the edge distance term must also result in units of mm. Therefore, the linear function for the edge distance is an acceptable simplification.

9.6 Equation for Characteristic Application

Simplifying the terms of the equations led to an equation in the form:

$$P_U = 0.0170C_1\sqrt{A_n f'_c} \quad \text{eq. 9.6}$$

the curve fit constant, 0.0170, resulted from a regression analysis on the 57 edge bar tests. Equation 9.6 predicts the blowout capacity of a deeply-embedded edge bar with no development length. The predicted capacities using Equation 9.6 are compared with the measured capacities for the 57 edge bar tests in Figure 9.4. Equation 9.6 was reasonably accurate over the range of measured values. For the 57 tests, the average value of the measured capacity divided by the predicted

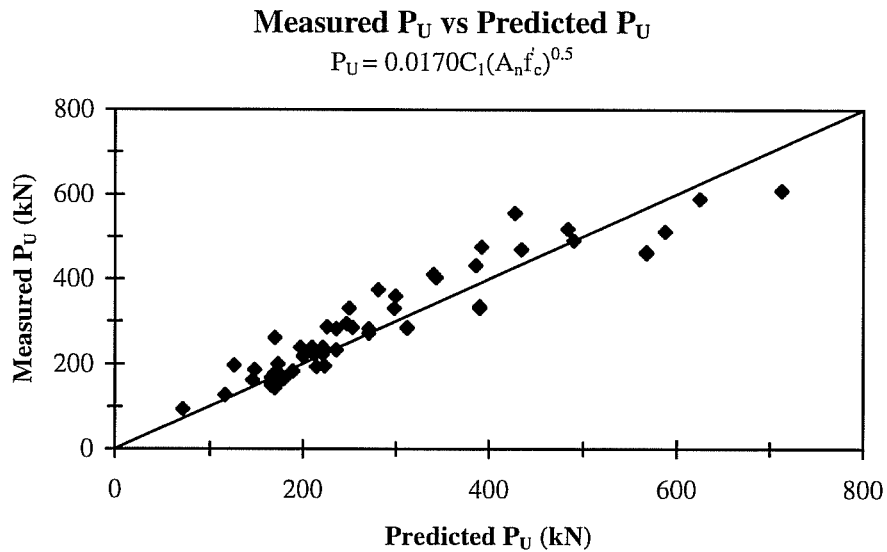


Figure 9.4 - Comparison of Measured Capacities with Capacities Predicted by Characteristic Equation (Equation 9.6)

capacity was 1.07 with a standard deviation of 0.168, and a range of values from 0.810 to 1.56.

Equation 9.6 is identical in form to the one proposed by Furche and Eligehausen [18] (Equation 6.13) for the blowout capacity of anchor bolts. The constant proposed by Furche and Eligehausen, for P_U in units of kN, was 0.0168.

9.7 Comparison of Characteristic Equation with Physical Model

The general form of the equation for blowout capacity derived from the physical model, with P_U in N, was:

$$P_U = \frac{R_U}{\alpha} = \frac{k(C_1)^x m (f'_c)^y}{n \left(\frac{P_U / A_n}{f'_c} \right)^z} \quad \text{eq. 9.7}$$

which can be rearranged into:

$$P_U = \left(\frac{km}{n} \right)^{\frac{1}{1+z}} (C_1)^{\frac{x}{1+z}} (A_n)^{\frac{z}{1+z}} (f'_c)^{\frac{y+z}{1+z}} \quad \text{eq. 9.8}$$

The characteristic equation, Equation 9.6, can be substituted into Equation 9.8 and since there are three unknowns: x , y and z , and three equations: the exponents for C_1 , A_n and f'_c in Equation 9.8, the values of x , y and z can be calculated.

Substituting these results into Equation 9.7 yields:

$$P_U = \frac{k(C_1)^2 m (f'_c)^0}{n \left(\frac{P_U / A_n}{f'_c} \right)} = \frac{k(C_1)^2 m}{n \left(\frac{P_U / A_n}{f'_c} \right)} \quad \text{eq. 9.9}$$

which implies the resistance force, R_U , is:

$$R_U = km(C_1)^2 \quad \text{eq. 9.10}$$

and is not a function of the concrete strength. However, Equation 9.7 is based on the assumption α (the denominator of Equation 9.7) varies with the ratio of bearing stress at the head and the compressive strength of concrete as proposed by

Furche and Eligehausen. Instead the ratio of bearing stress at the head and tensile strength of concrete can be assumed using $0.5\sqrt{f'_c}$ for the tensile strength. Replacing f'_c in the denominator of Equation 9.7 with $0.5\sqrt{f'_c}$, repeating the substitutions and solving for the exponents x , y and z , Equation 9.7 becomes:

$$P_U = \frac{k(C_1)^2 m (f'_c)^{0.5}}{n \left(\frac{P_U / A_n}{0.5\sqrt{f'_c}} \right)} \quad \text{eq. 9.11}$$

The resistance equation, R_U , is of the same form originally assumed:

$$R_U = 36(C_1)^2 0.5\sqrt{f'_c} \quad \text{eq. 9.12}$$

Based on Equation 9.12 and the characteristic equation, Equation 9.6, the equation for α becomes:

$$\alpha = 0.0311 \frac{P_U / A_n}{0.5\sqrt{f'_c}} \quad \text{eq. 9.13}$$

Figure 9.5 compares measured values for α based on the measured capacity, P_U , and Equation 9.12, for the 57 deep-embedment edge bar tests with the values predicted by Equation 9.13. Figure 9.6 shows the distribution of α with the ratio of bearing stress, f_b , and tensile strength, f_t . Equation 9.13 provides reasonable agreement with the measured data, though it should be noted that since the values

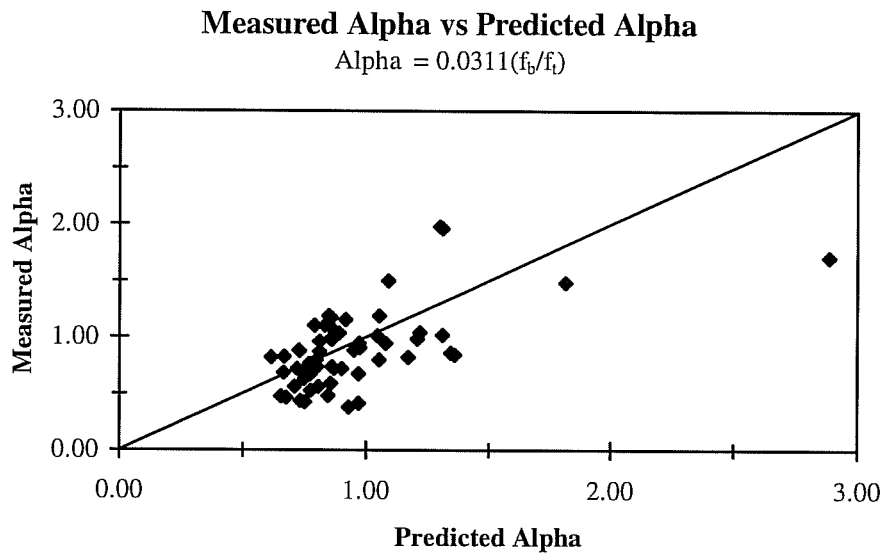


Figure 9.5 - Comparison of Measured and Predicted Alpha

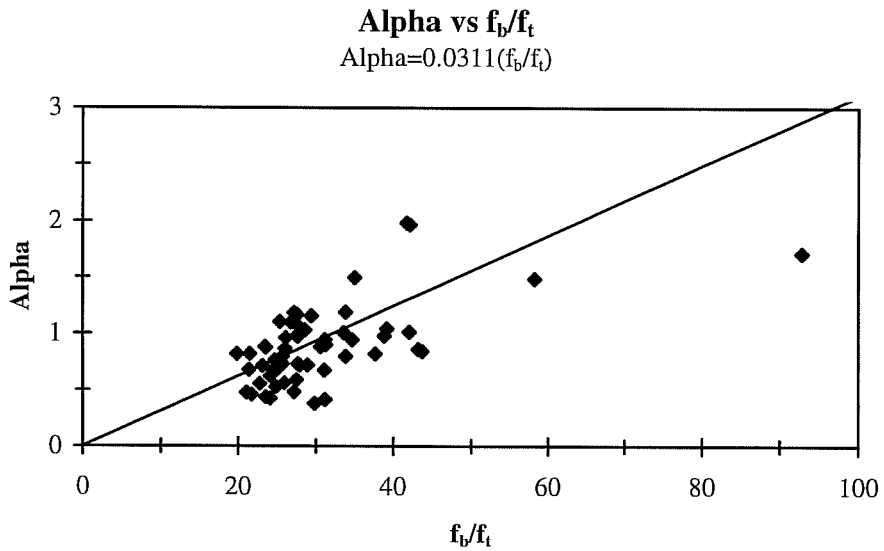


Figure 9.6 - Comparison of Alpha with f_b/f_t

for α are grouped so closely together that a variety of functions based on the ratio of f_b/f_t could be as accurate.

9.8 Development Length

It was observed during testing that development length along the bar increased the anchorage capacity of deeply-embedded headed reinforcement. It was also observed that the increase could be accurately predicted using provisions for development length in the current ACI code. It is, however, conservative to ignore the increase in strength provided by development length. In many applications of headed reinforcement the available development length will not be significant. For example, in a beam-column joint with headed beam longitudinal reinforcement, the available development length is less than the depth of the column. The strength increment provided by development length is likely to be minimal. Ignoring the contribution from development length will provide reserve strength and not increase material cost appreciably.

In Figure 9.7 the measured capacities for 20 edge bar tests with development length along the bar are compared with predicted capacities from Equation 9.6. The maximum value of the measured capacity divided by the predicted capacity for this comparison of twenty tests was 1.67 with a minimum of 1.12. The average value of measured capacity divided by predicted capacity

was 1.49 with a standard deviation of 0.143. As expected, the characteristic equation underestimated the capacities for bars with development length.

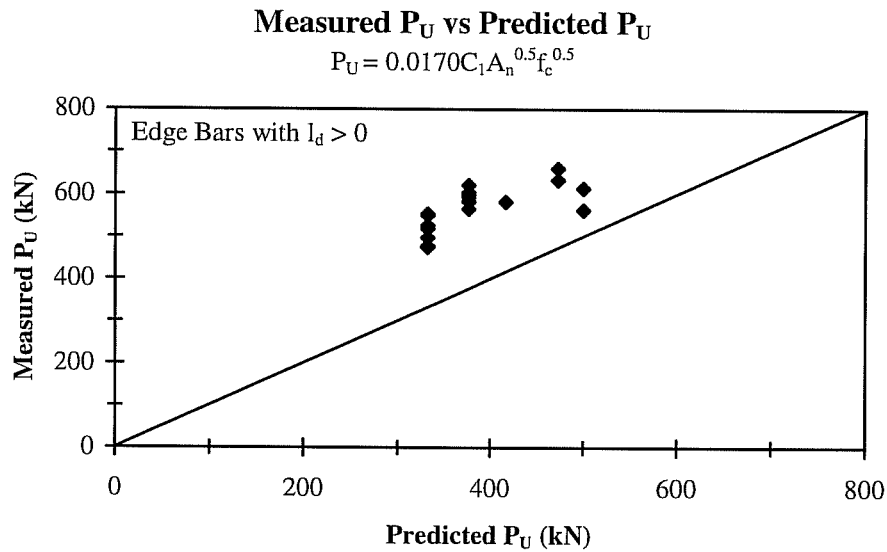


Figure 9.7 - Comparison of Measured Capacities of Bars with Development Length with Capacities Predicted by Characteristic Equation (Equation 9.6)

9.9 Corner Placement and Close Spacing

The test results showed that corner placement or close spacing of headed reinforcement reduced the anchorage capacity compared with the characteristic situation of a single edge bar. In reviewing existing code provisions, the CEB method [13] for blowout capacity of anchor bolts was a comprehensive approach covering both corner placement and close spacing.

In the CEB method, the capacity of corner bolts or groups of bolts is reduced by a ratio of the available failure surface area and the typical failure surface area of a single bolt. The area used for the failure surface area of a single bolt near an edge, A_{bon} (A_c^0 in CEB notation) was identical to the average area measured for the 77 deep-embedment pullout tests on edge bars:

$$A_{\text{bon}} = 36C_1^2 \quad \text{eq. 9.14}$$

The failure area is based on a pyramidal blowout cone with a base measuring $3C_1$ on each side of the headed reinforcing bar. In Figure 9.8, blowout failure areas, A_{bo} , are defined for single edge bars, closely spaced edge bars and corner bars. The characteristic capacity, P_{UO} , predicted by Equation 9.6 is corrected for corner placement and close spacing by:

$$P_U = \frac{A_{\text{bo}}}{A_{\text{bon}}} P_{\text{UO}} \quad \text{eq. 9.15}$$

In Equation 9.6, the blowout capacity is based on the resistance of the available failure surface area. In the tests on paired edge bars, the tensile load on each bar was measured and reported. The value calculated using Equation 9.15 would have to be divided by the number of bars in the group (two for the tests on paired bars) to determine the ultimate tensile load that can be applied to each bar in the group. The measured and predicted values reported for tests on paired bars represent the load on each bar.

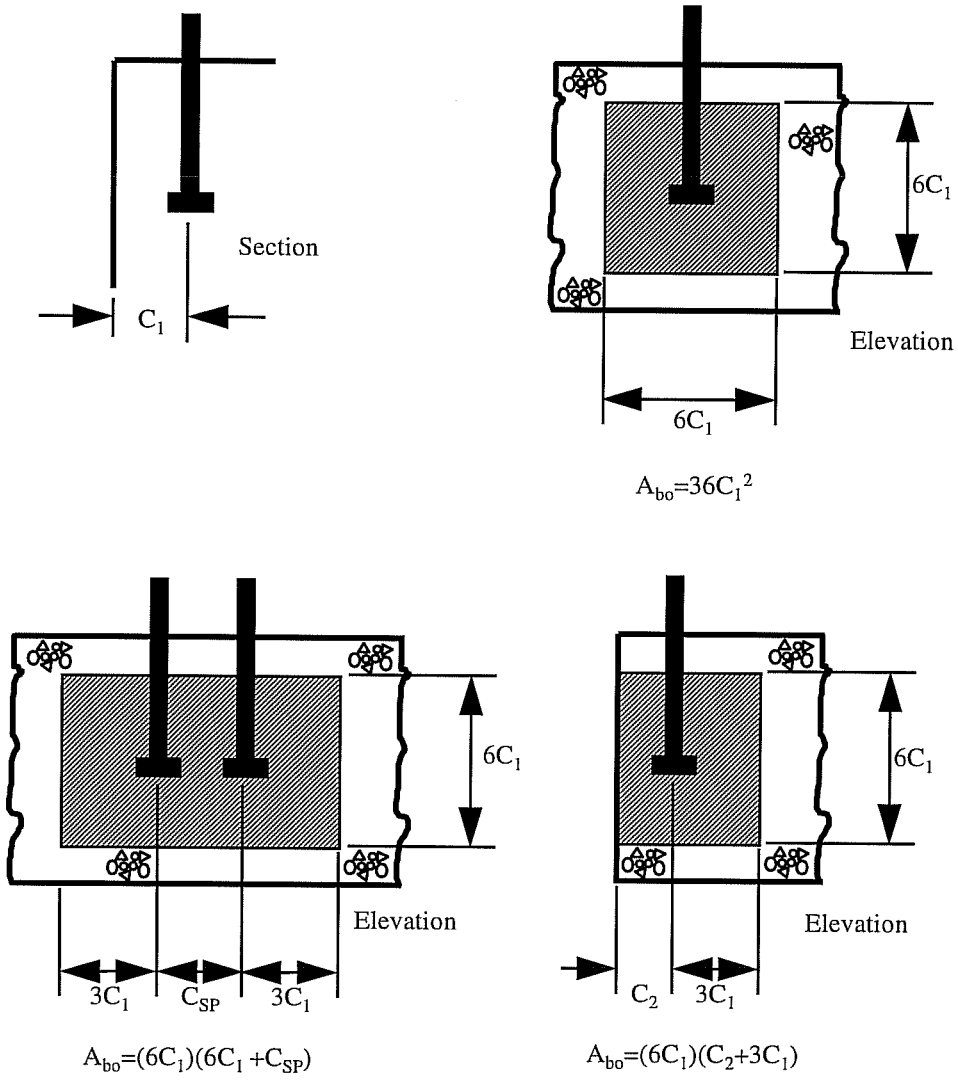


Figure 9.8 - Blowout Areas, A_{bo} , for Various Configurations

In addition to taking into account the reduced failure surface area, the CEB method also employs a factor for corner bars. This factor takes into account the disturbance of radial stresses from a corner. The CEB equation is:

$$\Psi_C = 0.7 + 0.3 \frac{C_2}{3C_1} \leq 1 \quad \text{eq. 9.16}$$

Note that the ratio $C_2/3C_1$ represents the borderline between edge and corner bars and matches observations made from the deep-embedment tests on corner bars. The general form of Equation 9.16 is also used in the Concrete Capacity Design for pullout cone capacity of anchor bolts.

Combining Equations 9.6, 9.15 and 9.16 results in the capacity of headed reinforcement closely spaced or placed in a corner:

$$P_U = \left(0.7 + 0.3 \frac{C_2}{3C_1} \right) \frac{A_{bo}}{A_{bon}} 0.017 C_1 \sqrt{A_n f'_c} \quad \text{eq. 9.17}$$

with the value $(0.7+0.3(C_2/3C_1))$ less than or equal to 1.

The measured blowout capacities from 31 corner bar tests and 6 tests on paired edge bars are compared with the predicted capacities of Equation 9.17 in Figure 9.9. The measured capacity divided by the predicted capacity ranged from 0.573 to 2.07 with an average of 1.29 and a standard deviation of 0.356. These procedures for corner placement and close spacing seem to model the behavior of the tests. However, they are more conservative than the characteristic equation and there is more scatter in the predicted values.

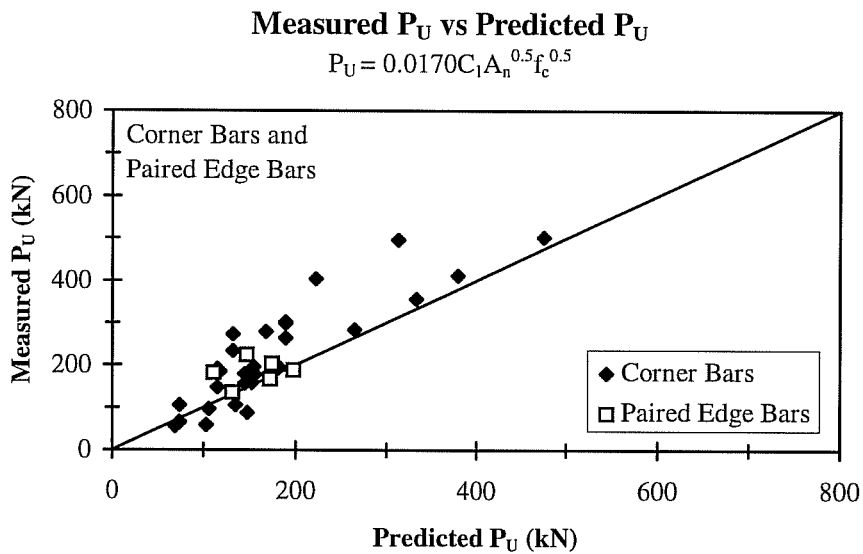


Figure 9.9 - Comparison of Measured Capacities of Corner and Paired Bars with Capacities Predicted by Modified Characteristic Equation (Equations 9.6, 9.15 and 9.16)

9.10 95% Fractile of Characteristic Equation

The final step in formulating the design procedure was to reduce the constant, 0.0170, in Equation 9.6 to the 95% fractile. To determine the new constant for the 95% fractile, the measured capacities for the 57 deep-embedment pullout tests conducted on single edge bars with no development length that resulted in blowout failures were divided by the primary terms of Equation 9.6:

$$k = \frac{P_U}{C_1 \sqrt{A_n} f_c'} \quad \text{eq. 9.18}$$

The average and standard deviation of the values of k were then calculated. The average, \bar{k} , was 0.0181 and the standard deviation, s , was 0.00286. The 95% fractile constant was calculated from:

$$k_{95\%} = \bar{k} - 1.96s \quad \text{eq. 9.19}$$

which resulted in a value of $k_{95\%}$ equal to 0.0125, which is slightly lower than the 95% fractile value proposed by Furche and Eligehausen, which for units of kN, was 0.0134. The design characteristic equation is therefore:

$$P_U = 0.0125C_1\sqrt{A_n f'_c} \quad \text{eq. 9.20}$$

The measured capacities of the 57 characteristic tests are compared with the values predicted by Equation 9.20 in Figure 9.10. The predicted value from Equation 9.20 was less than the measured capacity for all 57 tests. The measured capacities for all 114 deep-embedment pullout tests (77 edge bar; 31 corner bars and 6 paired edge bars) are compared with capacities predicted using Equations 9.20, 9.15 and 9.16 in Figure 9.11. 112 of the 114 tests, 98%, had measured capacities higher than predicted. The two bars with measured capacities lower than predicted were both corner bars, Tests C4B6 and C7B7. The measured capacities for these two tests were approximately 80% of the predicted design capacity.

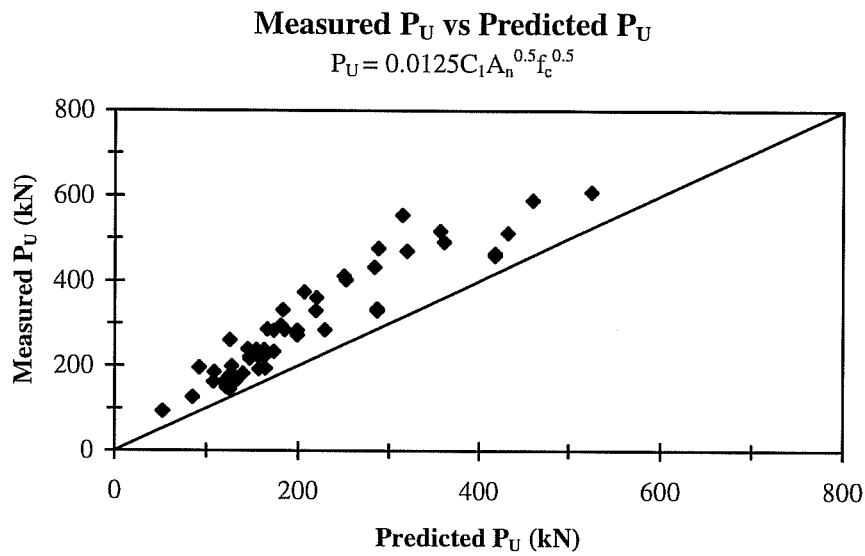


Figure 9.10 - Comparison of Measured Capacities of Edge Bars with No Development Length with Capacities Predicted by Characteristic Design Equation (Equation 9.20)

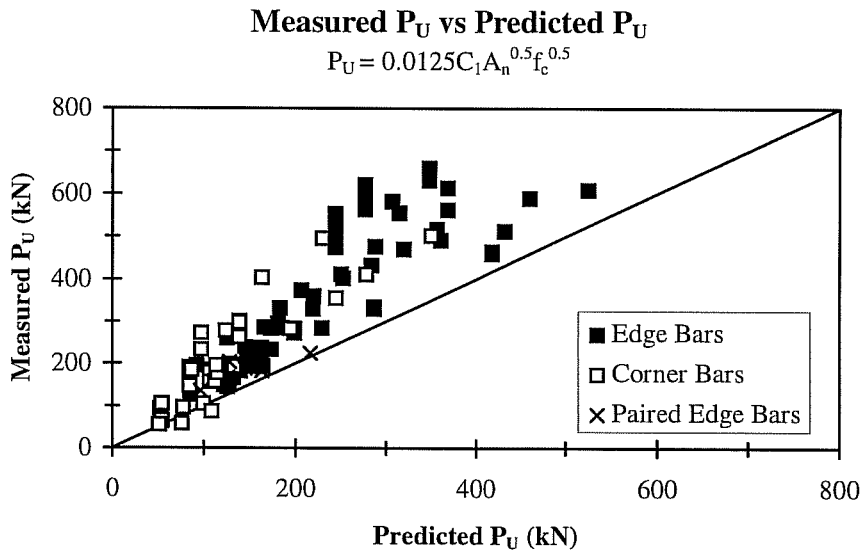


Figure 9.11 - Comparison of Measured Capacities of All Deep-Embedment Tests with Capacities Predicted by Design Equations (Equations 9.20, 9.15 and 9.16)

9.11 Comparison with Other Research

In previous research projects at the University of Stuttgart and the University of Texas, the blowout capacity of anchor bolts was investigated. The results of these projects provide additional comparisons of the effectiveness of the design equations for the blowout capacity of headed reinforcement (Equations 9.20, 9.15 and 9.16).

University of Stuttgart

Furche and Eligehausen [18] conducted twenty tests on anchor bolts that resulted in side blowout failures. The parameters for these tests are listed in Table 9.2. The parameters are nominal values taken from tables and the results are taken from figures presented by Furche and Eligehausen. There may be slight errors in the data presented in Table 9.2 due to differences between nominal and actual values and inaccuracies in reading the figures. However, it is assumed that these errors are less than 5% and insignificant for the comparisons. The second edge distance was not reported by Furche and Eligehausen and it is assumed that it was sufficient (greater than $3C_1$) for the tests to behave as edge bars. It is also assumed that the bolts tested had no deformations along the length and therefore no development length.

The predicted capacities for the parameters of Furche and Eligehausen's tests are compared with the measured capacities in Figure 9.12. The measured capacity was greater than the predicted capacity for all twenty tests.

Test ID	d_b (mm)	A_n (mm ²)	C_1 (mm)	h_d (mm)	f'_c (MPa)	P_U (kN)
F1	25	766	40	400	26	100
F2	25	766	40	400	26	110
F3	25	766	40	400	26	115
F4	25	766	60	400	26	130
F5	25	766	60	400	26	135
F6	25	766	60	400	26	142
F7	25	766	60	400	26	148
F8	25	766	60	400	26	150
F9	25	766	60	500	26	120
F10	25	766	60	500	26	160
F11	25	766	60	500	26	170
F12	25	766	80	400	26	185
F13	25	766	80	400	26	190
F14	25	766	80	400	26	205
F15	25	264	60	400	26	100
F16	25	264	60	400	26	105
F17	25	264	60	400	26	110
F18	25	1100	60	400	26	155
F19	25	1100	60	400	26	178
F20	25	1100	60	400	26	180

Table 9.2 - Parameters and Results of Tests by Furche and Eligehausen

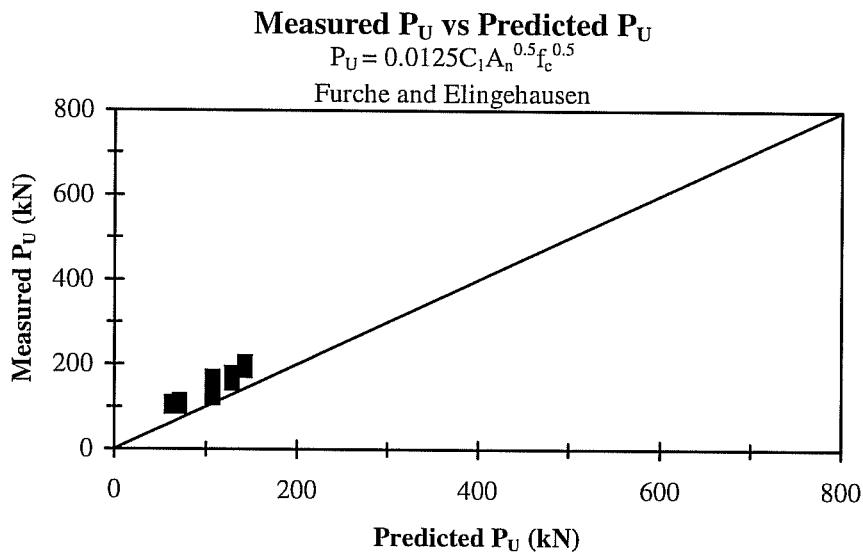


Figure 9.12 - Comparison of Measured Capacities from Furche and Eligehausen with Design Equations (Equations 9.20, 9.15 and 9.16)

University of Texas

Fifty-three tests reported by Hasselwander [22] resulted in blowout failures. The parameters for these tests are listed in Table 9.3. The data from 48 tests, H1 through H48, were used to generate the best-fit and design equations proposed by Hasselwander (see Section 6.4). In addition, Hasselwander conducted one test to determine the effect of transverse reinforcement, H49R; one test with cyclic loading, H50C; and three tests on paired edge bars, H51G, H52G and H53G, which were not included in the formulation of his equations but are included in this comparison. The reported capacities for the paired bars are the

Test ID	d_b (mm)	A_n (mm ²)	C_1 (mm)	C_2 (mm)	C_{SP} (mm)	h_d (mm)	f'_c (MPa)	P_U (kN)
H1	25	2660	38	457	0	381	38	276
H2	25	2660	76	457	0	381	27	343
H3	25	2660	102	457	0	381	24	342
H4	25	2660	76	457	0	508	27	353
H5	44	6556	86	457	0	667	27	622
H6	44	6556	111	457	0	667	25	665
H7	44	6556	137	457	0	667	32	793
H8	44	6556	137	457	0	667	30	748
H9	44	6556	175	457	0	667	27	947
H10	44	6556	111	457	0	889	25	638
H11	44	6556	137	457	0	889	34	838
H12	44	3009	111	457	0	667	18	303
H13	44	3800	111	457	0	667	30	692
H14	44	4655	111	457	0	667	38	663
H15	44	11116	111	457	0	667	19	524
H16	44	6556	111	457	0	667	37	728
H17	44	11116	111	457	0	667	27	699
H18	32	1572	48	305	0	318	32	228
H19	32	1572	76	305	0	318	32	259
H20	32	1572	111	305	0	318	32	330
H21	32	1572	143	305	0	318	32	305
H22	32	1572	76	305	0	318	17	215
H23	32	1572	76	305	0	318	17	204
H24	51	3762	76	406	0	508	33	553
H25	51	3762	102	406	0	508	36	478
H26	51	3762	152	406	0	508	36	691
H27	51	3762	203	406	0	508	33	779
H28	51	3762	102	406	0	508	15	320
H29	51	3762	102	406	0	508	15	338
H30	13	831	19	114	0	191	24	51

Table 9.3 - Parameters and Results of Tests by Hasselwander

Test ID	d_b (mm)	A_n (mm ²)	C_1 (mm)	C_2 (mm)	C_{SP} (mm)	h_d (mm)	f'_c (MPa)	P_U (kN)
H31	13	831	25	114	0	191	24	71
H32	13	831	25	114	0	191	22	75
H33	13	831	32	114	0	191	38	85
H34	13	831	32	114	0	191	21	58
H35	13	443	32	114	0	191	22	68
H36	13	1425	32	114	0	191	22	58
H37	13	1425	38	114	0	191	25	67
H38	13	443	38	114	0	191	24	63
H39	13	1425	38	114	0	191	22	79
H40	13	831	44	114	0	191	27	69
H41	13	831	51	114	0	191	23	80
H42	13	443	51	114	0	191	21	47
H43	13	831	57	114	0	191	21	83
H44	13	443	64	114	0	191	24	93
H45	13	831	25	114	0	254	20	67
H46	13	831	32	114	0	254	21	62
H47	13	831	38	114	0	254	24	78
H48	13	443	38	114	0	254	24	74
H49R	44	6556	111	114	0	667	37	925
H50C	44	6556	111	114	0	667	35	717
H51G	25	2660	76	114	127	381	18	144
H52G	25	2660	76	114	254	381	27	220
H53G	25	2660	76	114	381	381	19	169

Table 9.3 - Continued

ultimate loads measured on each bar. All anchor bolt tests reported by Hasselwander employed smooth anchor bolts so there was no development length for any of the tests.

Due to the sizes of Hasselwander's test specimens, 13 of the tests would be classified as corner bars with C_2 less than $3C_1$. Equation 9.16 was used to take into account the disturbance of radial stress patterns on one side by the corner. However, the test specimens used by Hasselwander were square and the corner bars had the radial stress patterns disturbed on two sides. To take this into account the reduction factor (Equation 9.16) was squared to represent both corners.

The measured capacities of the 53 tests reported by Hasselwander are compared with the predicted capacities in Figure 9.13. The measured capacities of 45 tests were higher than the predicted capacities. Of the eight tests with predicted capacities higher than measured, five were edge bar tests, two were corner bar tests and one test was on paired edge bars. On average, the measured capacities of these five edge bar tests were 89% of the predicted design capacity and 85% for the corner bar and paired bar tests.

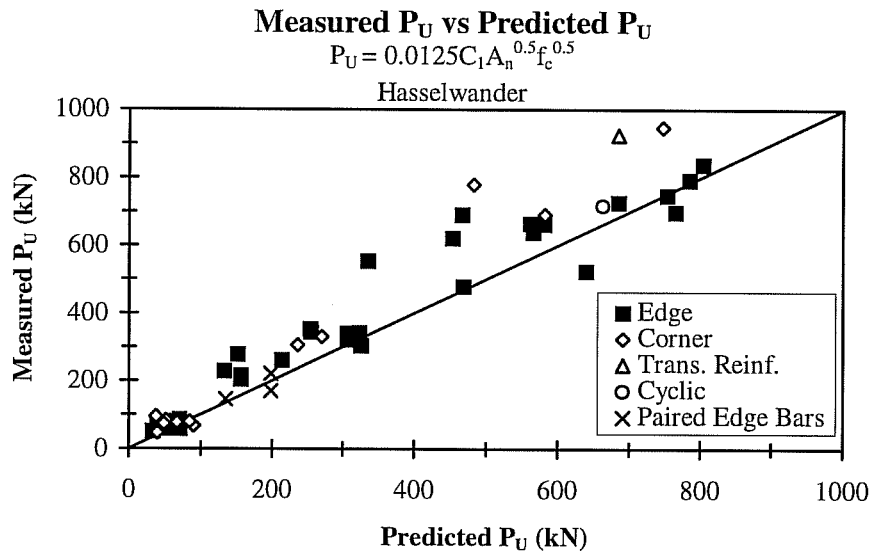


Figure 9.13 - Comparison of Measured Capacities by Hasselwander with Capacities Predicted by Design Equations (Equations 9.20, 9.15 and 9.16)

Combining the 114 tests on deeply embedded headed reinforcement, 20 tests by Furche and Eligehausen and 53 tests reported by Hasselwander, the measured capacities were greater than the predicted capacities from the design equations (Equations 9.20, 9.15 and 9.16) for 177 of the 187 tests or 95% of the data. The measured capacities of these 187 tests are compared with the predicted design capacities in Figure 9.14. Statistical measures of the measured capacity divided by the predicted design capacity for various groups of tests are listed in Table 9.4. Example calculations for the blowout capacity of edge, corner and paired bars are shown in Table 9.5.

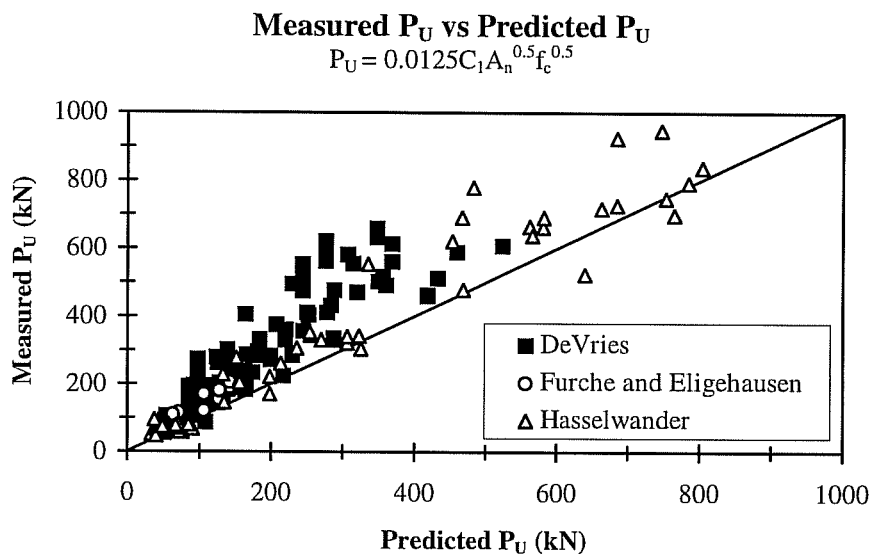


Figure 9.14 - Comparison of Measured Capacities for 187 Tests with Capacities Predicted by Design Equations (Equations 9.20, 9.15 and 9.16)

Tests	Measured P_U /Predicted Design P_U			
	Maximum	Minimum	Average	Standard Deviation
57 Tests on Edge Bars with $l_d=0$	2.12	1.10	1.45	0.229
114 Tests on Headed Reinforcement	2.82	0.779	1.65	0.396
20 Tests by Furche and Eligehausen	1.76	1.13	1.43	0.167
53 Tests by Hasselwander	2.46	0.745	1.27	0.313
All 187 Tests	2.82	0.745	1.52	0.394

Table 9.4 - Summary of Statistical Measures for Various Comparisons Based on Design Equations (Equations 9.20, 9.15 and 9.16)

	Test ID					
	Edge		Corner		Paired	
	C7B4	C13B1	C2B4	C9B7	C12B5	C12B6
d_b (mm)	35	35	25	25	25	25
h_1 (mm)	55	55	70	70	40	40
h_2 (mm)	100	100	70	70	80	80
t (mm)	25	25	16	16	18	18
C_1 (mm)	102	64	60	61	25	25
C_2 (mm)	457	457	60	61	457	457
C_{sp} (mm)	#N/A	#N/A	#N/A	#N/A	102	152
l_d (mm)	0	305	0	305	0	0
Trans. Reinf.	None	TE-3	None	TC-1	None	None
f'_c	24	21	25	27	25	25
P_{UO} (kN)	419	246	249	263	81	81
A_{bo} (mm ²)	374544	147456	86400	89304	18900	22500
A_{bon} (mm ²)	374544	147456	129600	133956	22500	22500
A_{bo}/A_{bon}	1.00	1.00	0.67	0.67	0.84	1.00
PSI	1.00	1.00	0.80	0.80	1.00	1.00
P_{UBO} (kN)	419	246	133	140	68	81
P_U (kN)	460	517	197	298	135	182
P_U/P_{UBO}	1.10	2.10	1.48	2.13	1.98	2.24

Table 9.5 - Example Calculations for Blowout Capacities

9.12 Summary

The best fit equations generated from the physical model and regression analyses were simplified into one equation better suited for design. The simplified characteristic equation provides an estimate of the blowout capacity of a headed reinforcement edge bar. The simplified characteristic equation was further modified to provide a lower bound blowout capacity at the 95% fractile. For a comprehensive design method, reduction factors were formulated for corner placement and close spacing.

Chapter 10

Design Implications for Headed Reinforcement

10.1 Introduction

In the previous chapters procedures have been outlined to determine the pullout-cone and blowout capacities of headed reinforcement. In this chapter, implications for design of these procedures will be discussed and two design examples given.

The best-fit characteristic equation for the pullout-cone capacity of a single headed reinforcing bar away from edges is:

$$P_{UPC} = \frac{A_n}{A_{no}} \frac{h_d^{1.5} \sqrt{f'_c}}{65} \quad \text{eq. 10.1}$$

where P_{UPC} is the pullout-cone capacity in kN, h_d the embedment depth in mm and f'_c the concrete compressive strength in MPa. The ratio A_n/A_{no} represents the increase in failure area due to the size of the head. For the 95% fractile design equation, the value of 65 in Equation 10.1 is changed to 112.

The best-fit characteristic equation for the blowout capacity of a single headed reinforcing bar away from a corner is:

$$P_{\text{UBO}} = \frac{C_1 \sqrt{A_n f'_c}}{59} \quad \text{eq. 10.2}$$

where P_{UBO} is the blowout capacity in kN, C_1 the edge distance in mm, A_n the net bearing area in mm^2 and f'_c the concrete compressive strength in MPa. For the 95% fractile design equation the value of 59 in Equation 10.2 is changed to 80. Both Equations 10.1 and 10.2 are modified for placement near edges or close spacing of bars. Both equations require the head to have sufficient stiffness.

10.2 Failure Mode

A designer will proportion headed reinforcement and the variables affecting the anchorage capacity so the required bar force can be reached before either a pullout-cone or blowout failure occurs. An important value for designers using headed reinforcement is the ratio of embedment depth to edge distance when the mode of failure switches from a pullout-cone to blowout. This ratio of embedment depth to edge distance determines which design method to use as well as deflection and post-peak behavior of the member.

To determine the embedment depth for a given edge distance and head when the blowout capacity is less than the pullout-cone capacity, Equations 10.1

and 10.2 could be equated and solved for h_d . However, when the edge distance is less than 1.5 times the embedment depth Equation 10.1 is modified for edge placement. Because of this it is difficult to form a general equation for h_d . The standard heads supplied for this test program represent a typical range of sizes and aspect ratios, calculating the minimum value of C_1 with a blowout capacity less than the pullout-cone capacity for a given h_d for these heads and a range of embedment depth will show general trends.

The capacities based on Equations 10.1 and 10.2 for bars with standard heads over a range of embedment depths and edge distances are shown in Figures 10.1 through 10.6. A concrete strength was assumed for calculation purposes though the trends should be independent of concrete strength since both the pullout-cone and blowout capacities are functions of the square root of the concrete strength. At shallow embedment depths, the pullout-cone capacity is less than the blowout capacity. With deeper embedments the failure mode switches with the blowout capacity being less than the pullout-cone capacity, represented by the flat part of the curves. Note that the pullout-cone capacity is nearly independent with respect to edge distance. Included on the figures are the yield and ultimate bar strengths based on a yield stress of 500 MPa and an ultimate stress of 650 MPa. For rectangular heads it was assumed that the long side of the head would be placed parallel with the nearest edge of concrete ($h_1 < h_2$). The

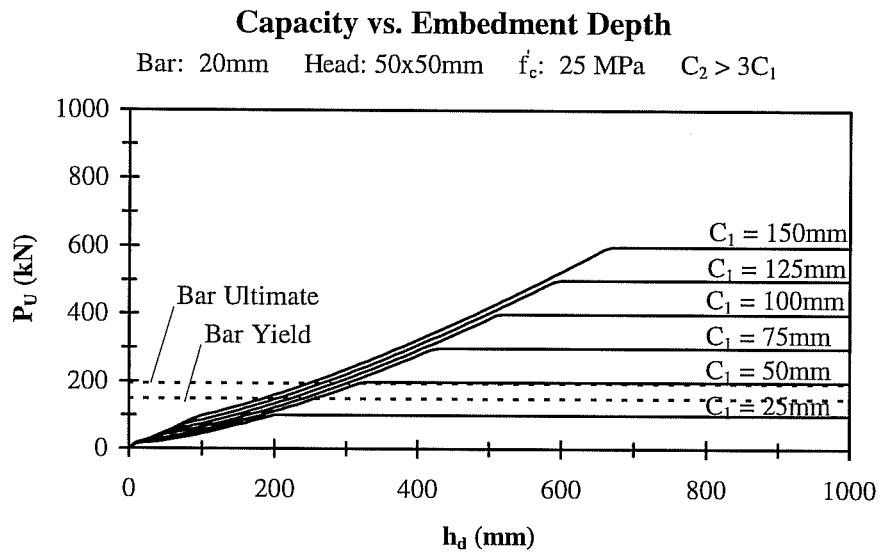


Figure 10.1 - Anchorage Capacity of 20mm Bar with 50x50x12mm Head

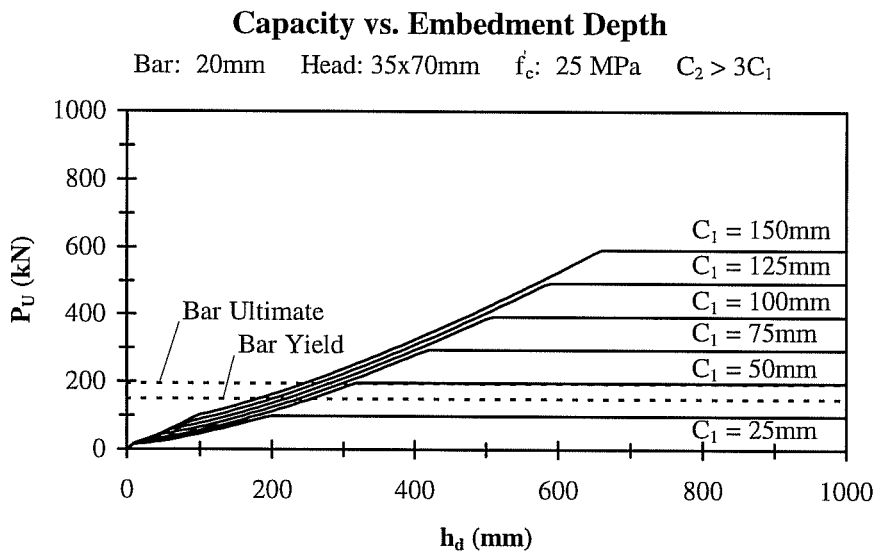


Figure 10.2 - Anchorage Capacity of 20mm Bar with 35x70x16mm Head

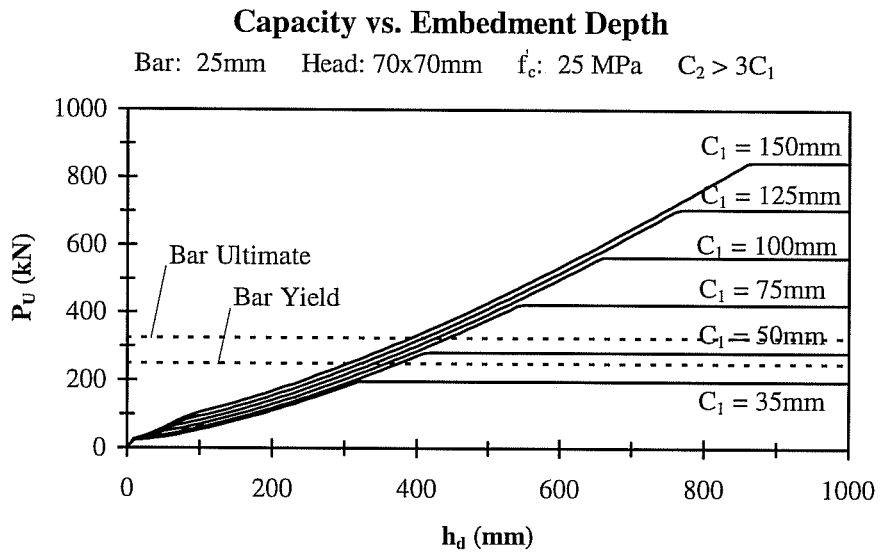


Figure 10.3 - Anchorage Capacity of 25mm Bar with 70x70x16mm Head

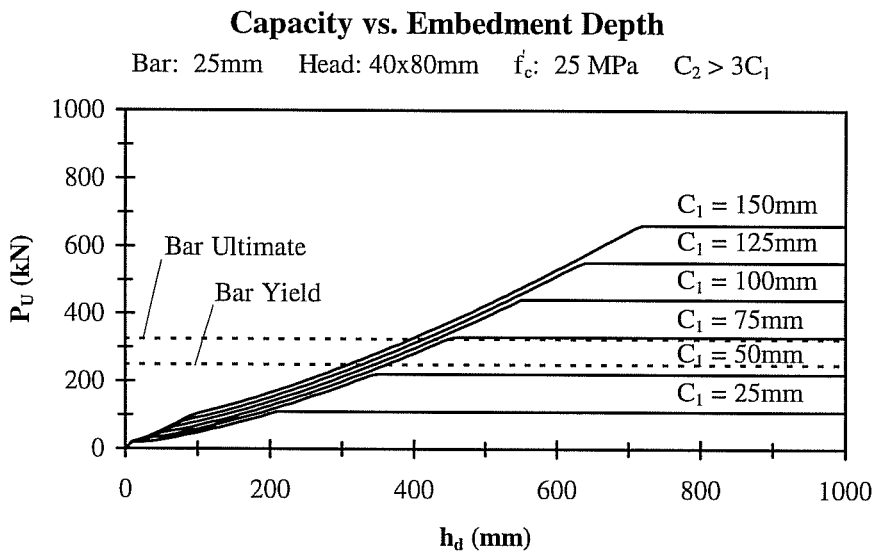


Figure 10.4 - Anchorage Capacity of 25mm Bar with 40x80x18mm Head

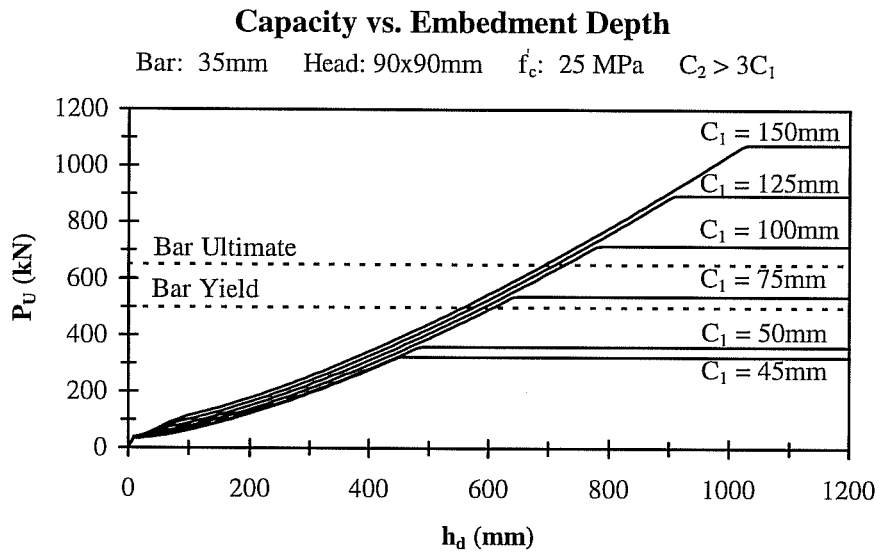


Figure 10.5 - Anchorage Capacity of 35mm Bar with 90x90x20mm Head

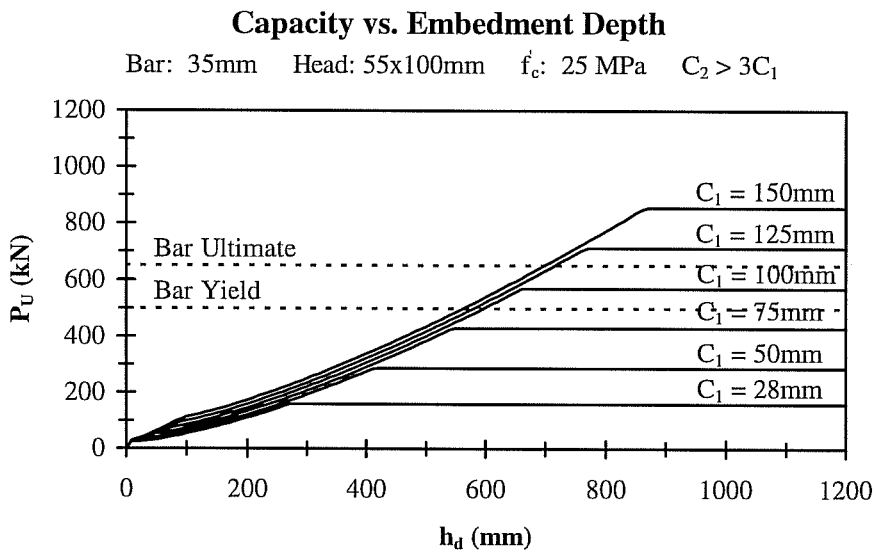


Figure 10.6 - Anchorage Capacity of 35mm Bar with 55x100x25mm Head

orientation of rectangular heads has a slight effect on the pullout-cone capacity of headed reinforcement near an edge since the failure area is based on the perimeter of the head. The relationships between h_d and C_1 when the pullout-cone capacity and blowout capacity are equal are plotted in Figure 10.7 for 50x50mm and 90x90mm heads. For the range of expected head sizes, when the ratio of h_d/C_1 is less than 5, the pullout-cone capacity will be less than the blowout capacity, for ratios of h_d/C_1 between 5 and 10 the blowout capacity could be less than the pullout-cone capacity depending on head size, and when h_d/C_1 is greater than 10 the blowout capacity will be less than the pullout-cone capacity.

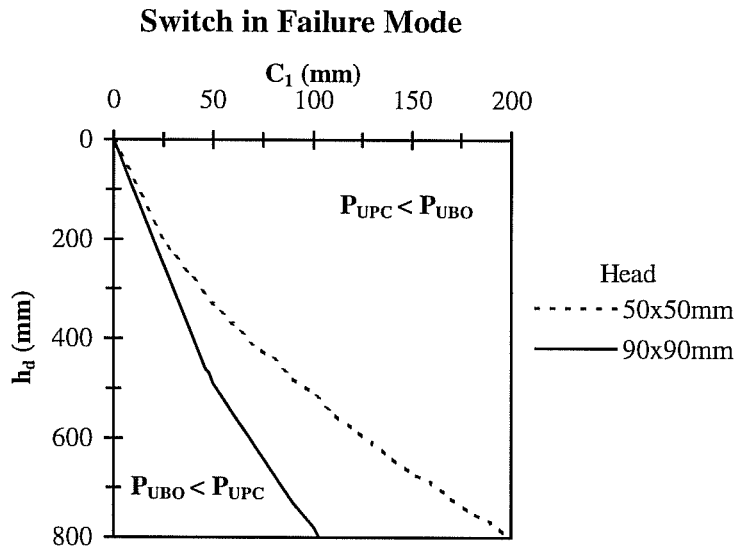


Figure 10.7 - Relationship Between h_d and C_1 for Switch in Failure Mode

10.3 Minimum Distances for Bar Yield

For most applications the anchorage needs to be strong enough to provide the yield force of the bar. Designers have the most control over concrete strength and placement of bars and may have little control over head size and yield strength of steel. Knowing the embedment depth or edge distance required to reach a given level of stress in the bar for a given head and concrete strength would be very useful.

For headed reinforcement, the pullout-cone capacity is a function of the perimeter of the head. For this reason it is difficult to form a general equation for the required embedment depth to yield a bar placed away from any edges. However, the embedment depth can be calculated if the head and bar size are known. Beginning with the characteristic design equation for a single headed bar placed away from any edges:

$$P_{UPC} = \frac{A_n}{A_{no}} \frac{h_d^{1.5} \sqrt{f'_c}}{112} \quad \text{eq. 10.3}$$

$A_b f_s / 1000$, where A_b is the bar area and f_s the required stress level (for example the yield stress, f_y) can be substituted for P_{UPC} and Equation 10.3 rearranged so that the stress terms, f_s and f'_c , are on one side:

$$\frac{f_s}{\sqrt{f'_c}} = \frac{8.9}{A_b} \left(\frac{A_n}{A_{no}} \right) h_d^{1.5} \quad \text{eq. 10.4}$$

Given a bar and head size, the embedment depth for a given ratio of $f_s/\sqrt{f'_c}$ can be calculated. In Figure 10.8 the curves based on Equation 10.4 are shown for the three standard square heads. Assuming a yield stress of 500 MPa, the ratios of $f_y/\sqrt{f'_c}$ for the pullout tests ranged between 55 and 115. In this range embedment depths greater than 6 to 15 times the bar diameter are required to yield a single bar.

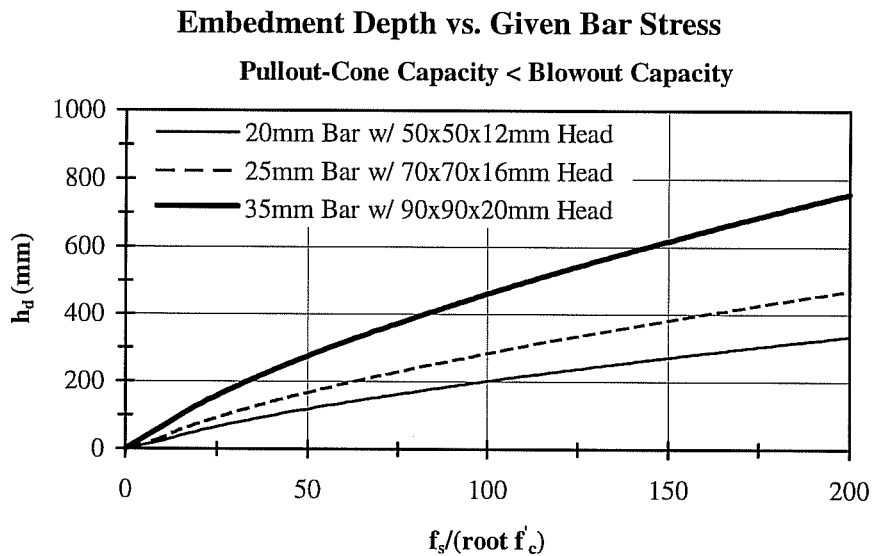


Figure 10.8 - Required Embedment Depth for Given Ratio of $f_s/(\sqrt{f'_c})$

When the ratio of embedment depth to edge distance is high enough that the blowout capacity is less than the pullout-cone capacity, an important value for designers is the minimum edge distance to yield the bar. Unlike the pullout-cone capacity equation, the blowout capacity, Equation 10.2 can be rearranged algebraically for the edge distance.

Beginning with the characteristic design equation for a single edge bar with deep embedment:

$$P_{UBO} = \frac{C_1 \sqrt{A_n f'_c}}{80} \quad \text{eq. 10.5}$$

and substituting $A_b f_s / 1000$ for P_{UBO} and the constant, m , defined as the ratio of net bearing area, A_n , divided by the bar area, A_b :

$$m = \frac{A_n}{A_b} = \frac{A_h}{A_b} - 1 \quad \text{eq. 10.6}$$

into Equation 10.5 yields:

$$A_b f_s = 12.5 C_1 \sqrt{m A_b f'_c} \quad \text{eq. 10.7}$$

and substituting $(\pi/4)d_b^2$ for A_b and rearranging so that f_s and f'_c are on one side gives:

$$\frac{C_1}{d_b} = \frac{1}{14.1 \sqrt{m}} \left(\frac{f_s}{\sqrt{f'_c}} \right) \quad \text{eq. 10.8}$$

Values for C_1/d_b are plotted against $f_s/\sqrt{f'_c}$ for various values of m in Figure 10.9. Assuming a yield stress of 500 MPa, $f_y/\sqrt{f'_c}$ varied from about 55 to 115 for the pullout tests and for the standard heads, m varied from 4 to 10. In this range of values, C_1/d_b for a single bar varied from 1 to 4. Since C_1 is the edge distance, the clear cover, C_{c1} , is one-half a bar diameter less, so the critical clear covers vary from 0.5 to 3.5 bar diameters. These covers are well within the range of covers for typical construction practices.

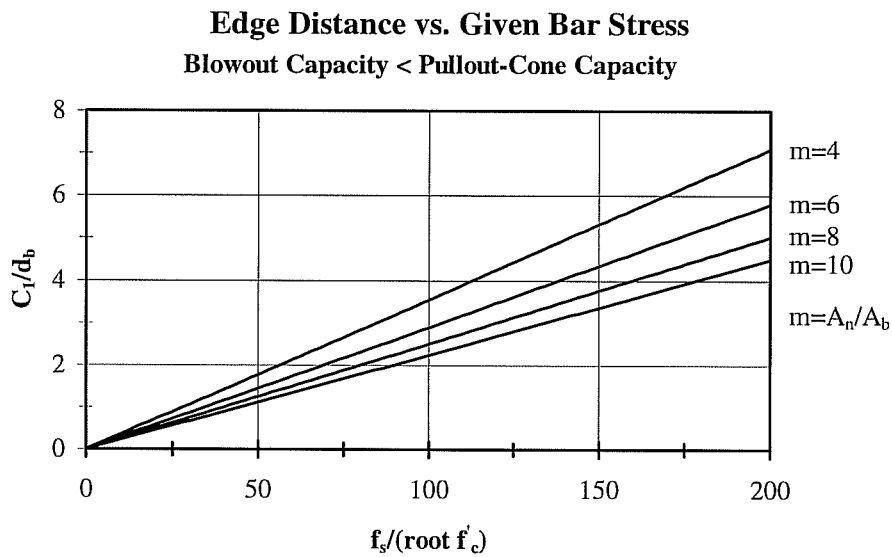
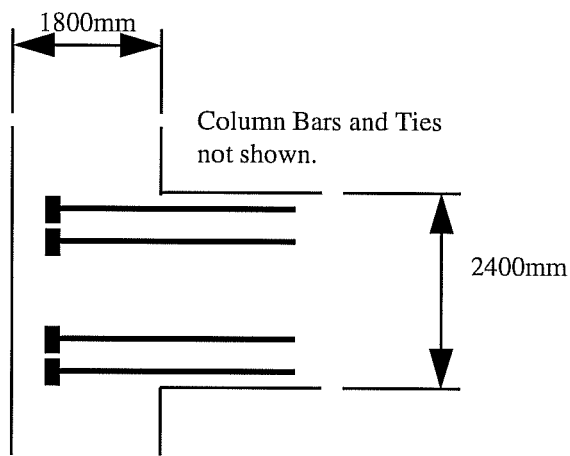


Figure 10.9 - Required Edge Distance for Given Ratio of $f_s/(\text{root } f'_c)$

10.4 Beam-Column Joint Design Example

Given a beam-column T-joint with dimensions and material properties as shown in Figure 10.10 design the top beam steel using headed reinforcement to provide a negative moment capacity in the beam of 10,000 kN-m. The anchorage must be strong enough to yield the bars.

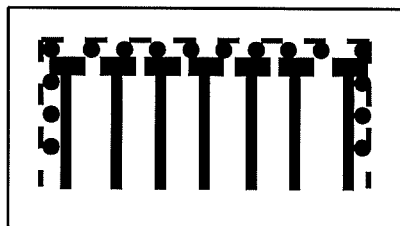


A. Elevation

Material Properties
Concrete Strength: $f'_c = 49$ MPa
Steel Yield Stress: 500 MPa
Steel Ultimate Stress: 650 MPa

Column
1200mm x 1800mm
Minimum Clear Cover: 50mm
Tie Diameter: 20mm
Bar Diameter: 45mm

Beam
1200mm x 2400mm
Tie Diameter: 16mm



B. Partial Column Plan

Figure 10.10 - Parameters for Beam-Column Joint Design Example

First, a preliminary size for the beam steel needs to be chosen. Assuming the moment arm of the beam is equal to 0.9 times the overall depth and using the yield stress of the steel, the area of steel required is equal to about $10,300\text{mm}^2$. This can be provided with 15-30mm diameter bars ($A_s = 10,500\text{mm}^2$) or 10-35mm diameter bars ($A_s = 10,000\text{mm}^2$). The minimum clear cover for the beam bars is equal to the minimum cover over the column ties plus the diameter of the column ties and bars, 115mm. With this minimum cover and assuming 10-35mm bars, the center-to-center spacing of the bars in one layer would be 104mm. Using 55mm wide heads will leave 49mm clear between the heads which should be adequate for construction. Using 90mm wide heads would result in 14mm clear spacing between the heads which would be inadequate to allow aggregate to pass between the heads during placement of concrete. Two layers of steel would be required to use this head size.

Based on Figure 10.8, an embedment depth of approximately 550mm is needed to yield a single 35mm bar with a 90x90x20mm head, assuming a pullout-cone failure. The embedment depth will likely be more than this since the overall depth of the column is 1800mm. The maximum possible embedment depth is equal to the column depth minus the minimum clear cover, column tie diameter, column bar diameter and the head thickness. With a 25mm thick head the maximum embedment depth is 1660mm. Using this embedment depth and a

single layer of steel with 55x100x25mm heads, the assumed pullout-cone failure area (Figure 10.11) interacts with the compression reaction of the beam. Given this it seems unlikely the pullout-cone mode will be the controlling mode.

With a 35mm bar and 55x100x25mm head the minimum edge distance is $115 + 35/2$ or 132.5mm or 3.8 bar diameters for bar yielding assuming a blowout failure. Based on the curves in Figure 10.9, this should be adequate to yield the bar. However, with an embedment depth of 1650mm, the distance from the bearing surface of the head to the back face of the column is only 140mm, less than $3C_1$ assumed for the failure area by the characteristic equation. The blowout

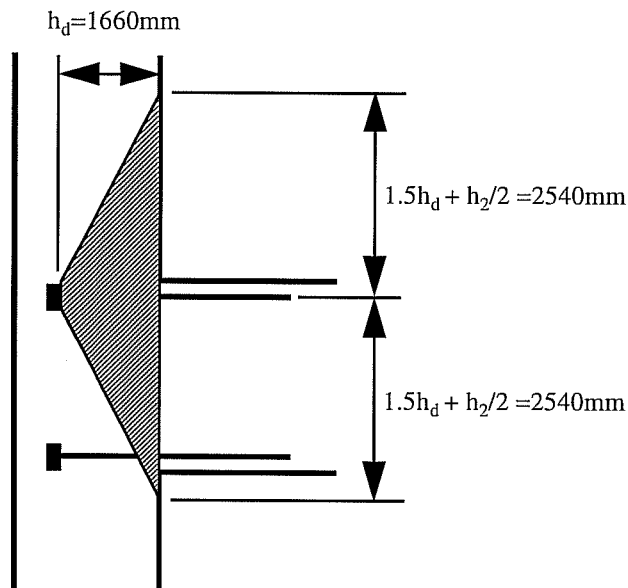


Figure 10.11 - Pullout-Cone Failure for Beam-Column Joint Design Example

failure surface for a single 35mm bar with 55x100x25mm head with C_1 of 133mm and h_d of 1660 is shown in Figure 10.12. The design blowout capacity for this bar is found using Equation 10.2 modified for the available failure area:

$$P_U = \frac{(539)(798)}{36(133)^2} \frac{133\sqrt{(4500)(49)}}{80} = 527\text{kN} \quad \text{eq. 10.9}$$

This capacity is 105% of the yield force of the bar. Using minimum cover, a single layer of 10-35mm bars with 55x100x25mm heads will provide the required moment ($\phi M_n = 10,200 \text{ kN-m}$) and anchorage (Figure 10.13). Since the edge distance of the next interior bar is greater than the outside bar, the anchorage capacity will also be greater and need not be checked.

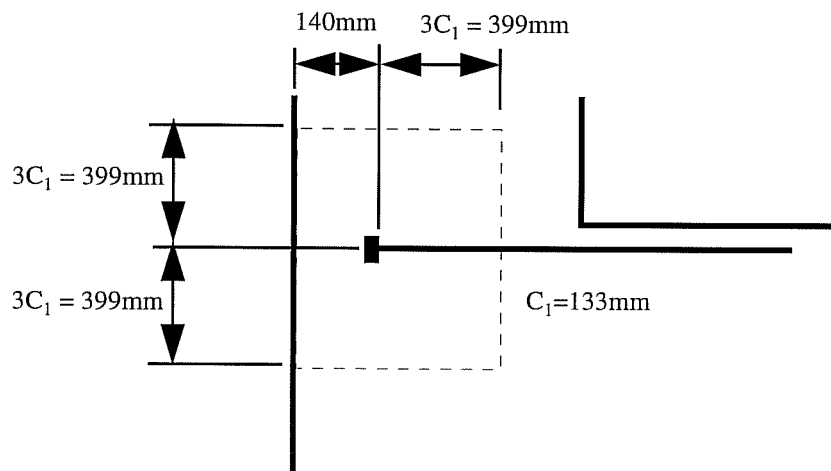


Figure 10.12 - Blowout Failure for Beam-Column Joint Design Example

The development length needed for a straight bar anchorage of 35mm bars placed the same way as the headed bars is 1510mm. The hooked bar development length for 35mm bars with this placement is 420mm. However, the use of headed bars avoids the congestion in the cage associated with the tail extensions of hooked bars.

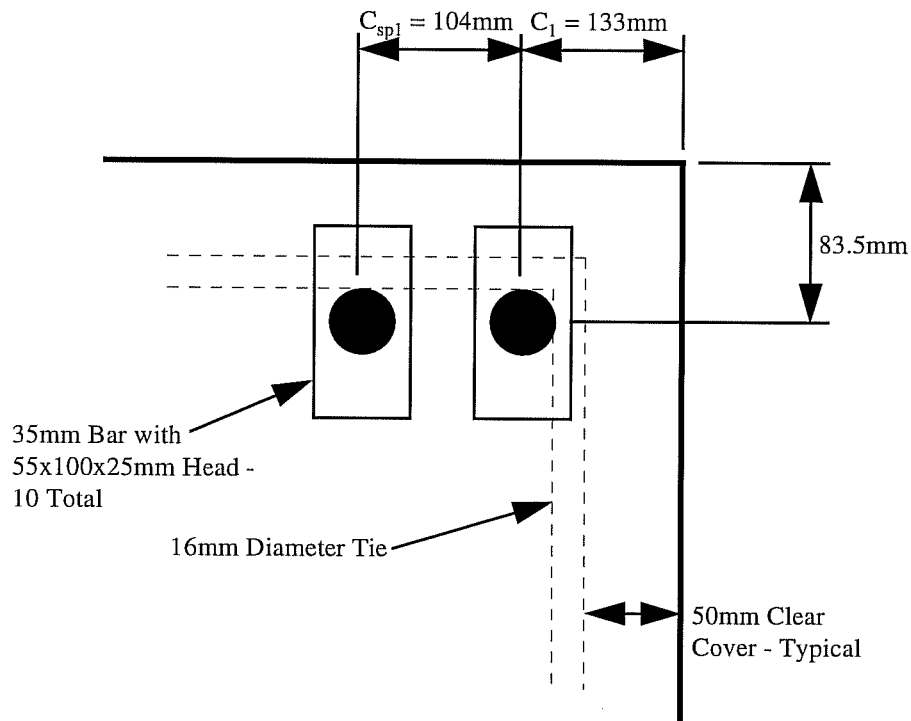
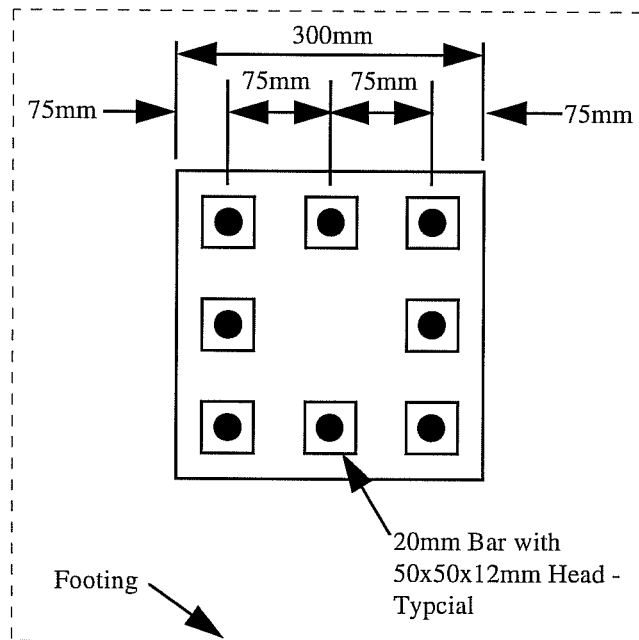


Figure 10.13 - Partial Beam Section for Beam-Column Joint Design Example

10.5 Column-Footing Design Example

The column in Figure 10.14 is part of a wind frame and under wind load the entire section is in tension. The column bars are anchored in a spread footing integral with the floor slab. Design the footing to provide anchorage for the headed column bars. The anchorage must provide enough capacity to yield the bars.



Material Properties

Concrete Strength: $f'_c = 28$ MPa

Steel Yield Stress: 500 MPa

Steel Ultimate Stress: 650 MPa

Figure 10.14 - Parameters for Column-Footing Design Example

Since footings are usually shallow, the pullout-cone capacity of the group of bars will likely control. Based on the curves in Figure 10.8, an embedment depth of 200mm would yield a single 20mm bar away from any edges. Since the center-to-center spacing of the bars is less than 1.5 times this embedment depth and all the column bars are in tension the column bars will be considered as a group. If a square footing is used, then the perimeter of the footing must be 1.5 times the embedment depth away from the group of bars. If the footing is smaller, the group of bars will be near four edges and the pullout-cone capacity will be based on the edge distance which would greatly reduce the capacity.

The design of the footing is a trial and error process. To yield all the column bars the total anchorage capacity of the group must be 1200 kN. The pullout-cone capacity for a group of bars is calculated from:

$$P_U = \frac{A_n}{A_{no}} \frac{h_d^{1.5} \sqrt{f'_c}}{112} \quad \text{eq. 10.10}$$

where A_n is based on the perimeter of the heads in the group. Since A_n and A_{no} are functions of the embedment depth, a first estimate of the embedment depth is required. A preliminary estimate for h_d can be determined by assuming the ratio of A_n/A_{no} is 1. With this assumption, h_d must be 863mm. Since the ratio of A_n/A_{no} is usually greater than 1 for headed reinforcement an embedment depth of 800mm may be sufficient. The pullout-cone failure surface for this embedment

depth is shown in Figure 10.15. The pullout-cone capacity for the group of column bars with an embedment depth of 800mm ($40d_b$) is:

$$P_U = \frac{(2600)^2 (800)^{1.5} \sqrt{28}}{9(800)^2 \cdot 112} = 1255\text{kN} \quad \text{eq. 10.11}$$

which is 105% of the required capacity. To provide sufficient cover between the head and earth surrounding the footing an overall depth of 900mm should be used. The plan dimensions of the footing should be slightly larger than the assumed

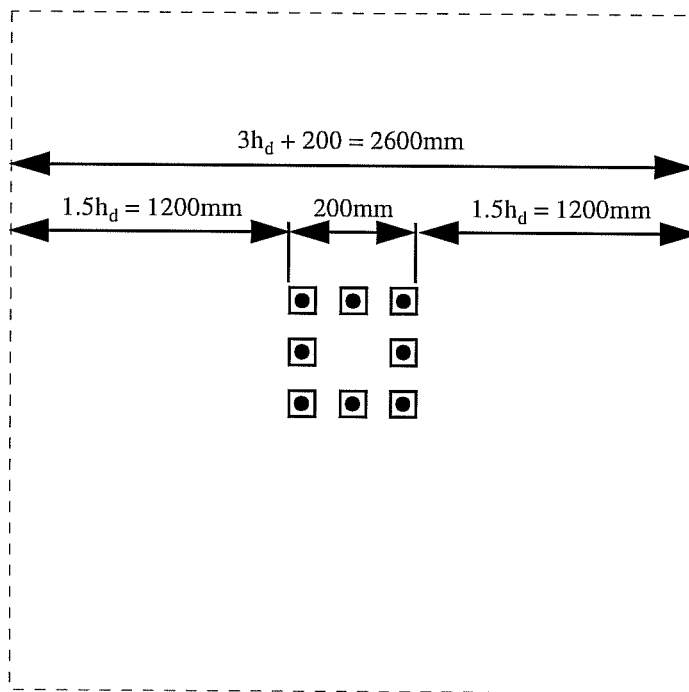


Figure 10.15 - Pullout-Cone Failure Area for Column-Footing Design Example

failure and 2700mm would be sufficient (Figure 10.16). The volume of the footing could be reduced by forming the bottom parallel with the assumed failure area. The straight bar development length required to yield the bars in the column is 920mm and the hooked bar development length is 320mm.

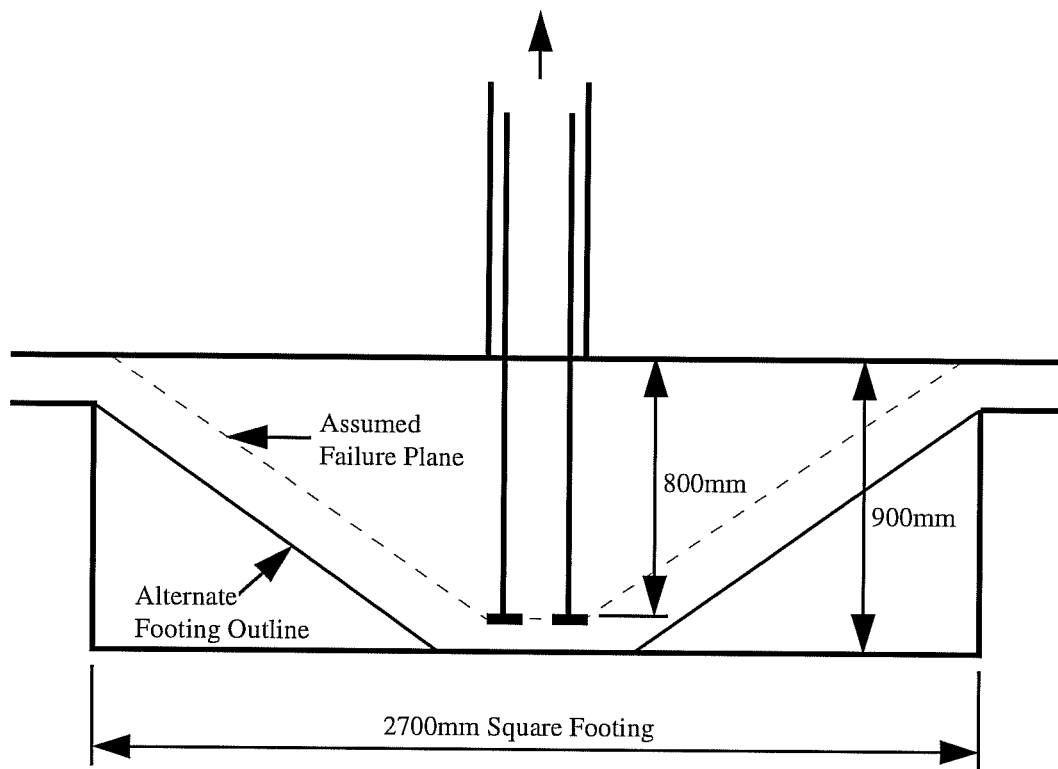


Figure 10.16 - Section of Footing for Column-Footing Design Example

Chapter 11

Summary and Conclusions

11.1 Summary

The results of over 140 pullout tests have shown that headed reinforcement is a viable method for providing anchorage of reinforcement in concrete members. Based on the results of shallow-embedment and deep-embedment pullout tests, comprehensive design methods have been proposed for the anchorage capacity of headed reinforcement in concrete members. The design methods are rational and transparent, allowing engineers to use headed reinforcement in a wide range of applications and include the effects of embedment depth, edge distance, close spacing, corner placement, concrete strength and head size. The methods cover two failure modes, pullout-cone and side blowout, with the yield and ultimate strengths of the reinforcing bar being other limits on the anchorage capacity. The pullout-cone capacity was found to be less than the side-blowout capacity for headed bars with low ratios of embedment

depth to edge distance. When the ratio of embedment depth to edge distance was high, the blowout capacity was less than the pullout-cone capacity.

11.2 Conclusions

Shallow-Embedment Tests

Based on the results of 21 pullout tests on headed reinforcement with shallow embedments the primary factors affecting the anchorage capacity were embedment depth, edge distances and concrete strength. For bars with low ratios of embedment depth to edge distance, pullout-cone failure and bar failure were the two modes controlling the anchorage capacity. Development length added strength to the anchorage but it is conservative to ignore this increase. Transverse reinforcement placed perpendicular to the headed reinforcing bar had no effect on the anchorage capacity or behavior. Bar placement near one edge reduced the anchorage capacity compared to placement away from all edges and corner placement reduced the capacity further.

The anchorage capacity of headed reinforcement with shallow embedments can be predicted with the Concrete Capacity Design method. The CCD method was developed to predict the pullout-cone capacity of anchor bolts. The CCD method assumes a pyramid shaped failure surface with height equal to the embedment depth. A distribution of tensile stress in the concrete over a

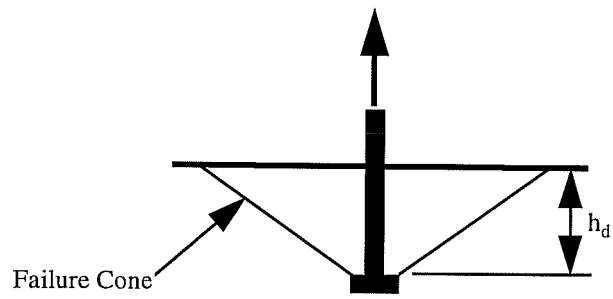
pyramidal shaped failure surface resists the tension in the bolt or bar. The size of the assumed failure area for a single bar away from an edge is $1.5h_d$ from the center of the bar and the area is $9h_d^2$. To take into account increased strength associated with the large heads typically found on headed bars, the size of the available failure surface is $1.5h_d$ from the perimeter of the head (Figure 11.1) provided the head has sufficient stiffness to act as a rigid head. The design equation for the pullout-cone capacity of a headed reinforcing bar in SI units is:

$$P_U = \Psi \frac{A_n}{A_{no}} \frac{h_d^{1.5} \sqrt{f'_c}}{112} \leq \frac{A_b f_y}{1000} \leq \frac{A_b f_u}{1000} \quad \text{eq. 11.1}$$

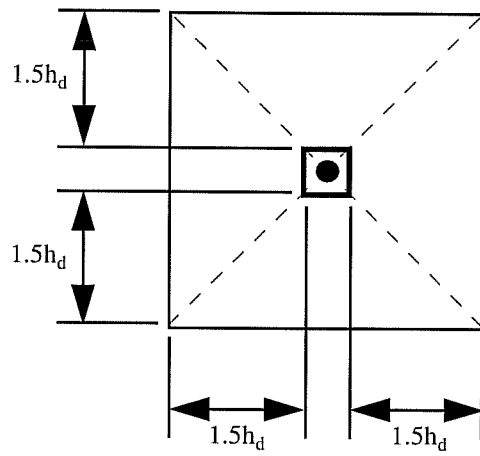
where P_U is the anchorage capacity in kN, h_d the embedment depth in mm and f'_c the concrete compressive strength in MPa. A_n is the available failure surface for a single bar or group of bars based on the perimeter of the heads and A_{no} the basic failure surface area equal to $9h_d^2$. The value Ψ takes into account the disturbance of radial stress for placements near edges and is calculated by:

$$\Psi = 0.7 + 0.3 \frac{C_1}{1.5h_d} \leq 1.0 \quad \text{eq. 11.2}$$

where C_1 is the minimum edge distance. The anchorage capacity is also limited by the capacity of the bar with A_b being the bar area in mm^2 and f_y the yield stress or f_u the ultimate bar stress in MPa.



A. Section



B. Plan

Figure 11.1 - Pullout-Cone Failure for Headed Reinforcement

Deep-Embedment Tests

Based on 123 pullout tests on headed reinforcement with deep embedments placed near edges or corners, the primary factors affecting the blowout capacity of the anchorage were edge distance, net bearing area of the head and concrete compressive strength. For bars with large ratios of embedment to edge distance, side blowout failure and bar failure were the two modes controlling the anchorage capacity. Development length increased the anchorage capacity but again it is conservative to ignore this increase in strength. Transverse reinforcement in the anchorage zone did not increase the ultimate capacity though large amounts of transverse reinforcement placed near the head did increase the level of load maintained after the initial blowout failure. Corner placement and close spacing of bars reduced the blowout capacity of headed reinforcement.

In the physical model proposed for blowout failures, tensile stresses in the concrete are distributed over the blowout failure surface. The assumed failure surface is a pyramid with height equal to the edge distance and base measuring $3C_1$ from the center of the bar (Figure 11.2). The driving force in the model is related to the tensile load on the bar and is a function of the bearing stress at the head and the concrete tensile strength.

The design equation for the blowout capacity of headed reinforcement in SI units is:

$$P_U = \Psi \frac{A_{bo}}{A_{bon}} \frac{C_1 \sqrt{A_n f'_c}}{80} \leq A_b f_y \leq A_b f_u \quad \text{eq. 11.3}$$

where P_U is the blowout capacity in kN, C_1 the minimum edge distance in mm, A_n the net bearing area of the head in mm² and f'_c the concrete compressive strength in MPa. The ratio A_{bo} over A_{bon} is the ratio of available failure area for a single bar or group of bars and the basic failure area, A_{bo} , equal to $36C_1^2$. The general form of Equation 11.3 is identical to an equation proposed by Furche and Eligehausen [18] for the blowout capacity of anchor bolts. The value Ψ takes into account the disturbance of radial stress by corner placement and is calculated by:

$$\Psi = 0.7 + 0.3 \frac{C_2}{3C_1} \leq 1.0 \quad \text{eq. 11.4}$$

where C_1 is the minimum edge distance and C_2 is the minimum orthogonal edge distance. The anchorage capacity is also limited by the capacity of the bar with A_b being the bar area in mm² and f_y the yield stress or f_u the ultimate bar stress in MPa.

The design equations for both the blowout and pullout-cone modes of failure assume the head is adequately stiff. Based on results of deep-embedment pullout tests on heads with reduced thickness, the head should be designed to prevent yielding of the head in bending under a uniform distribution of bearing stress at the ultimate load.

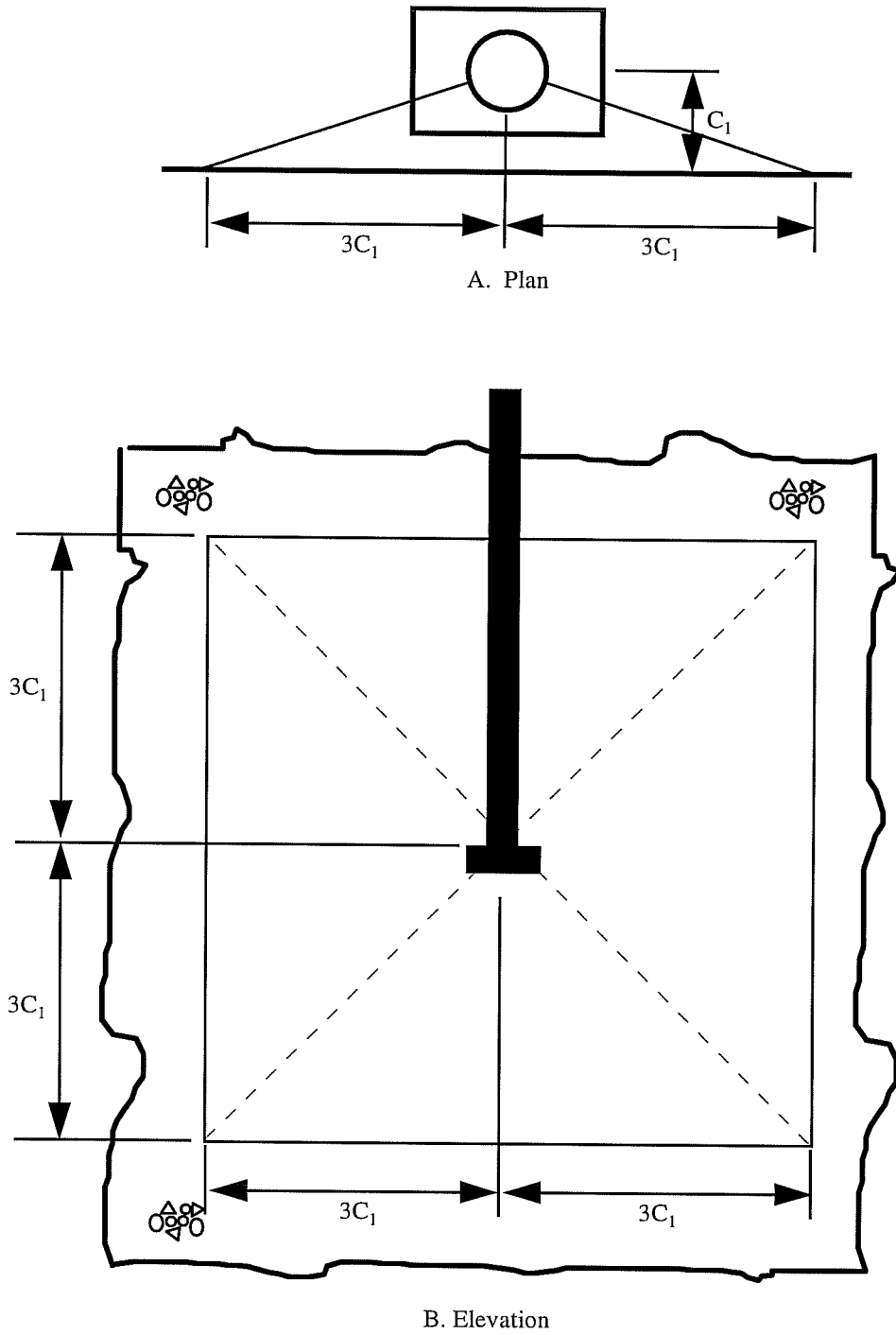


Figure 11.2 - Blowout Failure for Headed Reinforcement

11.3 Areas for Further Research

The research program in this report focused mainly on the behavior of single headed reinforcing bars under monotonic loading and used simple setups to model concrete members. The ease of construction and testing of these setups allowed a large number of variables to be tested. However, to fully understand the behavior of headed reinforcement in concrete members, tests should be conducted on specimens which more accurately model the dimensions, boundary conditions and forces of members. Further studies should be done looking at the effect of head thickness and whether head yielding or excessive head deformation reduces the anchorage capacity. Also more tests should be conducted on the behavior of groups of reinforcing bars. A total of six tests were conducted on pairs of closely spaced headed reinforcing bars. In typical applications like beam-column joints, many bars may be closely spaced and in multiple layers.

A few tests have been conducted on headed reinforcing bars with cyclic tensile loads. However, the test specimens did not accurately model the dimensions and boundary conditions of concrete members and the bars were never placed in compression. Since it is expected that headed reinforcing will be used in members subjected to earthquake loading, more accurate models of members with headed reinforcing should be tested under cyclic loading.

Another potential use of headed reinforcing bars in concrete members is as ties in column sections replacing traditional bent ties. The tests reported in this study focused applications of headed bars for longitudinal reinforcement. Tests should be conducted on column sections to verify that the headed bars provide confinement and bracing of the longitudinal column bars.

Finally, specific questions related to applications of headed reinforcement such as repair and strengthening of existing structures will have to be addressed.

Bibliography

1. American Concrete Institute (ACI 318-95), Building Code Requirements for Structural Concrete and Commentary, American Concrete Institute, Detroit, Michigan, 1995.
2. American Concrete Institute (ACI 349-85), Code Requirements for Nuclear Safety Related Concrete Structures and Commentary, American Concrete Institute, Detroit, Michigan, 1985.
3. American Concrete Institute, Ballot Item Code and Commentary CB-30 (Proposed Chapter 23 for ACI 318), American Concrete Institute, Detroit Michigan, 1995.
4. "ASTM C 234-91a Standard Test Method for Comparing Concretes on the Basis of the Bond Developed with Reinforcing Steel," 1991 Annual Book of ASTM Standards, American Society for Testing and Materials, Philadelphia, Pennsylvania, 1991.
5. "ASTM C 900-87 Standard Test Method for Pullout Strength of Hardened Concrete," 1987 Annual Book of ASTM Standards, American Society for Testing and Materials, Philadelphia, Pennsylvania, 1987.
6. Bazant, Z. P. and Sener, S. "Size Effect in Pullout Tests," ACI Materials Journal, Vol. 85, No. No. 6, September-October 1988, pp. 347-351.

7. Berner, D. E., Gerwick, B. C., and Hoff, G. C., "T-Headed Stirrup Bars," Concrete International, Vol. 13, No. 5, May 1991, pp. 49-53.
8. Berner, D. E., and Hoff, G. C., "Headed Reinforcement in Disturbed Strain Regions of Concrete Members," Concrete International, Vol. 16, No. 1, January 1994, pp. 48-52.
9. Brown, J. M., "W. B. Wilkinson (1819-1902) and His Place in the History of Reinforced Concrete," Newcomen Society Transactions, Vol. 39, No. 439, 1966-1967, pp. 129-142.
10. Collins, D. M., Klinger, R. E., and Polyzois, D., "Load-Deflection Behavior of Cast-In-Place and Retrofit Concrete Anchors Subjected to Static, Fatigue and Impact Tensile Loads," Research Report 1226-1, University of Texas at Austin, February 1989.
11. Comite Euro-International du Beton (CEB), Model Code for Concrete Structures, English Translation, proposed 1990.
12. Comite Euro-International du Beton (CEB), "Fastenings to Reinforced Concrete and Masonry Structures: State of the Art Report," Bulletin d' Information No. 206, August 1991.
13. Comite Euro-International du Beton (CEB), "Design of Fastening in Concrete: Fastening for Seismic Retrofitting, State of the Art Report on Design and Application," Bulletin d' Information No. 226, August 1995.
14. Cook, R. A., Collins, D. M., Klinger, R. E., and Polyzois, D., "Load-Deflection Behavior of Cast-in-Place and Retrofit Concrete Anchors," ACI Structural Journal, Vol. 89, No. 6, November-December 1992, pp. 639-649.
15. Cote, P., and Wallace, J. W., "A Study of Reinforced Concrete Knee-Joints Subjected to Cyclic Lateral Loading," Report No. CU/CEE-94/11, Clarkson University, Postdam, New York, February 1993.

16. Doerr, G. T., and Klinger, R. E., "Adhesive Anchors: Behavior and Spacing Requirements," Research Report 1126-2, University of Texas at Austin, March 1989.
17. Fuchs, W., Eligehausen, R., and Breen, J. E., "Concrete Capacity Design (CCD) Approach for Fastening to Concrete," ACI Structural Journal, Vol. 92, No. 1, January-February 1995, pp. 73-94.
18. Furche, J., and Eligehausen, R., "Lateral Blow-Out Failure of Headed Studs Near a Free Edge," Anchors in Concrete: Design and Behavior, ACI SP-130, American Concrete Institute, Detroit, Michigan, 1991.
19. Gerwick, B. C., Draft of "Application of Headed Reinforcement in Reinforced Concrete Structures," Ben C. Gerwick, Inc., San Francisco, California, 1995.
20. Hasselwander, G. B., "High-Strength Anchor Bolts Embedded Near the Edges of Concrete Piers," Ph.D. Dissertation, University of Texas at Austin, 1979.
21. Hasselwander, G. B., Jirsa, J. O., and Breen, J. E., "Strength and Behavior of Single Cast-in-Place Anchor Bolts Subject to Tension," Anchorage to Concrete, ACI SP-103, American Concrete Institute, Detroit, Michigan, 1987.
22. Hasselwander, G. B., Jirsa, J. O., Breen, J. E., and Lo, K., "Strength and Behavior of Anchor Bolts Embedded Near Edges of Concrete Piers," Research Report 29-2F, University of Texas at Austin, May 1977.
23. Hawkins, N. M., "The Bearing Strength of Concrete Loaded Through Rigid Plates," Magazine of Concrete Research, Vol. 20, No. 62, March 1968, pp. 31-40.
24. Hawkins, N. M., "The Bearing Strength of Concrete Loaded Through Flexible Plates," Magazine of Concrete Research, Vol. 20, No. 63, June 1968, pp. 95-102.

25. Hyatt, T., "An Account of Some Experiments with Portland-Cement-Concrete Combined with Iron, as a Building Material, with Reference to Economy of Metal in Construction, and for Security Against Fire in the Making of Roofs, Floors, and Walking Structures," A Selection of Historical American Papers on Concrete, 1876-21926, ACI SP-52, American Concrete Institute, Detroit, Michigan, 1976.
26. Ibell, T. J., and Burgoyne, C. J., "Experimental Investigation of Behaviour of Anchorage Zones," Magazine of Concrete Research, Vol. 45, No. 165, December 1993, pp. 281-291.
27. Ibell, T. J., and Burgoyne, C. J., "A Plasticity Analysis of Anchorage Zones," Magazine of Concrete Research, Vol. 46, No. 166, March 1994, pp. 39-48.
28. Ibell, T. J., and Burgoyne, C. J., "A Generalized Lower-Bound Analysis of Anchorage Zones," Magazine of Concrete Research, Vol. 46, No. 167, June 1994, pp. 133-143.
29. Ingham, J. M., "Seismic Design of Knee-Joints under Transverse Loading.," Applications of the T-Headed Bar in Concrete Design and Construction Workshop, St. John's, Newfoundland, 1994.
30. Klinger, R. E., and Burdette, E. G., "Research Needs in Design of Anchorage to Concrete," Concrete International, Vol. 11, No. 12, December 1989, pp. 72-76.
31. Klinger, R. E., and Mendonca, J. A., "Tensile Capacity of Short Anchor Bolts and Welded Studs: A Literature Review," ACI Journal, Vol. 79, No. 4., July-August 1982, pp. 270-279.

32. Kuchma, D. A., "Compressive Response of Reinforced Concrete Confined by T-Headed Reinforcement," Applications of the T-Headed Bar in Concrete Design and Construction Workshop, St. John's, Newfoundland, 1994.
33. Lieberum, K. H., and Reinhardt, H. W. "Strength of Concrete on an Extremely Small Bearing Area," ACI Structural Journal, Vol. 86, No. 1, January-February 1989, pp. 67-76.
34. Lee, D. W., and Breen, J. E., "Factors Affecting Anchor Bolt Development," Research Report 88-1F, University of Texas at Austin, August 1966.
35. Marzouk, H, and Jiang, D., "A New Design for Bridge Deck Slabs," Canadian Society for Civil Engineering, Fourth International Conference on Short and Medium Span Bridges, Halifax, Nova Scotia, 1994.
36. Meyerhof, G. G., "The Bearing Capacity of Concrete and Rock," Magazine of Concrete Research, Vol. 4, No. 12, April 1953, pp. 107-116.
37. Mitchell, D. W., and Rooney, A., "T-Headed Bars in the Hibernia G.B.S.," Canadian Civil Engineer, Vol. 11, No. 3, March 1994, pp. 3-4.
38. McConnell, S. W., and Wallace, J. W., "Use of T-Headed Bars in Reinforced Concrete Knee-Joints Subjected to Cyclic Lateral Loading," Report No. CU/CEE-94/10, Clarkson University, Postdam, New York, June 1994.
39. Orangun, C. O., Jirsa, J. O., and Breen, J. E., "A Reevaluation of Test Data on Development Length and Splices," ACI Journal, Vol. 74, No. 3, March 1977, pp. 114-122.
40. Roberts, C. L., "Behavior and Design of the Local Anchorage Zone of Post-Tensioned Concrete Members," Master's Thesis, University of Texas at Austin, May 1990.

41. Sherrod, P. H., "NLREG: Nonlinear Regression Analysis Program," Manual, 1995.
42. SINTEF Report No. STF65 F86083, "T-Headed Bars SP1: Static Pullout Tests," SINTEF, Trondheim, Norway, 1986.
43. SINTEF Report No. STF18 F86048, "T-Headed Bars SP2: Fatigue Tests - Bars in Air," SINTEF, Trondheim, Norway, 1986.
44. SINTEF Report No. STF65 F86088, "T-Headed Bars SP3: Fatigue Tests - Bars Embedded in Concrete," SINTEF, Trondheim, Norway, 1986.
45. SINTEF Report No. STF65 F86084, "T-Headed Bars SP4: Shear Tests," SINTEF, Trondheim, Norway, 1986.
46. SINTEF Report No. STF20 F90027, "Friction Welded Joints - Fatigue," SINTEF, Trondheim, Norway, 1990.
47. SINTEF Report No. STF20 F92127, "Fatigue in Friction Welding Joint for Reinforcement Bars," SINTEF, Trondheim, Norway, 1991.
48. SINTEF Report No. STF20 F92020, "Static and Dynamic Pull-Out Tests of T-Headed Bars Embedded in Concrete," SINTEF, Trondheim, Norway, 1992.
49. SINTEF Report No. STF70 F92077, "Sleipner Y-Tests Experimental Results," SINTEF, Trondheim, Norway, 1992.
50. Smee, D. J., "The Effect of Aggregate size and Concrete Strength on the Failure of Concrete Under Triaxial Compression," Civil Engineering Transactions, Institution of Engineers, Australia, Vol. CE 9, No. 2, October 1997, pp. 339-344.

51. Stone, W. C., and Carino, N. J., "Deformation and Failure in Large-Scale Pullout Tests," ACI Journal, Vol. 80, No. 6, November-December 1983, pp. 501-513.
52. Walker, S., and Bloem, D. L., "Effects of Aggregate Size on Properties of Concrete," ACI Journal, Vol. 57, No. 9, September 1960, pp. 283-298.
53. Walker, S, Bloem, D. L., and Gaynor, R. D., "Relationships of Concrete Strength to Maximum Size of Aggregate," Proceedings of the U.S. Highway Research Board, Vol. 38, 1959, pp. 367-385.
54. Williams, A., "The Bearing Capacity of Concrete Loaded Over a Limited Area," Technical Report 526, Cement and Concrete Association, 1979.

Vita

Richard Alan DeVries was born in Omaha, Nebraska on October 22, 1965, the son of JoAnn and Richard N. DeVries. He received the degree of Bachelor of Science in Civil Engineering with High Honors from the University of Texas in December 1987. He then entered the Graduate School of the University of California at Berkeley and received a Master of Science in Engineering in May 1989. In the following years, he worked as a structural engineer in Austin, Texas. In August 1992, he began his doctoral studies in the Graduate School of the University of Texas at Austin under the supervision of Dr. James O. Jirsa. He married Linda LaFrance on May 14, 1995; and in August of 1996, was appointed to the faculty of Oklahoma State University in Stillwater, Oklahoma.

Permanent Address: 1905 Wren Ct.
Edmond, Oklahoma 73034

This dissertation was typed by the author.